Berichte
aus dem
Institut für Meereskunde
an der
Christian-Albrechts-Universität Kiel

Nr. 88

1981

THE GATE LAGRANGIAN BATFISH EXPERIMENT
SUMMARY REPORT

by
John Woods, Harry Leach, Peter Minnett

DOI 10.3289/IFM_BER_88

Copies of this Report are available from
Prof. J.D. Woods
Institut für Meereskunde
Düsternbrooker Weg 20
D-2300 Kiel 1
Federal Republic of Germany

ISSN 0341 - 8561

Die „Berichte aus dem Institut für Meereskunde" erscheinen in unregelmäßiger Folge und sind gedacht als Arbeitsunterlagen für den sich mit dem jeweiligen Thema befassenden Personenkreis. Die Hefte werden fortlaufend numeriert. Sie sind unredigierte Beiträge und geben allein die Meinung des Verfassers wieder.

D 2300 Kiel 1, Düsternbrooker Weg 20

ABSTRACT

Thirteen quasi-Lagrangian box-surveys were carried out as part of the GATE-Experiment with a CTD mounted in a Batfish towed body. The experiment, the data acquisition and data processing are described; the uncertainties in the data are estimated and a selection of standard products from the data set are presented and described. By means of isopycnic analysis it has been possible to show that thermohaline and dynamic structures were present whose scales were comparable with those of mesoscale fronts.

ZUSAMMENFASSUNG

Als Teil des GATE-Experiments wurden dreizehn quasi-Lagrang'sche Box-Vermessungen mit einer CTD-Sonde, die in einem Batfish-Schleppkörper montiert wurde, durchgeführt. Das Experiment, die Datenerfassung und die Datenverarbeitung werden beschrieben. Die Ungenauigkeiten der Daten werden abgeschätzt und eine Auswahl von Standardprodukten des Datensatzes werden präsentiert und beschrieben. Mittels isopyknischer Analyse ist es möglich gewesen, zu zeigen, daß thermohaline und dynamische Strukturen vorhanden waren, deren Längenskalen vergleichbar waren mit denen mesoskaliger Fronten.

PREFACE

The Lagrangian Batfish experiment carried out on board RRS "Discovery" in 1974 during GATE was an important step in a long-term research programme that started in 1965 in the central Mediterranean and continued in 1981 in the North Atlantic. The research programme is designed to explore local structures associated with turbulence in the upper ocean on scales up to 100 km. This spectral range includes the microstructure (normally smaller than 1 metre) and the finestructure (vertical scales up to several tens of metres, horizontal scales up to several tens of kilometres). In terms of oceanic turbulence, it includes the mesoscale and microscale cascades flowing from the energy containing eddies on synoptic scale (~100 km). Exploration of oceanic structure on these scales has stimulated the development of new apparatus and methods. Our research programme has involved the use of flow visualization (for the microstructure), high-resolution profilers (for the temperature finestructure) and combined surveys by expandable bathythermographs and airborne radiation thermometer (for the mesoscale). Each method has yielded stimulating new images of a hitherto unexplored aspect of upper ocean turbulence. In 1974, thanks to our colleagues at the Institute of Oceanographic Sciences, Wormley, we were able to introduce another new tool to the research programme, a Conductivity-Temperature-Pressure probe mounted in a Batfish. This allowed us to survey the mesoscale thermohaline structure in three dimensions for the first time. A large data set was collected and systematically processed to yield a rich harvest of novel images. They are presented in the thirteen-part data report (Woods, Leach and Minnett, 1981) that accompanies this summary report. Here we describe the experiment, assess the experimental errors and present samples of the new mesoscale images chosen partly to show the best that has been achieved with the new apparatus and partly to compare the thirteen parts of the data report. Processing the data set to extract the new images involved an extension to the mesoscale of diagnostic techniques previously used only on the gyre scale. They have been discussed briefly by Woods and Minnett (1979), but as they are likely to be new to many readers we go into greater detail in this volume.

Our research was based initially at the Oceanography Department, University of Southampton (1974-1977) and then at the Institut für Meereskunde an der Universität Kiel (1977-1981). The fieldwork would not have been possible without the support of the Marine Physics group at the Institute of Oceanographic Sciences, Wormley, and the captain and crew of RRS "Discovery". Data processing was carried out at the Science Research Council Atlas Computer Laboratory, Chilton, University of London Computer Centre and the Regionales Rechenzentrum für Niedersachsen (Hannover). The Natural Environment Research Council helped finance the work through research grants GR3/2194 and GR3/2634 (1974-1977) and the Deutsche Forschungsgemeinschaft through research grants WO 254/1, 4, 6, 8 (1978-1980). We thank these agencies for their support, and our colleagues at Southampton, Wormley, Chilton, Kiel and Hannover for their help over the past years.

The following members of the research team at Southampton and Kiel contributed to the production of this report:
Wolfgang Barkmann, Gordon Blanchard, Bernd Burkert, Mike Butterfield, Jürgen Fischer, Bernd Frantz, Dieter Helm, Stefan Hesse, George Kimber, Harry Leach, Manfred Lüdtke, Isabelle Meurin, Peter Minnett, Beryl Noyce, Bernd Reklies, Linda Warren, Jan Wenzel, John Woods.

CONTENTS

1. INTRODUCTION

1.1 Aims of the experiment

The experiment was designed to explore the time varying, three-dimensional thermohaline finestructure of the tropical thermocline in the North Atlantic Equatorial Counter Current on horizontal scales of 0.1 to 25 km. Turbulence theory suggested that on these scales the finestructure should exhibit frontlike characteristics (for a review see Woods, 1980). The experiment thus appears under the heading "Fronts" in the SCOR (1973) plan for the Oceanographic Sub-Programme of GATE. The measurements were also expected to provide a direct estimate of the contribution made by finestructure advected by the North Atlantic Equatorial Counter Current to Eulerian fluctuations recorded by moored instruments and at fixed ship stations.

1.2 Experiment design

The experiment was designed to make a Lagrangian time series of repeated surveys of the three-dimensional thermohaline finestructure within an arbitrarily chosen 25 km square box drifting with the mean current velocity at hull depth (about 35 km/day). Navigation was based on integration of ship velocity relative to the water, measured by an electromagnetic log mounted on the ship's hull. The initial starting position was chosen such that the mean current promised to carry the survey box through the array of moorings and stationary ships in the GATE C-scale ship array (see section 1.5. below).

Each survey comprised a set of parallel legs spaced 1 or 2 nautical miles apart and running north-south or east-west in successive surveys in the time series. Care was taken to design the surveys in each time series in a way that promised to yield a ground track (predicted from the mean current) that would minimize direct encounters with moorings and stationary ships.

The Batfish undulation was designed to have a sawtooth waveform, with turning depths near the surface and at 60 metres depth and a nominal ascent/descent rate of 1 m/s. With a ship speed of 4 m/s this would give a cycle wavelength of 500 metres. The Batfish would intersect an isopycnic surface about 50 times along each 25 km long leg. The time for each leg would be about 100 minutes and the total time for a 12 leg survey would be about 24 hours. The length and number of legs was increased in succesive surveys in the third experiment in the hope of compensating for unknown displacements due to vertical shear of the current and to navigational inaccuracies.

1.3 The experimental site - oceanographic conditions

The experiment was performed during September 1974 within 100 km of the GATE Origin 8°N, 24°W. The site lies in the North Atlantic Equatorial Counter Current which flows most swiftly in late summer; the mean speed derived from our navigation data was 35 km/day to the east. The reader is referred to Merle's (1978) Atlas of the Equatorial Atlantic for a recent summary of the seasonal variation of oceanic distribution in the area; and to Hastenrath and Lamb's (1977, 1978) Atlases for the surface meteorology and air-sea exchange. Montgomery's (1938) famous analysis of salinity and depth on isopycnals is still of interest, especially in view of our use of isopycnic analysis.

In the top 70 metres of the ocean where we collected our Batfish data set, the hydrography is dominated by a shallow mixed layer over a pycnocline of rather uniform density gradient. The mean temperature profile shows a transition at 35 metres between an upper weak gradient and a deeper thermocline with a gradient of -0.25 K/m, and the mean salinity profile exhibits a transition at 35 metres between a weak stable gradient above, and a deeper (stable) halocline with a gradient of +0.1 ppt/m to a maximum of 36.18 ppt at 42 metres: below the maximum salinity decreased rather uniformly at about 0.02 ppt/m. The mean profiles offer no possibility of double diffusive convection above the salinity maximum (42 metres), but it may occur below.

1.4 GATE

The experiment was a part of the GATE Oceanographic Sub-Programme. GATE was the Atlantic Tropical Experiment of the Global Atmospheric Research Programme (GARP 1972). GATE was a meteorological experiment designed to investigate the role of the tropics in the general circulation of the atmosphere. The meteorological observing system including a large-scale (A) array of 40 research ships stationed as shown in fig. 1.1. Smaller B-scale arrays of ship stations were nested within the A-scale array, centred on 8°N, 24°W. An oceanographic sub-programme was organized by SCOR to take advantage of this unique array of research ships (SCOR 1973). Some of the early results of the oceanographic sub-programme have been published in special editions of Deep-Sea Research (Siedler and Woods, 1980; Düing, 1980) and an analysis of the large-scale distributions has been published as a GATE Oceanographic Atlas (Düing, Ostapoff, Merle, 1980). Siedler and Philander (1982) summarize the sub-programme results for the upper ocean available up to 1980.

1.5 The "Discovery" Batfish experiment in relation to GATE Oceanography

The experiment summarized in this volume was performed on board RRS "Discovery" as part of the C-scale part of the GATE Oceanographic Sub-programme. The C-scale array comprised 5 research ships at fixed station subject to certain constraints (e.g. at synoptic observing times). A sixth ship, "Columbus Iselin", was not committed to a fixed station; she had a primary responsibility for servicing the Cyclesonde moorings (Van Leer, Düing, Evath, Kenelly and Speidel, 1974), but was free to make spatial surveys, including some joint work with "Discovery", which was free to rove throughout the C-scale area. An array of current meter and Cyclesonde moorings lay within the C-scale ship array at positions shown in fig. 1.2.

On three occasions "Discovery" made repeated Batfish surveys of water masses drifting through the C-scale array. These are described in

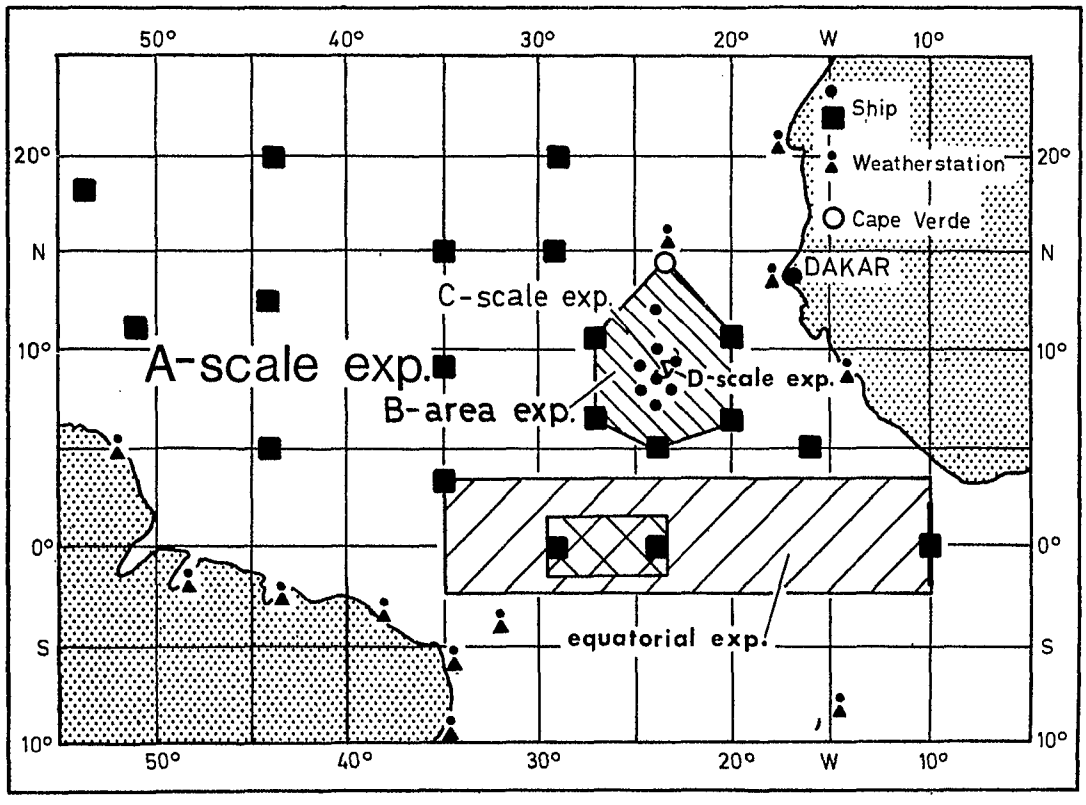

Figure 1.1 : Map indicating GATE observational areas in the tropical Atlantic, covering dominant scales A to D.

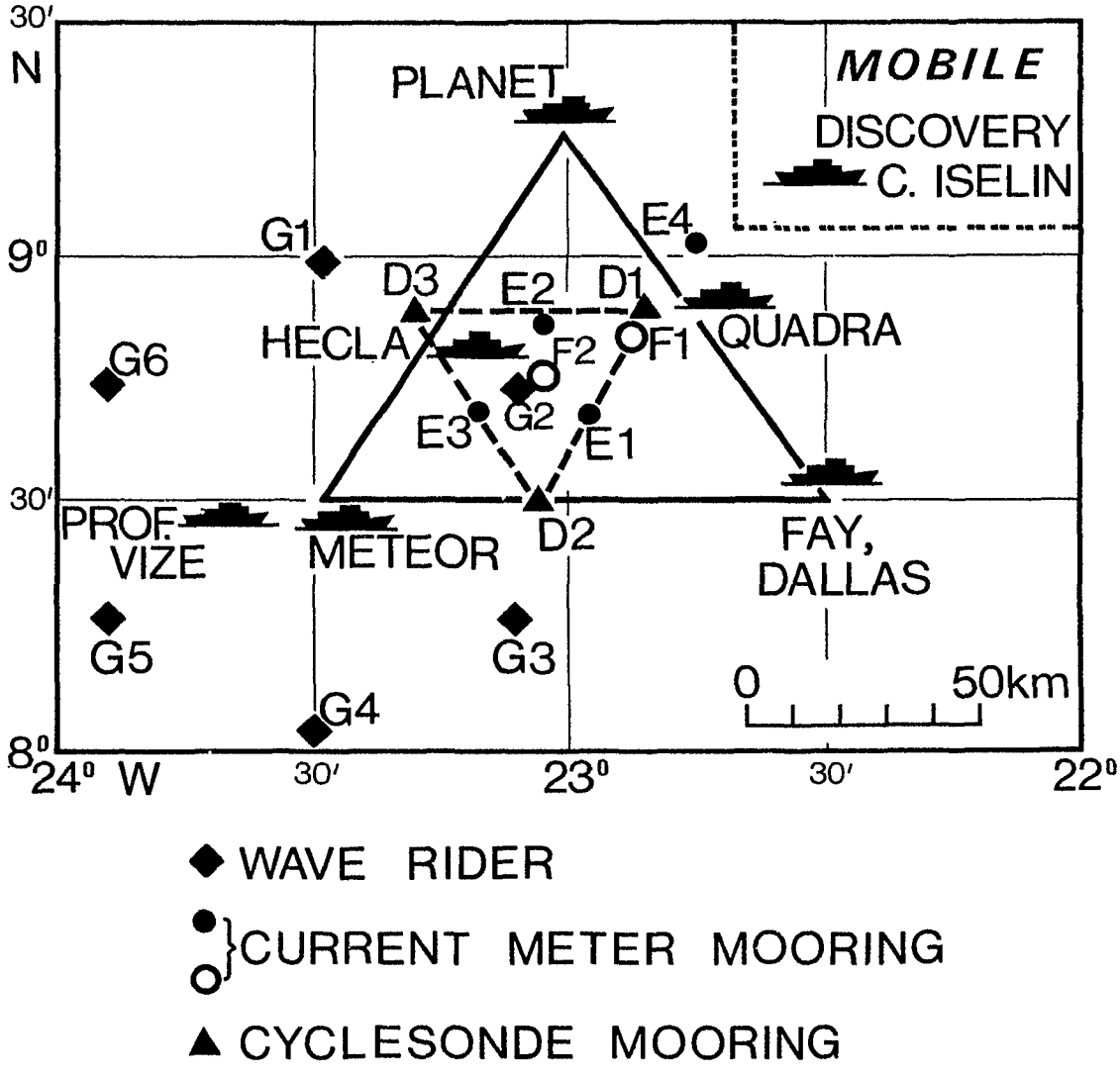

Figure 1.2 : The GATE C-Scale observational array.

chapter 2 of this summary report. The Batfish surveys provide information about the thermohaline variations on horizontal scales (0.5 - 25 km) too small to be resolved by the fixed ship and mooring array. Before the experiment Rooth (1973) and Ostapoff et al. (1973) had drawn attention to patches of salinity anomaly with these scales at the proposed site of the B-scale array. It was feared that Eulerian fluctuations measured at the fixed ships would be seriously contaminated by the rapid advection of such anomalies in the Equatorial Counter Current.

The C-scale oceanography programme (Philander, 1975) included a study of internal waves using moored current meters, Cyclesondes and profilers at fixed ships. The Batfish experiment also contributed to the internal wave programme by measuring the undulations of isopycnals.

1.6. Other GATE experiments contributing to the "Discovery" Batfish surveys

The research programme on board RRS "Discovery" included a number of other measurements in addition to the Batfish survey experiment. First, there were the routine observations of sea surface temperature and salinity, and meteorological variables, recorded every two minutes. Second, the Batfish was also used for experiments for Dr. R.T. Pollard during the period spent in the GATE C-scale array. The third experimental programme on "Discovery" involved a series of profiles with the free-fall PROTAS sonde of Dr. J. Simpson. The site for the PROTAS profiles was designed to be the centres of some of the Batfish surveys in the Lagrangian time series, so as to collect some information concerning the current shear finestructure in the water surveyed by the Batfish. The penalty was an interruption to the Lagrangian time series that increased the risk of misalignment of successive surveys relative to the drifting water mass.

The RRS "Discovery" cruise 66 report (Institute of Oceanographic Sciences, 1975) has additional information on the general experimental programme.

1.7 Other GATE experiments directly related to the "Discovery" Batfish surveys

It has already been noted that the starting position of each Lagrangian time series was chosen with the intention that the water mass being surveyed by the Batfish would pass through some of the moorings and fixed ship stations in the GATE C-scale array. The data from these moorings and fixed ships is therefore directly relevant to the interpretation of our expertimental data set.

The two other roving ships, "Quadra" and "Columbus Iselin" also contributed to the "Discovery" experiment, by making parallel measurements with a Batfish ("Quadra"), a Hydroglider and an acoustic profiler ("Columbus Iselin"), on a number of occasions.

1.8 Publications relating to the "Discovery" data set

(a) Chee (1976)

The variation of temperature and salinity measured with a fish towed at a nominally constant depth of 2 m alongside "Discovery", was recorded every second during a calm sunny day. It was shown that there is a systematic diurnal variation of temperature and temperature variance in the records, but not of salinity and salinity variance. The Equatorial Counter Current advects these time-varying spatial patterns of temperature and more steady spatial patterns through fixed stations giving Eulerian changes that have amplitudes and frequencies comparable with those measured at RV "Meteor".

(b) Pegler (1976)

The effect of lateral variation of sound speed on sonar range was

analyzed using the Batfish data set. The result was that horizontal variability of sound speed is more important than horizontal variability of thermocline depth.

(c) Minnett (1978)

The first detailed description of the experiment is given including data processing, an analysis of errors and a preliminary account of the principal features in one survey (3L3). The following properties were given particular attention:

(i) The contamination of data products (notably the spacing between pairs of isopycnals) by internal waves and by measurement inaccuracies.

(ii) The scale, concentration and distribution of microscale density inversions.

(iii) The spacing between isopycnic and isothermal surfaces.

(iv) The diurnal cycle of heating and depth change of the mixed layer.

(v) The pattern of isotherms on isopycnic surfaces.

(vi) A comparison of the calibration of measurements by the "Discovery" Batfish and the "Columbus Iselin" Hydroglider above the thermocline.

(d) Kassler (1980)

A detailed analysis of microscale density inversions in the Batfish data set. The size and concentration and distribution relative to mesoscale structure are similar to those found in other experiments, but as no reliable method was discovered for identifying those inversions that were caused by instrumental malfunction (mainly residual lag in the thermometer) the validity of the results remains in doubt.

(e) Woods and Minnett (1979)

The first results of the isopycnic analysis of the data from one of the Batfish surveys (3L3). They considered the statistics and spatial distribution of scalar variables on one isopycnic surface. This revealed that the pressure difference between an isopycnal and its mean isothermal surface could be spatially divided into "disturbed" and "undisturbed" regions, the disturbed regions being where this pressure difference varied rapidly between adjacent measurement positions.

(f) Leach (1984)

Statistical analysis of the spatial structure of static stability and thermohaline anomalies in the Batfish surveys reveals significant differences in lateral (along isopycnal) and vertical scales.

(g) Woods (1981)

Features of the mesoscale structure in Batfish survey 3L3 are shown to be consistent with the predictions of theoretical models of mesoscale fronts.

(h) Tang (1984)

The probability distribution and spectrum of variations of spacing between pairs of isopycnals are analyzed. Part of the observed variation is due to internal waves, but it seems likely that some is due to front-like mesoscale turbulence. Assuming that the effect of microscale mixing is negligible, the measurements are interpreted in terms of the probability distribution of relative vorticity.

(i) Kronfeld (1982)

The space-time variation of temperature and salinity measured by the Batfish above the thermocline (i.e. above 40 m) were analyzed with the aim of discriminating between relatively steady spatial patterns and the diurnal modulation due to surface heat exchange and mixing to discriminate between spatial patterns encountered sequentially and temporal changes occuring during the sampling. The results of the

analysis show that the discrepancy between heat lost and gained at the surface can be accounted for by making reasonable assumptions about the advection of heat, estimated using the thermohaline information.

(j) Woods, Leach and Minnett (1981)

This is the companion to this report. A systematic coverage of all parameters in all thirteen maps of the experiment is graphically presented.

(k) Leach, Minnett and Woods (1984)

This is essentially a shortened version of the present report.

2. THE LAGRANGIAN EXPERIMENTS

This chapter contains a brief account of the Batfish Lagrangian experiments, based on the bridge log and the experimental log. Earlier accounts are to be found in Woods (1974), Minnett (1978) and the "Discovery" 66 cruise report (IOS 1975), which also refer to other experiments on the same cruise.

The "Discovery" 66 cruise plan called for two Lagrangian experiments each following a mesoscale water mass as it drifted some 150 km with the North Atlantic Equatorial Counter Current through the GATE C-scale from west of "Meteor" to east of "Quadra" in about 5 days. The first experiment was successfully completed from 3 - 7 September, yielding seven maps. The second experiment, starting on 13 September, was abandoned after completing the second map, when it became necessary to recover the F2 mooring (which had broken loose on 12 September). A third experiment was therefore started on 14 September and terminated after completing four maps on 16 September, when the deadline for leaving the GATE area was reached. Details of the three experiments are listed in Table I and their positions in relation to the fixed C-scale ships and moorings are illustrated in fig. 2.1.

Nomenclature

RAW DATA WORD - One sample of one of the sensors,

DERIVED DATA WORD - One sample of a variable derived from the raw samples,

DATA CYCLE - One set of data words, based on a set of raw data words collected in rapid sequence,

DOWN DIP - A set of data cycles collected sequentially while the Batfish was descending from its upper to its lower turning level,

UP DIP - A set of data cycles collected sequentially while the Batfish was ascending from its lower to its upper turning level,

LEG - A set of up and/or down dips collected sequentially while the ship was following one straight line segment of a survey track,

Map Name	Date/Time (GMT) September 1974 Start	End	Position of Centre of Map at Start Latitude	Longitude	No.	Legs Heading during First Leg	Length km	Spacing km	Mean Surface Current Direction	Speed m/s
1L1	3/1427	3/2218	08°26.0'N	23°50.5'W	5	W	22	4	056°	0.33
1L2	4/0324	4/1307	08°30.5'N	23°44.0'W	6	S	22	4	052°	0.33
1L3	4/2209	5/1030	08°30.5'N	23°32.0'W	6/2	W/S	22	4/0	084°	0.45
1L4	5/1535	6/0529	08°33.5'N	23°17.0'W	8	S	22	4	073°	0.41
1L5	6/0540	6/1407	08°44.0'N	23°14.0'W	6	E	22	4	066°	0.35
1L6	6/2031	7/0717	08°47.0'N	23°02.5'W	6	N	26	4	069°	0.54
1L7	7/0724	7/2323	08°51.5'N	22°44.5'W	7	E	22	4	080°	0.59
2L1	13/2145	14/0350	08°48.5'N	22°57.5'W	6	S	11	2	075°	0.34
2L2	14/0354	14/0911	08°52.5'N	22°52.0'W	7	E	9	2	070°	0.37
3L1	14/1650	14/2229	08°48.5'N	22°57.5'W	6	S	9	2	065°	0.46
3L2	14/2240	15/0842	08°53.0'N	22°49.0'W	9	E	13	2	075°	0.41
3L3	15/0850	16/0633	08°57.5'N	22°43.5'W	13	N	22	2	116°	0.30
3L4	16/0638	16/2000	08°56.5'N	22°30.0'W	8	E	26	4	109°	0.23

Table I: Summary of Lagrangian Batfish Surveys from "Discovery"

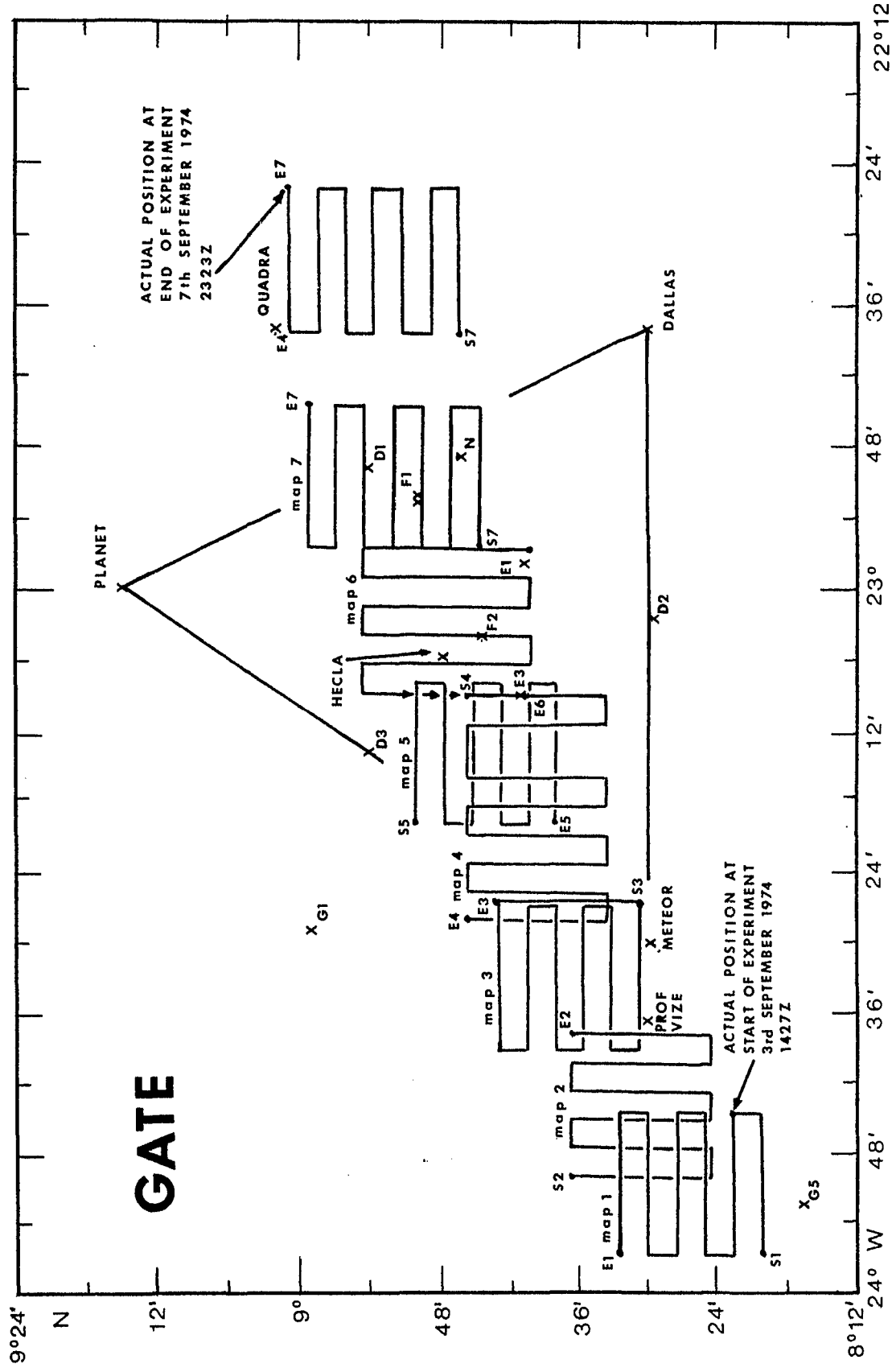

Fig. 2.1 a) : 1st LAGRANGIAN BATFISH EXPERIMENT

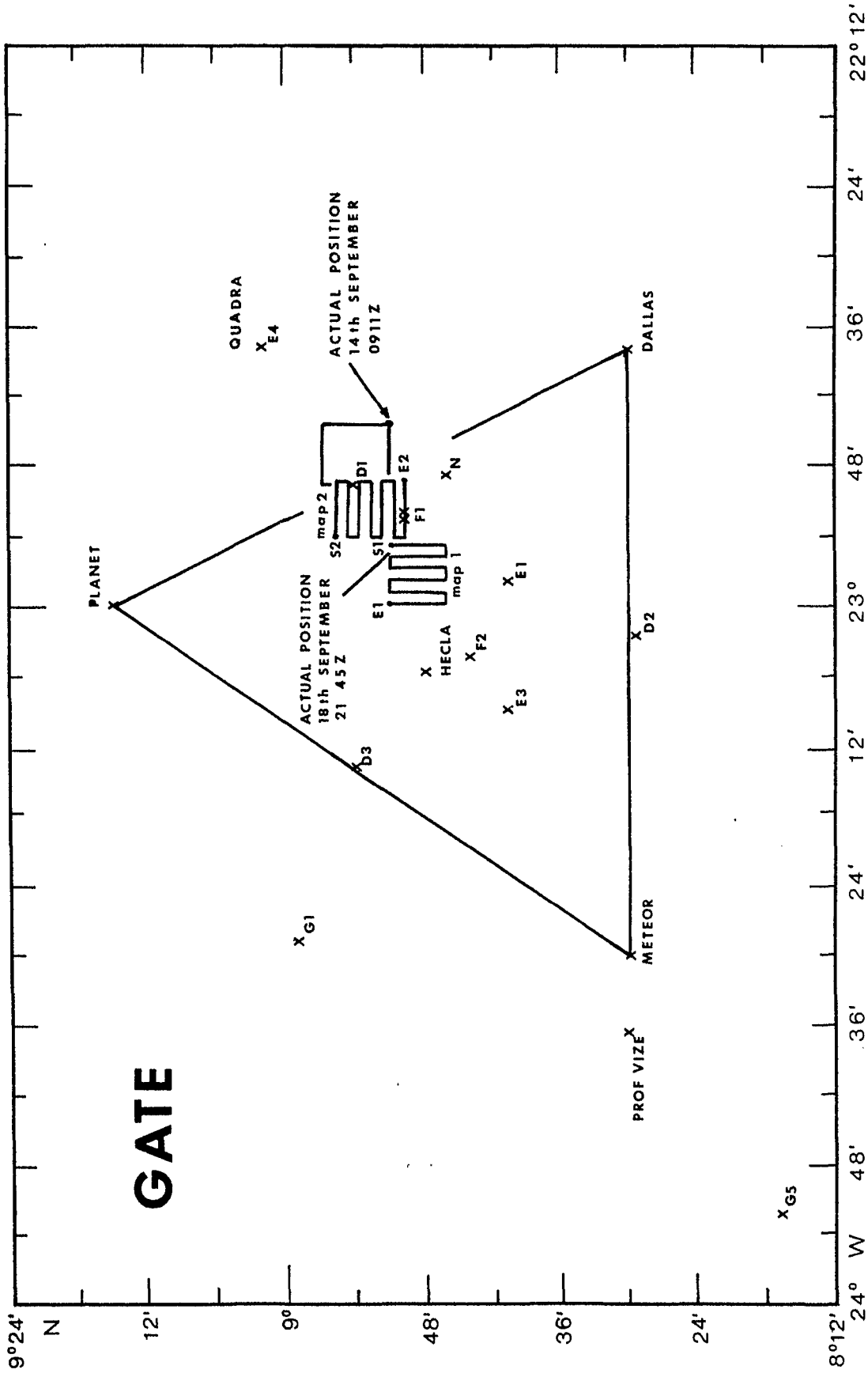

Fig. 2.1 b) : 2nd LAGRANGIAN BATFISH EXPERIMENT

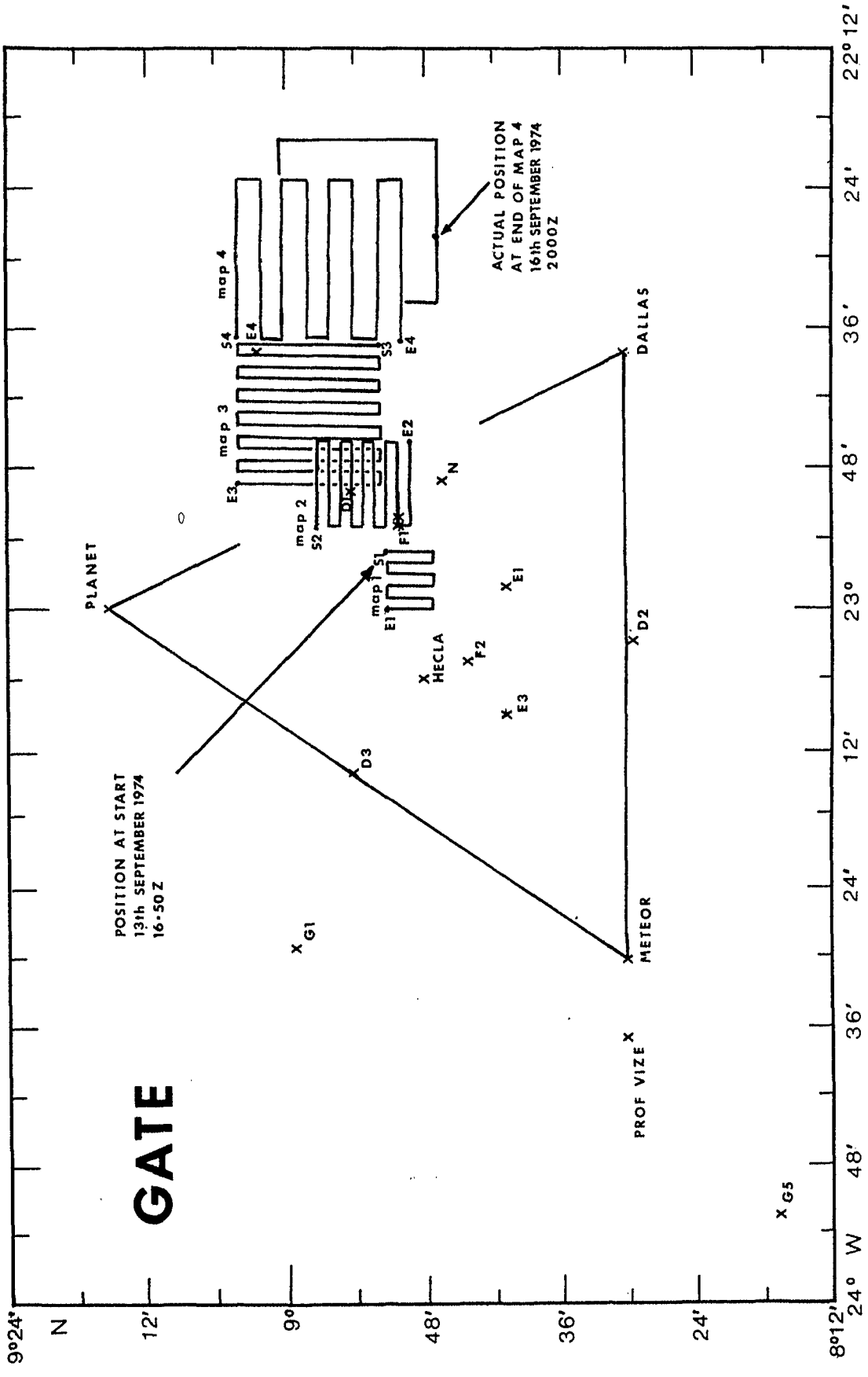

Fig. 2.1 c) : 3rd LAGRANGIAN BATFISH EXPERIMENT

MAP - A set of legs making one complete survey of a mesosale water mass,

LAGRANGIAN EXPERIMENT - The collection of one time series while following a mesoscale water mass, plus supporting measurements.

The following simplified code is used to refer to parts of the data set. (Experiment number) - L - (Map number) - (Leg number) - Dip number followed by D or U to designate down dip or up dip.

2.1. The first Lagrangian time series: 3 - 7 September

Map 1L1: The location of the first Map was chosen so that water being surveyed would be expected to drift centrally through the C-scale area towards the vicinity of "Quadra". On September 2, the US P3A aircraft carried out a reconnaissance of the sea surface temperature patterns around the wave-rider buoy G5 (8°17'N, 23°52'W), and reported a temperature jump of 1.5 K (possibly a front) at three locations along a line running approximately NW-SE through G5. The position of 1L1 was slightly adjusted to cover the predicted location of this feature, assuming advection at 070°, 0.38 m/s.

Map 1L2: Starting 5 hours after the end of 1L1, the location of 1L2 was displaced according to the current velocity measured during 1L1. During this Map, and in the period between 1L2 and 1L3, the water being surveyed passed through the position of "Meteor", from which an 8 hour series of rapid CTD profiles to 100 m was made.

Map 1L3: An interval of 9 hours elapsed between the end of 1L2 and the start of 1L3 to allow for other work to be done from "Discovery". As before, the start position of the new map was displaced to allow for advection during this period.

The experimental plan for this first Lagrangian time series turned critically on ending this third map just to the west of mooring E3, so that the difficult fourth map, which would survey the water mass as it passed through the high concentration of ships and moorings in the

centre of the C-triangle could be based on a navigationally simple (and therefore safe) series of north-south legs creeping to the west (i.e. against the current). The aim was to complete the fourth map without actually risking the Batfish by towing it amongst the moorings, while still surveying the T-S distribution. Added to this navigational constraint was the plan to carry out the fourth map as joint operation with "Columbus Iselin". Thus the plan required us to start the fourth map at just the right time and place; this rendevous had been calculated on the basis of an assumed advection of 070°, 0.38 m/s. As we entered the sixth leg 1L3 it became clear that the current was slower than we had predicted (on the basis of earlier measurements up to September 2). So it was decided to add two extra legs on the eastern edge of the map, running north-south over as precisely the same track as could be done using the relative navigation facilities (see section 3.3).

Difficulty in controlling the Batfish was encountered during the early part of this map, leading to a comparatively poor waveform and suspension of data acquisition between 0003 and 0023 GMT (during 1L2-2). After a period of manual control, the response of the Batfish was sufficiently improved to permit the continuation of the survey.

A small course deviation was made at the beginning of Leg 1L2-1 to avoid approaching too close to "Meteor".

Map 1L4: This survey was begun some 5 hours after completing 1L3. A navigation error caused the start of the map to be about 11 km to the east of the intended position (i.e. to the east instead of to the west of the mooring E3). This was corrected by increasing the separation legs 1L4-3 to 4 n.miles (7.4 km) and adding two extra legs to the end of the survey pattern. The last six legs (1L4-3 to 1L4-8) were centred on the calculated position of the advected body of water being surveyed. Acoustic equipment was used to monitor internal waves from the "Columbus Iselin", which took up position about 1 n.mile (about 1.8 km) to the east of "Discovery" for legs 1L4-3 to 1L4-6. On leg 1L4-6, the "Columbus Iselin" towed the Hydroglider (a towed undulating fish similar to Batfish). During these joint operations the ship reduced speed to about 7 knots to improve the quality of the acoustic

data.

The conductivity cell of the Batfish CTD became contaminated during leg 1L4-4 (see section 6.1.3) with the result that much of the data from this leg are unreliable. The contamination was recognized just after the end of this leg, and was cleared by stalling the Batfish during the turn into leg 1L4-5.

Map 1L5: This map began without pause after the end of Map 1L4. During the period of the survey, the water body is believed to have passed through the positions of moorings E3 and F2, and "Hecla". An 8 hour series of STD profiles to 100 m was made from "Hecla" during this time.

Map 1L6: After a break of 6½ hours for PROTAS measurements "Discovery" continued the Lagrangian Experiment with Map 1L6, which had legs extended to 17 n.miles length (26 km) to reach the mooring E1. The "Columbus Iselin" accompanied "Discovery" at a distance of about ½ n.mile (about 1 km) to the east, using acoustic equipment as in Map 1L4. An apparently disabled tanker was encountered during this map, which necessitated some slight changes of course during legs 1L6-5 and 1L6-6.

Map 1L7: This map followed Map 1L6 directly. It was interrupted after leg 1L7-3 for 3 hours for PROTAS work, but when resumed, the start position of 1L7-4 was appropriately displaced. As in the previous map, the "Columbus Iselin" collaborated during 1L7, making a parallel course about ¼ n.miles (½ km) to the south of "Discovery". It was noted that the current had increased in speed to about 1 knot (≈ 0.5 m/s) and veered to 080° as the position of "Quadra" was approached. This had the effect of moving our survey to the south of the E4 mooring. However, the water body moved through the moorings F1 and D1 during Map 1L7.

The course of legs 1L7-1 and 1L7-7 had to be altered to avoid the disabled tanker and an unidentified buoy. A short break in the CTD data acquisition was caused during leg 1L7-2 by computer failure.

2.2 The Second Lagrangian time series: 13 - 14 September

It was intended that this series should continue until the evening of September 16, but the need to recover the mooring F2 on September 14 brought it to a close after two maps had been completed. The original intention had been to modify the procedure followed in the first Lagrangian series, firstly by halving the leg spacing to 1 n.mile (1.8 km) and secondly by progressively increasing the size of successive maps in the series from the first one that had approximately the linear dimension of a series 1 map to a final map with twice the series 1 dimensions. The object of this plan was to overcome tracking errors due to inadquacies in the navigation, and to vertical current shear about which we had no information while the experiment was in progress.

Map 2L1: This was positioned upstream of F1 and D1 current meter moorings, with the intention that the measured water body would pass through them during the latter stages of 2L1 and the early part of 2L2.

Map 2L2: Following directly after the completion of 2L1, the dimensions of this second map were not increased over those of the first, in view of the need to terminate the experiment in time to recover F2. As expected the water mass passed through F1 and D1. During leg 2L2-3 it was necessary to alter course to avoid the mooring D1. The response of the Batfish deteriorated towards the end of this map. When the fish was recovered it was seen that the stabilizing rudder had been damaged. This was repaired and the hydraulic system was overhauled before the next survey.

2.3 The Third Lagrangian time series: 14 - 16 September

Map 3L1: This map was a repeat of 2L1, lying upstream of the F1 mooring. By making north-south legs creeping west against the current it was possible to avoid hazarding the Batfish close to F1. The

"Columbus Iselin" co-operated during this map by making a series of north-south legs about 1 n.mile (1.8 km) to the east of F1 using acoustic apparatus and, when clear of the mooring, making temperature profiles with XBTs with 1 km spacing.

Map 3L2: Using the same 1 n.mile (1.8 km) leg spacing as the previous map, but covering an area about 8 n.miles (15 km) square, this map was begun directly after the completion of 3L1. The "Columbus Iselin" continued to make relating measurements along an east-west line about 1 n.mile north of D1. During the period 3L2, the water body being passed through F1 and D1.

Map 3L3: Maintaining the same leg separation but increasing the length to 12 n.miles (22 km), map 3L3 was begun without pause. During 3L3 the current veered to south of east and decreased markedly in speed, so that the anticipated passage of the water mass centrally through E4 did not occur. (Nevertheless the edge of the surveyed water did just pass through it.) The "Columbus Iselin" made supporting measurements along a north-south line east of D1. "Quadra" made a series of Batfish tows to the north-east of E4 during lege 3L3-1 to 3L3-6, and then a sequence of frequent CTD profiles at E4 up to the end of leg 3L3-12.

The conductivity cell of the "Discovery" Batfish CTD became fouled during legs 3L3-3 and 3L3-7. The first impact went unnoticed and led to corrupted conductivity data being logged for the last part of leg 3L3-3 and for most of 3L3-4. The effect of the second impact was recognized and, because suitable action was taken to clear the cell, the resulting data loss covered only a few kilometres of 3L3-7.

Map 3L4: Starting directly after the completion of map 3L3, 3L4 was a combined operation for "Quadra", "Columbus Iselin" and "Discovery". The plan for "Discovery" involved a series of eight east-west legs with 2 n.miles (3.6 km) spacing, creeping south from a starting position 2 km north-east of E4. "Quadra" maintained position 1 n.mile north in time with "Discovery". "Quadra" and "Discovery" maintained a speed through the water of between 9 and 10 knots throughout the map.

The "Columbus Iselin", towing the Hydroglider at a maximum speed of 4 knots, covered the central part of the map area, starting the turn at the end of each leg in time with "Discovery" and "Quadra" (but reaching the start of each new leg later because of the reduced speed). Each of "Columbus Iselin's" legs was located midway between the track of "Discovery" and "Quadra", so that after the turn she took up a position ahead of and between the two fast ships which overhauled and passed either side of her. The tracks of the ships, relative to the water, are shown in figure 2.2. The time available for the Lagrangian Experiments expired at 2000 GMT, September 16, and the survey was terminated in leg 3L4-8.

The conductivity cell was again fouled in legs 3L4-5 and 3L4-7, leading to loss of data in these legs and also in leg 3L4-8.

3. INSTRUMENTATION

The description in this chapter of the instruments and procedure used to collect the CTD data is restricted to those directly related to the Batfish Lagrangian Experiments. A schematic representation of the Batfish system is shown in fig. 3.1. The meteorological instruments and measurements are discussed in the next chapter.

3.1 The Batfish

The Batfish (Dessureault, 1976) is a vehicle that can be towed at 10 knots while undulating under control from the towing ship, using a command signal based on the difference between the actual depth (derived from the CTD) and a prescribed analogue signal. The control signal operates a hydraulic ram that tilts the Batfish hydroplanes; hydraulic pressure is maintained by a screw turned by the flow past the fish.

The Batfish used in our experiments was built by Hermes, Ltd., Dartmouth, Nova Scotia, Canada, and modified at IOS Wormley, England, to carry a WHOI/Brown CTD probe. It was towed behind "Discovery" at 8 to 10 knots (4 to 5 m/s) on a faired cable 150 metres long (200 metres in some early legs). The control signal was a symmetric saw tooth. The Batfish undulated between a minimum depth of 10 m or shallower to about 60 or 70 metres. An example of the Batfish track is shown in fig. 3.2.

3.2 The CTD probe

The WHOI/Brown CTD probe is an instrument designed to measure conductivity, temperature and pressure in the ocean (Brown, 1974; Brown and Morrison, 1978). The instrumenent used during GATE was equipped with a miniature four-electrode conductivity cell, with an internal diameter of 2 mm and a length of 8 mm. Temperature was measured by a fast response thermistor and a platinum resistance thermometer, the outputs

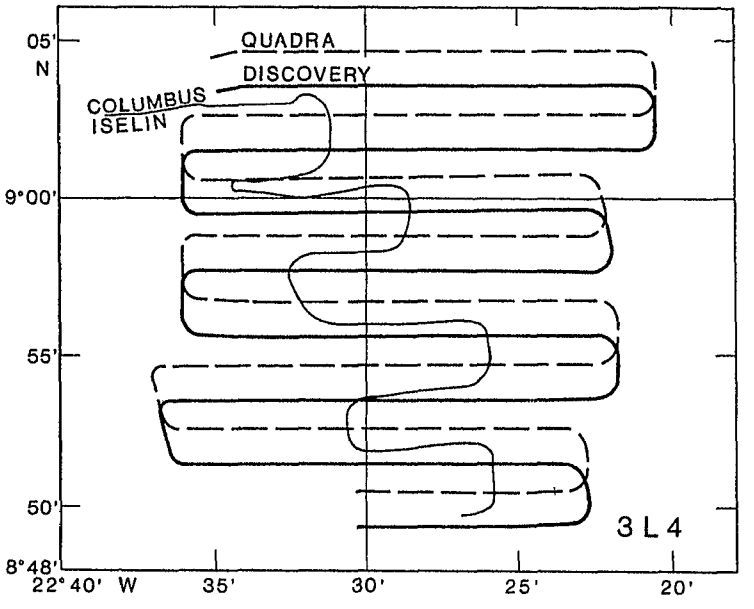

Figure 2.2 :

Tracks of "Discovery", "Quadra" and "Columbus Iselin" during the combined operation on 16th September 1974 forming Map 3L4.

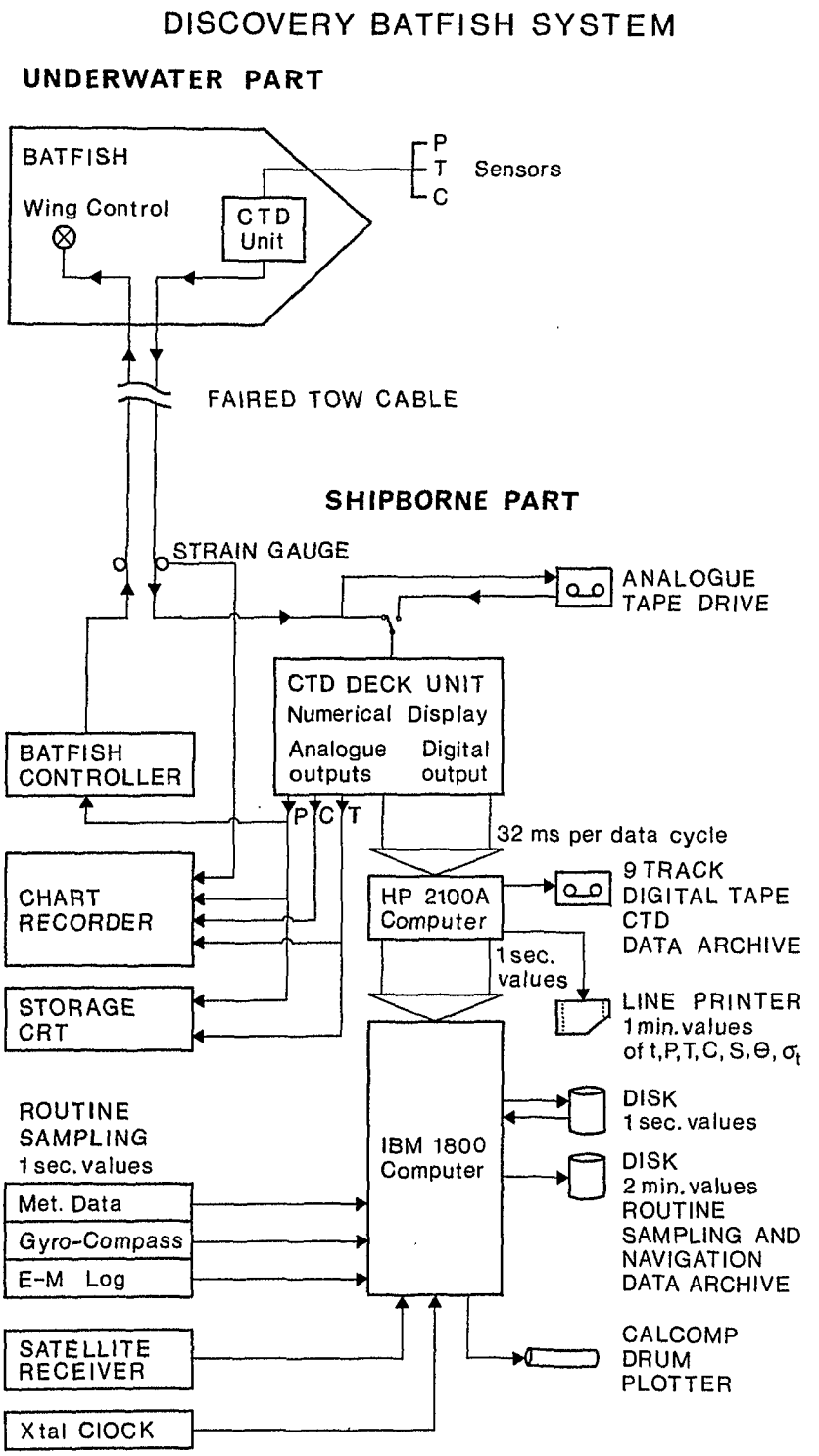

Figure 3.1 : Block diagram for the RRS Discovery Batfish System.

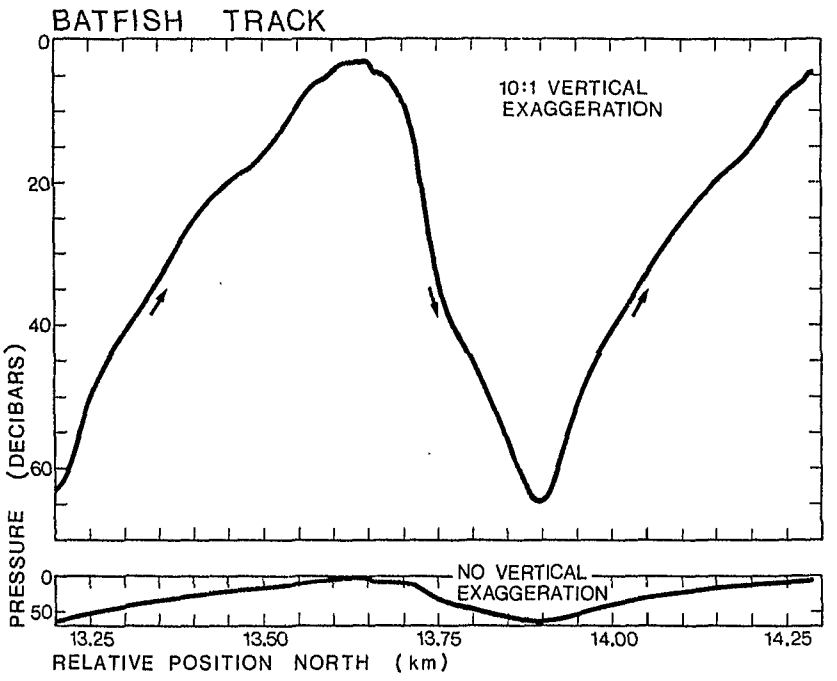

Figure 3.2 a) : Example of the Batfish Track as a function of depth and position, with and without vertical exaggeration.

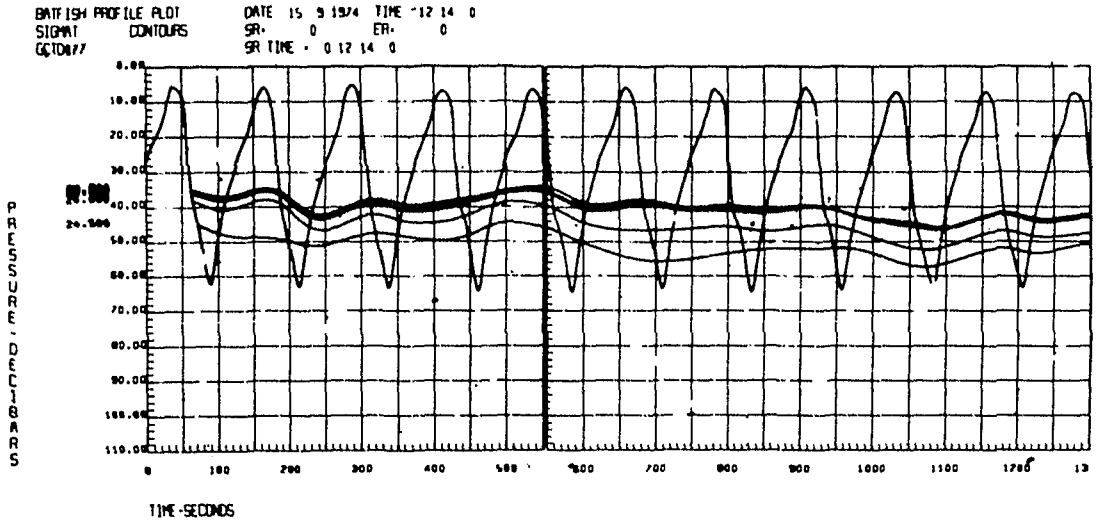

Figure 3.2 b) : Time series of the depth of the Batfish and of selected σ_t surfaces during Leg 3 of Map 3L3 on 15th September 1974.

of which were electronically combined in the underwater unit in an attempt to achieve a temperature signal with the stability of that from the platinum thermometer with the speed of response of the thermistor. The response time of the sensors is given by Brown to be less than 30 ms; they are scanned every 32 ms. The signals are digitized to 16 bit accuracy in the underwater unit and transmitted to the deck unit on board the ship through a conducting core in the towing cable. The digitizing interval of the electronic circuitry limits the sensitivity of the conductivity cell to 0.001 mS/cm, of the thermometer to 0.0005 K and the straingauge pressure sensor to 0.045 decibars. A more detailed account of the instrumental errors is given in chapter 6.

The thermometers and conductivity cell are mounted on a stalk. This protruded through a port in the fairing of the Batfish, exposing the sensors to water that had not been disturbed by the Batfish or by the towing cable.

3.3 Navigation

The absolute position of "Discovery" was obtained about every hour by satellite fixes. Intermediate positions were obtained by integrating the output of a two-component electromagnetic log (Tucker et al., 1970) on the hull. In calculating the intermediate positions it was assumed that the water moved at a constant velocity between each pair of satellite fixes, the vector current being calculated by comparing log and satellite displacements. The current velocities estimated in this way are presented in table I and fig. 3.3. They compare well with estimates of the near surface currents from moored current meters (Minnett, 1978).

The log was calibrated off Dakar on 27 August 1974 for straight runs; no attempt was made to correct for errors due to uneven flow under the hull during turns. Ignoring this uncertainty, the log measure the velocity of the ship relative to the water at hull depth. This

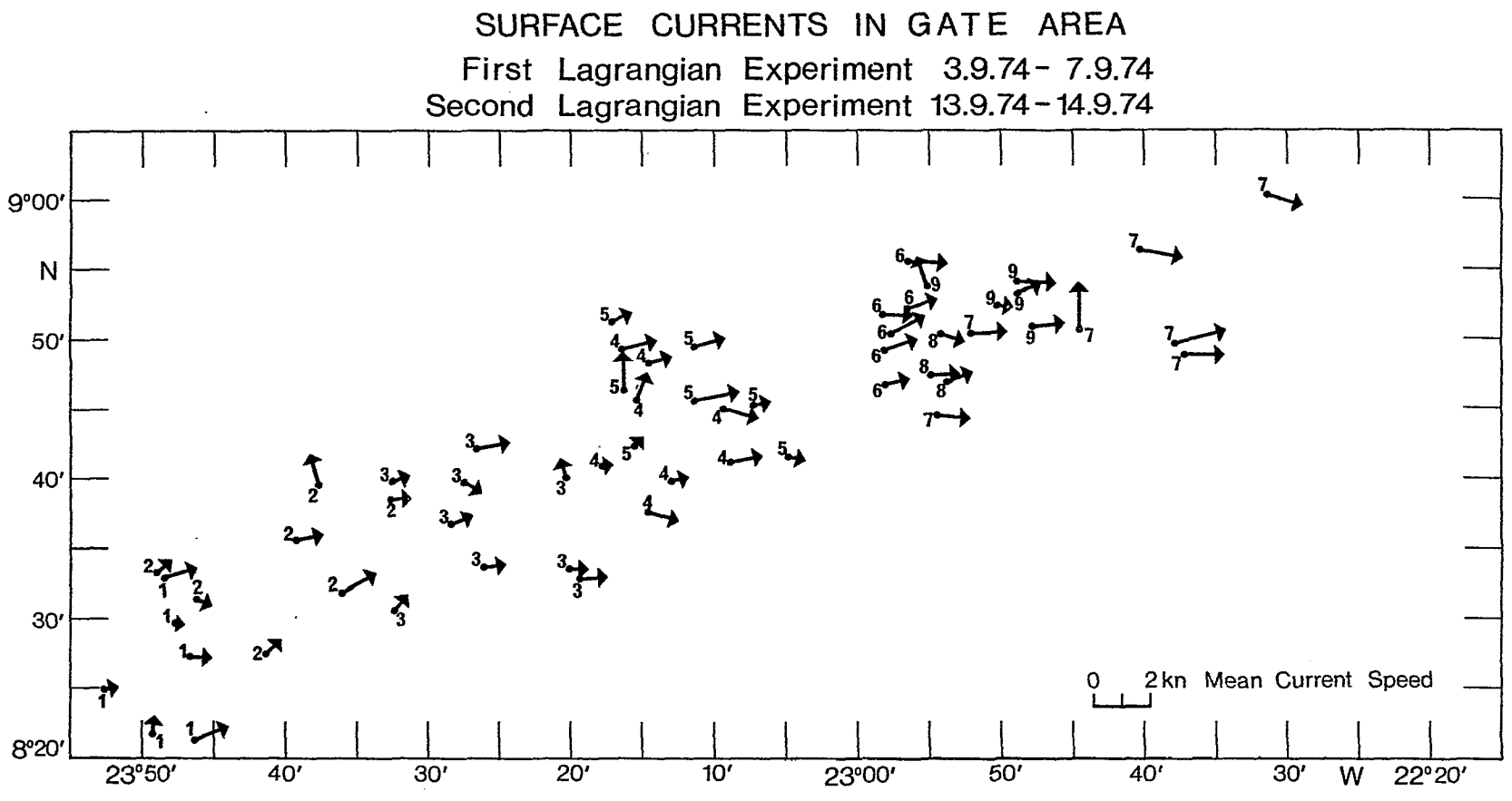

Legend

1 Experiment 1L1 3.9.74, 14^{27h} — 3.9.74, 22^{18h}
2 Experiment 1L2 4.9.74, 3^{24h} — 4.9.74, 13^{07h}
3 Experiment 1L3 4.9.74, 22^{09h} — 5.9.74, 10^{30h}
4 Experiment 1L4 5.9.74, 15^{35h} — 6.9.74, 5^{29h}
5 Experiment 1L5 6.9.74, 5^{40h} — 6.9.74, 14^{07h}
6 Experiment 1L6 6.9.74, 20^{31h} — 7.9.74, 7^{17h}
7 Experiment 1L7 7.9.74, 7^{24h} — 7.9.74, 23^{23h}
8 Experiment 2L1 13.9.74, 21^{45h} — 14.9.74, 3^{50h}
9 Experiment 2L2 14.9.74, 3^{54h} — 14.9.74, 9^{11h}

Fig. 3.3 a) :
The surface currents were calculated from the difference in the position of the ship obtained using a satellite fix and dead-reckoning from the ship's log signal integrated since the previous satellite fix.

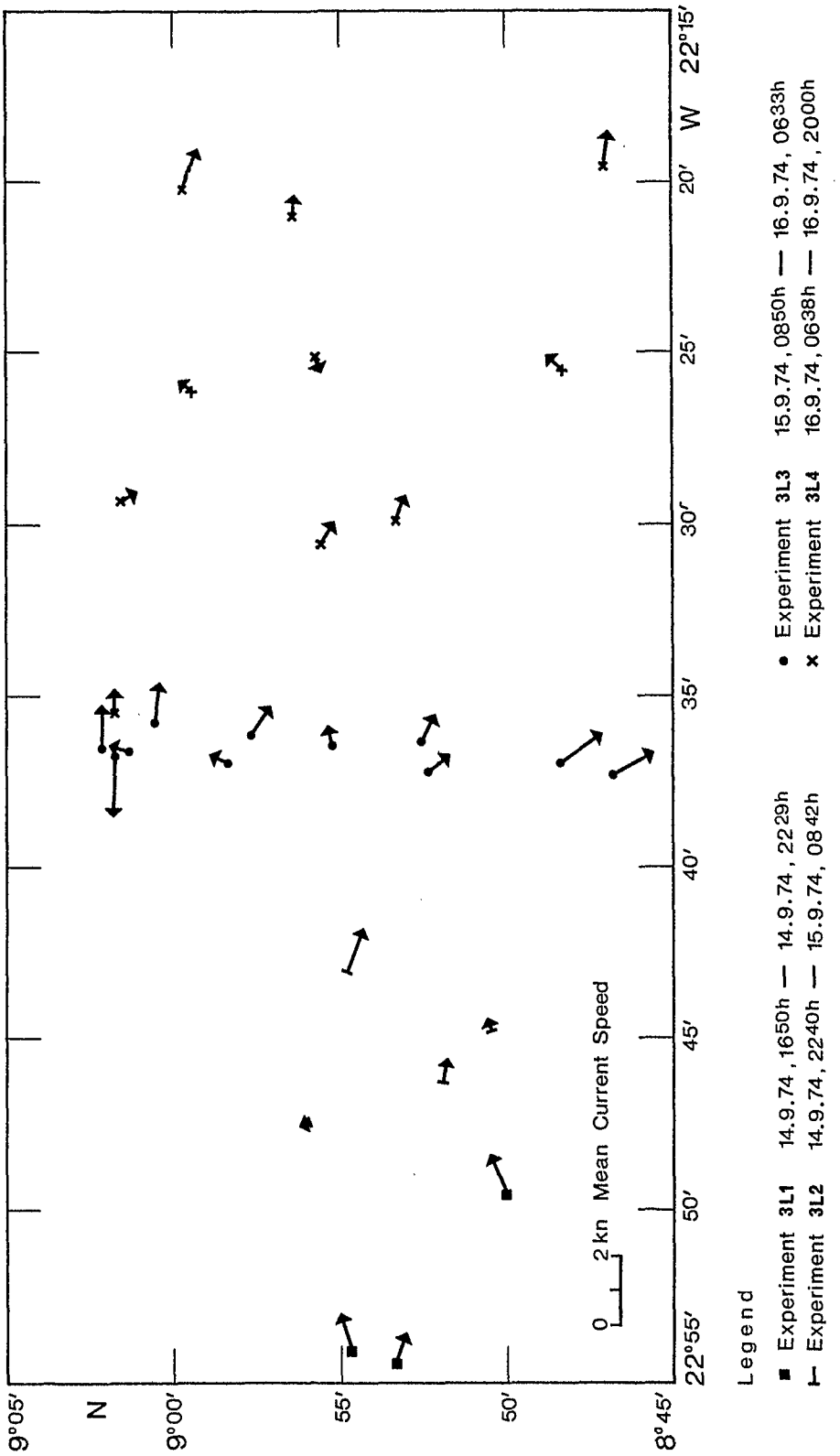

Fig. 3.3 b) :
The surface currents were calculated from the difference in the position of the ship obtained using a satellite fix and dead-reckoning from the ship's log signal integrated since the previous satellite fix.

provided the basis for the "relative positions" used in our Lagrangian surveys. The prescribed survey track was drawn on a Visual Display Unit connected to the ship's computer (which controlled the navigation). Relative positions of the ship were displayed on the VDU every two minutes. Instructions were given to the officer of the watch to alter course as required to keep the ship moving along the specific track. In this way it was possible to follow a survey pattern that was advected with the mean flow, assuming that the spatial variation of surface current on scales smaller than the survey pattern were negligible.

3.4 Data acquisition and real-time monitoring

The WHOI/Brown CTD underwater unit transmits data in real-time in serial form using "frequency shift key" modulation. As a consequence the raw data can be recorded on an audio tape deck, and can be re-played through the CTD deck unit. During GATE this option was kept available for periods when the normal digital data acquisition was interrupted by computer failure.

The CTD data signal is demodulated and decoded in the CTD deck unit, which also scales the measured variables into physical units for immediate display. These values are also made available on digital and analogue outputs. Along with the required Batfish waveform the Batfish controller and the output from a strain gauge measuring the towing cable tension, the analogue signals were monitored on a precision chart recorder. The most recent temperature profile was displayed on a storage oscilloscope as a function of pressure. The digital data were archived on nine-track magnetic tape by the HP 2100A computer. One minute spot values were recorded on a line printer together with calculated values of potential temperature, salinity and density (sigma-t).

The ship's computer (IBM) monitored the meteorological instruments, the gyrocompass and electromagnetic log, once per second on a routine

basis. After low-pass filtering to give values every two minutes these data were archived on disk.

At intervals of one second the ship's computer received a CTD data cycle from the HP 2100A computer. These data were augmented with calculated salinity and density and assigned a time and position (as calculated by integration of the signals from log and compass) before being stored on disk. It was from these data that quick-look plots were drawn to enable further quality control and preliminary scientific assessment.

At the end of each leg it was possible to plot sections along the leg showing the depth of chosen isopleths of temperature, density or salinity with a line representing the path of the Batfish through the water (fig. 3.2 b). Vertical sections cutting through several legs could also be drawn at the end of each map. Further, values of temperature, salinity or density could be plotted as horizontal sections at a specified constant depth, for each completed map. These fields could then be contoured by hand.

It was planned to conduct a preliminary analysis of the data with these plots and, if necessary, alter the course of the investigation to achieve an optimal survey pattern about a chosen thermohaline structure. In practice, the effect of corrupted data caused by cell-fouling and heat-flow problems in the sensors in the large temperature gradients of the thermocline (see section 6.1), was so great as to mask the sought-after signals. Furthermore, as the computer was over-burdened in producing these plots in addition to its routine load, the plots were rarely available in time for tactical adjustment to the survey pattern.

4. METEOROLOGICAL MEASUREMENTS

Routine meteorological measurements were made throughout GATE using the automatic sampling, averaging and computer logging system on RRS "Discovery". The instruments are described in this chapter. The time series of two-minute average values for Phase III of GATE are presented, with a brief description of the meteorological conditions during the Lagrangian Batfish experiments.

4.1 Meteorological instrumentation

The meteorological instruments are mounted at various positions on the ship, aimed at providing optimum measurements. The solarimeter is mounted above the roof of the wheel-house, at a height of 14.6 m above the waterline, where it is least likely to fall in shadow. A set of wet and dry thermometers is mounted each side of the wheel-house, at 14.0 m, so that at least one set is not in direct sunlight. The thermometers and solarimeters are cleaned and serviced daily, during which time the measurements are, of course, not reliable. Wind velocity is measured by an anemometer and vane mounted at 19.8 m on the foremast. An aneroid barometer, located in the gravimeter room at a nominal height of 2.6 m above the waterline, completes the meteorological instrumentation.

4.2 Data acquisition

Signals from all meteorological instruments are recorded once per second as part of the routine sampling procedure of the ship's computer. The scalar meteorological variables are low-pass filtered to give two-minute values which are archived. Both port and starboard wet and dry thermometer signals are archived, and, since the effect of direct heating is discernable during periods of high insolation, it is prudent to use the thermometer set which gives the lower air temperature.

The one-second measurements of the ship's heading, from the gyrocompass, are used to resolve the measured wind speed and direction into north and east components which are filtered and stored, also at intervals of two minutes, as components of the "relative wind". In the routine navigation procedure, the velocity of the ship through the water is also resolved into north and east components. These values are added to the components of relative wind to give wind over the water, which is archived as a speed and a direction. During the course correction by "satellite updating" (see section 3.3), the values of the wind speed and direction are also corrected using the improved course and direction of the ship. When the measured wind speed is less than one knot, the wind direction, and therefore the components of relative wind, become unreliable quantities because of measurement difficulties at the threshold of instrumental response.

4.3 Meteorological data from GATE Phase III

In this section the meteorological measurements made on RRS "Discovery" during Phase III of GATE are presented as time series plots (fig. 4.1). They cover the entire period of the Lagrangian Batfish surveys, the times occupied by the individual maps being shown in the plot. The data were collected as the ship navigated the survey patterns (fig. 2.1), or made other manoeuvres in between, and have been processed as described in the previous section to give the two-minute samples which appear in the figure. To avoid the effect of direct solar heating on the thermometer, the lower value of the port and starboard air temperatures (and corresponding wet bulb depression) has been used. Gaps in the data are due to computer down-time or routine servicing of the instruments. Diagrams, with an expanded time scale, showing the meteorological data relevant to each Lagrangian Map are presented in the corresponding comparison volumes of the Data Report (Woods, Leach and Minnett, 1981). Rainfall was not measured automatically, but a raingauge was examined twice per day. The measured rainfall is shown in table II (after Institute of Oceanographic Sciences, 1975).

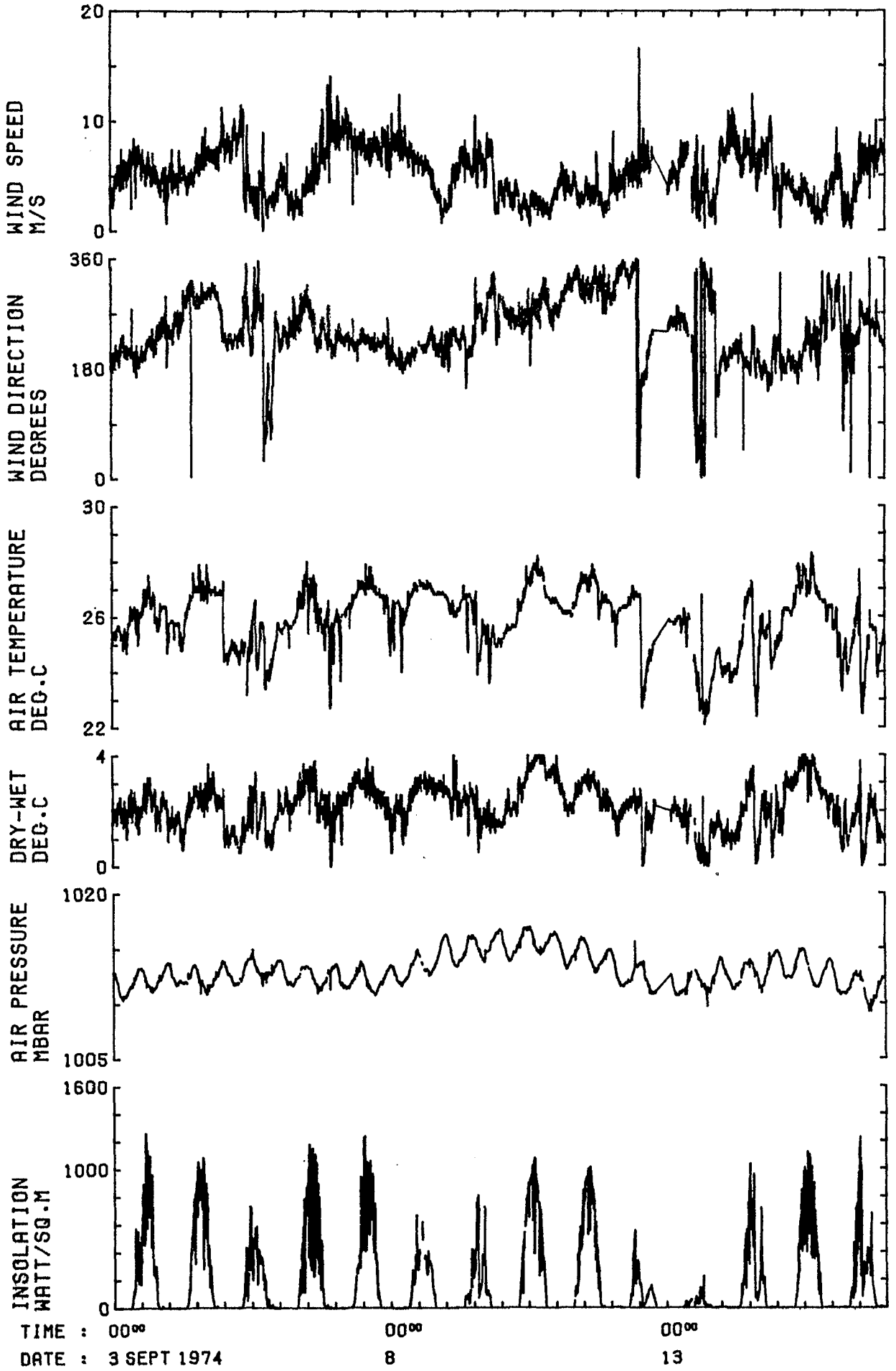

Fig. 4.1 :
The meteorological data were collected by the standard meteorological instrumentation on board the RRS "Discovery".

Table II: Rainfall Data

Date 1974	Time Read	Amount (mm)	Comments
01.09.	2000	0.0	
02.09.	0900	0.0	
"	1300	0.3	Between 1200 and 1250
"	1900	29.0	" 1700 and 1900
03.09.	0050	1.7	
"	0900	0.0	
"	2000	0.0	Short sharp showers during day
04.09.	0830	1.7	
"	2000	0.0	Light showers during day
05.09.	0800	6.3	Between 0600 and 0700
"	1700	2.1	1.2 mm by 1013
06.09.	0800	0.8	
"	2100	0.0	
07.09.	0830	2.7	
"	2000	0.0	
08.09.	0800	3.5	
"	2000	0.0	
09.09.	1940	0.8	1400 rain
10.09.	0800	0.0	
"	2000	0.0	
11.09.	0800	0.0	
"	2000	0.0	
12.09.	0800	0.8	
"	1945	6.7	Between 1325 and 1400
13.09.	0800	0.0	
"	1610	17.7	4.4 mm in storm 0805 rain most
"	1900	33.7+	of day from 1230
14.09.	0800	0.2	
"	1645	9.2	1420 to 1645
15.09.	0900	4.9	
"	2000	0.0	
16.09.	0800	5.5	
"	1530	5.5	Heavy 1320
"	2000	0.0	
17.09.	0800	0.8	
		151.9	Total rainfall in 17 days

As can be seen from fig. 4.1, the winds experienced during the Lagrangian Experiments were mostly slight, very rarely reaching 10 m/s and less than 5 m/s for a considerable part of the time. At the start of the first Lagrangian Experiment, occasional whitecapping was observed, and rainfall was restricted to short showers. Similar conditions prevailed during the following day, but on September 5, the sky was overcast and several squalls were experienced, with many more observed on the horizon. The next day was sunny with small cumulus clouds (ca. 2/10), with a calm sea and slight swell. Slicks were observed on the sea surface during the late morning (10:55 GMT). The sky was again overcast on September 8 and 9, but with little or no rain; occasional whitecapping was seen. Two very sunny, calm days followed, with practically no sea surface waves and only a slight swell. In the early afternoon of September 12 a very severe squall was experienced. This can be seen in the meteorological records as a sudden change in wind direction and drop in insolation. The torrential rain was accompanied by a fall in air temperature of more than 5 K. Rain fell for most of the following day, and also during the next afternoon, on September 14, when the wind also strengthened and whitecaps were observed. During the two days of the third Lagrangian Experiment, high insolation was recorded and the wind weakened to less than 2 m/s in the afternoon of September 15, becoming a little stronger during the night and following afternoon. The sea was slight with no whitecapping noted.

More complete descriptions of the weather in the whole GATE area are to be found in the GARP reports (ICSU/WMO, 1975a, b).

5. DATA PROCESSING

The data set brought back from the RRS "Discovery" cruise contained the raw time series of CTD samples every 32 ms on computer compatible tapes and "Discovery" two-minute navigation and meteorological data on disks. The data processing scheme summarized in fig. 5.1 was designed to combine these two data sources, into a standard data cycle format, to add new, derived variables in each data cycle, to apply corrections for instrument lags, to edit bad data and to create new files with reduced versions of the data set suitable for scientific analsyis. The total data set comprised $6 \cdot 10^6$ data cycles of eleven variables. The standard products illustrated in this report were derived from a re-organized data set of ca. $5 \cdot 10^5$ data cycles.

5.1 First Processing

In the first processing stage the raw measurements of pressure, temperature and conductivity were converted to physical units and the time correction applied to the temperature. Then the data cycles were averaged together in threes to give an interval of 96 ms. Subsequently the derived variables salinity, density (σ_t), potential temperature and sound speed were calculated. Apart from the speed of sound which was calculated according to Wilson's (1960) formula, these variables were computed using IOS (Institute of Oceanographic Sciences) software derived by Crease and Sankey (1974). Finally the "Discovery" two-minute navigation data were used to calculate the ship's position in kilometres east and north of the GATE origin (24°W, 8°N).

5.2 Second Processing

In the second processing stage the "Discovery" two-minute data were used to calculate the ship's position relative to the water at the start of each survey ("Map"). This was achieved by integrating the fore-aft and port-starboard speeds of the ship as measured by an

DATA PROCESSING FLOW DIAGRAM

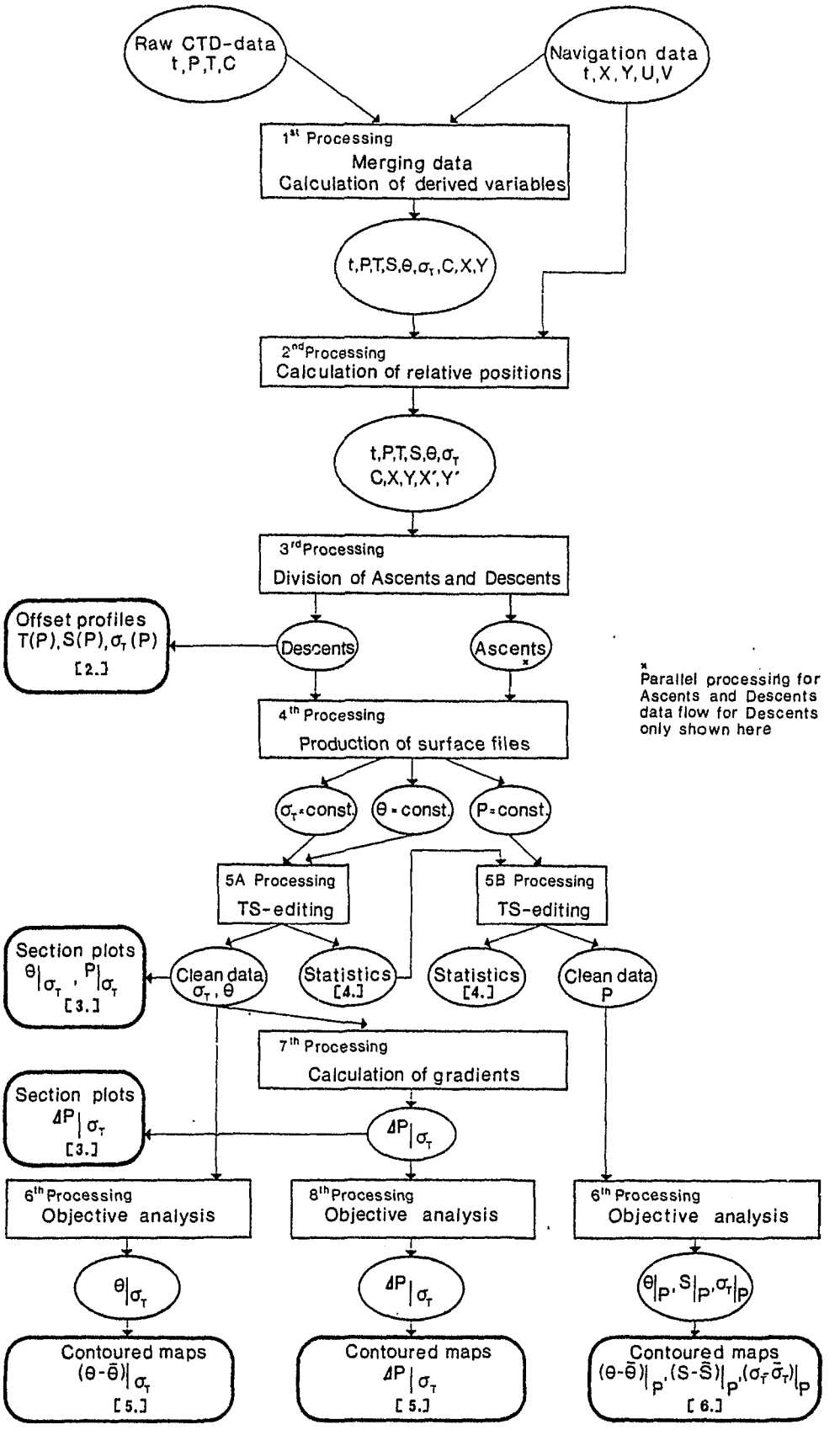

Figure 5.1 : Flow diagram of the processing of the data from the GATE Lagrangian Batfish Experiment.

electromagnetic log together with the ship's heading as recorded from the gyrocompass. Each data cycle of the data from the first processing stage was thus extended by two variables, the relative position north and the relative position east.

5.3 Third Processing

The third processing stage separated the data into two parts, collected while the Batfish was descending or ascending repsectively. During the first part the Batfish was passing from warmer to cooler water, so that thermal lag on the sensors (in partcicular the thermometer and pressure sensor) was positive, and in the second part, vice versa. The lag in the thermometer was corrected to first order with the result that for most of the isopycnal products there is no significant difference between those obtained from the descending or ascending part of the data set (see fig. 5.2). No scheme was found which made a consistent correction for the thermal lag in the pressure sensor, with the result that isopycnals are recorded as lying several metres deeper in the ascending part than in the descending part of the data set. This presents a serious problem in the products based on pressure (rather than density) coordinates.

5.4 Fourth Processing

In the fourth stage of processing the data set was interpolated onto standard surfaces of pressure, density and potential temperature. Up till this stage the data had retained the original time-series form in which it was collected. The interpolation was achieved by scanning the data and testing to see if a standard surface passed between each pair of data points (cycles). If this was the case, then a new data cycle on the standard surface was produced from the two adjacent time-series data cycles by linear interpolation. The data produced by this processing were ordered by surface with the data points within each surface ordered by time.

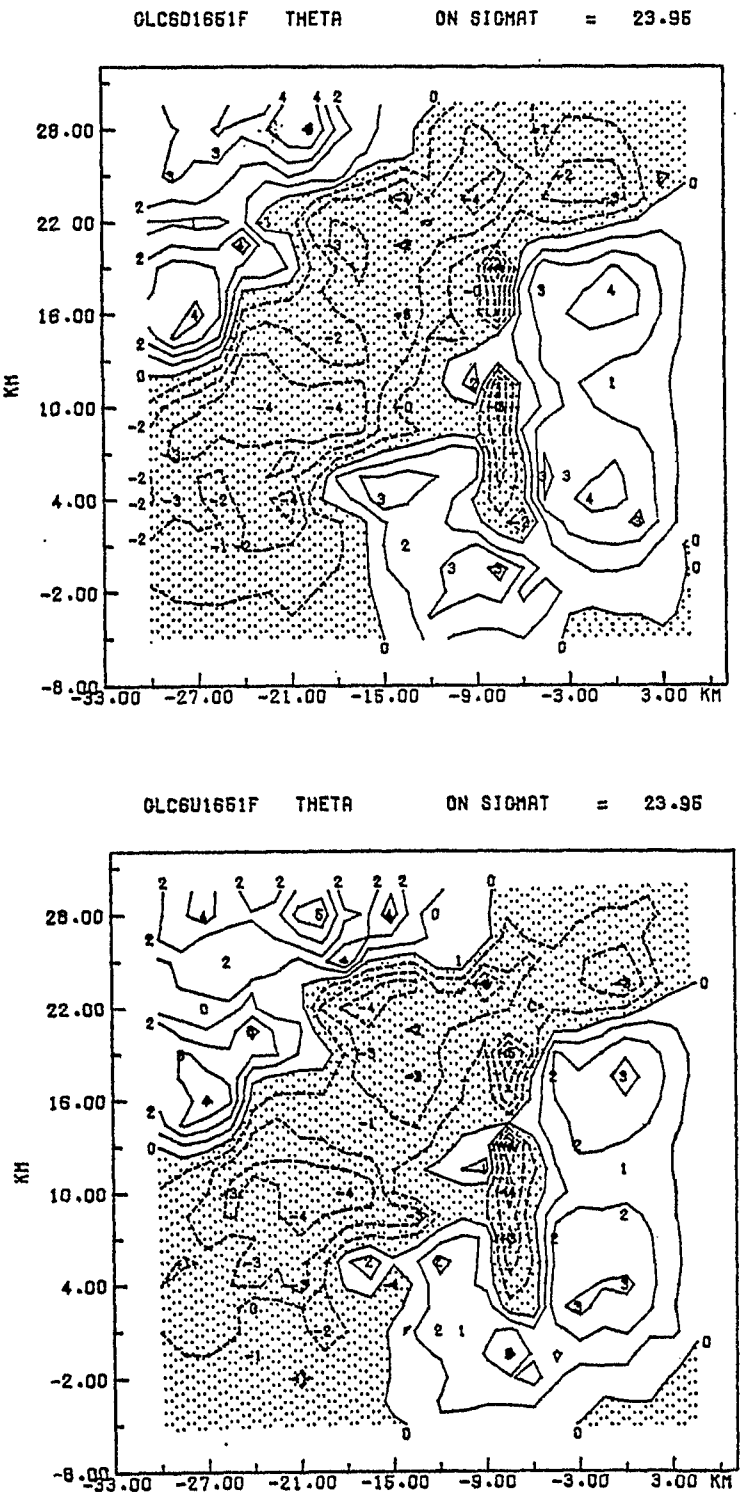

Figure 5.2 :

Two maps of potential temperature on the density surface σ_t = 23.95 kg m^{-3} produced independantly from data from Batfish "down-dips" and Batfish "up-dips" respectively. Despite time-lag problems the pictures show considerable similarity.

5.5 Fifth Processing

The fifth stage of the data processing scheme consisted of removing corrupted data cycles using a criterion based on a statistical T-S relationship for each map. A simpler method had been tried before the data had been interpolated on to the standard surfaces, but had been found inadequate in discriminating between good and bad data (Minnett, 1978).

The major cause of irretrievably corrupt data collected by the WHOI/Brown CTD probe during GATE was fouling of the conductivity cell. Impact with the contaminant was characterized by a sudden shift to lower conductivity (and consequently lower derived salinity and, to a lesser extent, derived density). While the sensor was fouled the output contained fluctuations, which appear similar to those in the desired signal, superimposed on an offset from the environment level (fig. 5.3), but it is impossible to recover the signal as one cannot be sure that the fluctuating part was entirely environmental in origin.

The other source of corrupt data was the residual salinity spikes which were caused by the imprecise matching of thermometer and conductivity cell time constants. The spikes appear when the temperature gradient underwent a rapid change.

As the signal cannot be recovered from these corrupted data, the erroneous data cycles must be removed prior to scientific analysis. This was achieved by making use of the narrow range of the T-S relationship expected on a given isopycnal. The density of seawater, expressed as σ_t, is a function of salinity and temperature; erroneous values of salinity caused by conductitivy cell fouling or salinity spiking produce temperature values on isopycnals that are different from those given by uncontaminated data. Thus corrupted data can be identified and removed from those on isopycnals by determining rejection limits on salinity or temperature. Equally, corrupted data can be identified on potential isothermal surfaces by examination of

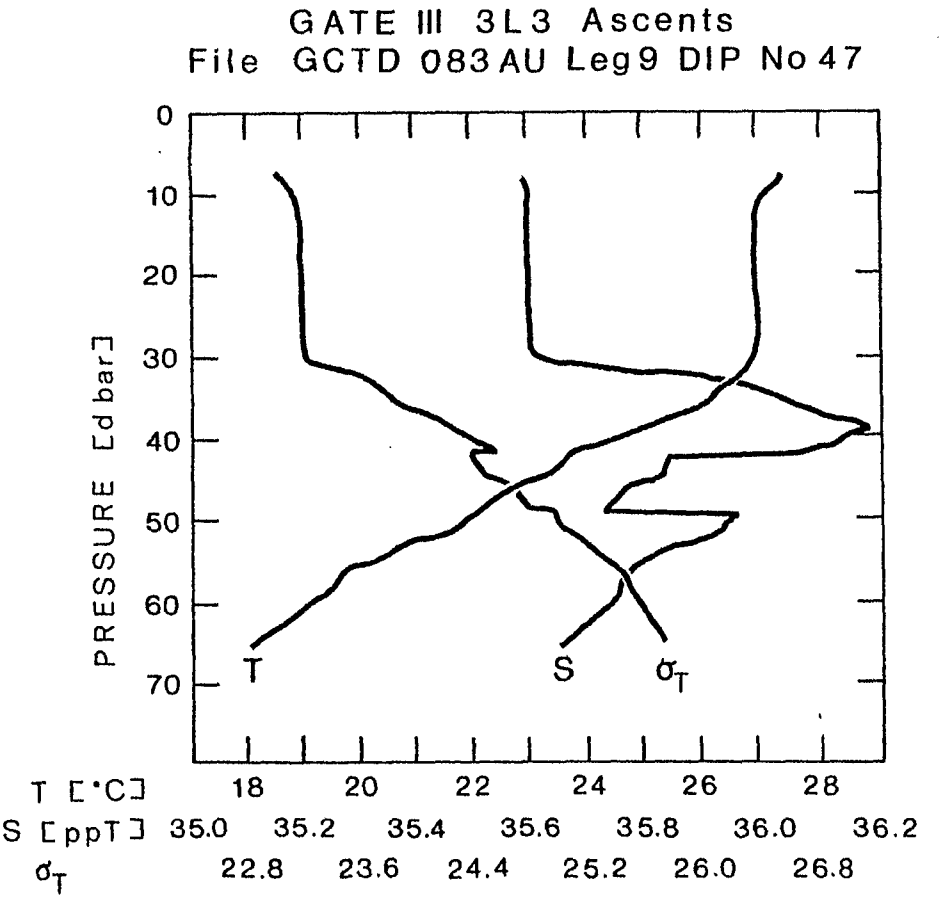

Figure 5.3 :

Temperature, salinity and density profiles for Dip 3L3-9-47U. The contamination seen in the salinity and density signal between 42 and 49 decibars is thought to be caused by temporary fouling of the conductivity cell. The temperature signal appears to be unaffected.

the salinity or density signal. In practice potential temperature on isopycnals and salinity on potential isotherms were used. The data were edited surface by surface, map by map.

An example of the potential temperature signal on isopycnals is shown in fig. 5.4; the conductivity cell appears to have been badly contaminated at about 1300 GMT and again at about 2200 GMT. Numerous other smaller collisions reveal themselves as vertically coherent excursions to lower values. The errors in salinity, which appear as horizontal spikes in profiles, are isolated vertical spikes in this representation. Comparison between the mean levels of the signals before and after fouling events show that the conductivity cell calibration does not appear to have been permanently affected, although in the worst cases the recovery time was several hours.

The editing procedure consisted of two parts. Firstly, changes of more than a specified amount between successive values on the isopleths were identified. These are the result of salinity spikes or of the impact with suspended matter. In some of the fouling events and in most cases of salinity spikes the next value on the isopleth was found to be uncontaminated and the corrupt point was easily removed. When the conductivity cell fouling had persisted over several profiles, data values from the first erroneous one to that one which lay within one standard deviation of the mean were rejected. The statistics used here had been calculated for values of the variable being scanned on each isopleth in that map. In practice 0.1 Kelvin degrees for potential temperature on isopycnal surfaces and 0.1 ppt for salinity on potential isothermal surfaces were found suitable threshold values for this process. This intermediate set of "clipped" data was purged of the most erroneous values but retained some undesirable features from the recovery periods after bad fouling events.

To remove the data points which could still be classed as erroneous the "clipped" data were subjected to the second part of the editing process. Statistics of these data were found on each isopleth for each map, and those data points lying beyond a given number of standard

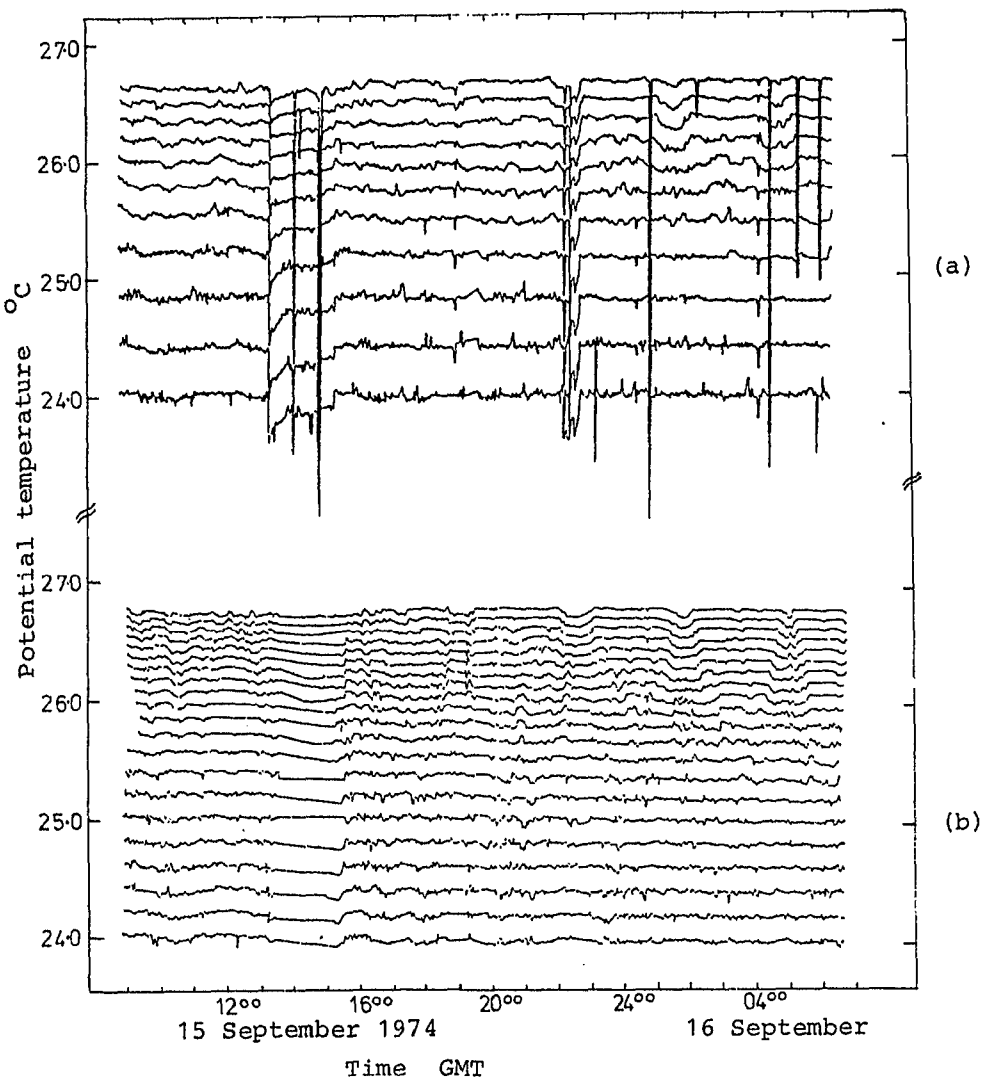

Fig. 5.4 :

Potential temperature on the isopycnals σ_t = 24.55 to σ_t = 25.75 as raw data (a) and after editing (b). The raw data are shown for values every 0.1 in σ_t and the edited data every 0.05.

deviations from the mean were rejected. After several trial runs it was decided that the acceptance window had to be as narrow as two standard deviations centred on the mean (i.e. ± 1 standard deviation) to ensure that all obviously corrupt data had been removed. In having so stringent a criterion one inevitably runs the risk of removing data that should be classed as signal, but it was thought better to endeavour to remove all corrupted data and risk rejecting some signal than to leave erroneous values in the data set which might be misinterpreted during subsequent scientific analysis. This procedure constituted the 5A processing stage and was applied to the data on density and potential temperature surfaces.

The editing of data on pressure surfaces was more problematical as internal waves moved large vertical gradients through the isobaric surfaces and so produced signal comparable to the effect which had to be eliminated. Again, use was made of the relatively narrow range of salinities and temperatures found on a given isopycnic surface. Salinity values on the isobaric surface were scanned and compared with rejection limits determined from the statistics of the edited salinity signal on the isopycnic surface for data from that map. The expected salinity value was found by linear interpolation between the mean salinities on the isothermal surface either side of the temperature value in the data cycle being considered. The larger of the standard deviations for salinity of the two adjacent isothermal surfaces was used to give the rejection limits centred on the expected salinity value. Editing the pressure surface data formed the 5B processing stage.

In general between 75 % and 85 % of all data in the surface files were accepted as being good, within the limits of accuracy discussed in chapter 6.

5.6 Sixth Processing

In the sixth processing stage the irregularly spaced data on standard surfaces were objectively analyzed onto a regular x - y (east-north) grid. The eight processing was identical to the sixth, the only difference being that the input data was the product of the seventh processing; namely pressure difference on density surfaces.

The objective analysis was accomplished by first computing the two-dimensional auto-correlation function of the data to be analyzed. This raw auto-correlation function was smoothed, multiplied by a conical taper and had negative values set to zero. This was done because the irregular spacing of the input data leads to an irregular auto-correlation function. The taper was used so that the modified auto-correlation function would reach a value of zero within a finite number of lags. The modified auto-correlation function was then used as a weighting function to determine the influence of each measured data point at each of the grid points to be interpolated. The weighting function was calculated separately for each surface to be objectively analyzed to avoid influencing the results with statistics with other characteristics to those of the surface in question.

5.7. Seventh Processing

The pressure signal on isopycnals is dominated by large, vertically coherent displacements (fig. 5.5). The residual signal can be revealed by generating a relative pressure, or thickness, by referring the pressure signal on an isopycnal to that on a chosen reference isopycnal (fig. 5.6). The seventh processing stage was applied to data after editing stage. It consisted of generating a new variable, being the pressure interval between alternate pairs of isopycnals, as measured along the Batfish track, which was assigned to the data points lying on the intermediate isopycnal.

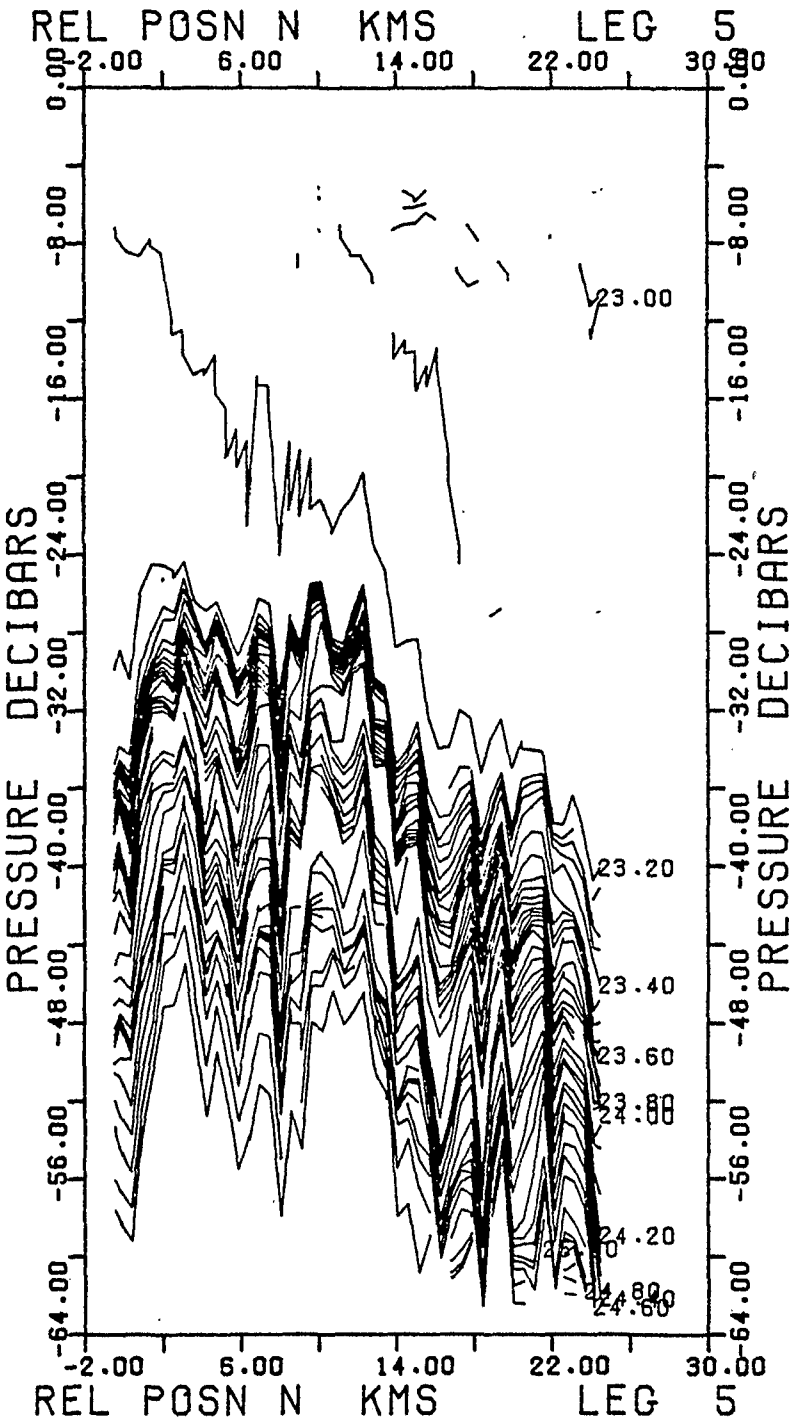

Fig. 5.5 :

Pressure on isopycnals in the range of σ_t = 23.00 - 25.00 kg m^{-3}.
Contour interval 0.05 kg m^{-3}.

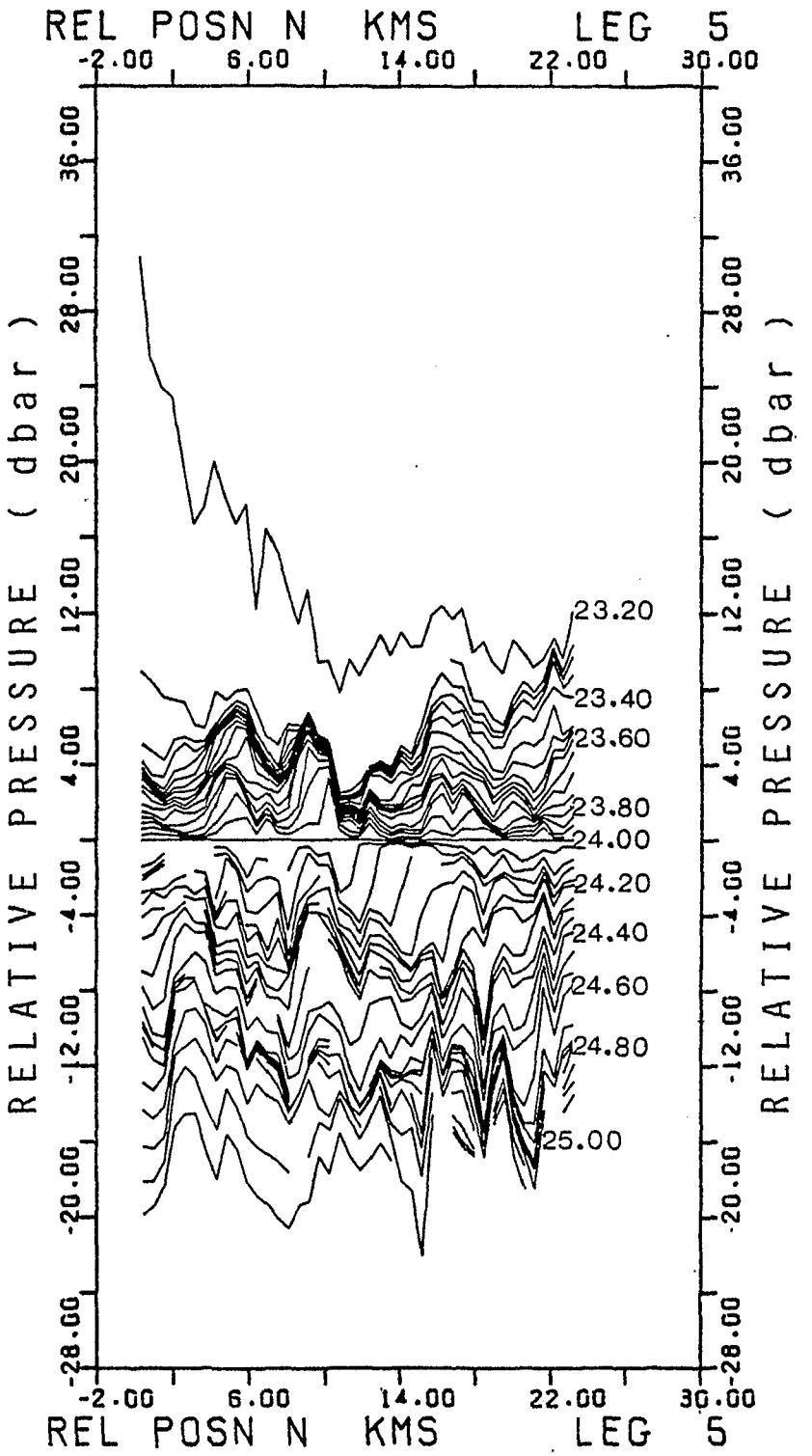

Fig. 5.6 :

Pressure, relative to the pressure on σ_t = 24.00 kg m^{-3}, on surfaces of constant σ_t in the range σ_t = 23.20 - 25.00 kg m^{-3}.

6. ASSESSMENT OF UNCERTAINTIES

The uncertainties associated with the variables shown in chapter 7 and in the Data Report (Woods, Leach and Minnett, 1981) are discussed in this chapter. An assessment of the inaccuracies in the data measured by the WHOI/Brown CTD is made, and the effect of these on derived variables is considered. Estimates of inaccuracy derived from static calibration are inappropriate as the instrument error in our measurements is dominated by non-equilibrium effects due to rapid passage through a spatially inhomogeneous environment. The nature and size of these uncertainties can be deduced from close examination of the data themselves. As the data have been separated into two subsets from ascending and descending profiles (chapter 5) to reduce the effects of systematic but incorrectable errors, the estimates of "relative accuracy" apply only to data within each subset. The signal-to-noise level in some variables especially those specified on isopleths, is not as good as might be hoped. However the critical test for features which appear in a noisy data set is to compare the two subsets. Features appearing in both are presumed, with a fair degree of certainty, to be environmental signals (see fig. 5.2).

A discussion of the uncertainties in the relative navigation is also presented in this chapter.

6.1 Measurement errors

All measurements of physical quantities are subject to inaccuracies resulting from the shortcomings of the measuring system. In the CTD, random errors arise from the electronic's noise and the finite digitizing interval. Systematic errors have been caused by the response time of the sensors to rapidly changing fields and the dependency of the output of the sensor on a variable other than the one it measured.

The WHOI/Brown CTD is equipped with a 16-bit digitizer (Brown, 1974, Brown and Morrison, 1978) which gives a digitizing interval of

0.0005 K in the temperature signal, 0.045 decibars in the pressure signal and 0.001 mS/cm in the conductivity signal. The electronic's noise is stated to be smaller than the digitizing interval, and Brown claims to have achieved temperature stability over six months of ± 0.003 K. The accuracy of the computed salinity is given a ± 0.0024 ppt when compared with water bottle samples taken in the range of 0 to 4500 m (Fofonoff, Hayes and Millard, 1974).

Equilibrium laboratory calibration and comparison with water bottle samples taken during the cruise were used to give linear correction terms to the temperature and conductivity signals. After this correction it was presumed that the measurements complied with the manufacturers' specification. However, the most important source of inaccuracies in the Batfish CTD data is thought to be heat flow in the sensors. The water temperature changed through some 9 K in the part of the thermocline which was investigated and this change occured in about 30 seconds. Consequently the sensors were not in thermal equilibrium with the fluid so the output of the thermometer does not give a precise measurement of the water temperature. The output from the pressure sensor is also temperature dependent. We have no indication whether the conductivity cell is sensitive to this rapid temperature change, but as the electrodes are mounted on a small ceramic stalk with small thermal capacity and heat conductance, it has been assumed in the subsequent error analysis that the output from the conductivity cell is uncontaminated by this problem. Such temperature dependent errors would be classified as systematic, but as they reflect the variability in the environmental temperature field they are very difficult to separate from the desired signal.

6.1.1 Measurement errors from the pressure sensor

The output of the strain-gauge pressure sensor is dependent on the temperature of the sensor; the manufacturer's specification gives a temperature coefficient of about 0.3 decibar/K. In the WHOI/Brown CTD the pressure sensor is mounted in the aluminum end plate of the

presssure vessel, which has a thermal capacity much larger than the sensor itself and with which the sensor is in good thermal contact. Consequently, the temperature of the pressure sensor is difficult to estimate and a correction employing a reduced amplitude, phase shifted heat wave failed to produce a consistent decrease in the difference between the mean isopycnal pressure encountered on ascending and descending profiles. This discrepancy is shown in fig. 6.1 for Map 3L3. It was decided to divide the GATE Batfish CTD data into two sets derived separately from the ascending and the descending parts of each Batfish cycle (see chapter 5).

The errors in the pressure signal in the two subsets can be estimated from the difference between mean isopycnic pressures, which arise from the different temperature histories of the pressure sensor up to the point where it encounters a given density on ascending or descending profiles. As the temperature history at these points will have much smaller variation when one considers the ascending or descending profiles separately, and to the relative error in pressure differences between close points on the same profile or similar points on different profiles will be much less, say 10 %, of the systematic error. While the absolute error in the pressure signal remains of the same order as the mean isopycnal pressure discrepancy between ascending and descending profiles, say ± 1 decibar at worst, the relative error in pressure along isopleths in either of the subsets of data is put at ± 0.1 decibar.

The effect of the dynamic pressure, caused by the passage of the Batfish through the water, is thought to be negligible. For the experiment considered here the pressure sensor was screened from the flow of water by the end plate in the nose of the Batfish. Had the pressure sensor been unprotected from the flow a dynamic pressure equivalent to a depth of water of less than 0.5 m would have been experienced. This would have resulted in a constant offset to the pressure signal.

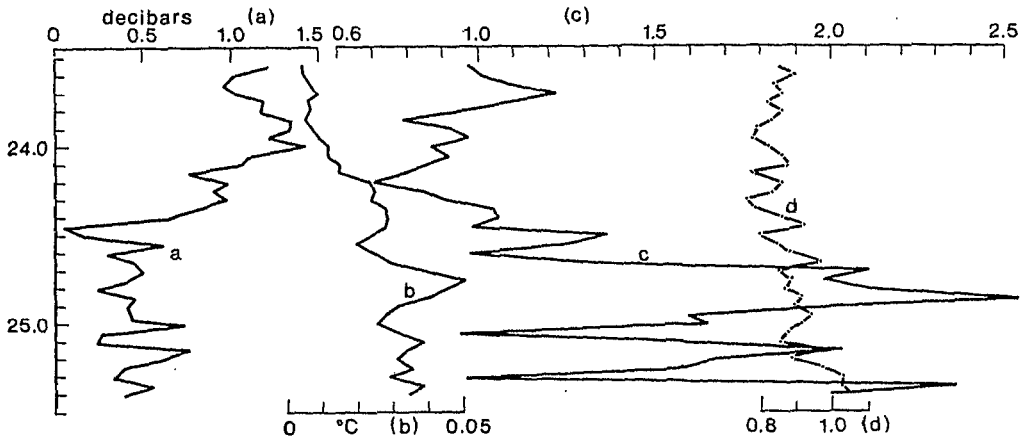

Figure 6.1 : The difference in the up- and down-going data can be seen in statistics of pressure and potential density on σ_t surfaces: (a) $P_u - P_d$; (b) $\theta_u - \theta_d$; (c) variance (θ_u) : variance (θ_d); (d) Variance (P_u) : variance (P_d).

6.1.2 Measurement errors in conductivity

There is no evidence in our data set that the output of the conductivity cell is affected by temperature changes. It is possible that such a dependency exists and contributes to the residual errors in the derived variables.

The main source of error in the conductivity signal is fouling of the cell by material in the water. Judging from remains of jelly-like matter, frequently found adhering to the Batfish on recovery of the vehicle, it is quite possible that the conductivity cell fouling was often caused by collision with jellyfish or similar creatures. Such incidents have produced a characteristic signature in the derived salinity which moves very rapidly to lower values. Sometimes the signal returned to normal values very slowly, as though the contaminant were being gradually washed away, while on other occasion the recovery from fouled data happened as quickly as did the onset, see, for instance, fig. 5.3. In the former cases it is often impossible to tell, by examination of the plots of salinity along the Batfish track, when the fouling has entirely cleared.

Only rarely was the conductivity cell fouling recognized at the time of the event and if it was seen to persist for more than a few minutes the cell was flushed out by reducing the speed of the ship causing the Batfish to stall, thus producing a reverse flow of water through the cell. The majority of such collisions went unnoticed at the time and as there is no certain way of recovering the data from the signal during the times when the cell was fouled, they were removed after identification at the editing stage, leaving a number of gaps in the data (see chapter 5).

Except where the cell has been fouled it has been assumed that error in the conductivity signal is negligible with that due to temperature in calculating salinity and density values.

6.1.3 Measurement errors in temperature

From examination of the raw data it was clear that the measurement errors in temperature were greater than the 1 - 2 mK accuracy to be expected from the static calibration, and a simple heat flow correction was applied to the temperature signal at stage 1 of the processing (chapter 5 and section 6.2.1).

However, after Stage 5 of the data processing (chapter 5) it was possible to examine meaningful statistics of potential temperature on isopycnals and it was apparent that the simple correction was inadequately modelling the physical processes causing errors in the temperature measurement. For example, the variability of temperature on an isopycnal should be independent of the direction of the Batfish track, but the ratio of isopycnic temperature variance on up and down profiles is sometimes far from unity in the deeper portion of the Batfish wave-form (as can be seen in fig. 6.1). Internal waves were moving the depths at which isopycnals were found through typically 10 m, and this, along with the variability in the density at which the lower turning points in the Batfish profile occured. This leads to large variability in the temporal rate of change of temperature at these densities and the increased ratio of the temperature variance can be explained if one assumes that there is a residual thermal lag effect contaminating the temperature on isopycnals with some function of the recent temperature history of the CTD. This process might be identified with heat flow to and from the pressure casing of the CTD along the stem of the thermometer, or with thermally induced changes in resistance of the wire connecting the platinum resistance thermometer to its interface circuitry (Morrison, 1977, private communication). Temperature changes of 25 K could cause errors of about 15 mK (Millard, 1977, private communication), so the observed temperature change of about 9 K along the Batfish profiles could have caused measurement errors of about 5 mK.

6.1.4 Uncertainties in navigation

The principal source of error in the electromagnetic log is thought to arise from the difficulty in aligning the sensor head, so that the two components of flow which are measured correspond to forwards and sideways motion of the ship. Calibration of the log at sea is usually undertaken in flat calm conditions by steaming a circuit round a drifting buoy. Navigation during this exercise is by radar fixes on the buoy and it is assumed that the surface currents are uniform in space and time. The accuracy is further limited by errors in the radar fixes. Although such a calibration procedure was undertaken just before the GATE cruise it cannot be assumed that the absolute accuracy of the electromagnetic log is better than half a knot or 0.9 km/h (Fasham, 1974, private communication).

The gyrocompass is digitized to 20 minutes of arc. This alone can produce a maximum error of a 0.1 km displacement after a straight course of 20 km. This error could be increased to 0.25 km as the accuracy of the instrument is only believed to be about 30 minutes of arc.

Comparison of the measured current at a mooring and that estimated by the satellite update process suggests that these values are too pessimistic. The surface current, which was calculated as the mean of those from 210 satellite updates taken during a 15.5 day interval ending on 17th September at 0800 GMT, was 37 cm/s in a direction of 082° true. During this time "Discovery" was in the vicinity of the C-scale array of moored buoys (fig. 2.1). The E3 mooring, at 8°41'N, 23°10'W, had a vector averaging current meter at a depth of 7.6 m which gave values of 38.9 cm/s and 070° true for the speed and direction of the mean current (Halpern, 1975). These values were derived from 2304 15-minute samples taken from 19th August to 12th September. The difference between the "Discovery" and E3 mean values is a surface flow of 8.7 cm/s in a direction of 358° true. Assuming that the temporal and spatial variability in the surface current is sufficiently small to allow direct comparison between the two methods

and assuming that the E3 current meter was accurate, the discrepancy between the results could be attributed to errors in the "Discovery" navigation system. As the mean time between satellite fixes during this period was 1.78 hours the discrepancy could arise from errors which amounted to a displacement of about 330 m after each hour of steaming at 8 knots (14.8 km/h).

Perkins and Van Leer (1977) have shown that the easterly and northerly components of the mean current at D1 (fig. 6.2) measured at a depth of about 18 m changed from 31 and 17 cm/s to 36 and 24 cm/s between the periods 8th to 9th September and the 12th to 14th September with extreme fluctuations of some ± 120 % of the mean. Consequently it is probably that much of the discrepancy between the E3 and "Discovery" surface current is caused by variability in the flow, so that the error in the navigation is less than that derived above; say 200 m displacement per hour at 8 knots, or 270 m after 20 km.

As the geographical extent of the manoeuvres of RRS "Discovery" was limited to a small range it was decided to express the position of the ship as a distance, in kilometres, north and east of a fixed point, taken as 8°00'N, 24°00'W (see chapter 5). In calculating positions relative to this origin the curvature of the globe was neglected. The error introduced by this local flat earth approcimation, at a position ϕ°N, (24-θ)°W, can be expressed as:

$$\frac{\theta \pi a}{180} (\cos \phi - \cos 8°)$$

where a is the radius of the Earth. Taking a as the equatorial radius (6378.2 km) this error is 823.6 m at 9°24'N, 22°00'W (which lies beyond the experimental area). At 8°N two degrees of latitude correspond to 220.5 km so the error, which lies in a zonal direction, is less than 0.4 %. The length scale of the Batfish experiments was about 20 km and over such a distance the error introduced is 82 m, about the length of the ship, and is much less than the navigational errors derived above.

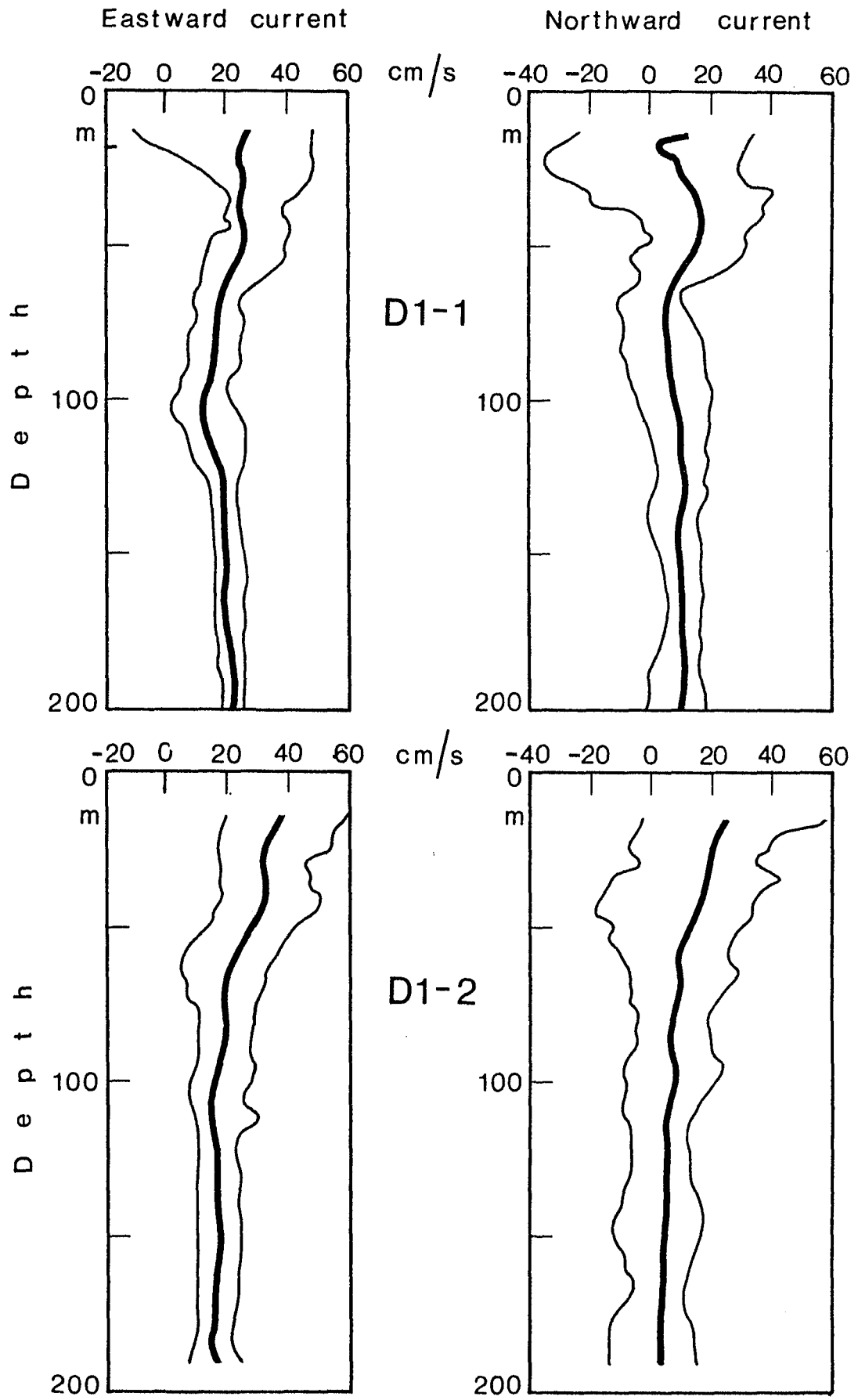

Figure 6.2 a) : Variability in the currents at D1 can be seen in the mean components for the periods 1730 GMT Sept. 8 to 2050 GMT Sept. 9 (D1-1) and 0030 GMT Sept. 12 to 1150 GMT Sept. 14 (D1-2). The minimum and maximum values are shown as thin lines. (after Perkins and Van Leer, 1976).

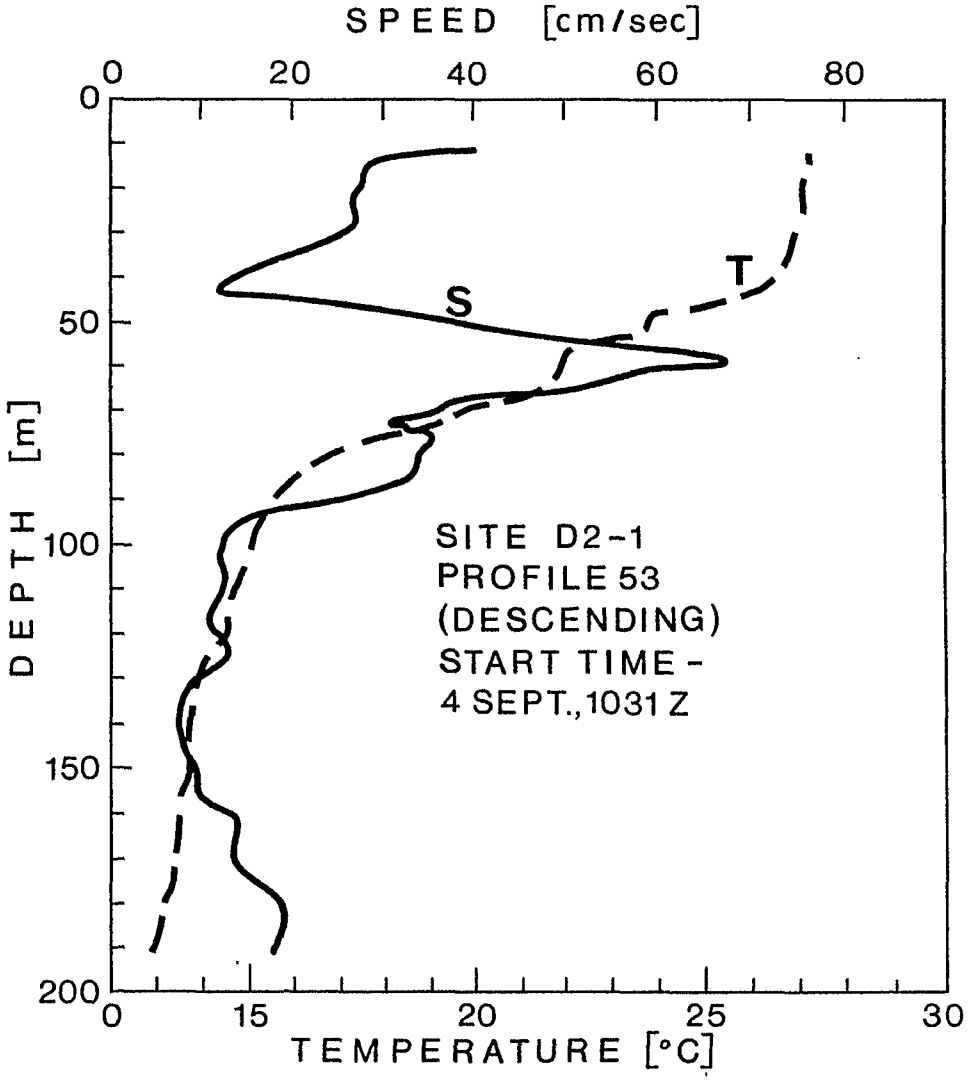

Figure 6.2 b) : Vertical profiles of temperature and current speed at the D2 Cyclesonde mooring. (from Perkins and Van Leer, 1976)

It is already been mentioned that the presence of surface currents results in the position of the ship calculated by the log-integration method, relative to the body of water being surveyed, being different from the geographical position (see fig. 6.3). Consequently it is necessary to have two sets of navigation data and those derived solely by log-integration from an origin at the beginning of a survey pattern are referred to as the "relative positions" (chapter 5).

In calculating the relative positions it was decided to identify them with the Batfish rather than the surface vessel, which required consiering the shape of the Batfish cycle. The dynamic response characteristics of the Batfish resulted in the pressure signal, expressed as a function of time, differing from the desired sawtooth waveform. In particular the turning points were much smoother and the rate of ascending was less than that descending. To express the pressure signal as a function of relative position the horizontal displacement of the fish from the ship is important, especially as this can change through about 30 m between the crests and troughs of the Batfish waveform. While this fluctuation is small in comparison with the errors in the navigation it is appreciable on the scale of a single Batfish cycle which had a typical wavelength of 550 m

Eames (1956) has addressed the problem of the shape of a cable towing a submerged body in equilibrium conditions for a variety of ideal configurations and has published tables to aid the calculation of the position of the towed body with respect to the surface ship. The calculation depends on several parameters which were not known accurately, such as the cable drag and the fish drag, and as the cable was continously accelerating as the Batfish undulated the results of such a calculation would be imprecise. The alternative approach was to approximate the cable to a rigid rod pivoting at the position of the sheave at the stern of the ship. The calculation was very simple and produced estimates of the position of the fish behind the ship marginally further away than those resulting from the much lengthier calculation described by Eames. For example, the rigid-rod approximation increased the distance between the ship and fish by 3.5 m when the latter was at a depth of 69.3 m.

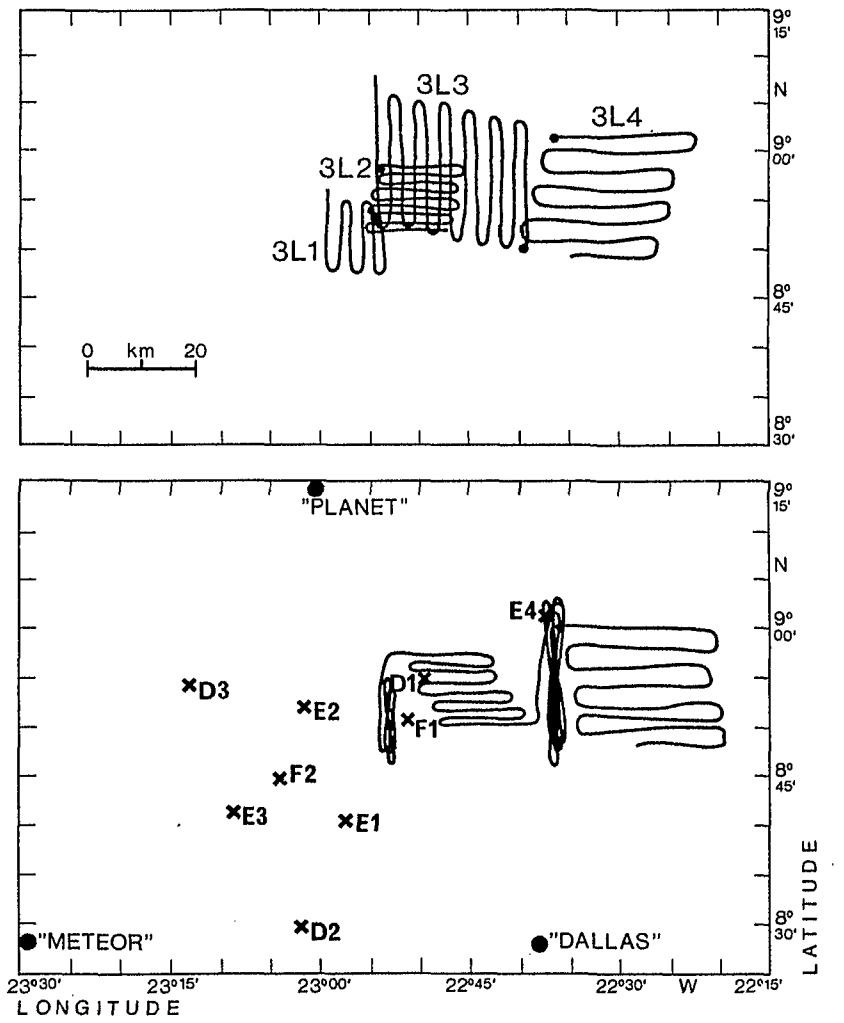

Figure 6.3 : The track of RRS "Discovery" during the Third Lagrangian Experiment, in geographical co-ordinates (bottom) and in co-ordinates relative to the origin of each map, shown as a circle (top).

Often the fish was seen not to follow directly behind the ship and a tow-off angle of 1.21° would produce an uncertainty in the relative position comparable to this figure. On some occasions when the fish broke surface it was observed to lie up to about 30 m to one side of the wake of the ship while for the deeper portions of each cycle the cable was generally seen to tow directly behind the ship; no attempt has been made to correct this somewhat haphazard effect. Consequently, the rigid-rod approximation, with the assumption that the fish is always directly behind the ship, was adopted to calculate the relative position of the Batfish. These co-ordinates are expressed as kilometres north and east of a geographical position designated as the origin of the current sruvey pattern. A typical vertical section of the path of the Batfish through the water is shown in fig. 3.2. The navigation data, relative and true are shown in fig. 6.3.

6.2 Corrections applied during data processing

Efforts were made during the data processing (chapter 5) to correct the systematic errors in the raw data. Corrections were incorporated into the processing sequence only if they produced a consistent improvement in quality throughout the data. Other schemes, such as a correction for the temperature dependence of the pressure sensor or a more complicated heat flow correction for the thermometer (Minnett, 1978) were not implemented, even though localized improvements might have resulted.

Although the editing procedure cannot be considered as a correction to the data, it is included in this section because of the removal of data know to be false leads to an improvement in the quality of the data set as a whole.

6.2.1 Time constant correction in temperature

The salinity calculated from CTD measurements made in conditions of rapidly changing temperature is a very sensitive indicator of the quality of the data. The spikes in salinity which result, in regions where the temperature gradient quickly changes, from a mismatch between the time constants of the thermometer and conductivity cell, can be used to estimate the correction parameter from the data set itself. By trying to reduce the size of these salinity spikes at the same time as minimizing the differences in the signal between successive profiles. A value of the correction parameter τ (which is the lag in response of the thermometer behind the conductivity cell) of 208 ms was determined. This is compatible with the value of 180 ± 30 ms used for the MODE data (Fofonoff, Hayes and Millard, 1974). The correction applied was the same as that used by Fofonoff et al. (1974), namely,

$$T_i^* = T_i + \tau \cdot \frac{\Delta T_i}{\Delta t}$$

where T_i is the measured temperature at data point i

T_i^* is the corrected temperature at data point i

$\Delta T_i/\Delta t$ is the rate of change of temperature at data point i, approximated by

$$\Delta T_i/\Delta t = (T_{i+1} - T_{i-1})2\delta t$$

where δ is the sampling interval.

This correction greatly reduced the salinity spikes seen in the raw date, but, after Stage 5 of processing (chapter 5) when the effects of conductivity cell blockage were removed, it became apparent that this simple correction was not perfect. The mean temperature found on isopycnals during the ascending part of the Batfish waveform is consistently higher than that found on the descending parts (see fig. 6.1). This effect could be caused by an overestimate of the thermometer lag. Reducing the value to 188 ms resulted in a slight

improvement in this discrepancy, but at the cost of less effective reduction of the salinity spikes. One must conclude that this simple correction does not entirely model the processes involved in inducing the errors (see Minnett, 1978).

6.2.2 T-S Editing

Unlike the principle of error in the temperature signal, which was systematic and so could be quite well modelled to recover the data, that in the conductivity signal was not. The data which should have been recorded during the periods when the conductivity cell was blocked were not recoverable, and had to be identified and removed. This was done in the fifth stage of the data processing and the procedure is described in chapter 5.

As the conductivity cell was occasionally blocked or at least contaminated for about an hour, the consequence of editing is that some of the resulting gaps in the data set are appreciable. furhtermore, on these occasions the return to normal operation of the cell was gradual with the result that, in order to remove these bad data, the window of acceptability had to be narrow, typically 50 ppm in salinity at constant density. The resulting risk is that uncontaminated data from regions of large signal might be outside this range and falsely rejected as corrupted data. This is known to have happened, but has been accepted as a necessary consequence of being sure that practically all bad data points had been rejected.

6.2.3 Navigation correction

As a result of irregularities in the navigation data it was necessary to apply corrections here as well. To eliminate occasional bad positions, a box was drawn around each survey pattern and points lying outside this box were replaced by values linearly interpolated from good points adjacent in time. To ensure a continuity in the positions

the additional constraint was introduced that the ship's speed could not have exceeded some reasonable value (6 m/s).

6.3 Inaccuracies as a consequence of data reduction

In reducing the data set to a series of objectively contoured fields on standard surface two separate interpolation schemes were used. An assessment of the possible inaccuracies introduced by these operations is the subject of this section.

6.3.1 Inaccuracies caused by interpolation onto isopleths

The assumption in the interpolation scheme used to derive the value of variables on isopleths (stage 4 of the data processing sequence) is that the variables change linearly between data cycles. This can give rise to an error which may be estimated from the separation of the variables and the gradients between them. Fig. 6.4 shows (schematically) the data cycles, B and C separated by P', on the Batfish track which occur either sie of an isopleth upon which has been interpolated a set of variables, at A. the line BDC shows a possible variation in a variable between the data cycles where it has been measured. The error introduced by the interpolation, ε, can be estimated as $p' \cdot Dq/DP$, where Dq/DP is the gradient of variable q along the Batfish track.

Taking p' as 0.09 decibars (assuming a dive or climb rate of about 1 decibar/s) and Dq/DP as the mean gradient of the profile we have (using the mean profiles from Map 3L3)[1],

[1]Value calculated using the "Experiment Mean" profile could be used here.

(i) above the salinity maximum,

potential temperature; $D\theta/DP = -0.12$ K/decibar

so $\varepsilon = 1.08$ mK

density; $D\sigma_t/DP = -0.072$ kg $\cdot m^{-3}$/decibar

so $\varepsilon = 0.00065$ kg m^{-3}

salinity; $DS/DP = 0.040$ ppt/decibar

so $\varepsilon = 0.00036$ ppt

(ii) beneath the salinity maximum,

potential temperature; $D\theta/DP = -0.33$ K/decibar

so $\varepsilon = 2.97$ mK

density; $D\sigma_t/DP = -0.072$ kg $\cdot m^{-3}$/decibar

so $\varepsilon = 0.00065$ kg m^{-3}

salinity; $DS/DP = -0.026$ ppt/decibar

so $\varepsilon = 0.00023$ ppt

The inaccuracies caused by the interpolation are thought to be generally less than these figures. Deviations from the linear approximation are expected not to have usually been as great, nor the whole width of the interval between cycles always to have contributed to the errors. With the possible exception of salinity specified on interpolated potential isotherms, the inaccuracies caused by interpolation onto isopleths are less than those arising from the measurement errors.

6.3.2 Inaccuracies introduced by Objective Analysis

As a measure of the error introduced during the objective analysis, the root mean square deviation of the data points from a surface linearly interpolated through the grid data points was calculated (see fig. 6.5). The size of this error compared with the standard deviation of the signal is a measure of the success of the objective analysis. If the error is small compared with the standard deviation of the signal then the interpolated surface must pass relatively close to the

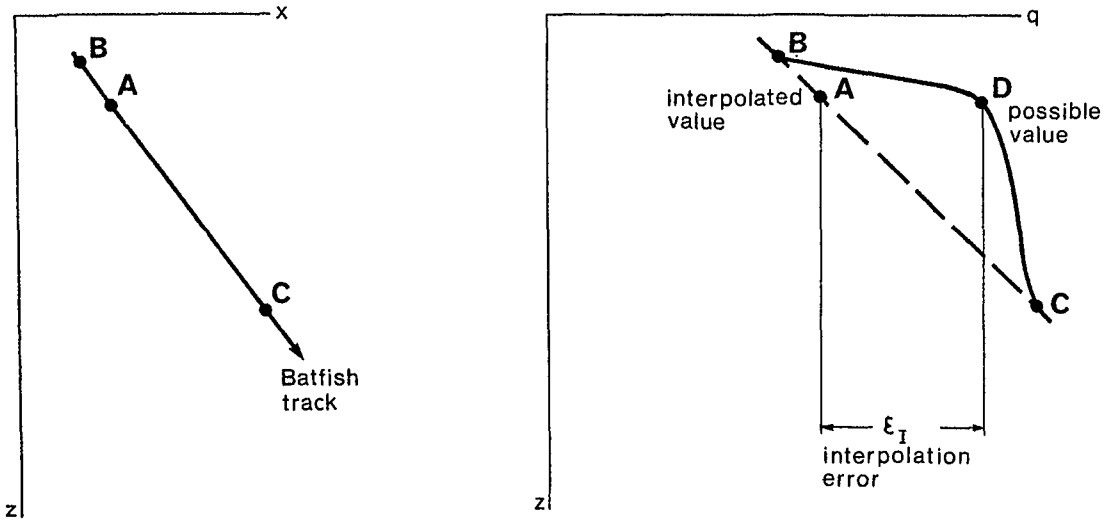

Figure 6.4 : Illustrating the posible error introduced by linearly interpolating the variable, q, between data samples, B and C, onto the isopleth A.

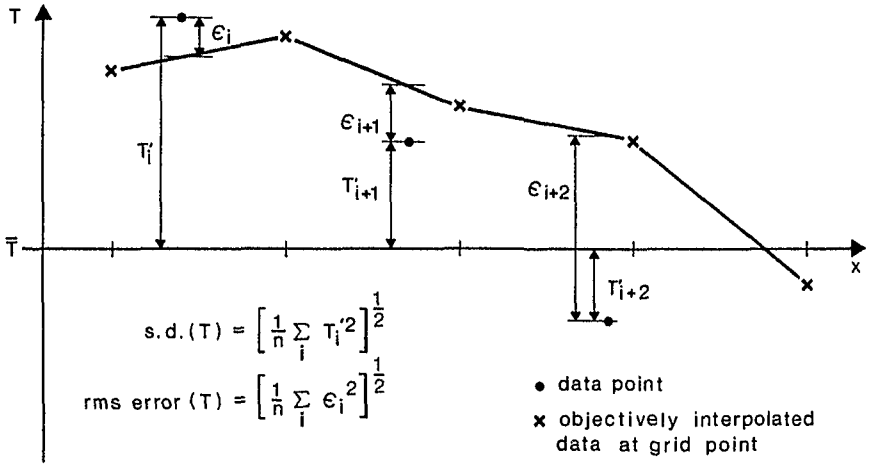

Figure 6.5 : Diagram to show the relationship of the standard deviation and rms error of irregularly spaced data to the data interpolated onto a regular grid. The dots represent the irregularly spaced data and T'_i is their deviation from the mean $\bar{T}$. The crosses represent the data interpolated onto grid points and the ε_i are the deviations of the irregularly spaced data from the value obtained at the same point by linear interpolation from the two nearest grid points. The ε_i thus represent the residual of the signal not represented in the grid point data.

data points; if the error is of the same order as the standard deviation then the interpolated surface is hardly a better approximation to the data than the horizontal plane with the mean value of the data points.

Profiles of the root mean square error as a function of σ_t are shown in figure 6.6. From these profiles it can be seen that the temperature distribution on density surfaces a root mean square error of 10 mK was typical. For thickness distributions on density surfaces the error was typically 0.5 decibar; this represents in general a rather large fraction of the standard deviation of the input data than in the case of temperature on density. The lower degree of success of the interpolation in the case of thickness is due to the signal having typically shorter horizontal length-scales which are rather less well resolved in the raw data and rather less well represented in the objectively interpolated data, since this is to some extent a smoothed field which follows the detail of the input data less well. The use of the data's own auto-correlation function as the weighting function should tend to compensate for difference in the spectral characteristics of the different spectral window of the observation.

6.4 Assumptions implicit in the data processing

The complex track followed by the Batfish during the Lagrangian Experiments means that various assumptions have been implicitly made in order to be able to process the data and present it in the forms shown in the next chapter. These assumptions relate to both the nature of the variability being investigated and to unwanted effects appearing from other scales and other phenomena.

6.4.1 The synoptic assumption

In reducing the data to a convenient form for interpretation, the data from each map have been contoured on isobaric, isothermal and iso-

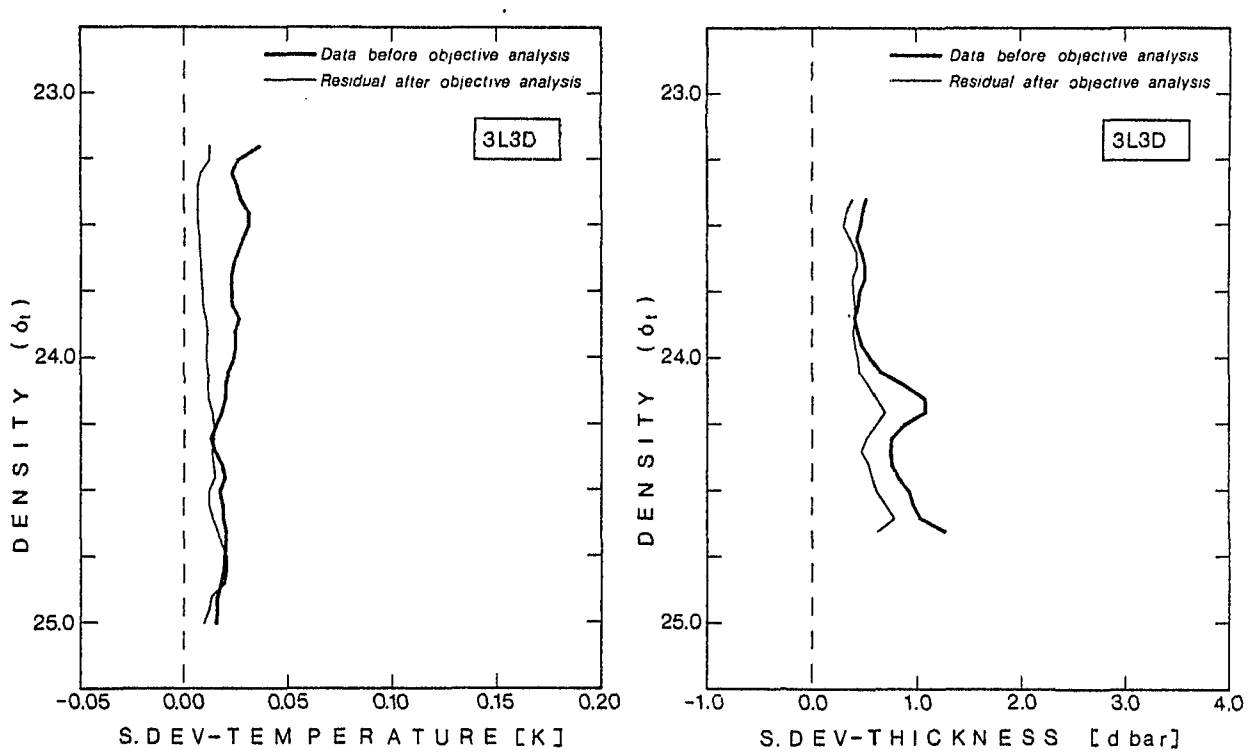

Fig. 6.6 :

Profiles of the residual (rms error) after objective analysis onto regular grids and the standard deviation before objective analysis of potential temperature and thickness on constant σ_t = 23.20 - 25.00 for potential temperature and σ_t = 23.40 - 24.65 for thickness.

pycnic surfaces (chapter 5). In objectively contouring the fields, the contributions of data points to any given grid point were weighted only on a basis of spatial separation. No account was taken of whether data points lay along a leg, and were recorded with time intervals of a few minutes between them, or lay across legs, in which case data points separated by only a few kilometres in space could be several hours apart in time. In other words, it was necessary to assume that the measurements within each map were synoptic. That significant changes can be seen in the contoured fields between maps made without pause between them means that either the structure has drifted out of the survey pattern (section 6.4.2) or that the structure has changed during the experiment.

The scales of the mesoscale features resolved in the maps lies between those of MODE type eddies, with length scales of about 100 km and time scales of many weeks, and those of Kelvin-Helmholtz billows and three-dimensional turbulence, with length scales of less than 1 m and time scales of a few minutes (Woods and Wiley, 1972). Although there is no dispersion relationship for mesoscale turbulent variability, it is reasonable to assume that the time scales of non-wavelike structures resolved in the Lagrangian data will have time scales between these two values.

Numerical modelling of mesoscale frontogenesis, which would be resolved in the data, by MacVean and Woods (1980) has shown that it is possible to form upper ocean fronts on time scales of 3 - 4 days. These calculations used a horizontal stretching deformation field with a deformation rate of 10^{-5} per second, acting on an initially weak baroclinic zone. The parameters used in the model are typical of those likely to be found in a field of MODE type eddies (MacVean, 1977).

More recent numerical modelling of the instabilities of upper ocean fronts has shown that frontal meanders with wavelengths of order 10 km have doubling times of a little more than 30 hours (MacVean, 1980).

Observational evidence of the time-scales of mesoscale structures is scant. Although Voorhis (1969) claims that the large scale manifesta-

tion of points appear to persist over several weeks, Katz (1969) found that the mesoscale frontal meanders could not be identified after a lapse of a few days between surveys. A comparable result has been found for deeper structures from the observations of the depth of an isopycnic surface in the Sargasso Sea (Katz, 1973). At a depth of almost 600 m, a dome shaped structure was observed to raise an isopycnal through about 100 m in a feature which extended along 560 km of a survey. It was also observed on an orthogonal section made at the same location two weeks later. The cause of the dome was not determined, but, along with other repeatable features it prompted Katz to propose that structures of 50 km or more are "quasi-stationary". Features on scales of 20 km showed high correlation on resampling after 24 hours.

Consequently, although it is clear that structures with length scales resolved in the Lagrangian surveys are likely to have evolved in the time taken to complete a map, it is reasonable to assume that the changes are unlikely to have been so great as to render the objective contouring false. The time scales of changes in resolved structures, determined numerically and observationally, are greater than the time needed to complete even the longest map. For further discussion in the context of structures diagnosed in the data set, see Woods (1981).

6.4.2 The effect of vertical current shear

In executing the Lagrangian Experiments with the relative navigation system, the assumption was made that the water under investigation moved as a slab, being advected by the larger scale currents. However, measurements from profiling current meter moorings show large shears within the depth range sampled by the Batfish (10 to 70 m). Nevertheless it can be shown that it is unlikely that the effect of these shears could have moved water out of our survey patterns, at least for the Third Lagrangian Experiment where the size of successive maps was increased to avoid this danger. Nor is it likely that the distortion of the survey pattern within a map could have been so great to render the pattern meaningless.

Data from the "D" moorings, which were equipped with Cyclesonde profiling current meters (Van Leer et al., 1974) show the presence of a strong shear layer at about 50 m, where values of up to 0.05 per second were observed over a depth range of 15 m (Perkins and Van Leer, 1977). While such strong signals are not seen in the mean profiles in horizontal velocity at, for example, D1 (8°54.7'N, 22°49.5'W), the difference in the mean current at 35 m and that at 15 m is 5.8 cm/s in a direction of 214° true (fig. 6.2). The value of the current at 50 m referred to that at 15 m is 10.3 cm/s in a direction 212° true. These values are taken from the mean of 118 profiles measured between September 8 and 14. If these values are taken as typical, then water at 15 m could have been advected through 5 km each day with respect to that at 35 m, and through 9 km with respect to that at 50 m depth.

The largest map of the Lagrangian series (3L3) covered an area of about 22 km square is about 22 hours, being preceded by a smaller map (13 km square, 10 hours) and succeeded by a quicker one (26 km square, 13.5 hours). So, even in this case, provided the mean shears in the pycnocline did not greatly exceed those given above, some of the water, even at the deepest penetration of the Batfish, should be common to successive maps.

Figure 6.2 shows the temperature and current profile from September 4 at D2 (8°29.7'N, 23°02.2'W). A pronounced speed maximum in the thermocline can be seen. This plot, said to be of an extreme example (Perkins and Van Leer, 1977), shows a speed at the centre of the jet, at 50 m depth, of 67.7 cm/s. At 44 m the current is 11.4 cm/s. The shear between these two levels, in this profile, is between 0.049 per second and 0.035 per second. A shear of 0.05 per second, acting over 10 m in the vertical could produce a relative displacement comparable to the Batfish wavelength (0.5 km) in about 20 minutes. However, as these large shears appeared irregularly in the Cyclesonde data, they may have only rarely produced displacements comparable to the Batfish wavelength. Some of the fluctuating shears appeared to have strong tidal and inertial components. In the 11 hours of Map 3L3 the tidal component will have caused both compressive and dilative effects while

the inertial component will have completed about one quarter of a cycle, thus introducing a progressive distortion. The magnitude of these relative displacements depends on the amplitude, phase and vertical structure of the internal tide and inertial wave. As the maximum speed fluctuation (in the Cyclesonde data) at a given depth was comparable to the mean value, it seems unlikely that the relative displacement produced by the inertial wave during Map 3L3 was greater than that caused by the mean shear.

The relative positions of the data points have been calculated assuming the current in the region of the map was spatially uniform (chapter 5); the effect of the mean shear to move the north-west corner of Map 3L3 (fig. 6.3) by up to 5 km towards the north-east, with displacements along the track proportional to the elapsed time from the map origin. The inertial wave could produce a further displacement of the north-west corner by probably less than 5 km with progressive displacements through the map; the tide probably causes relative distortion within the map and short duration fluctuations may cause irregular displacements of individual data points.

6.4.3 Internal waves

The near surface pycnocline in the C-scale area sustained a wide spectrum of internal waves between the inertial and buoyancy frequencies, that is with horizontal wavenumbers in the range 0.004 cycles/km to 6 cycles/km (derived from the first mode dispersion curve given by Käse and Clarke, 1978). These wavenumbers include the comparatively narrow spectral window of the Lagrangian surveys. The higher frequency waves, including a local spectral maximum at 4 cph, are aliased in the horizontal by the Batfish sawtooth waveform. The fluctuations caused by aliased internal waves in, for example, the pressure signal of isopycnals or isotherms, are therefore a major source of noise.

The high vertical coherence of the internal waves, over the depth range of the Batfish survey, as revealed in repeated CTD profiles in-

dicates that the waves are of low mode, mainly first mode (Käse and Clarke, 1978).

The vertical displacements caused by internal waves can be removed by using density (σ_t) as the independent vertical co-ordinate. This technique was first used by Parr (1936) and Montgomery (1938) and was given the name isopycnic analysis. The component of the internal wave motion along isopycnals can distort the pattern of existing thermohaline variability by compression and dilation, to the same extent as the distortion of the pattern of data points in a map (section 6.4.2). However, apart from small scale mixing events caused by wave induced shear instability (Woods, 1968) which might have influenced individual data points on an isopycnal, the internal waves themselves cannot generate the mesoscale thermohaline variability revealed in sections and maps in density co-ordinates.

Given that the internal waves were of low mode, the pressure differences between isopleths should also be free from internal wave contamination, provided that the separation between the isopleths remains a small part of the vertical wavelength of the waves. This is the case for the data measured in the relatively small depth range of the Batfish experiments. However, as the pressure differences between isopleths are found along the Batfish track, an uncertainty is introduced into the measurement by the fact that the Batfish track is inclined to the vertical and the isopleths undulate with internal waves.

Consider two isopleths I and J (shown schematically in fig. 6.7) separated by δP decibars in the vertical, but which have an apparent separation δP_m decibars where this is found from the Batfish CTD data. The error introduced depends on the slope of the Batfish track and the inclination of that isopleth which was the second of the pair encountered. The angle made by the Batfish track to the horizontal, β, varied with the position in the cycle and can be derived from the pressure signal and the computed relative positions. For example, the average Batfish cycle time in Map 3L3 was 130.4 seconds, with a standard deviation of 19.3 seconds, which is divided into about 55 seconds

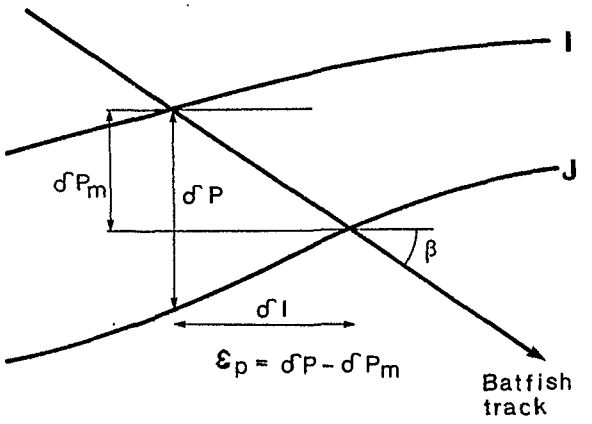

Fig. 6.7 :

Illustrating the error, ε_p, in the difference in pressure between two isopleths, labelled I and J, when measured along the Batfish track.

diving and 75 seconds ascending. With an amplitude of about 60 m this gives a dive and climb rate of 1.1 m/s and 0.8 m/s. The ship's speed during Map 3L3 was 4.27 m/s (standard deviation of 0.47 m/s) and this can be taken as the horizontal component of the Batfish velocity to an accuracy of only about 25 %. The horizontal separation between the ship and the fish varied by about 30 m between the extrema of the Batfish cycle. Thus on dives the average horizontal speed of the fish relative to the ship is about 0.5 m/s and of about 0.3 m/s on ascent, but the range of values is likely to include zero to twice these speeds. With a ship's speed of 4.3 + 0.5 m/s the Batfish speed can be set at 5.3 to 3.5 m/s. The inclination of the Batfish track to the horizontal (β) is such that $\tan \beta = 0.26 \pm 100$ % on down dips and $\tan \beta = 0.19 \pm 100$ % on up dips. For the parts of the dips away from the turning points the range of these values will be much less, but the values themselves will be increased.

Provided that the internal wave field which produces the tilting of the isopleths is not nearly monochromatic with a wavelength comparable to that of the Batfish cycle, the average error in the pressure difference will be zero over a sufficiently large sample; $\varepsilon_p = \delta P - \delta P_m = 0$. The error will be largest at the nodes of internal waves and close to zero at trough and crests, and given the probability distribution of a harmonic wave the likelihood of encountering a large error is smaller than meeting a small one.

An expectation value of the error can be calculated by considering the effect between the sloping Batfish track and a spectrum of internal waves with characteristics appropriate to the C-scale area (Minnett, 1978). This gives

$$\sqrt{\langle \varepsilon_p^2 \rangle} = 0.194 \sqrt{\delta \ell}$$

where $\sqrt{\langle \varepsilon_p^2 \rangle}$ is the root of the expectation value of the squared error, in decibars, and $\delta \ell$ is the horizontal displacement between the points where the isopleths cross the Batfish track, given in metres. For measured vertical separations of about 1 m, $\delta \ell$ is about 4 m on

descending profiles given an expected error of 0.39 decibar, and is about 5 m on ascending profiles leading to 0.43 decibar. Thus the error is about 40 % of the 1 m measured separation, and is slightly smaller for descending profiles. The expectation error is greater than 100 % for horizontal displacements larger than 26 m.

An alternative approach to estimate this error is to approximate the internal waves by inclined planes. Elliott and Oakey (1975) have measured the inclination of isotherms using a free fall probe, and found that the most frequently encountered slopes lay between 10° and 15°. There is some uncertainty in these measurements in that what Elliott and Oakey have attributed to curvature and tilt could have been caused by vertical motions. Assuming these results can be applied to the tilt of isopycnals in the C-scale area, and taking a most probable tilt of 12.5° gives an error of ± 85 % in pressure difference between isopleths measured on descending profiles, and ± 120 % on ascending profiles. These estimates would indicate that there should be no similarities between patterns of pressure differences measured on ascending profiles and descending profiles. As similarities are seen, it must be concluded that this error estimate is over-pessimistic.

6.4.4 Adiabatic change in density

The data analysis depends on interpolation of variables onto isopycnals. We followed Montgomery (1938) in using σ_t as our density variable. It might be argued that we should have used potential density. Here we consider the error arising from neglecting adiabatic changes of particles on the σ_t surfaces on which pressure varies by ± 10 decibar due to internal waves. It is convenient to introduce a new density variable σ_* defined as the in situ density that a particle has after adiabatic compression from its observed pressure p to a reference pressure p_*. The salinity variation on the density surface makes a corresonding variation of adiabatic lapse rate so, even if the surface had originally been isobaric, any compression will produce a range of σ_* values. Histograms of σ_* for 3L3 surfaces σ_t = 24.00 and

24.05 moved adiabatically to $p_* = 0$, 40, 100 and 500 decibar are shown in fig. 6.8. The density scatter introduced on a single σ_t surface, ± one g/m^3, is small compared with the uncertainty due to instrumental errors (section 6.1). For a mean vertical density gradient of 1 kg/m^4 this is equivalent to an error of one millimetre in the depth of particles on the isopycnic surface, which is small compared with the CTD sampling interval (30 mm). This error is too small to cause significant modulation of spacing between pairs of surfaces, even if their thermohaline anomalies are uncorrelated. Although the result is not unexpected (indeed oceanographers normally assume that σ_t is an adequate density variable for most purposes in the upper ocean), our unique data set has permitted a demonstration that it is still the case in the specially demanding analysis of mesoscale thermohaline anomalies in the North Atlantic Equatorial Counter Current.

6.5 Estimate of errors in standard products, as deduced from internal evidence

In the first sections of this chapter it was shown that the principle sources of inaccuracy in the data set have arisen from non-equilibrium effects and as such are not related to the estimate of accuracy which would be derived from equilibrium calibration techniques. Consequently one must use internal consistency checks to estimate inaccuracies and particular use has been made of comparison of signals seen in ascending profiles ($dT/dt > 0$) and descending profiles ($dT/dt < 0$).

Since all of the data considered here originated from a single instrument an estimate of the "relative accuracy" within each subset of ascending or descending data is all that is required to determine whether features seen in the data can be considered as environmental or not.

The estimated accuracies of variabiles as presented in the diagrams of chapter 7, and the data report (Woods, Leach and Minnett, 1981) are summarized in tables III and IV.

Table III: Estimates of Errors* in Measured and Derived Variables

Variable	Error
Pressure	± 0.1 dbar
Temperature	± 4 mK
Conductivity	± 5 μS cm
Potential temperature	± 4 mK
Salinity	± 5 ppm
Density (σ_t)	± 4 • 10^{-3} kg•m^{-3}

* These are the relative errors for each subset of data derived from ascending or descending profiles.

Specified Variable / Measured Variable, Error	$\theta)_{\sigma_t}$	$S)_{\sigma_t}$	$P)_{\sigma_t}$	$\sigma_t)_\theta$	$S)_\theta$	$P)_\theta$	$\theta)_P$	$S)_P$	$\sigma_t)_P$
	mK	ppm	dbar	10^{-3} kg•m^{-3}	ppm	dbar	mK	ppm	10^{-3} kg•m^{-3}
1. Above Salinity Maximum									
T, ΔT = 4 mK	10.2	-5.2	0.03	-6.0	-4.5	0.02	4.0	3.2	3.6
G, ΔG = 5 µS/cm	3.4	5.1	0.02	2.8	3.7	$4 \cdot 10^{-7}$	$8 \cdot 10^{-2}$	3.7	2.8
P, ΔP = 0.1 dbar	0.001	0.04	0.1	$-8.2 \cdot 10^{-3}$	-0.02	0.1	20.0	6.4	12.0
Accuracy	±12	±8	±0.1	±7	±6	±0.1	±21	±8	±13
2. Below Salinity Maximum									
T, ΔT = 4 mK	20.8	-2.2	0.05	-4.6	-3.2	0.01	4.0	-3.5	3.7
G, ΔG = 5 µS/cm	14.9	3.1	0.04	3.3	4.3	$1 \cdot 10^{-6}$	$4 \cdot 10^{-2}$	9.3	3.3
P, ΔP = 0.1 dbar	0.1	0.03	0.1	-0.03	-0.04	0.1	34.0	2.7	7.5
Accuracy	±25	±4	±0.1	±6	±6	±0.1	±35	±6	±9
(Uncertainties and pressure difference between isopleths are not given here, but are discussed in the text.)									

Table IV: Estimate of Accuracy of Variables specified on Isopleths

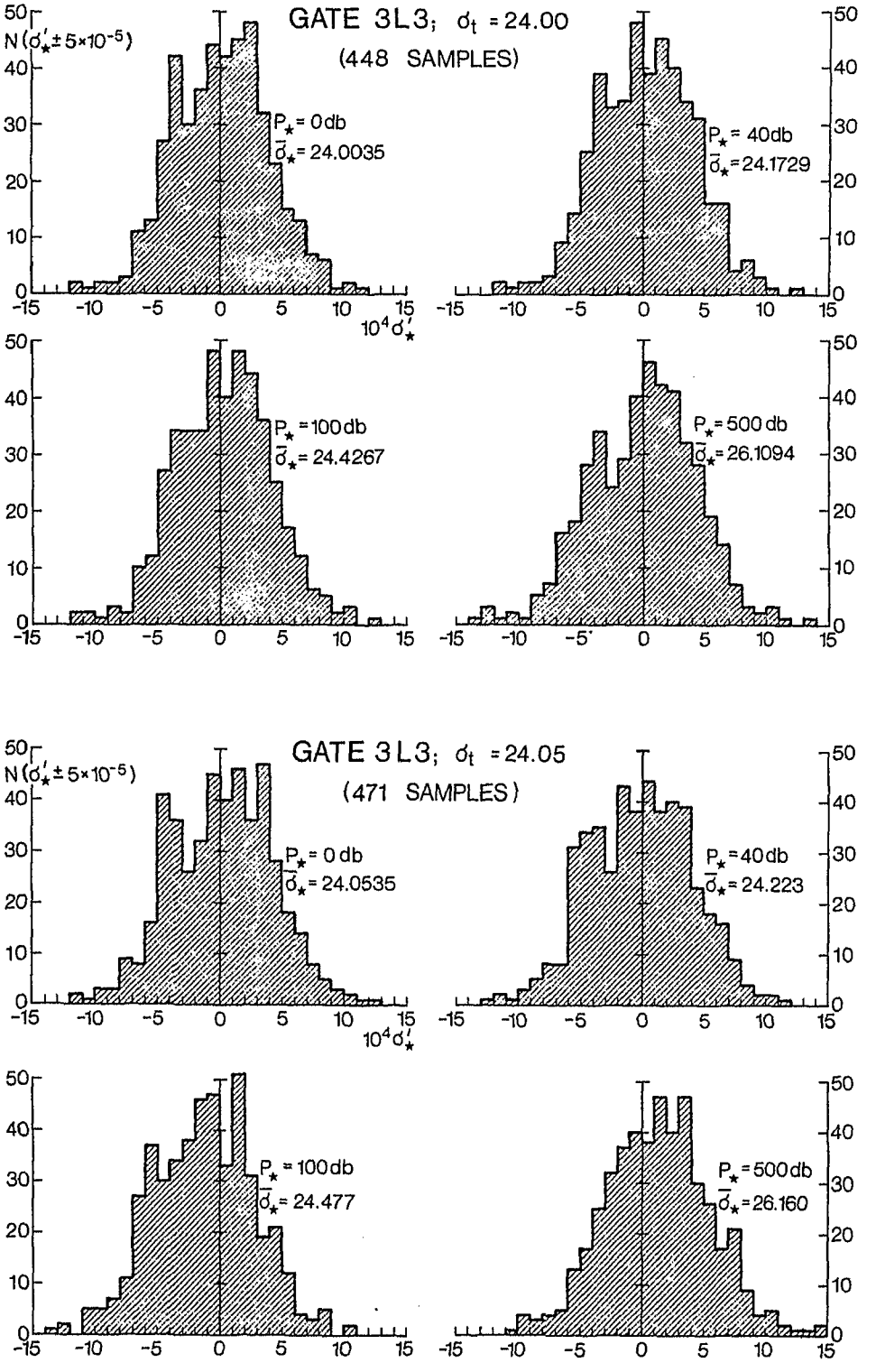

Figure 6.8 : Histograms of the scatter in density after adiabatic transformation of the data from two selected σ_t surfaces (24.00 and 24.05 kg m^{-3}) to various pressure levels. The typical scatter of 0.001 kg m^{-3} is less than the error due to instrumental inaccuracies.

The errors in the position of the data points have been dealt with in the discussion of the accuracy of the relative navigation (section 6.1.4).

6.5.1 Profiles

In displaying temperature or conductivity as profiles along the Batfish track, as a function of pressure, the inaccuracies are those incurred at measurement. These induce errors in salinity, potential temperature and density according to the functional dependence on the measured variables shown by the computational algorithms. The inaccuracies introduced by the failure of the algorithms to precisely model the physical properties of seawater (see, for example, Lewis and Perkin, 1978) are of no consequence in the framework of "relative accuracy".

As discussed in section 6.1.1, the main inaccuracy is the pressure signal caused by temperature hysteresis, can be estimated by comparing mean pressure on isopycnals found on ascending or descending profiles, and is about 1 decibar (fig. 6.1). The relative accuracy within each subset, which is relevant when considering changes in the pressure on isopleths from profile to profile, is smaller, say ± 0.1 decibar. The shapes of the profiles are subject to distortion along the pressure axis by the errors in pressure differences measured along the Batfish track, as discussed in section 6.4.3.

The inaccuracy in measured temperature has also been estimated by comparison between mean potential temperatures seen on isopycnals on ascending profiles. This quantity is highly derived and contains a factor which magnifies the measurement error (see section 6.5.2). The inaccuracy in measured temperature thus estimated is about ± 5 mK. A more severe test is to compare the shapes of histograms of salinity encountered on isopycnals in the two subsets of data (fig. 6.9). To achieve the best comparison it is necessary to shift the data from ascending profiles through + 5 ppm in salinity and 0.005 kg m^{-3} in σ_t.

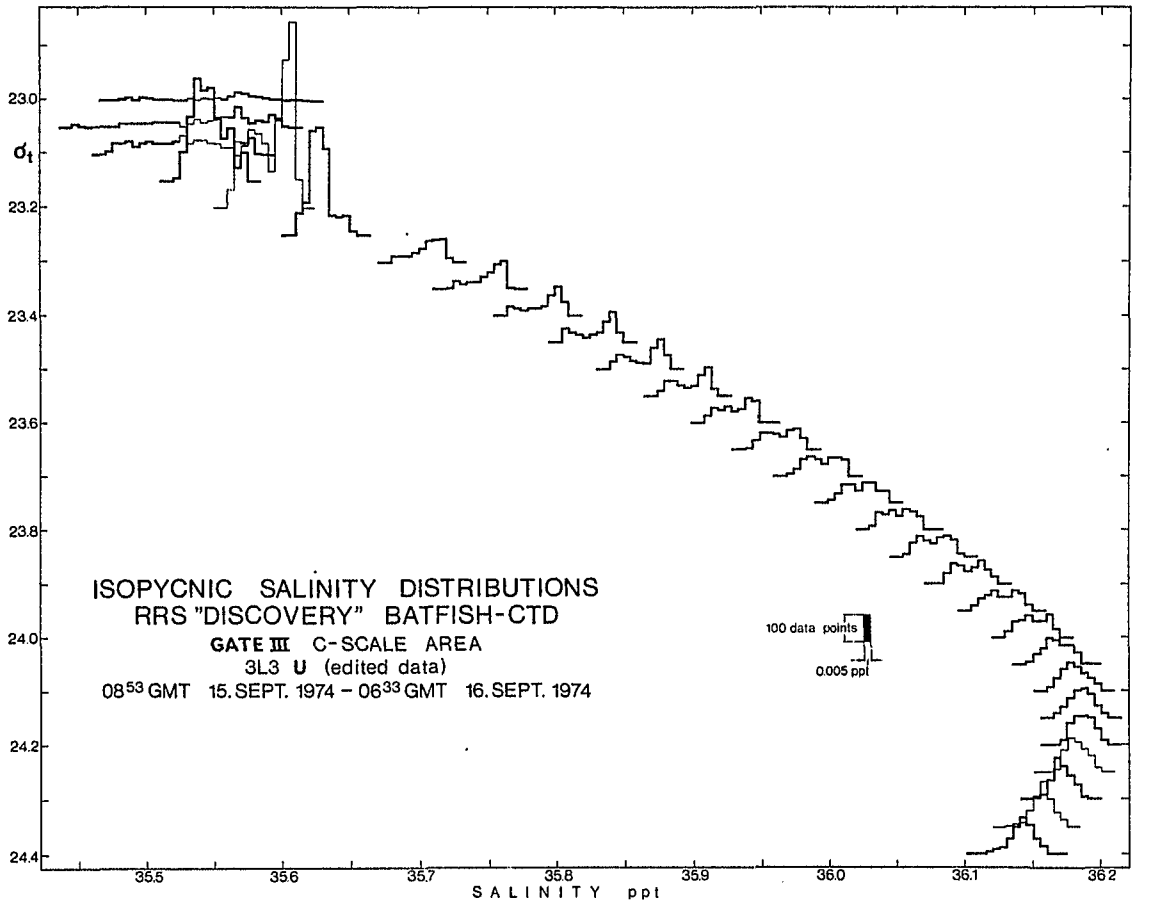

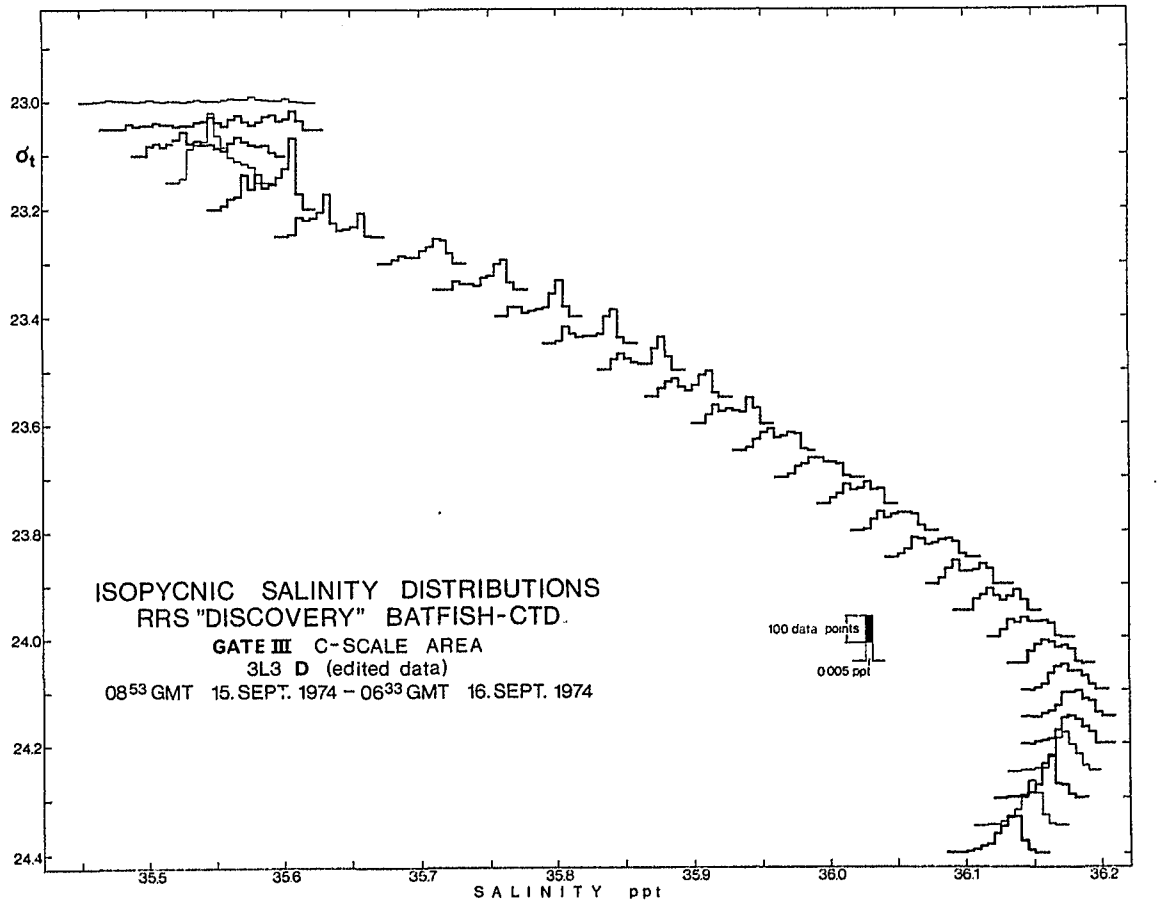

Fig. 6.9: Histograms of salinity on surfaces of constant σ_t produced independently from data from Batfish "down-dips" (lower figure) and Batfish "up-dips" (upper figure) respectively.

This is due to residual systematic errors, probably in temperature, but are of no consequence when considering relative accuracies. The shapes of the historgrams then compare well to within 5 ppm. This could result from an uncertainty in measured temperature of less than 4 mK, which is the value taken as the inaccuracy in the measured temperature.

During the periods when the conductivity cell was blocked (chapter 2 and section 6.1.2) the conductivity signal is not accurate at all. Otherwise the accuracy of the conductivity cell as stated by the manufacturer, which is ± 0.005 mS/cm, has been assumed (Brown and Morrison, 1978). This measurement inaccuracy is sufficient in itself to have accounted for the uncertainties attributed to measurement errors in temperature. However, since the temperature signal is known not to be entirely accurate in non-equilibrium conditions (section 6.2.1) it would appear that the estimates of measurement inaccuracies in temperature and conductivity have not always behaved additively or that the estimates are pessimistic.

The coefficients describing the dependence of the derived variables on the input parameters are themselves functions of these input variables, particularly temperature. However, no account is taken here of the changes in the estimated inaccuracies in the derived variables introduced by the 9 K temperature range found in the data, as these changes are less than 25 % (Minnett, 1978).

The uncertainties in the derived variables are ± 5 ppm in salinity ± 4 mK in potential temperature and ± 4 • 10^{-3} kg m^{-3} in σ_t.

6.5.2 Variables on isopleths

In specifying a variable on an isopleth, for example potential temperature on an isopycnal $\theta)_{\sigma_t}$, the measurement inaccuracies introduce uncertainties in both potential temperature and density. This can be envisaged as a shift of the density profile with respect to that of potential temperature. This error is given by

$$\Delta\theta)_{\sigma_t} = \Delta\theta + \frac{D\theta}{D\sigma_t} \Delta\sigma_t$$

where $\Delta\theta$, $\Delta\sigma_t$ are the uncertainties in potential temperature and dentity, as given in section 6.5.1, and $D\theta/D\sigma_t$ is the gradient of potential temperature with respect to density along the Batfish track. The contribution from the possible errors in the interpolation on to isopleths (section 6.3.1) can be neglected in comparison with the inaccuracies associated with the measured variables.

The subsurface maximum in the vertical salinity profiles (fig. 6.10) divides the water column into two regimes characterized by different mean values of $DS/D\sigma_t$. Consequently the uncertainties in $\Delta\Theta)_{\sigma_t}$ are different in the two regimes and have to be assessed separately.

Expanding the expression for $\Delta\Theta)_{\sigma_t}$ gives

$$\Delta\Theta)_{\sigma_t} = \left(\frac{D\Theta}{D\sigma_t} \frac{\partial}{\partial T} \sigma_t + \frac{\partial\Theta}{\partial T} \right) \Delta T + \left(\frac{D\Theta}{D\sigma_t} \frac{\partial}{\partial G} \sigma_t + \frac{\partial\Theta}{\partial G} \right) \Delta G$$

$$+ \left(\frac{D\Theta}{D\sigma_t} \frac{\partial}{\partial P} \sigma_t + \frac{\partial\sigma}{\partial P} \right) \Delta P$$

$$= a_{\Theta,T} \Delta T + a_{\Theta,G} \Delta G + a_{\Theta,P} \Delta P$$

Thus the measurement uncertainties (ΔT, ΔG, ΔP) are modified by the factors $a_{\Theta,T}$, $a_{\Theta,G}$ and $a_{\theta,P}$, which can be evaluated given a value for $D\Theta/D\sigma_t$. In the stratified layer above the salinity maximum, the mean value of $D\Theta)_{\sigma_t}/D\sigma_t$ is -1.7 K (for 3L3) which gives

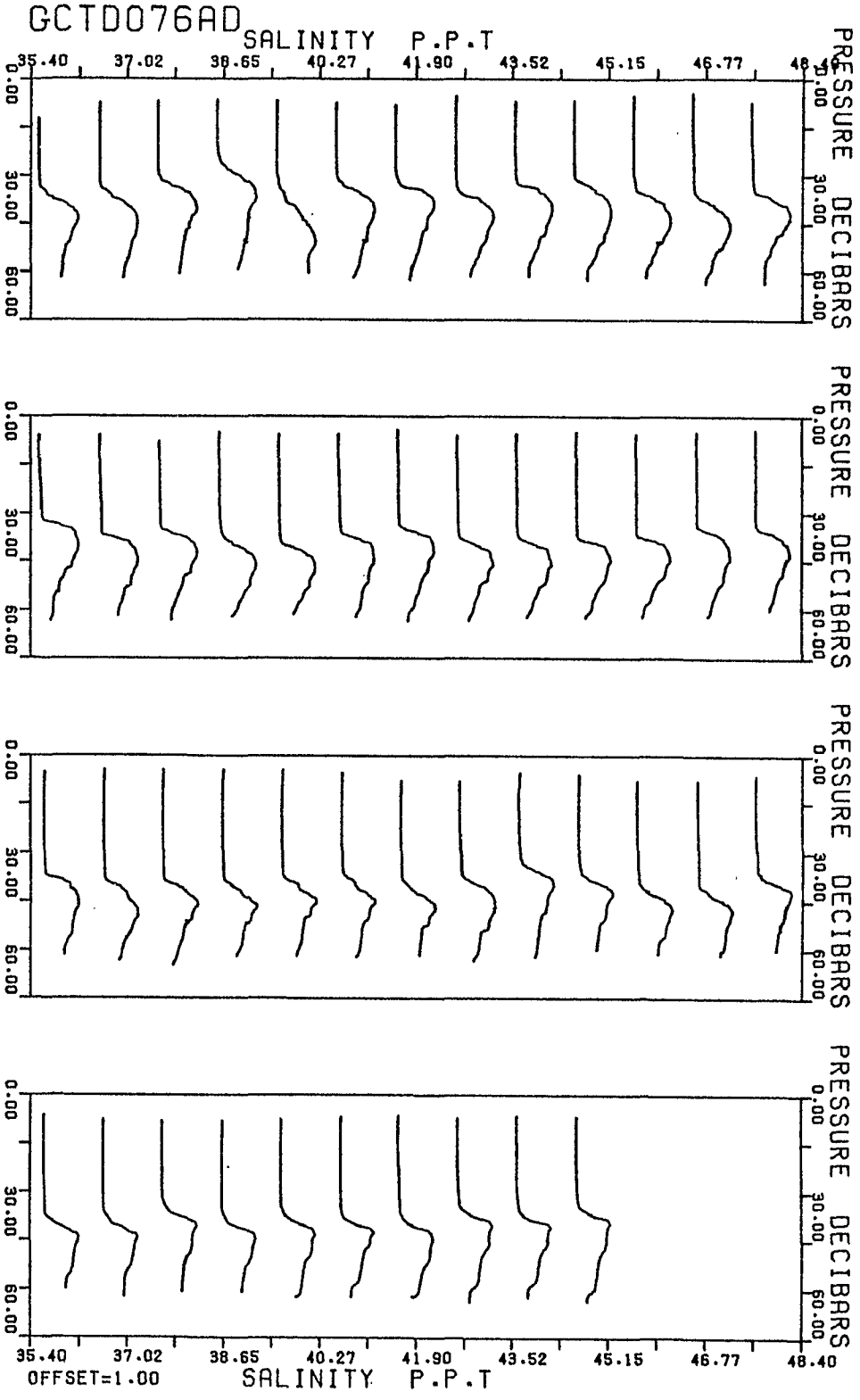

Fig. 6.10:

A series of salinity profiles from one leg of Map 3L3 showing the variability of the structure of the salinity maximum and of the profile above and below the maximum.

$$a_{\Theta,T} = 2.54 \text{ K/K}$$

$$a_{\Theta,G} = 0.96 \text{ K/(mS/cm)}$$

$$a_{\Theta,P} = 1.4 \cdot 10^{-4} \text{ K/decibar}$$

so,

$$a_{\Theta,T} \cdot \Delta T = 10.17 \text{ mK}$$

$$a_{\Theta,G} \cdot \Delta G = 3.45 \text{ mK}$$

$$a_{\Theta,P} \cdot \Delta P = 0.001 \text{ mK}$$

Thus, the uncertainty in potential temperature on isopycnals above the salinity maximum is about ± 12 mK.

Beneath the salinity maximum $D\Theta)_{\sigma_t}/D\sigma_t = -4.55$ K
which gives

$$a_{\Theta,T} = 5.19 \text{ K/K}$$

$$a_{\Theta,G} = 2.98 \text{ K/(mS/cm)}$$

$$a_{\Theta,P} = 1.2 \cdot 10^{-3} \text{ K/decibar}$$

so,

$$a_{\Theta,T} \cdot \Delta T = 20.76 \text{ mK}$$

$$a_{\Theta,G} \cdot \Delta G = 14.90 \text{ mK}$$

$$a_{\Theta,P} \cdot \Delta P = 0.12 \text{ mK}$$

Thus, the uncertainty in potential temperature on isopycnals below the salinity maximum is estimated at ± 25 mK.

Similar calculations give estimates for uncertainties of other variables specified on isopleths, which are shown in table IV. Each row in

the table shows the inaccuracy induced by uncertainties in the measured variables, as shown in the first column. These components are combined to give a geometric mean (thus making the assumption that the uncertainties in the different variables are uncorrelated) which is shown at the foot of each column and is taken as the estimate of accuracy.

6.5.3 Products based on objective analysis

In section 6.3.2 it was pointed out that objective analysis using the auto-correlation function as a weighting function tended to smooth the fields. The concept of a root mean square error as a measure of the success of the objective analysis was introduced. Provided that the deviation of the interpolated field from the input data, ε, (see fig. 6.5), is not correlated with the deviation of the temperature from its mean, T_i', then the mean square error $\frac{1}{n}\Sigma\varepsilon_i^2$ can be regarded as that proportion of the variance of the field, $\frac{1}{n}\Sigma T_i'^2$ not represented by the grid-point data. The energy spectrum of the data can thus be regarded as falling into two parts, a low-wavenumber part represented by the objectively analyzed data or grid points and a high-wavenumber part, unresolved by the grid, whose variance is the mean square error. In the preceding section 6.5.2 estimates have been made of the accuracy of variables on isopleths and it is assumed that the uncertainties are random. If this is the case there is no reason to suppose that the uncertainty of the grid-point data should be worse than that of the irregularly spaced data; indeed the low-wavenumber grid-point data should if anything have its uncertainty reduced since it is smoothed and represents only part of the spectrum.

7. A SELECTION OF THE STANDARD PRODUCTS

In this chapter an introduction to the data will be given. Of the thirteen Maps one, 3L3, has been chosen to illustrate the nature of the data in greater detail and this is discussed in section 7.1. The intermap variability will be considered by drawing on data from the other maps as well. The data shown here is only a selection from the whole data set which appears more comprehensively in Woods, Leach and Minnett (1981), where each Map has a whole volume devoted to it.

For the sake of readability all the figures for this chapter are collected together at the end of the chapter.

7.1 Examples from map 3L3

This Map of all the thirteen had the best resolution, namely thirteen legs some 25 km long with a spacing of one nautical mile. The Map is made up of some 500 individual Batfish profiles.

7.1.1 Statistics of the data

The variability of the temperature, salinity and density as a function of depth (pressure) is summarized in figure 7.1. Here the mean depth of the quasi-homogeneous layer (so-called "mixed-layer") of about 27 dbar can be seen and the salinity maximum of 36.2 ppt at about 45 dbar. It is interesting to note that the quasi-isothermal layer is deeper than the quasi-isohaline layer. The temperature and salinity as a function of density are shown in figure 7.2 as is the mean and deviation T-S diagram. Here the salinity maximum lies at σ_t = 24.2 at a temperature of about 25.5 °C. In these representations the very much smaller variability after the elimination of internal waves can be seen. In figure 7.3 this effect can be even more clearly seen where the temperature and salinity as a function of density have been redrawn in pressure coordinates making use of the mean density-pressure relationship; these curves can be compared with those in figure 7.1. The standard deviations of temperature and salinity as functions of pressure and as functions of density redrawn as functions

of pressure are also shown in figure 7.3. Here it is clear that the thermohaline variability (T or S as a function of σ_t) is an order of magnitude smaller than the total variability. This endorses our choice of working in σ_t-coordinates since the object of the investigation was largely quasi-geostrophic dynamics whose effects would be reflected in the spatial thermohaline structures. Close inspection of the statistics of the thermohaline structure using histograms of salinity on density surfaces as shown in figure 7.4 reveal that in the uppermost pycnocline, above the salinity maximum, two (local) water masses must have been present in the area being observed since the histograms show a double peak. Histograms of the spacing of isopyncals ("thickness") are shown in figure 7.5. Here it can be seen that the distribution is skew and that at some points the thickness observed was many times the mean thickness for the layer. In the absence of high-mode internal waves (Käse and Siedler, 1980) and errors in the observations the thickness should be related to the vorticity because of the conservation of baroclinic potential vorticity (Tang, 1984).

7.1.2 Profiles and sections from Leg 6

A glance at a set of individual profiles from Leg 6 (fig. 7.6) reveals the richness and variety of the structures of this area. Comparison of the individual temperature and salinity profiles again shows, as in the statistics (fig. 7.1), that the quasi-isothermal layer is deeper than the quasi-isohaline layer. The salinity profiles, modulated by internal waves, show steadily varying form in the shape of the maximum and detail of the junction between halocline and quasi-homogeneous layer and of the step-structures above and below the maximum. The step-like structures retain their form recognisably for a few profiles and then gradually change. The data from the same leg are shown again in figure 7.7a, where the depth and temperature of isopycnals are shown. Here it can be seen that the isopyncals are generally deeper in the north than in the south and that the spacing between them varies considerably. The temperature of isopycnals shows thermohaline structures dipping down towards the north. Figure 7.7b again shows the

depth of isopycnals but this time not only those in the pycnocline but also right up to the surface. The horizontal density gradient in the quasi-isopycnal layer ("mixed layer") can be seen and also the diurnal thermocline close to the surface. In order to be able to see the variability of isopycnal spacing more clearly the depths of isopycnals relative to the isopycnal σ_t = 24.00 kg m^{-3} are shown in figure 7.7c. Here it is also apparent that there is a band of greater thickness dipping downwards to the north.

7.1.3 Data on density surfaces

In figure 7.8 the spatial distribution of temperature and thickness for three adjacent density surfaces is shown. While the level of the temperature signal is relatively low, only a few tens of mK peak-to-peak, this is still clearly larger than the error of about ± 10 mK (Table IV) and the spatial consistency (from dip to dip and leg to leg) and the favourable comparison of data from ascending and descending profiles (fig. 5.2) gives confidence that the structures shown are genuine. The temperature distributions show a band of cold water running northeast-southwest through the area and that this band changes its position with depth, occurring more to the northwest with increasing depth. This is the spatial representation of the two water masses seen in the histograms of figure 7.4. The two water masses are separated by bands of relatively sharp horizontal temperature gradient where the isotherms "bunch" together. The spatial distribution of the thickness or spacing between isopycnals shows less similarity from surface to surface though the regions of increased thickness sometimes do show considerable spatial extent.

7.1.4 Data on pressure surfaces

Thermohaline structures with scales in the range 10 - 20 km were also observed in the so-called "mixed-layer", see figure 7.9, where the spatial temperature and salinity distribution at a depth of 10 dbar

are shown. Whereas the thermohaline structures in the pycnocline, being beyond the range of the diurnal heating cycle are presumably largely the result of quasi-(or semi-)geostrophic dynamics, those observed at 10 dbar include insolation and recent air-sea interaction effects (see Kronfeld, 1982). The diurnal heating cycle can account for most of the signal in temperature at 10 dbar.

7.2 Intermap variability

Map 3L3 was chosen to illustrate the results of the GATE Lagrangian Batfish experiment because its resolution and extent (spectral window) were better than those of the other maps. These however also show similar structures though sometimes spatially less well-defined than in Map 3L3 (see section 7.2.3 below).

7.2.1 Statistical comparison of the maps

The thirteen maps have been compared statistically in figure 7.10. here the mean and standard deviation for each map of temperature, salinity and density on pressure surfaces, temperature and salinity on density surfaces, salinity on temperature surfaces and thickness on density surfaces are shown. The temperature on pressure surfaces (fig. 7.10a) shows some hint of a general trend to lower temperatures as a function of time which may reflect the annual cycle. The salinity on pressure surfaces shows little sign of any general trend and seems to be rather variable, particularly during the First Time Series (Maps 1 - 7). The variance of salinity increases with depth and this is even more strongly seen in density on pressure surfaces (fig. 7.10c). This is undoubtedly due to internal wave activity. The lack of change in temperature variance with depth is presumably due to diurnal fluctuations at the shallower levels compensating for the reduced effect of internal waves there.

Since temperature and salinity must compensate each other on a density surface figures 7.10d and 7.10e are essentially identical apart from

the units. The general trend to lower temperatures is only apparent at the upper levels. The statistics of temperature for the First Time Series (Maps 1 - 7, i.e. 1L1 - 1L7) seem to be significantly different to those of the Second and Third Time Series (Maps 8 - 13, i.e. 2L1 - 2L2, 3L1 - 3L4); the mean values fluctuate much more and the standard deviations are considerably larger, often over 100 mK rather than of order 10 mK. The successive maps of the first time series were made with pauses between them and it is possible that the original water was lost, explaining the change in mean temperature whereas the later maps were made without break. The larger standard deviations must however reflect a greater variability in the thermohaline characteristics of the water at the earlier dates. The statistics of salinity on temperature surfaces (fig. 7.10f) show these same general features. Likewise it also shows that Map 7 (1L7) has an unusually low salinity for a given temperature, perhaps 0.2 - 0.3 ppt too low. It is implausible that this is genuine and it seems likely that the conductivity cell was partly blocked for the whole of the Map, or at least a sufficiently large part of it to affect the statistics used in the editing procedure (see chapter 5) thus allowing data, which elsewhere would have been classified as bad, to be accepted here as good.

The statistics of thickness or isopycnal spacing for selected isopycnals (fig. 7.10g) show considerable homogeneity throughout the experiment. The uppermost surface shown (σ_t = 23.45) appears to leave the pycnocline and enter the quasi-isopycnal layer ("mixed-layer") in some of the Maps of the First Time Series. The increasing variance at the lower levels reflects the decrease of the density gradient with depth; the thicknesses shown here are not normalized with the density gradient.

7.2.2 Statistics of the individual maps

The statistics of the individual Maps in profile form are shown in figure 7.11. Here appear the temperature and salinity as a function of density redrawn as a function of pressure using the mean density-

pressure relationship for the Map, the density as a function of pressure itself and also the temperature-salinity diagram. Perhaps the most striking feature seen when comparing these curve is the variability from Map to Map of the homogeneity of the quasi-homogenous layer, sometimes called "mixed-layer" and the transition from this layer to the pycnocline. In the first three Maps 1L1 -1L3 this layer shows considerable stratification with no clear-cut transition to the pycnocline. From Map 1L4 onwards the layer becomes more homogeneous and more sharply distinguished from the pycnocline. This is most extreme in Map 3L1. Maps 3L3 and 3L4 show increasing stratification again and a less distinct transition to the pycnocline.

The salinity maximum also shows fluctuations in its depth, value and shape; the depth is typically 40 dbar, the salinity 36.2 ppt and the temperature 25.5 °C. Here again Map 1L7 although apparently internally consistent has a considerably lower salinity than the other Maps.

7.2.3 The Maps

Figure 7.12 shows temperature on the density surfaces σ_t = 23.50, 24.00 and 24.50 kg m^{-3} for all thirteen Maps. In each case the mean temperature of the surface has been subtracted before plotting. The declared aim of the experiment (see chapter 1) was to follow the temporal development of structures with horizontal scales of about 10 km as they were advected eastward in the North Equatorial Counter Current. Inspection of individual Maps shows that there were indeed measurable structures with this sort of scale to be observed. Several of the Maps show similar characteristics to Map 3L3, namely regions of relatively weak temperature gradients separated by bands of strong temperature gradients, particularly Maps 1L3, 1L4, 1L6, 2L2, 3L1, 3L2.

The Maps of the First Time Series show relatively little similarity with one another, but as can be seen from Table I there were sometimes gaps of several hours between the individual Maps in which the ship was used for other work. The relative navigation was not conducted

continuously but instead the gaps were bridged by estimating the mean current and taking up the survey at the estimated position of the water mass at the time of continuation. It is clear that this could easily lead to loss of the water mass being studied. In addition vertical shears between the surface water, where the relative navigation was conducted, and the thermocline layers being observed could also have lead to loss of the water mass under investigation. Another problem, which is also apparent from the figures, is that the typical scale of the features observed is comparable or larger than the size of the Maps leading to difficulty in identifying the same feature in successive Maps. Finally there is the potential problem of the time scales of the temporal development of the structures observed being sufficiently short that a structure observed in one Map would be deformed out of recognition before the subsequent Map were completed (also implying that the individual Maps would be very unsynoptic).

Bearing these difficulties in mind it is interesting to look at the figures for the Second and Third Time Series. The Second Time Series consists of two small Maps (2L1, 2L2) surveyed in quick succession (see Table I). The patterns of temperature on density surfaces in these two Maps show considerable similarity to one another. All three surfaces shown have an area of colder than average water in the north and warmer than average water in the south. The mean temperatures of the respective surfaces are all with 0.01 K of each other, implying that more or less the same mass of water has been observed each time.

The Third Time Series (see Table I) consists of four maps of gradually increasing size. The size was progressively increased in order to compensate for inaccuracies in the relative navigation of slippage of the thermocline water due to vertical shear hoping that the water originally surveyed would be found somewhere within the larger survey later. Comparing the first two Maps, 3L1 and 3L2, reveals certain similarities. The upper surface (σ_t = 23.50 kg m^{-3}) shows warm water in the north and cold water in the south while the lower two surfaces (σ_t = 24.00 kg m^{-3}) show warmer water in the south. The lower two surfaces also have very similar mean temperatures. When we compare the

first two Maps in the Time Series with the Third we must remember that this map is rather larger (see Table I). However in the centre of Map 3L3 it is possible to identify an area in which in the upper surface there is an east-west band of stronger temperature gradient with warmer water to the north and colder water to the south, as in the upper surface of the first two Maps. If we now consider the lower two surfaces in the same part of Map 3L3 we find that cold water lies to the north of warm water, again as in the lower two surfaces of the two preceeding Maps. The mean temperatures of the surfaces of Map 3L3 also compare well with those of Maps 3L1 and 3L2. Comparing Map 3L4 with Map 3L3 is somewhat less fruitful though at the upper level the water is warmer in the west in both cases. At the middle level a band of cold water crosses the map through with somewhat different orientation and at the lowest level both Maps show a tongue of cold water projecting from the east though with different form. The mean temperatures of the surfaces are very similar.

In Figure 7.13 the isopycnal spacing distributions corresponding to the thermohaline structures of Figure 7.12 are shown. These distributions are more difficult to interpret. Even in the case of those Maps where there is some similarity in the thermohaline structures from Map to Map, 2L1 and 2L2, 3L1 and 3L2, there seems to be little similarity in the distribution of isopycnal spacing. In some of the maps of the First Time Series there is some hint of a similar strike of the structure of the isopycnal spacing and the thermohaline structure.

The temperature, salinity and density at a constant depth (16 dbar) in the surface layer ("mixed-layer") of all the Maps are shown in Figure 7.14. Whereas the thermohaline properties of the water in the thermocline can be regarded as conservative over the period of time required to conduct a Batfish survey of the type described in this report. This is certainly not true for the water close to the surface. The temperature is changed by insolation during the day and surface cooling at night and the salinity can be changed by precipitation from showers. The temperature distributions shown (Figure 7.14) are thus a

mixture of spatial variation plus the temporal variation convoluted by the time of day of the observation. The similarity of the salinity and density distribution to each other suggests that the surface layer density is principally determined by the salinity. In some of the Maps (2L1, 2L2, 3L2) there is some hint of similarity between the salinity distribution in the surface layer and thermohaline structure in the pycnocline below.

8 CONCLUSIONS

While the strongest signals in the finescale (1 - 20 km) in the North Equatorial Counter Current as observed in the GATE Lagrangian Batfish Experiment were internal waves, it is possible, using isopycnic analysis, to reveal and study structures which are the result of other dynamics. The curvature of the TS-distribution above the salinity maximum and the statistics of salinity on density surface rule out the possibility that the observed isopycnal thermohaline structures are the result of mixing by breaking internal waves. The stable salinity gradient also rules out the possibility of double diffusive phenomena playing a rôle above the salinity maximum. the presence of two local water masses suggests the action of quasi-isopycnal mixing by quasi-geostrophic motions. Judging from the maps these have scales of about 10 km. The sloping nature of the thermohaline structure (1:1000) is not unlike that of fronts, as described in the model presented by MacVean and Woods (1980). The thermohaline structures are however purely passive and in order to observe the dynamics the thickness was calculated. As a difference (differential) quantity calculated from data this variable is naturally somewhat less reliable than, say, temperature on density surfaces. Furthermore the thickness could be affected by high-mode internal waves, though their energy was small (Käse & Siedler, 1980), or by steeply sloping internal waves combining with the sloping (1:4) Batfish track. Inspection of the data show that the thickness is a more variable quantity than isopycnic temperature but it sometimes shows larger areas of anomalously high thickness supported by data from several legs. The rather poor spectral window of the data shown in the maps, perhaps one and a half decades, prevents precise determination of the horizontal length scales of the structures observed, nevertheless the length scales of order 10 km of the structures observed (see figures) do bear comparison with those predicted by MacVean's (1980) model of frontal instability.

Visual comparison of the isopycnal thermohaline structures from successive maps in the various time-series reveals only limited similarity and this seems to be due to the maps being rather small

relative to the size of the structures surveyed. In order to make some assessment of temporal development, it would seem to be necessary to have a combination of several of the isolated structures observed in these Maps so that reidentification of features would be more reliable. Additional difficulties are undoubtedly introduced by temporal development of the structures being observed and cumulative errors in the relative navigation leading to the structures surveyed in one map being (partly) lost before they were observed in the subsequent map. This seems to be the principal weakness of the data set and the chief recommendation for future experiments is that fewer surveys covering larger areas should be made. The power of isopycnic analysis to enable structures due to physical processes other than internal waves in the presence of strong internal wave fields to be seen has been amply demonstrated and this technique will undoubtedly find much application in the analysis of simlar data sets.

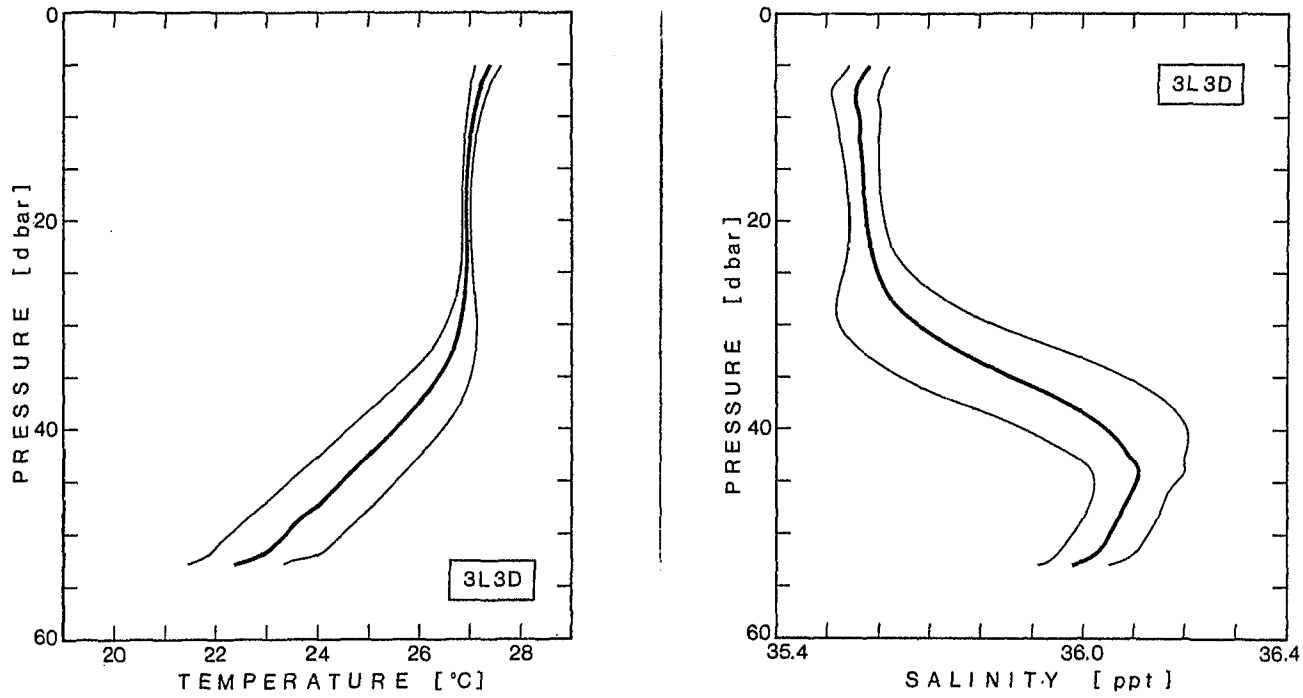

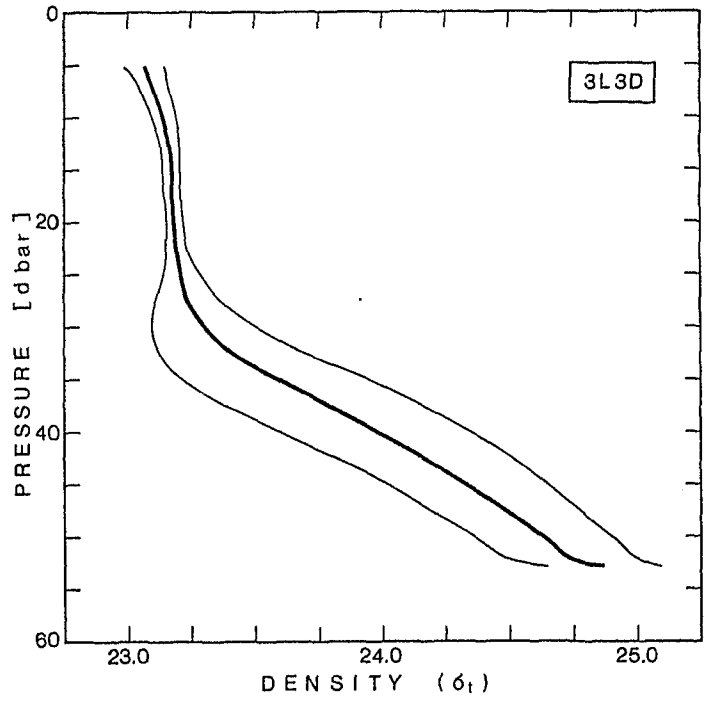

Figure 7.1 :
Profiles of the mean and standard deviation of potential temperature, salinity and density on surfaces of constant pressure.

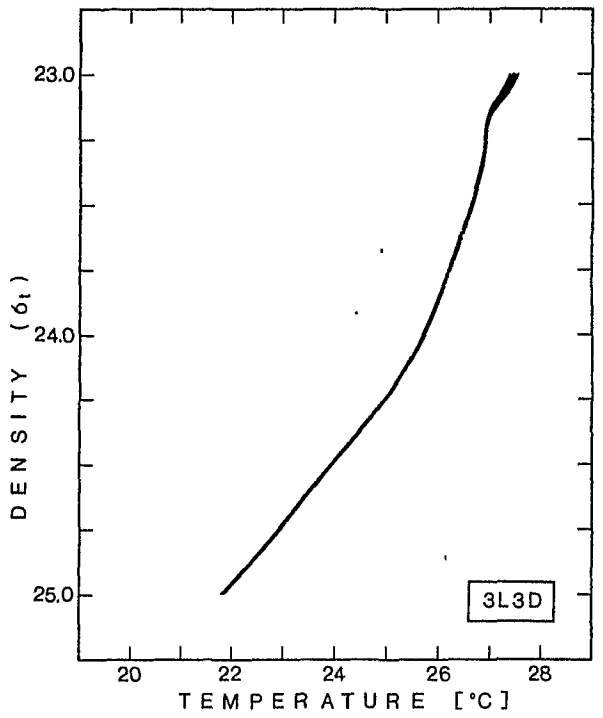

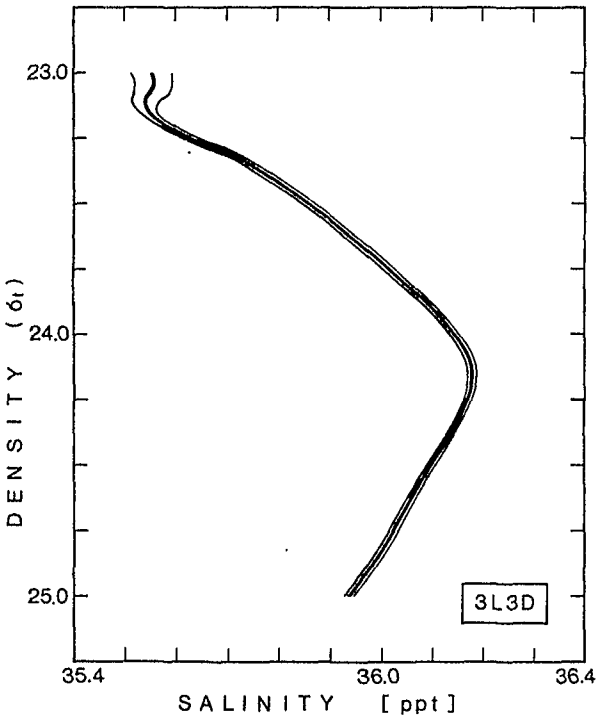

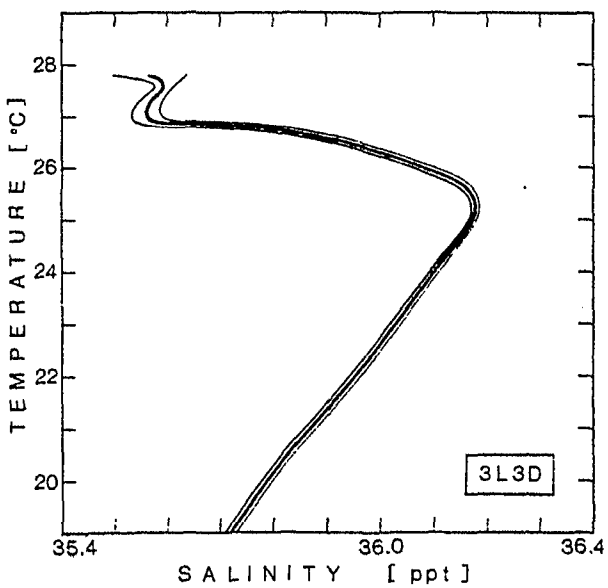

Figure 7.2 : Profiles of the mean and standard deviation of potential temperature and salinity on surfaces of constant σ_T (upper figures) and also salinity on surfaces of constant potential temperature (mean T-S diagram, lower figure).

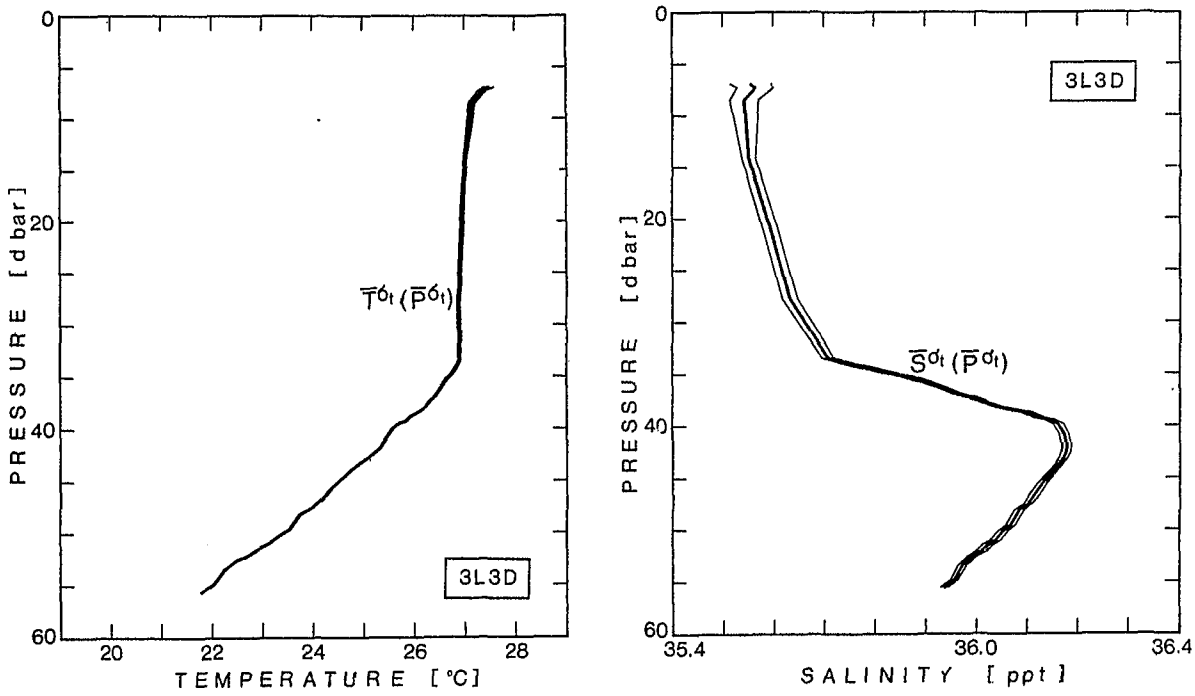

Fig. 7.3 a) : Profiles of the mean and standard deviation of potential temperature and salinity on surfaces of constant σ_T redrawn as functions of pressure using the mean relationship of σ_T to pressure.

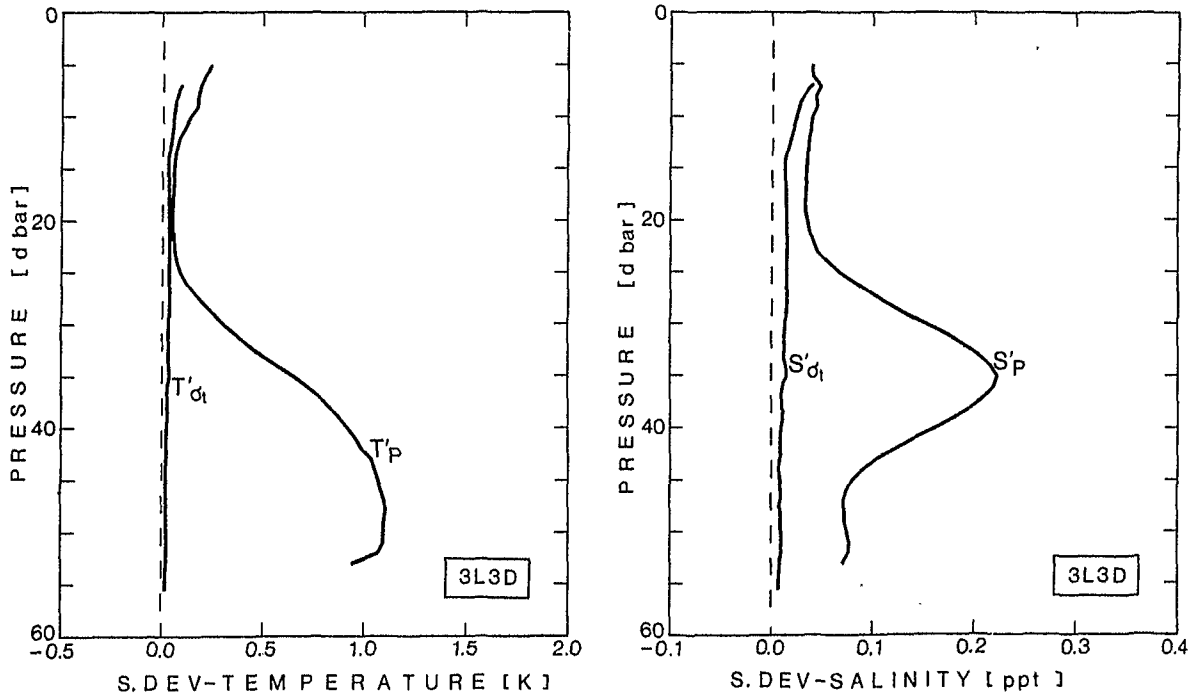

Fig. 7.3 b) : Profiles of the standard deviation of potential temperature and salinity on surfaces of constant pressure and on surfaces of constant density, redrawn as a function of pressure, for comparison.

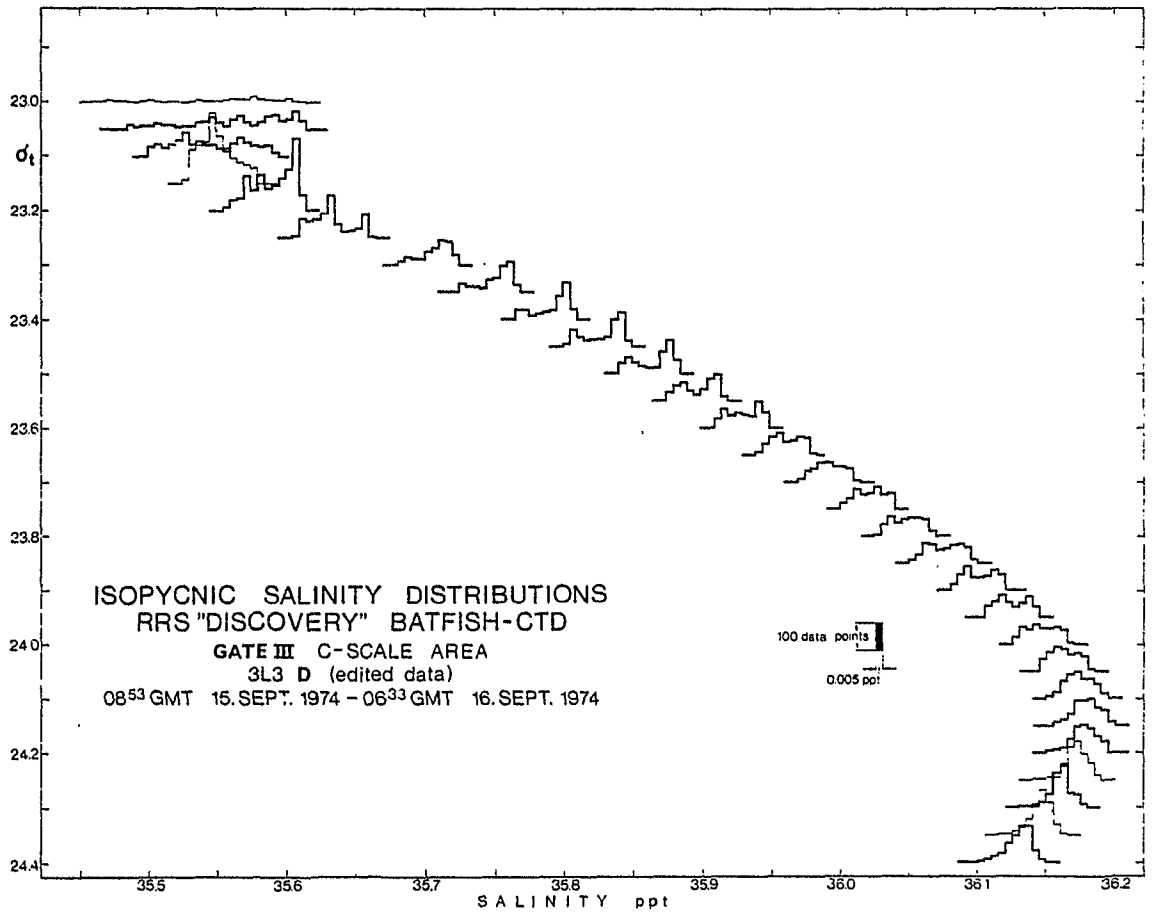

Figure 7.4 : Histograms of salinity on surfaces of constant density showing the bimodal distribution in the region above the salinity maximum.

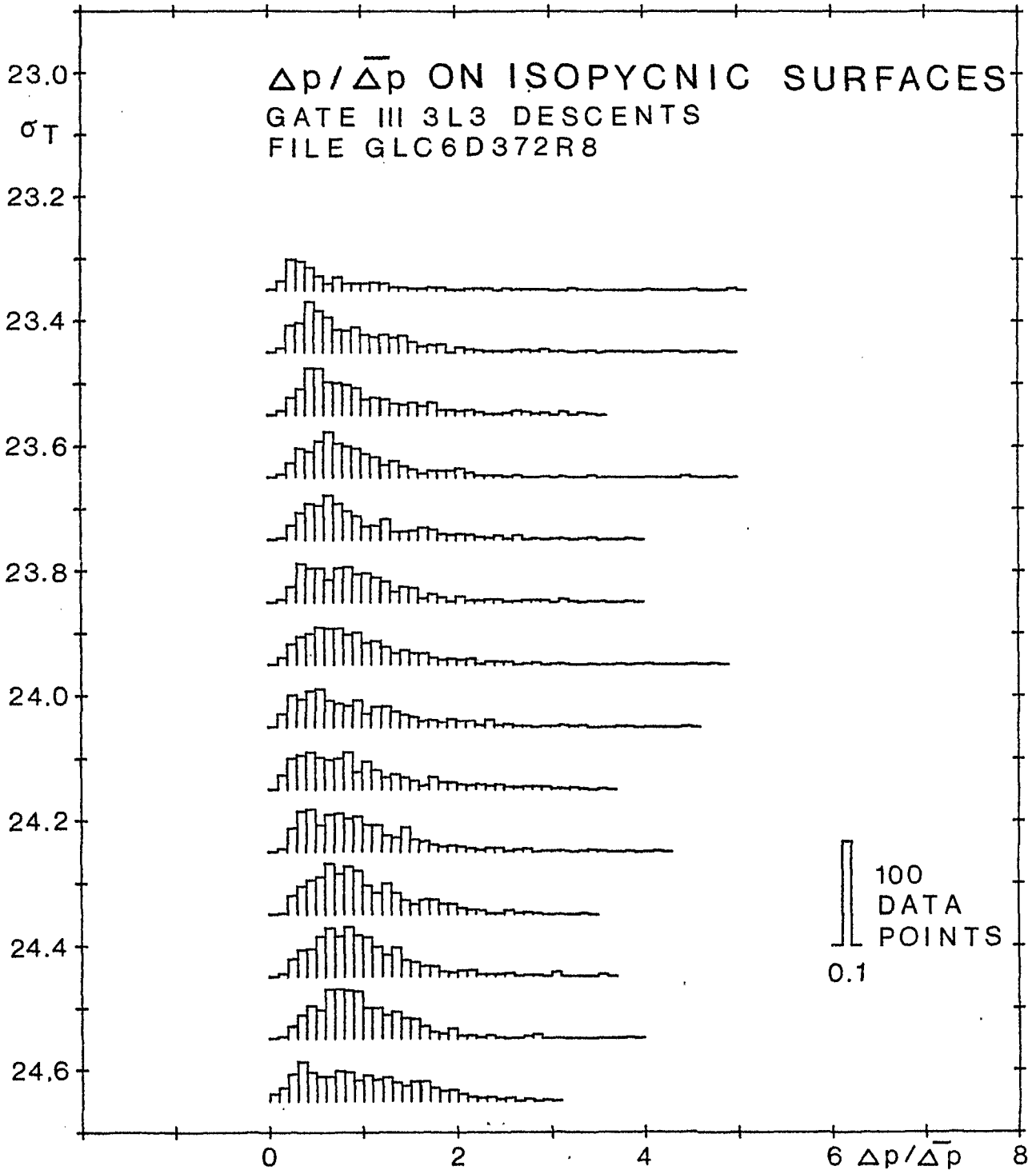

Fig. 7.5:

Histograms of normalized thickness on surfaces of constant σ_t. The thicknesses are normalized by the mean thickness on their surface to remove the effect of changes in the mean density gradient.

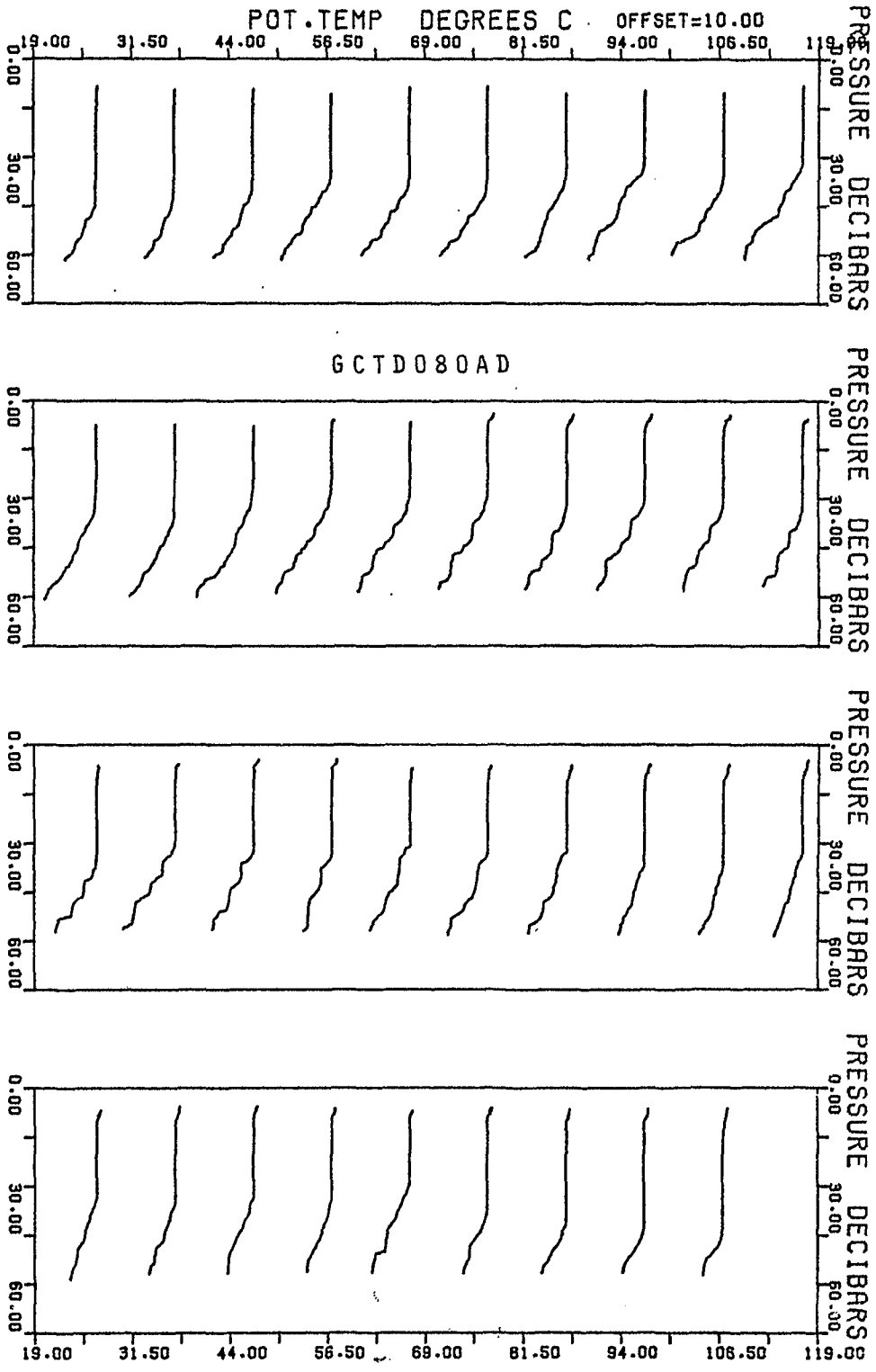

Fig. 7.6 a) :

Profiles of potential temperature as function of pressure from leg 6 of Map 3L3.

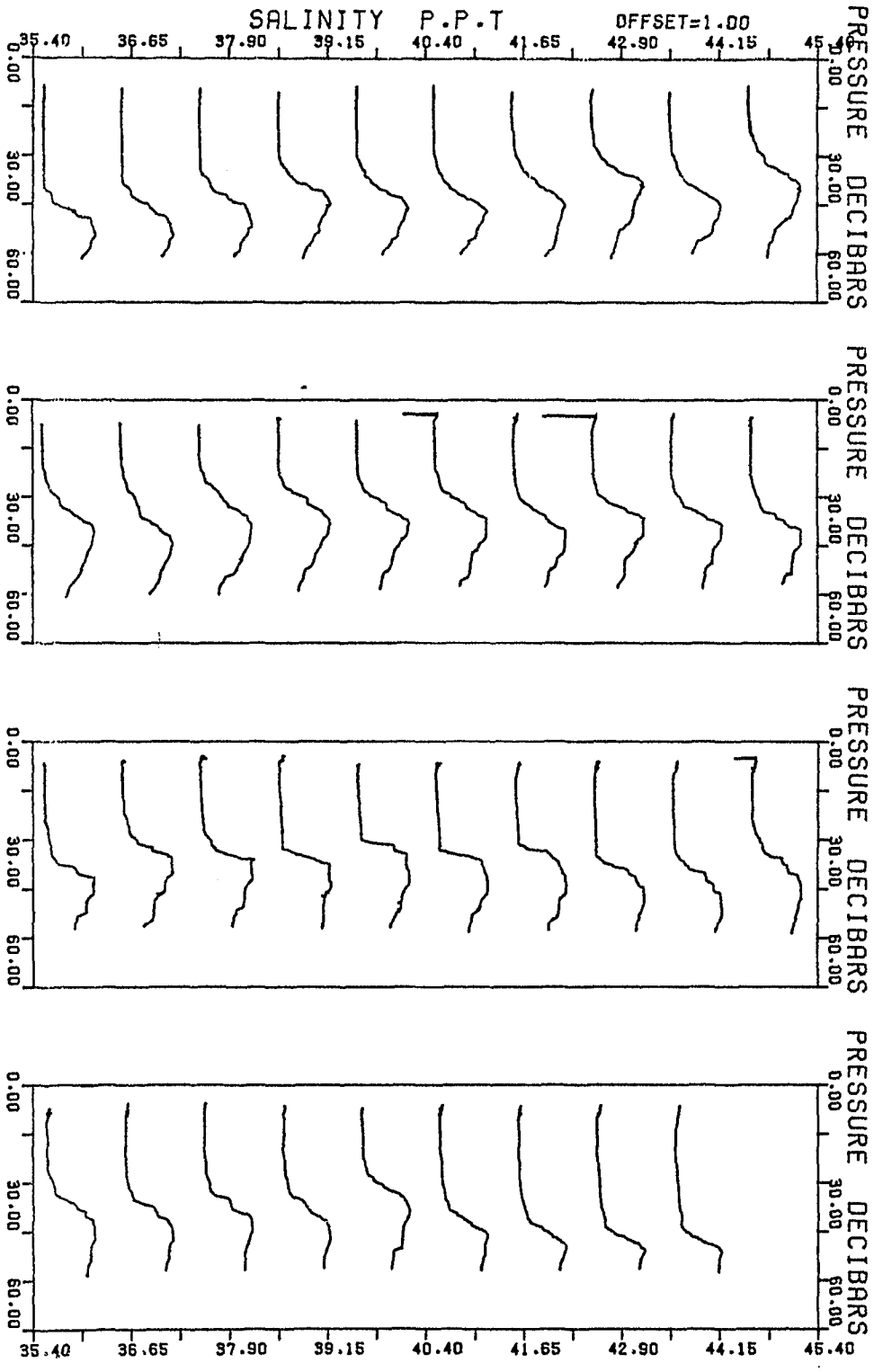

Fig. 7.6 b) :

Profiles of salinity as function of pressure from leg 6 of Map 3L3.

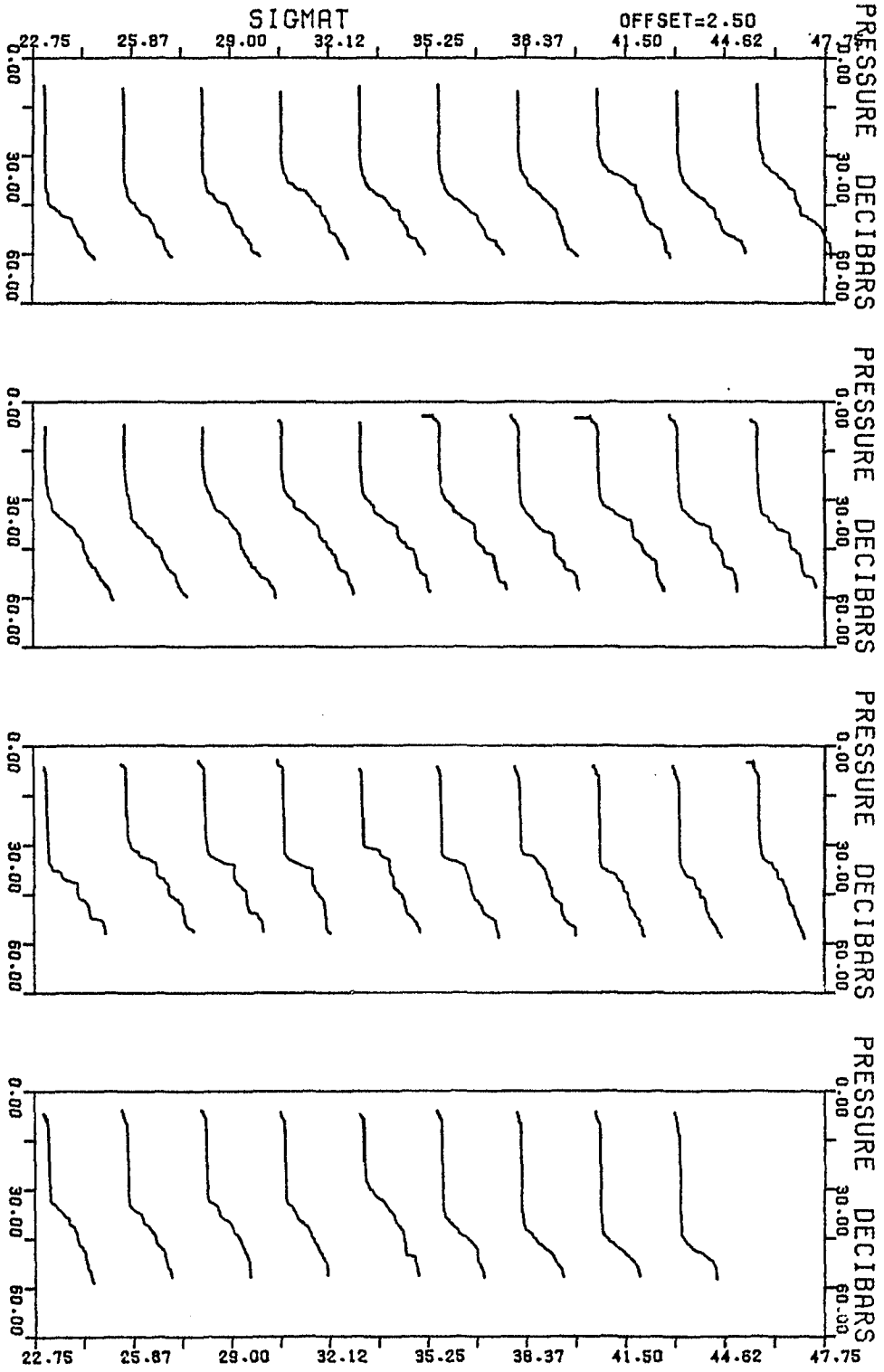

Fig. 7.6 c) :

Profiles of density as function of pressure from leg 6 of Map 3L3.

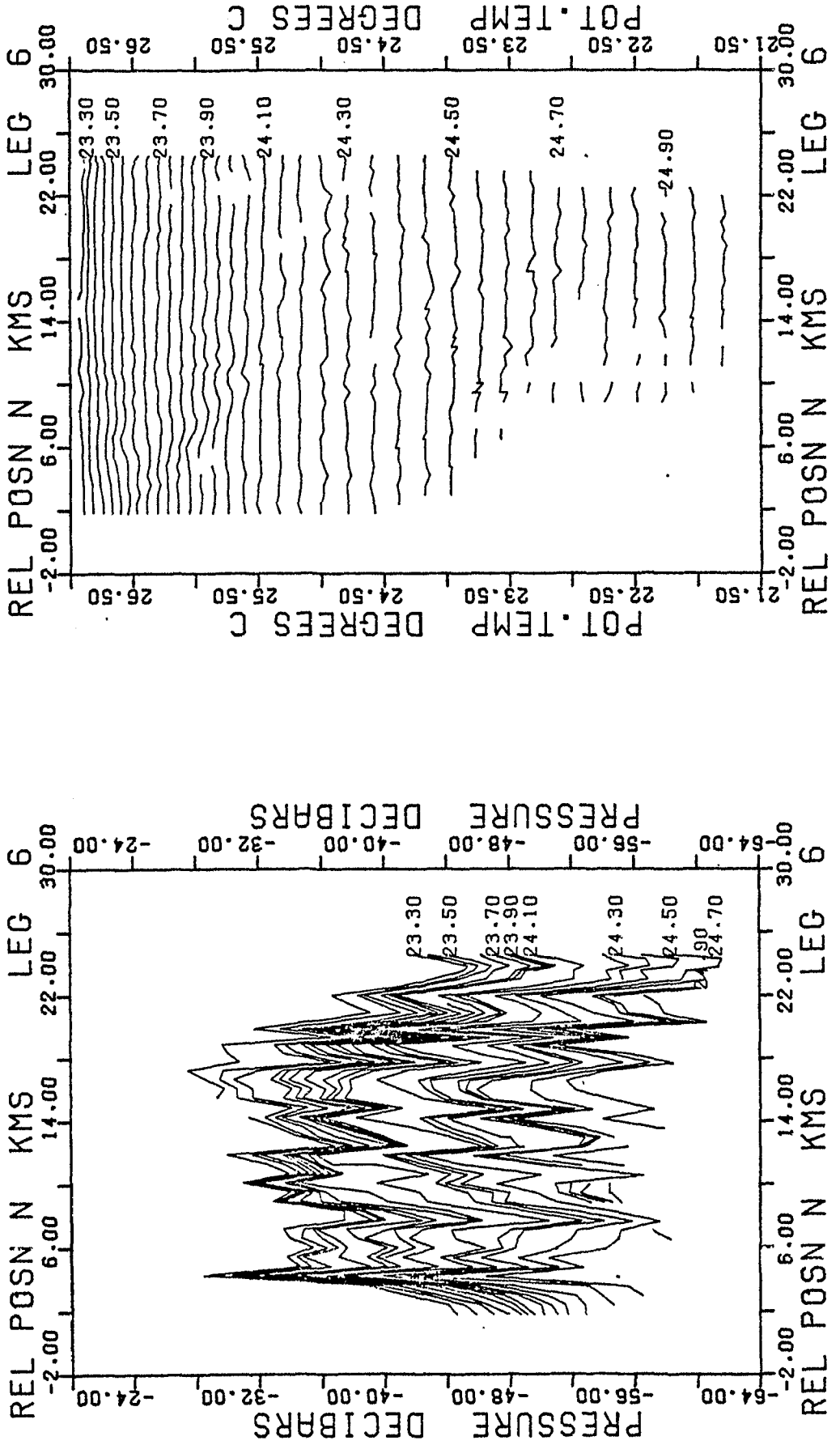

Fig. 7.7 a) : Pressure and temperature of isopycnals from leg 6 of Map 3L3. The pressure (or depth) of the isopycnals shows the internal wave activity . The temperature of the isopycnals shows thermohaline structures. Contour interval of potential temperature on isopycnals 0.05 kg m^{-3}. Contour interval of pressure on isopycnals 0.10 kg m^{-3}.

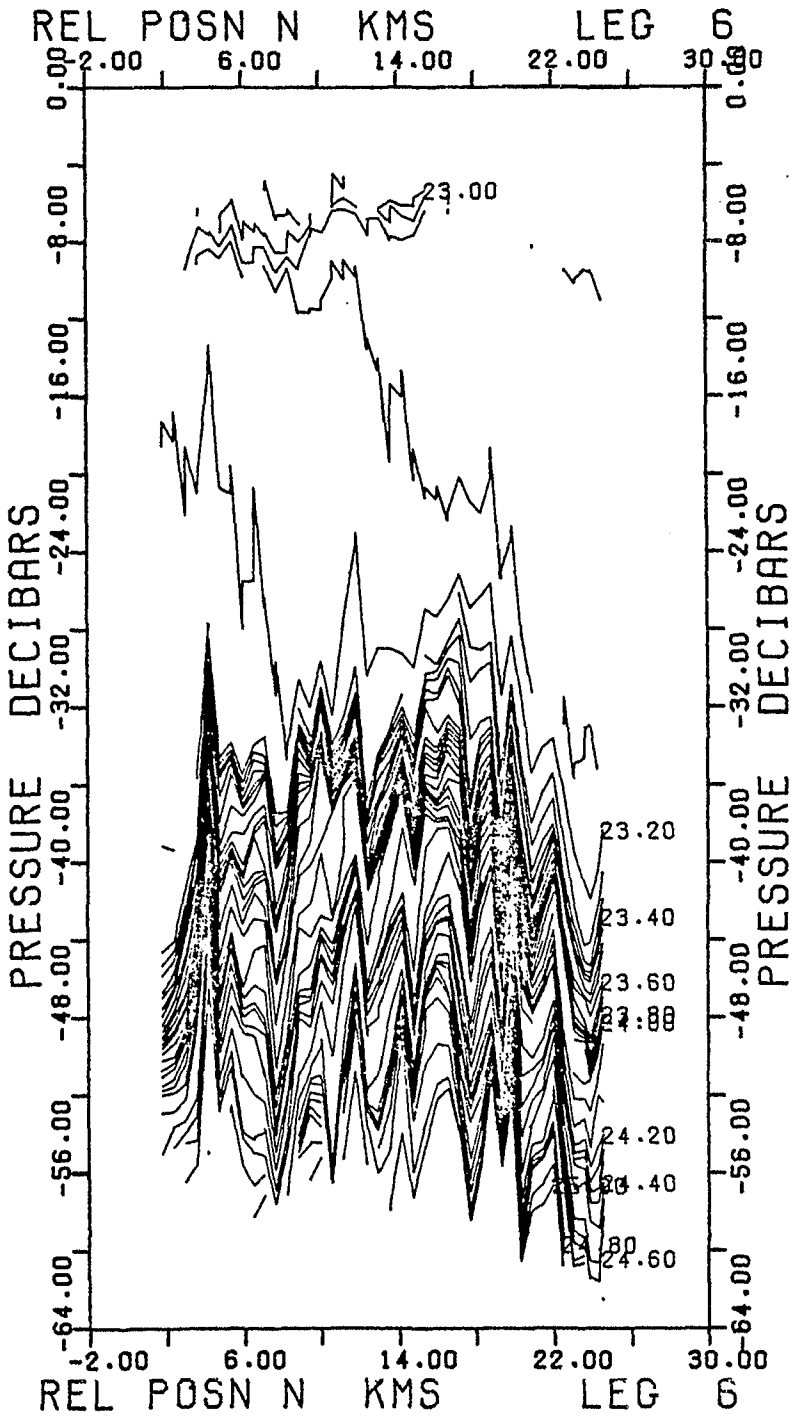

Fig. 7.7 b) : Pressure of isopycnals in the range σ_t = 23.00 - 25.00 kg m^{-3}.
Contour interval 0.05 kg m^{-3}.

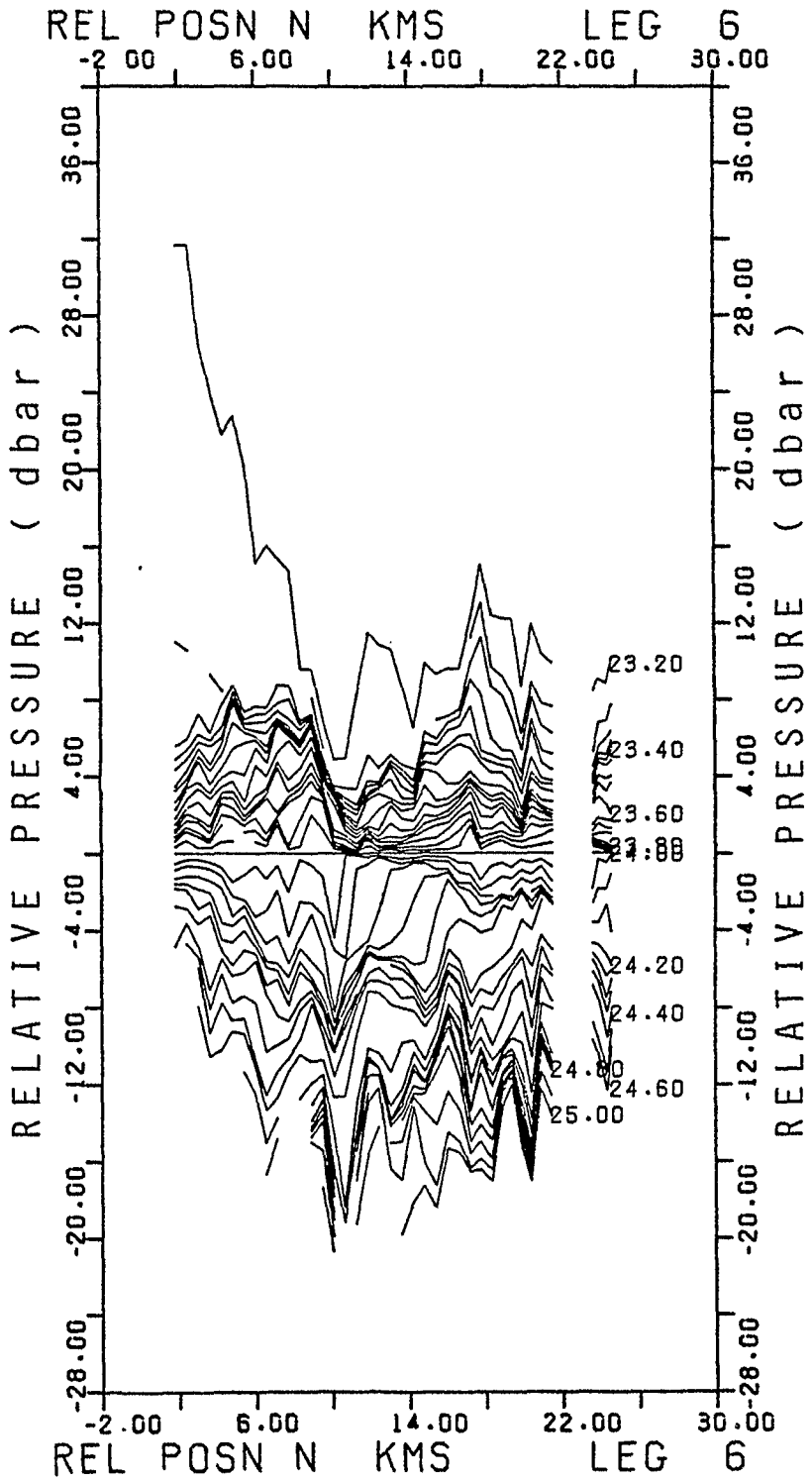

Fig. 7.7 c) : Pressure, relative to the pressure on σ_t = 24.00 kg m^{-3}, on surfaces of constant σ_t in the range σ_t = 23.20 - 25.00 kg m^{-3}.

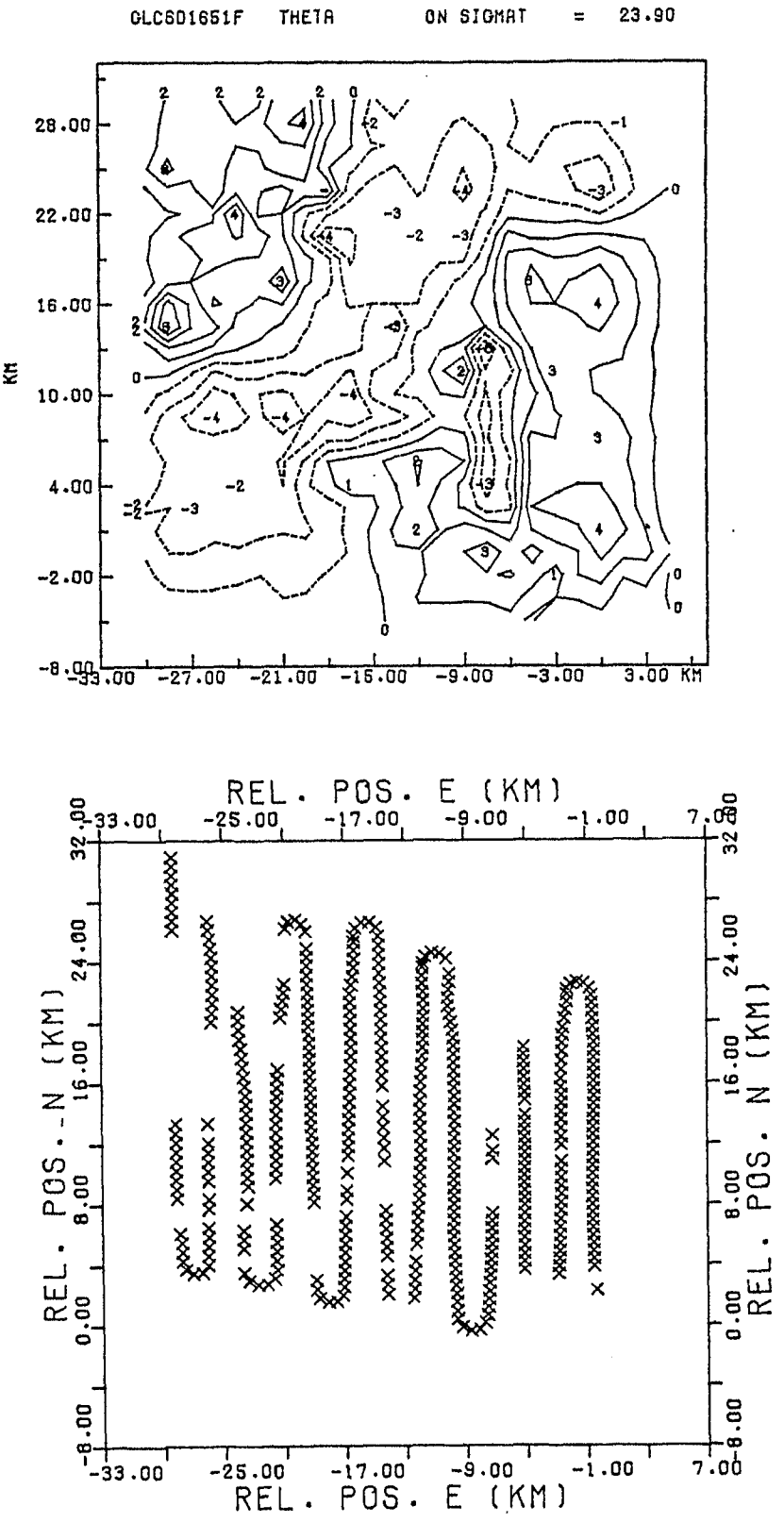

Fig. 7.8 a) :

Contoured map of potential temperature on the 23.90 kg m^{-3} isopycnal (upper figure). The contours are of the temperature deviation (units in 10^{-2} K) from the mean temperature (25.941 °C) on the surface.
Positions of the data relative to the origin of the map (lower figure).

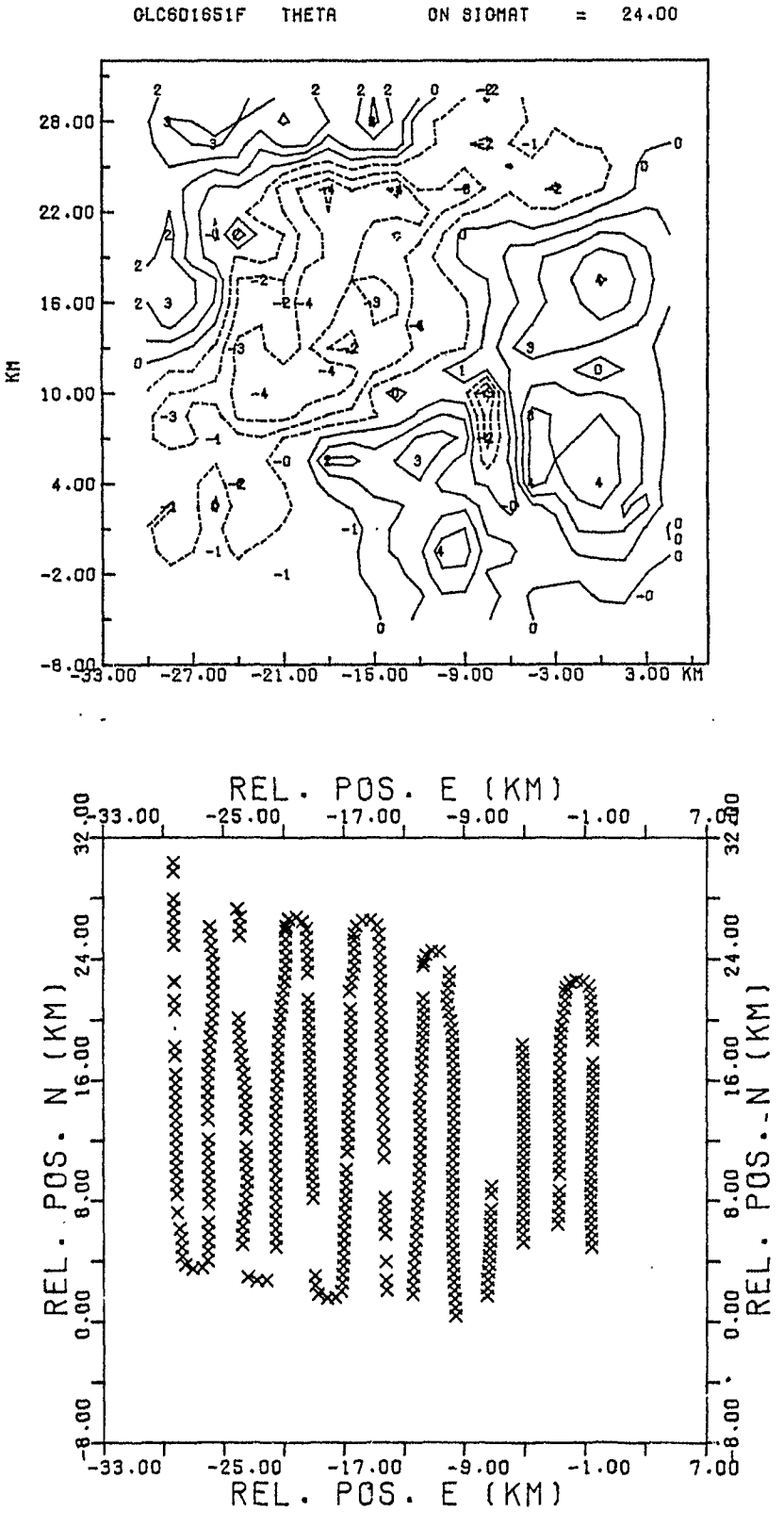

Fig. 7.8 b) :

Contoured map of potential temperature on the 24.00 kg m^{-3} isopycnal (upper figure). The contours are of the temperature deviation (units in 10^{-2} K) from the mean temperature (25.730 °C) on the surface.
Positions of the data relative to the origin of the map (lower figure).

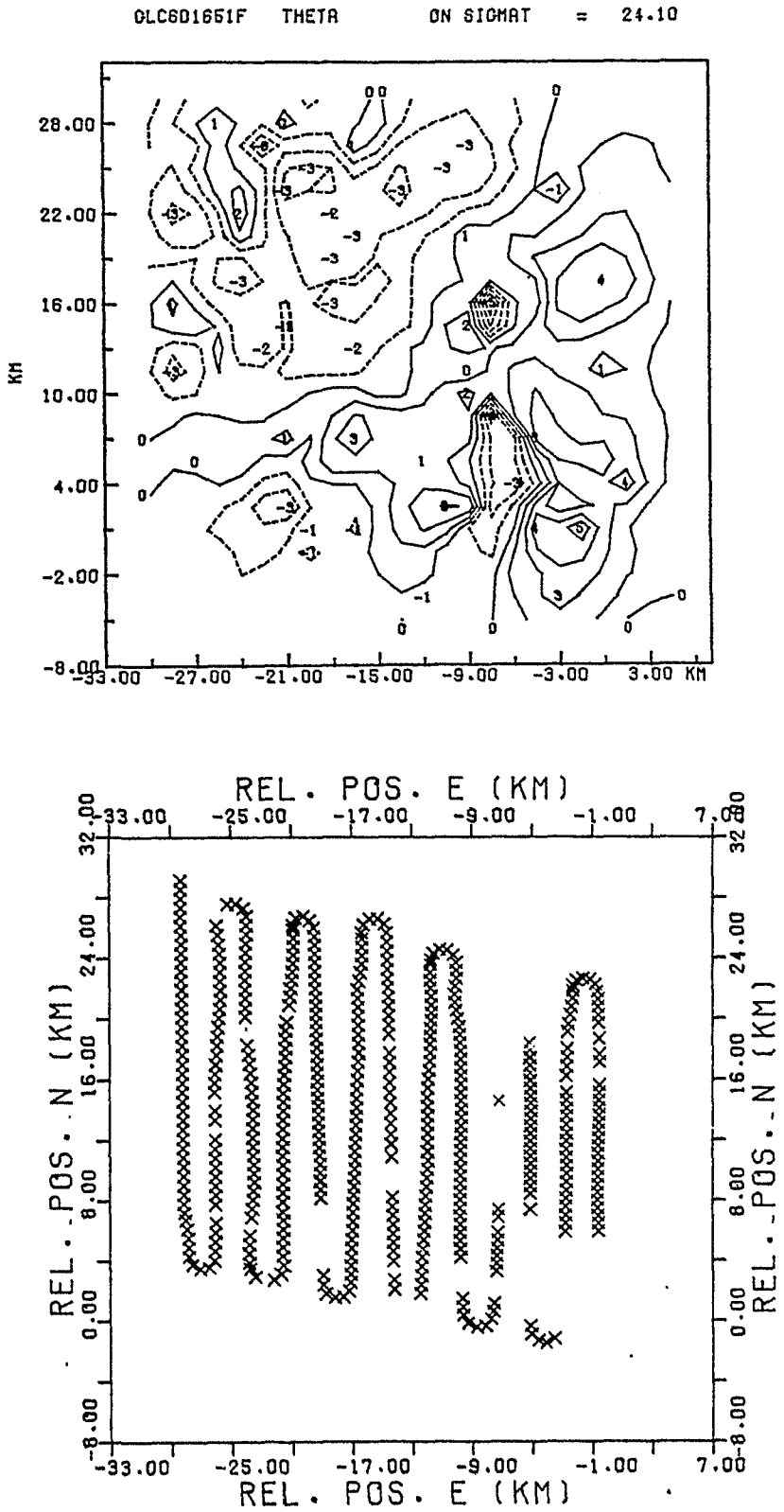

Fig. 7.8 c) :

Contoured map of potential temperature on the 24.10 kg m^{-3} isopycnal (upper figure). The contours are of the temperature deviation (units in 10^{-2} K) from the mean temperature (25.474 °C) on the surface.
Positions of the data relative to the origin of the map (lower figure).

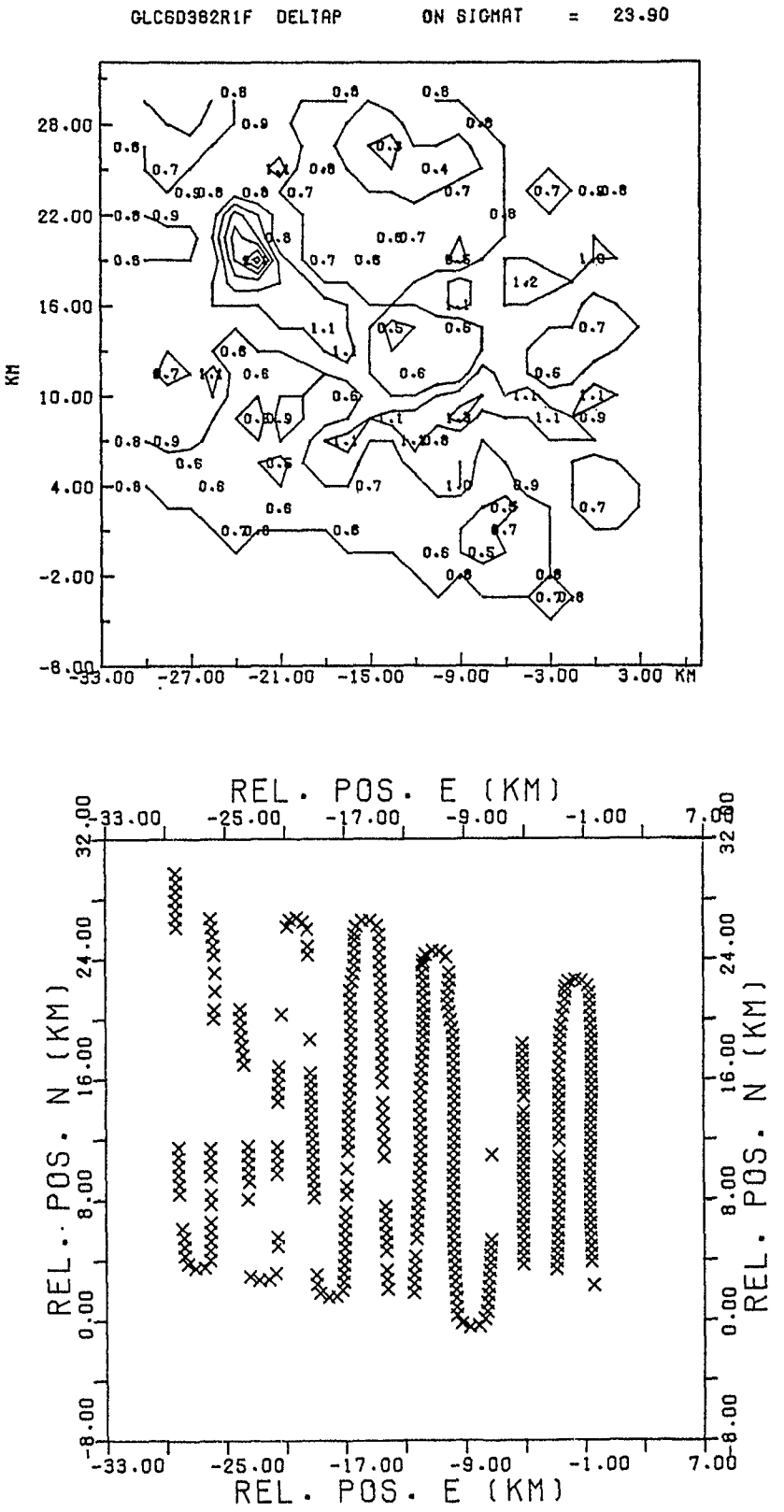

Fig. 7.8 d) :

Contoured map of thickness on the 23.90 kg m^{-3} isopycnal (upper figure, units in dbar) and the positions of the data relative to the origin of the map (lower figure).

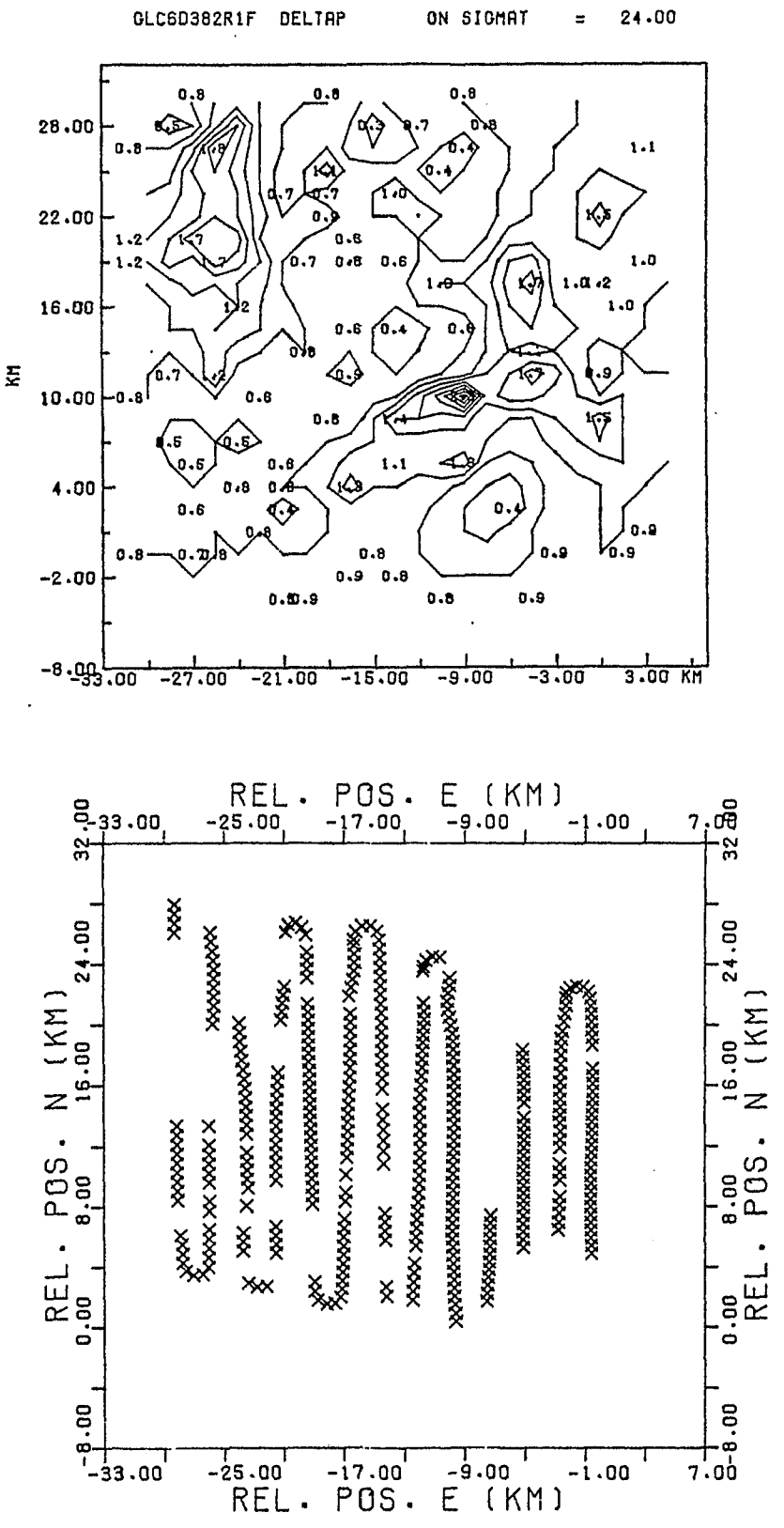

Fig. 7.8 e) :

Contoured map of thickness on the 24.00 kg m^{-3} isopycnal (upper figure, units in dbar) and the positions of the data relative to the origin of the map (lower figure).

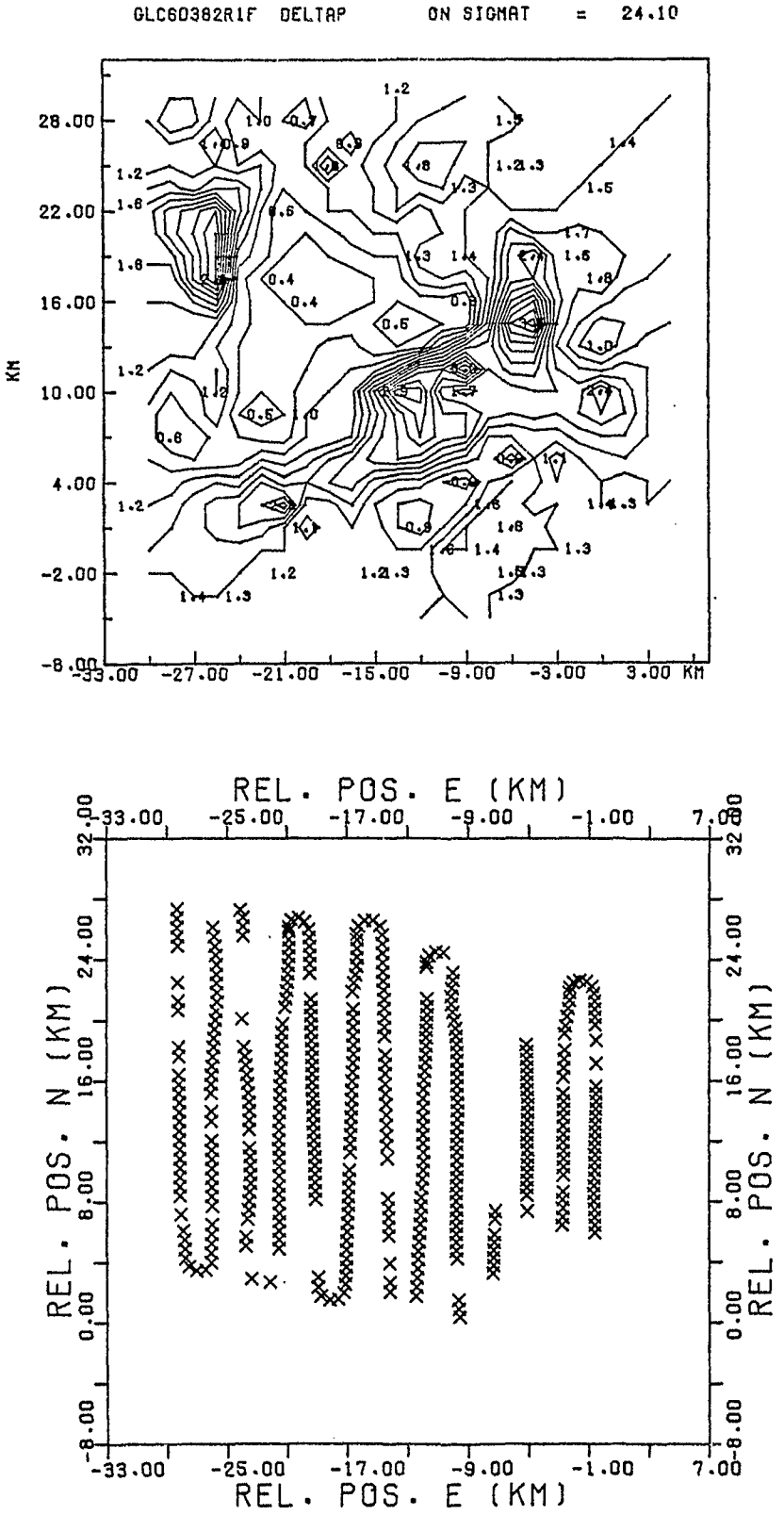

Fig. 7.8 f) :

Contoured map of thickness on the 24.10 kg m^{-3} isopycnal (upper figure, units in dbar) and the positions of the data relative to the origin of the map (lower figure).

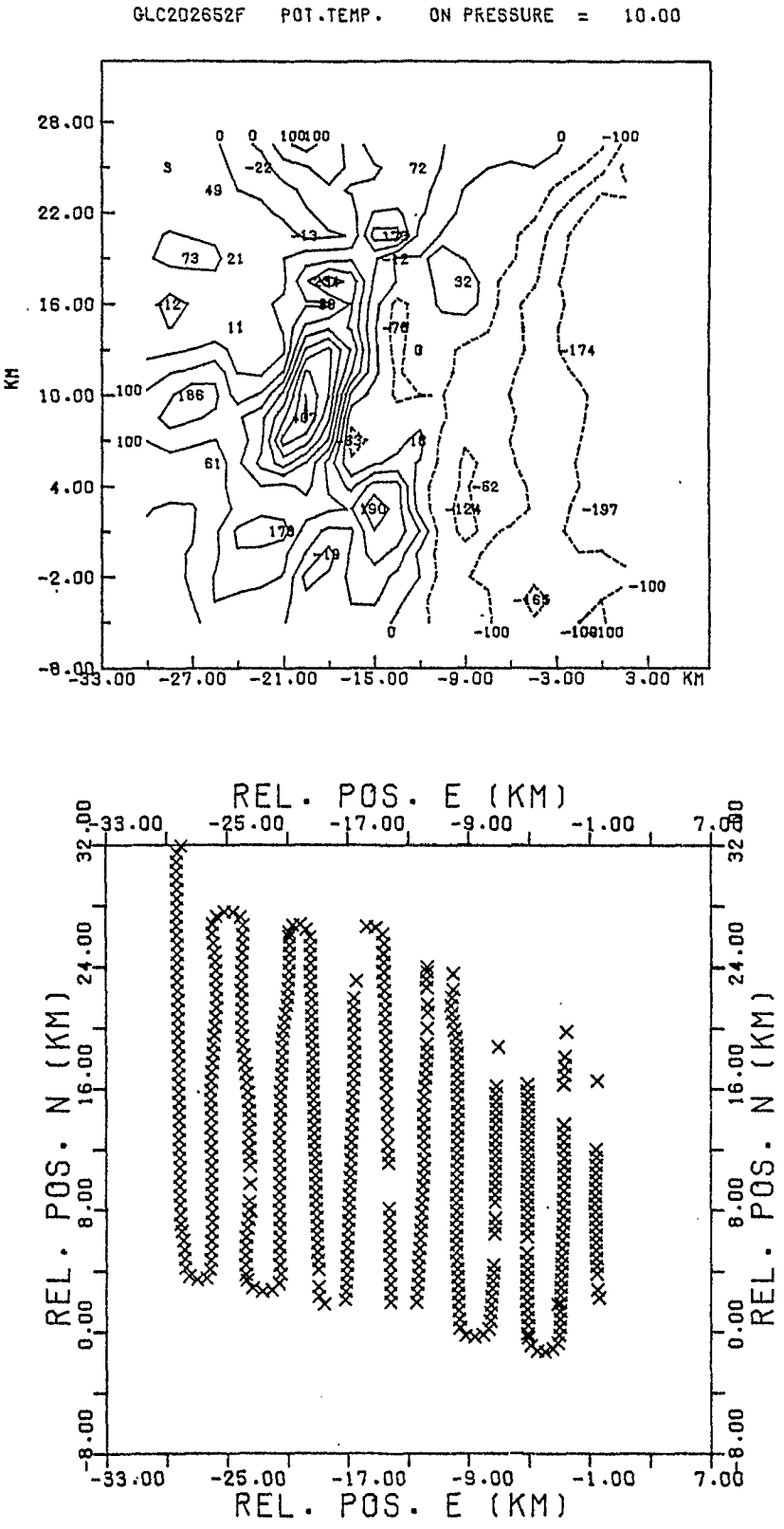

Fig. 7.9 a) :

Contoured map of potential temperature on the 10 dbar pressure surface (upper figure). The contours are of the temperature deviation (units in 10^{-3} K) from the mean temperature (27.029 °C) on the surface.
Positions of the data relative to the origin of the map. (lower figure).

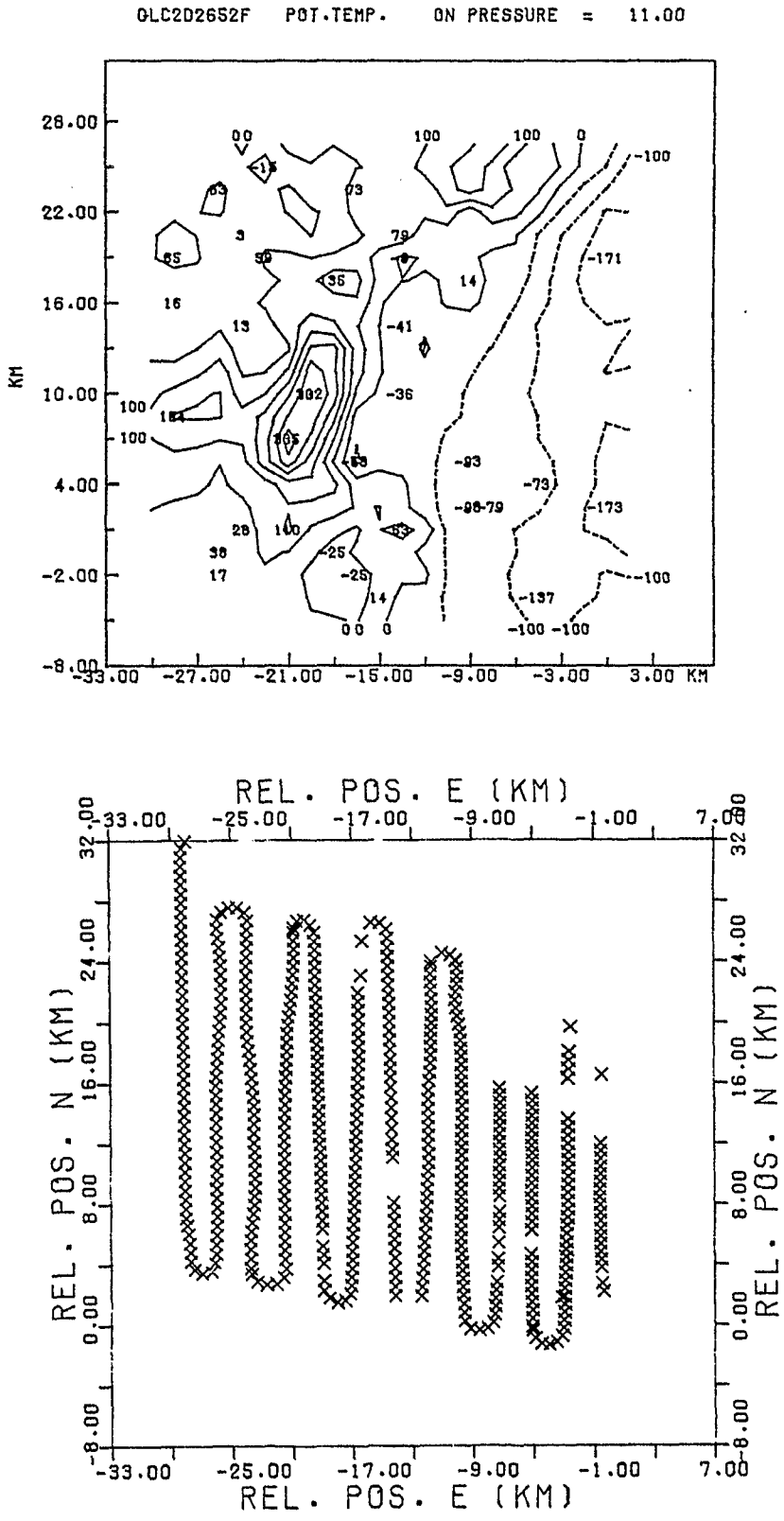

Fig. 7.9 b) :

Contoured map of potential temperature on the 11 dbar pressure surface (upper figure). The contours are of the temperature deviation (units in 10^{-3} K) from the mean temperature (27.007 °C) on the surface.
Positions of the data relative to the origin of the map (lower figure).

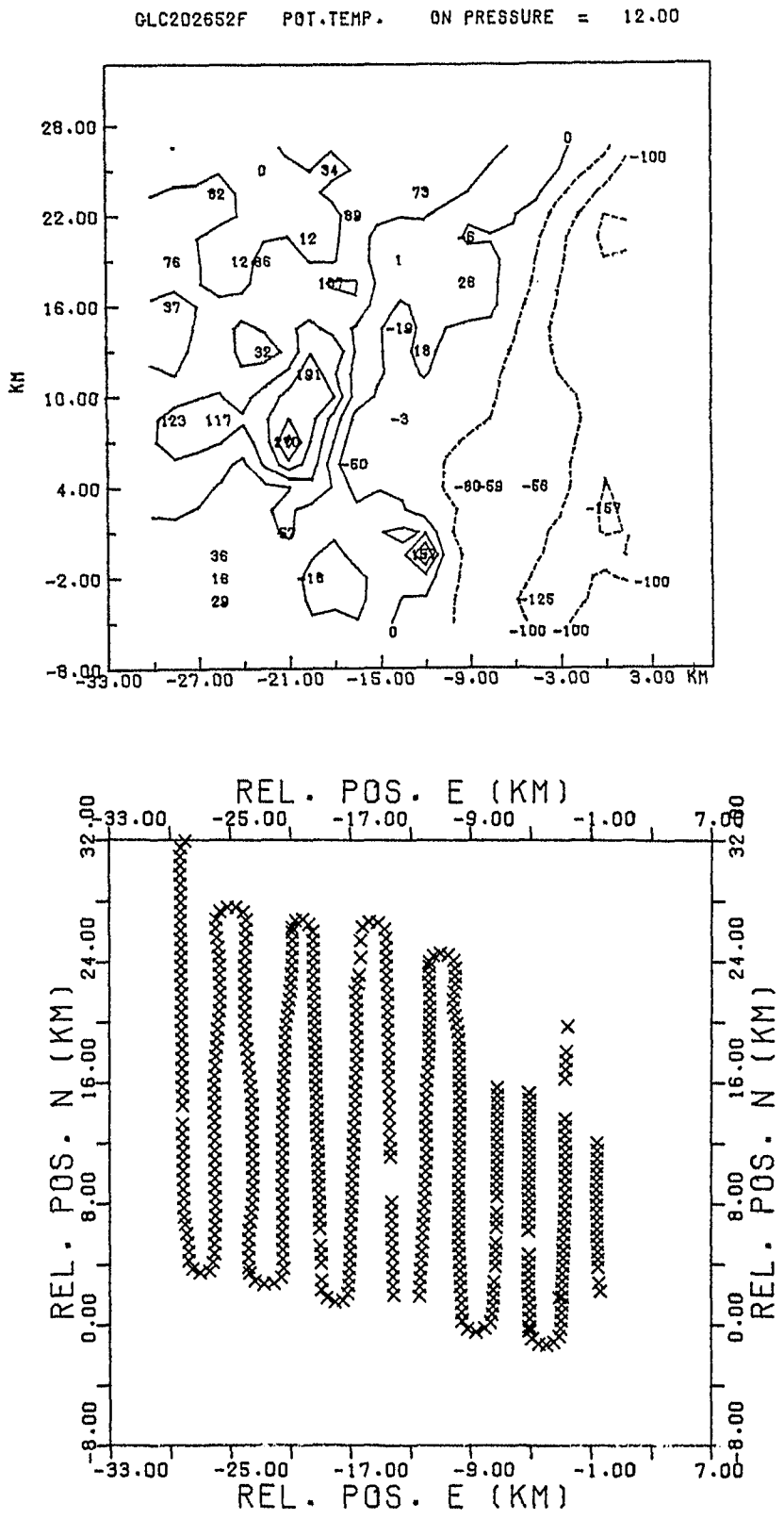

Fig. 7.9 c) :

Contoured map of potential temperature on the 12 dbar pressure surface (upper figure). The contours are of the temperature deviation (units in 12^{-3} K) from the mean temperature (26.982 °C) on the surface.
Positions of the data relative to the origin of the map. (lower figure).

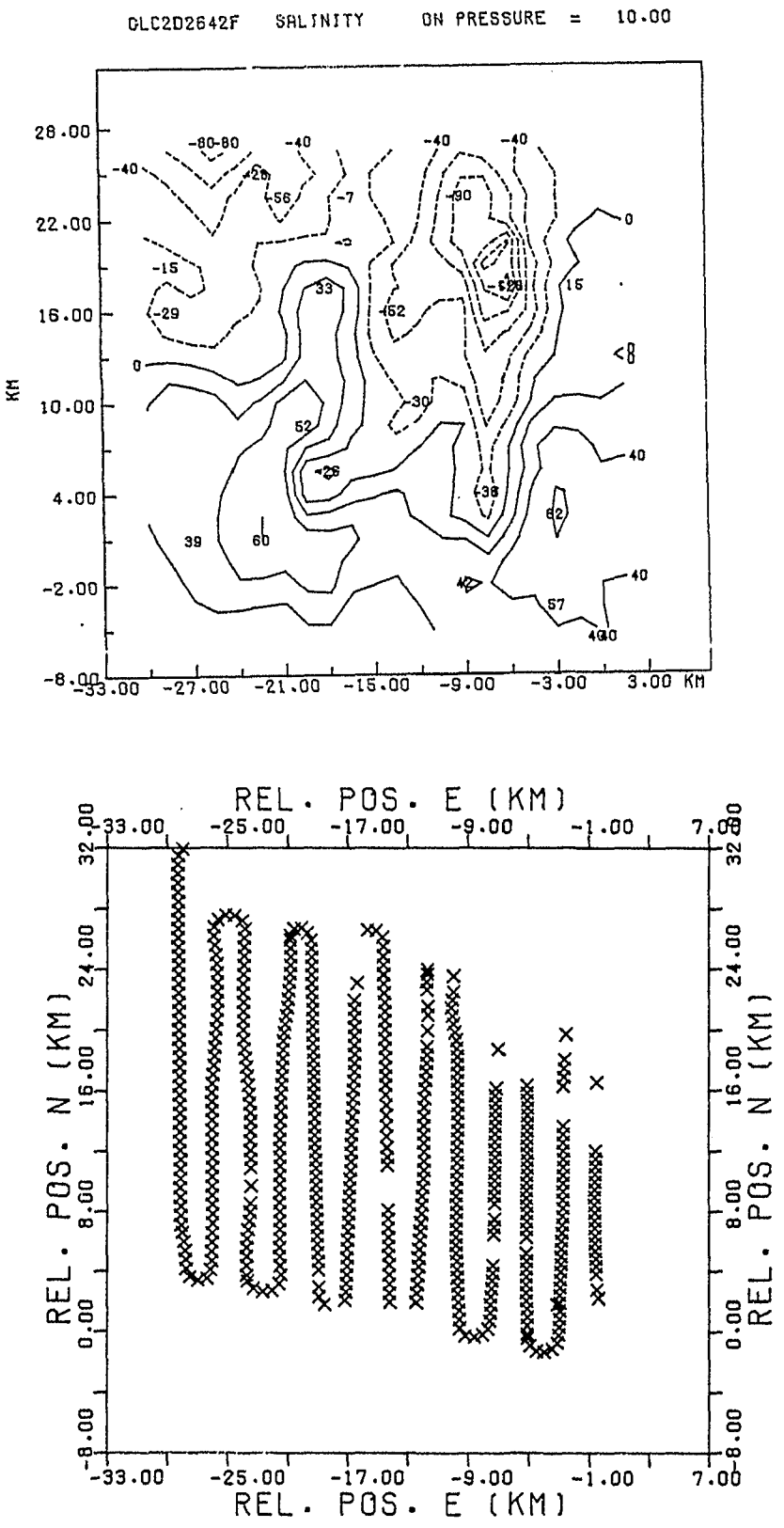

Fig. 7.9 d) :

Contoured map of salinity on the 10 dbar pressure surface (upper figure). The contours are of the salinity deviation (units in 10^{-6}) from the mean salinity (35.563×10^{-3}) on the surface.
Positions of the data relative to the origin of the map (lower figure).

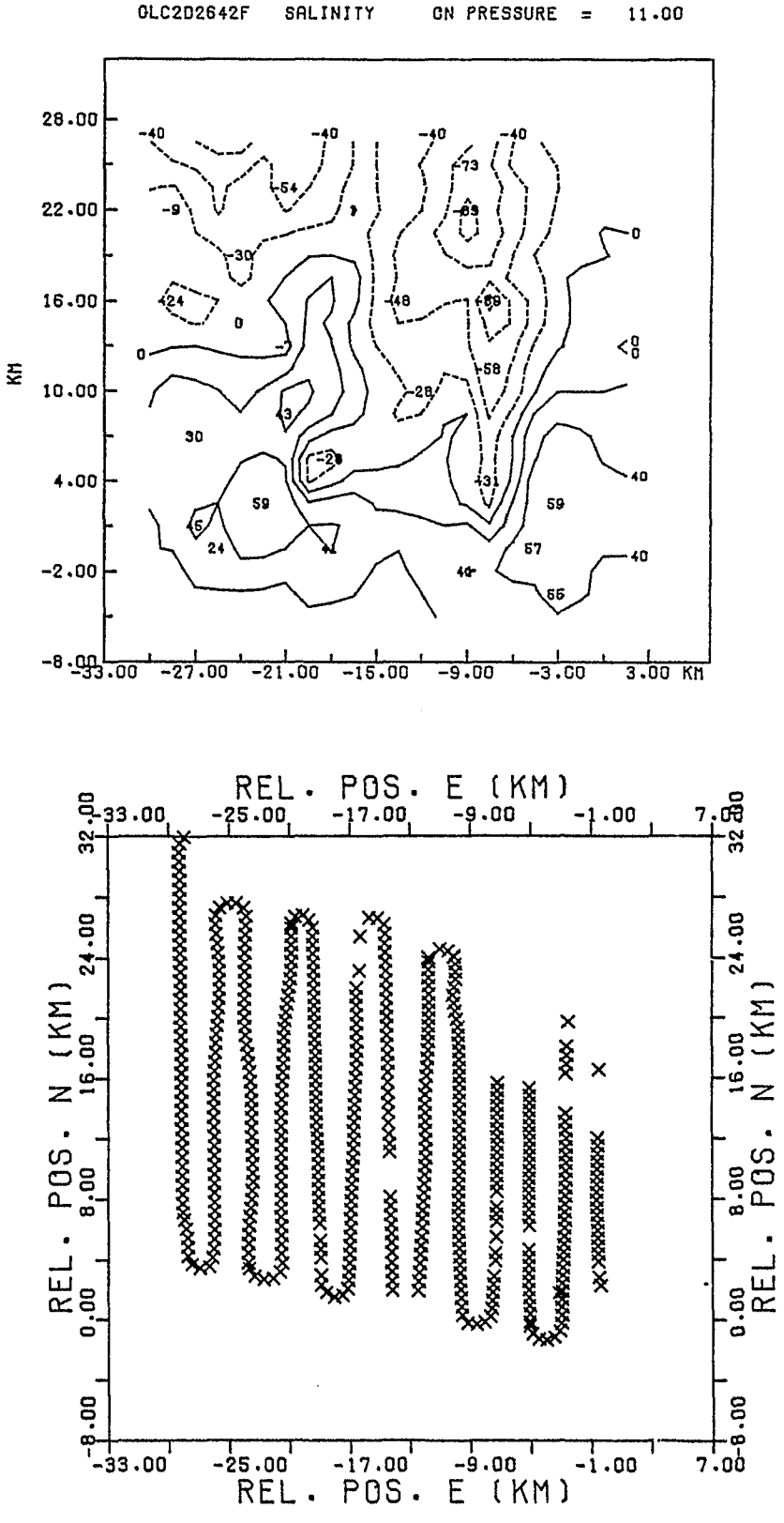

Fig. 7.9 e) :

Contoured map of salinity on the 11 dbar pressure surface (upper figure). The contours are of the salinity deviation (units in 10^{-6}) from the mean salinity (35.565×10^{-3}) on the surface.
Positions of the data relative to the origin of the map (lower figure).

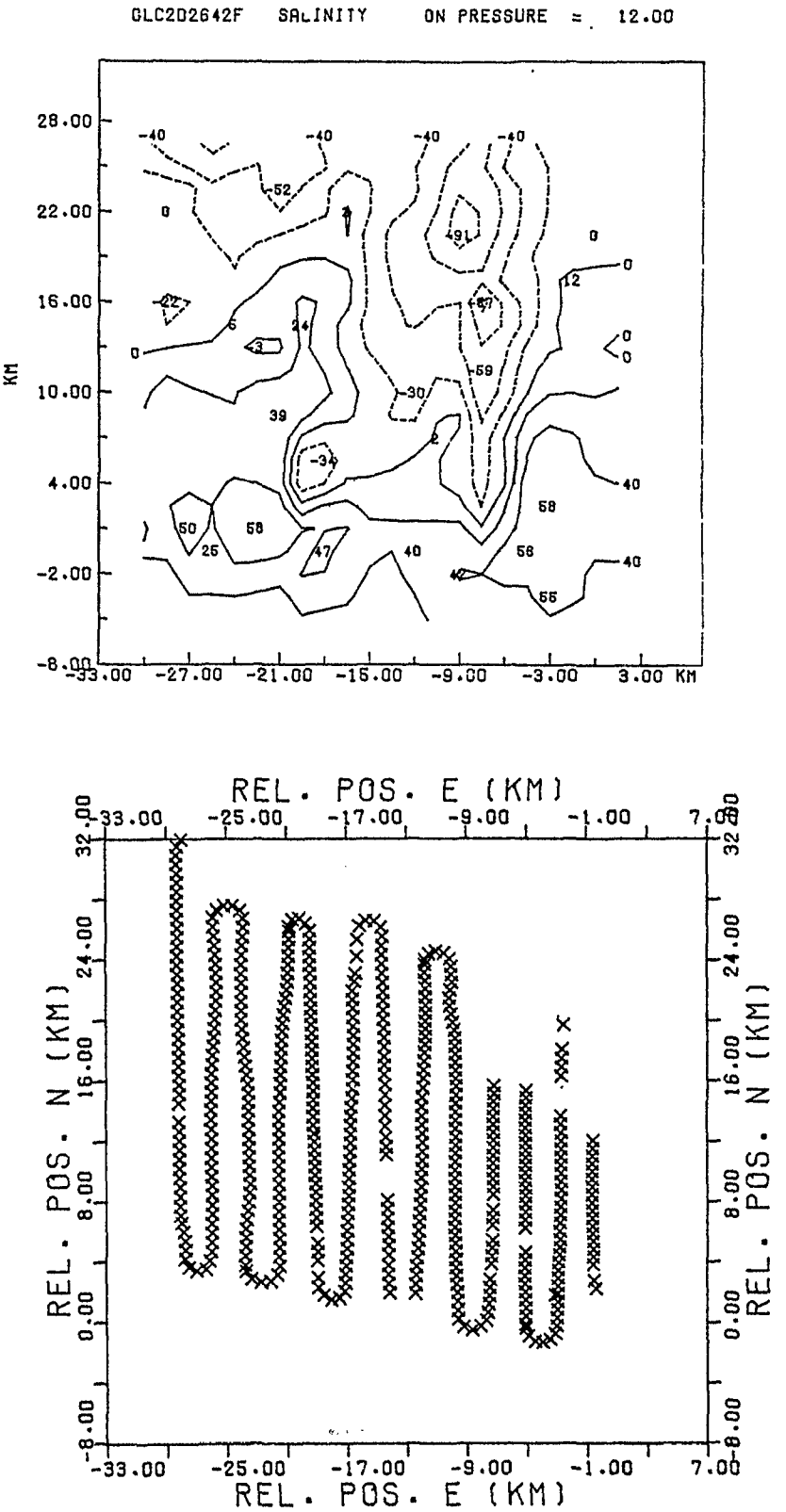

Fig. 7.9 f) :

Contoured map of salinity on the 12 dbar pressure surface (upper figure). The contours are of the salinity deviation (units in 10^{-6}) from the mean salinity (35.566×10^{-3}) on the surface.
Positions of the data relative to the origin of the map (lower figure).

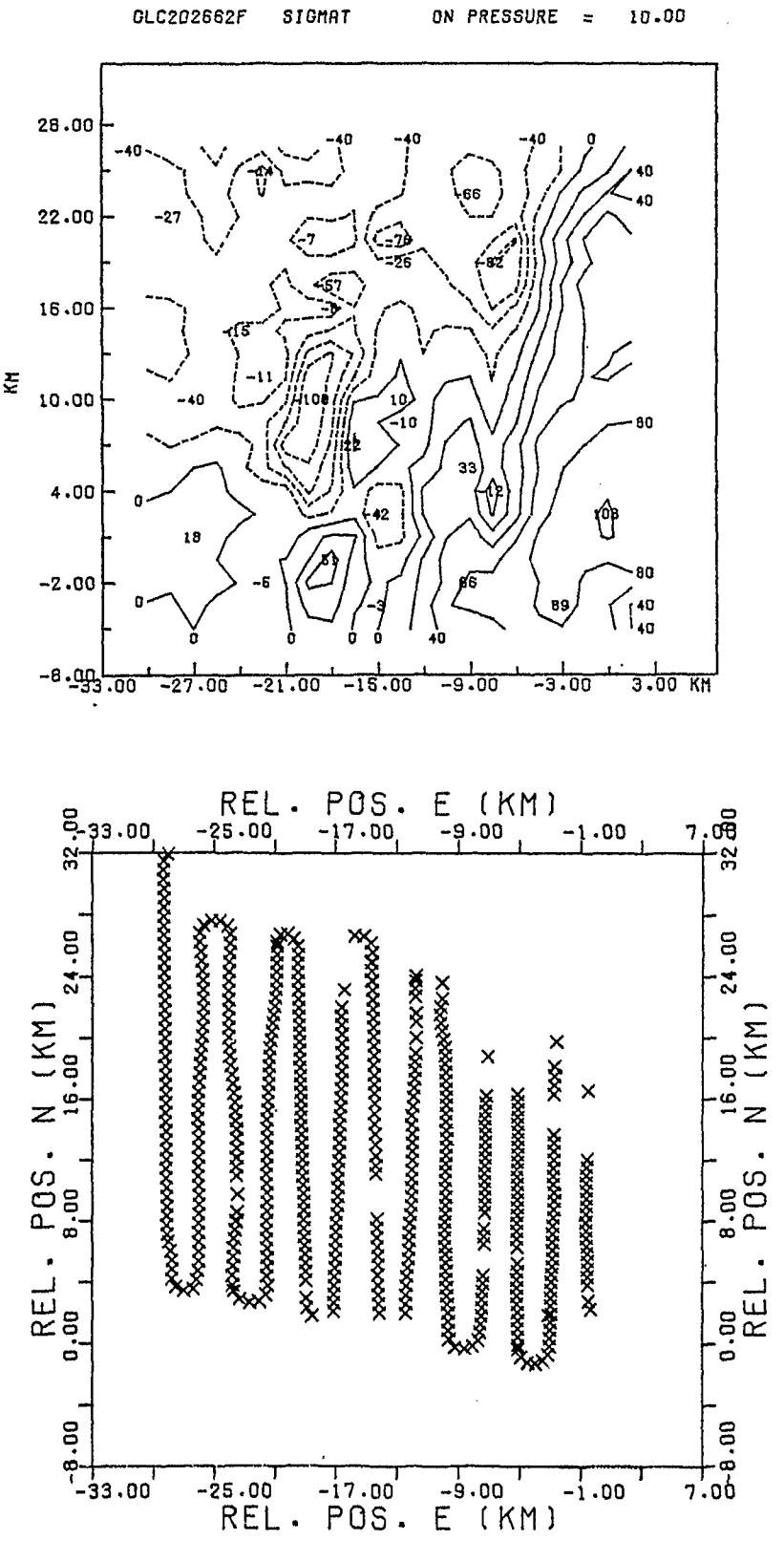

Fig. 7.9 g) :

Contoured map of density on the 10 dbar pressure surface (upper figure). The contours are of the density deviation (units in 10^{-3} kg m^{-3}) from the mean density (23.153 kg m^{-3}) on the surface.
Positions of the data relative to the origin of the map. (lower figure).

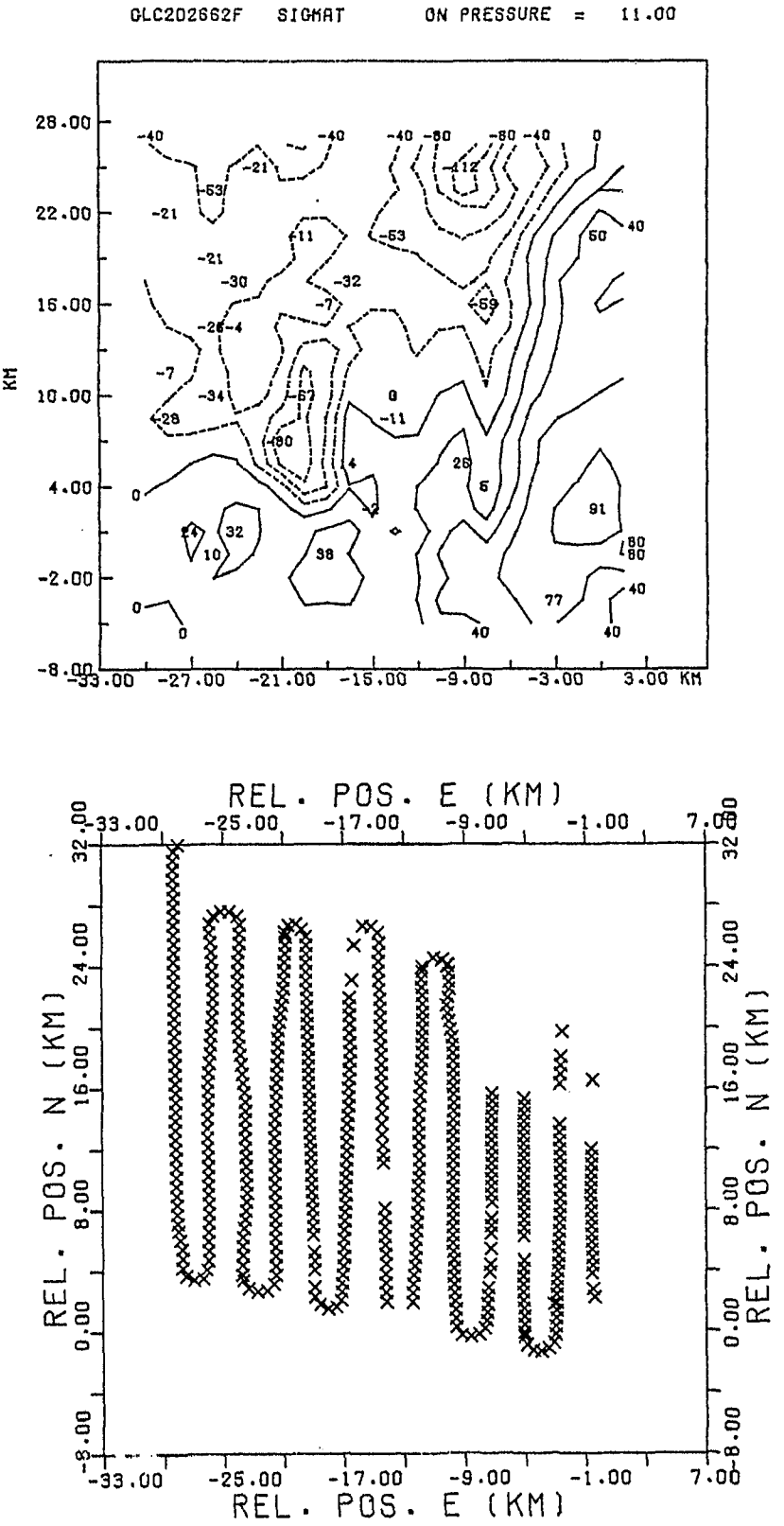

Fig. 7.9 h) :

Contoured map of density on the 11 dbar pressure surface (upper figure). The contours are of the density deviation (units in 10^{-3} kg m^{-3}) from the mean density (23.161 kg m^{-3}) on the surface.
Positions of the data relative to the origin of the map (lower figure).

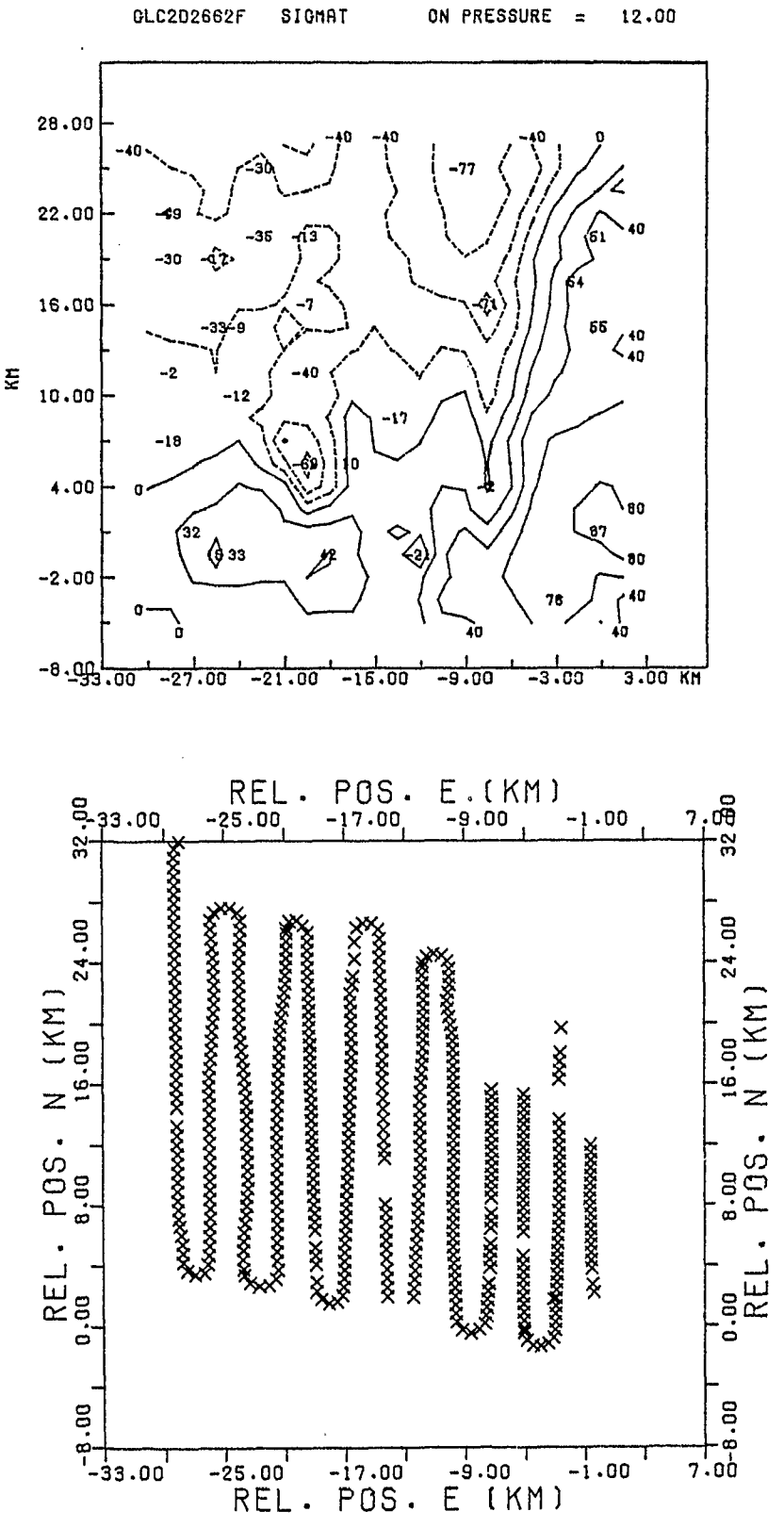

Fig. 7.9 i) :

Contoured map of density on the 12 dbar pressure surface (upper figure). The contours are of the density deviation (units in 10^{-3} kg m^{-3}) from the mean density (23.170 kg m^{-3}) on the surface.
Positions of the data relative to the origin of the map. (lower figure).

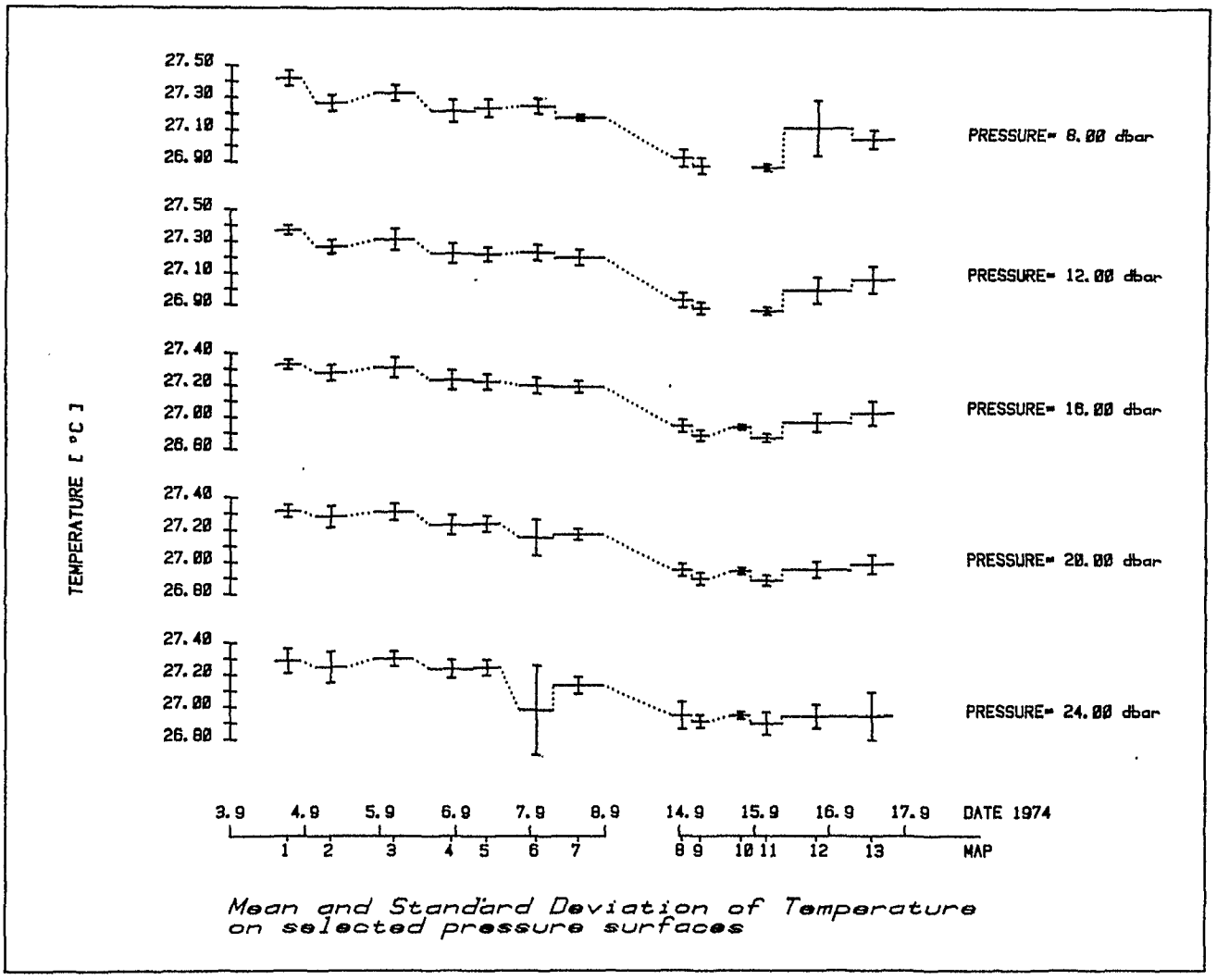

Figure 7.10 a) : Mean and standard deviation of temperature on selected pressure surfaces for all thirteen Maps of the GATE Lagrangian Batfish Experiment.

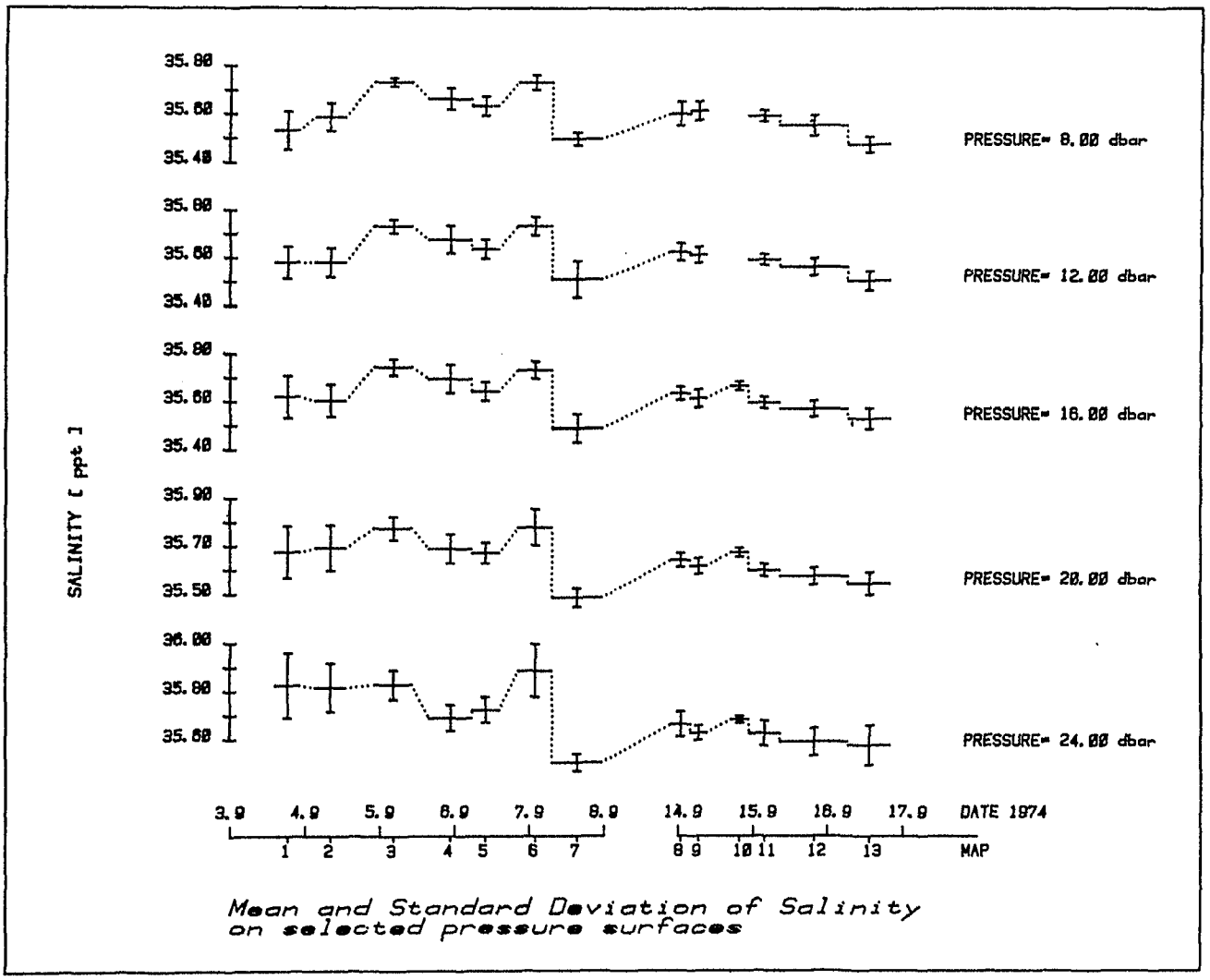

Figure 7.10 b) : Mean and standard deviation of salinity on selected pressure surfaces for all thirteen Maps of the GATE Lagrangian Batfish Experiment.

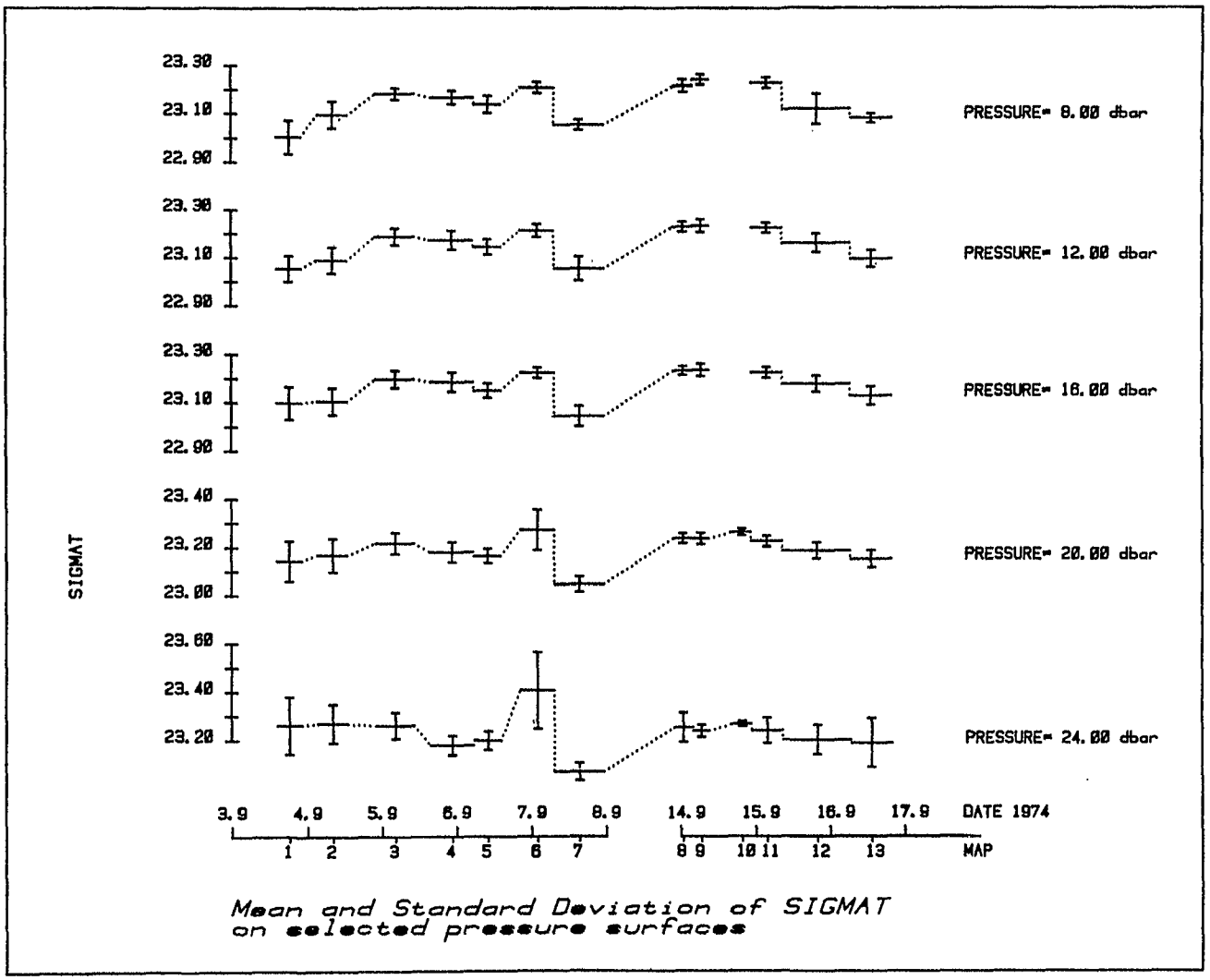

Figure 7.10 c) : Mean and standard deviation of density on selected pressure surfaces for all thirteen Maps of the GATE Lagrangian Batfish Experiment.

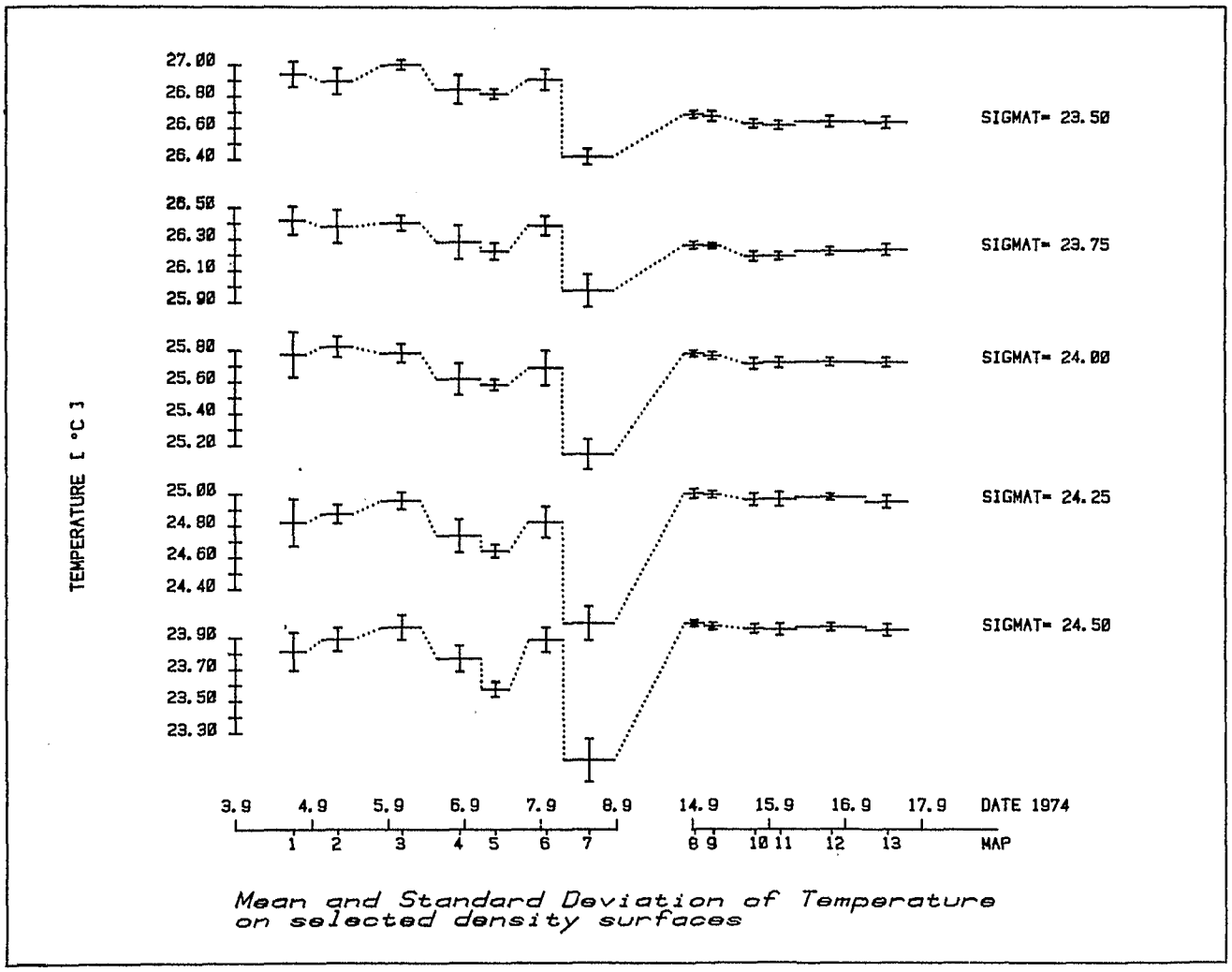

Figure 7.10 d) : Mean and standard deviation of temperature on selected density surfaces for all thirteen Maps of the GATE Lagrangian Batfish Experiment. Particularly noticeable is the greater thermohaline variability during the first timeseries, Maps 1 to 7 (i.e. 1L1 - 1L7).

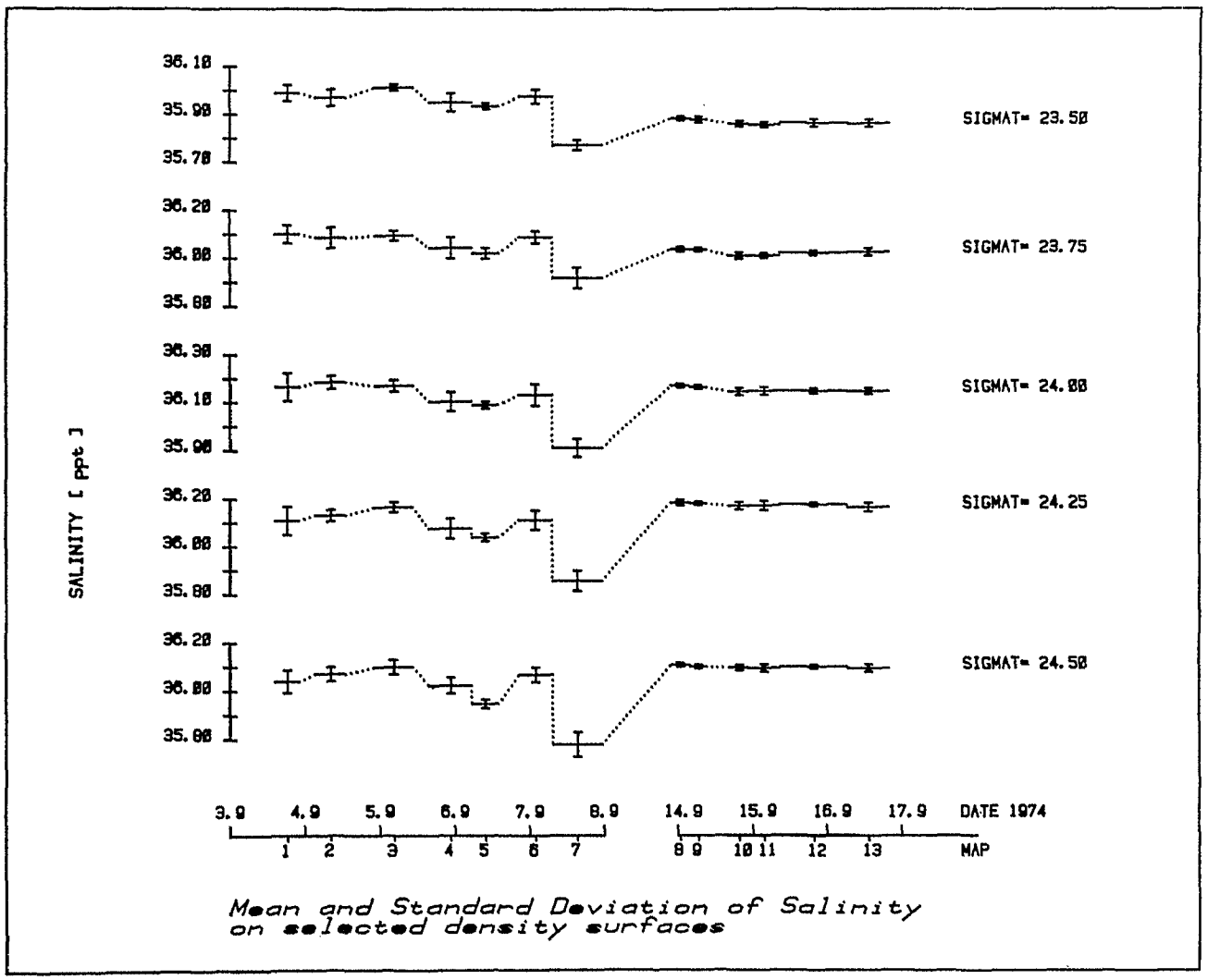

Figure 7.10 e) : Mean and standard deviation of salinity on selected density surfaces for all thirteen Maps of the GATE Lagrangian Batfish Experiment.

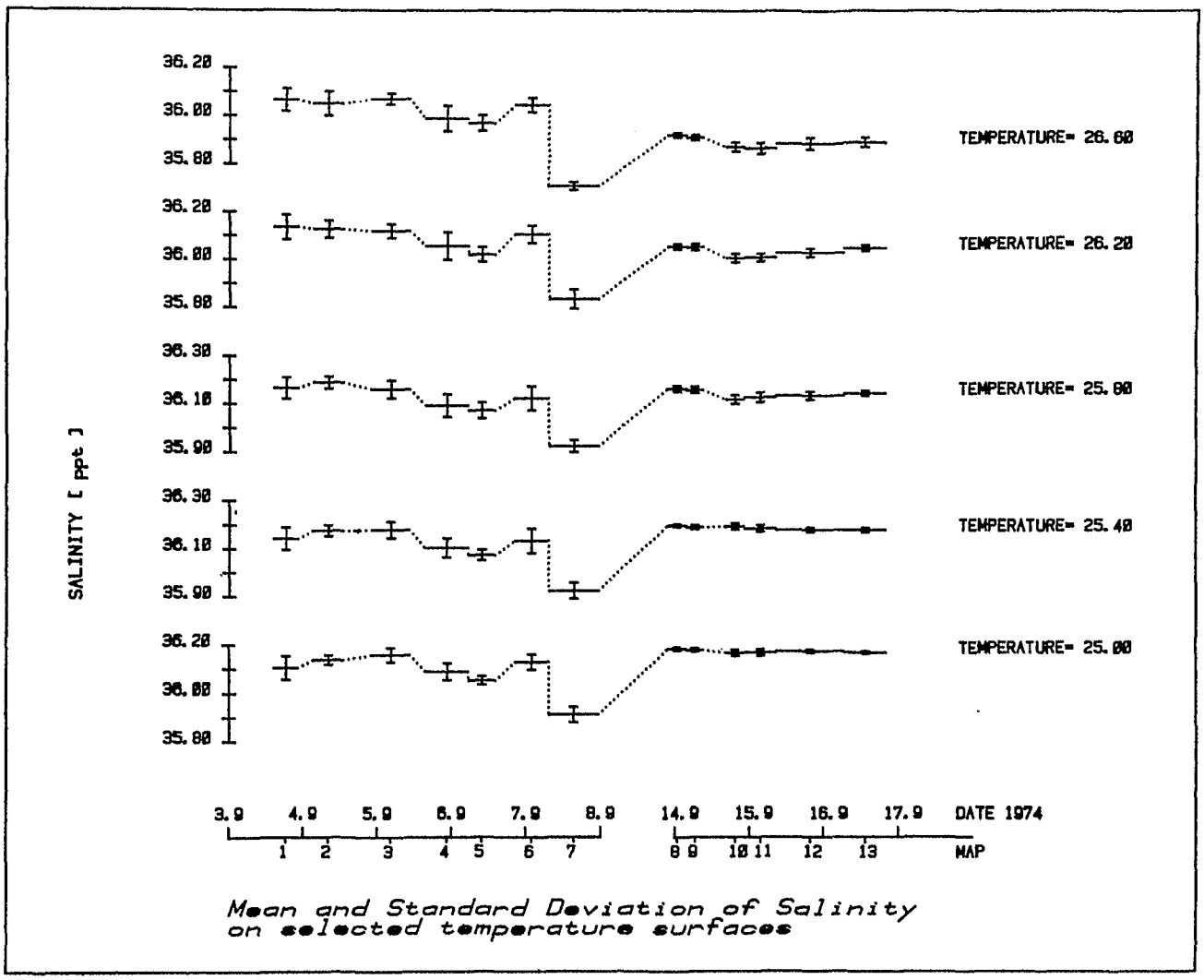

Figure 7.10 f) : Mean and standard deviation of salinity on selected temperature surfaces for all thirteen Maps of the GATE Lagrangian Batfish Experiment.

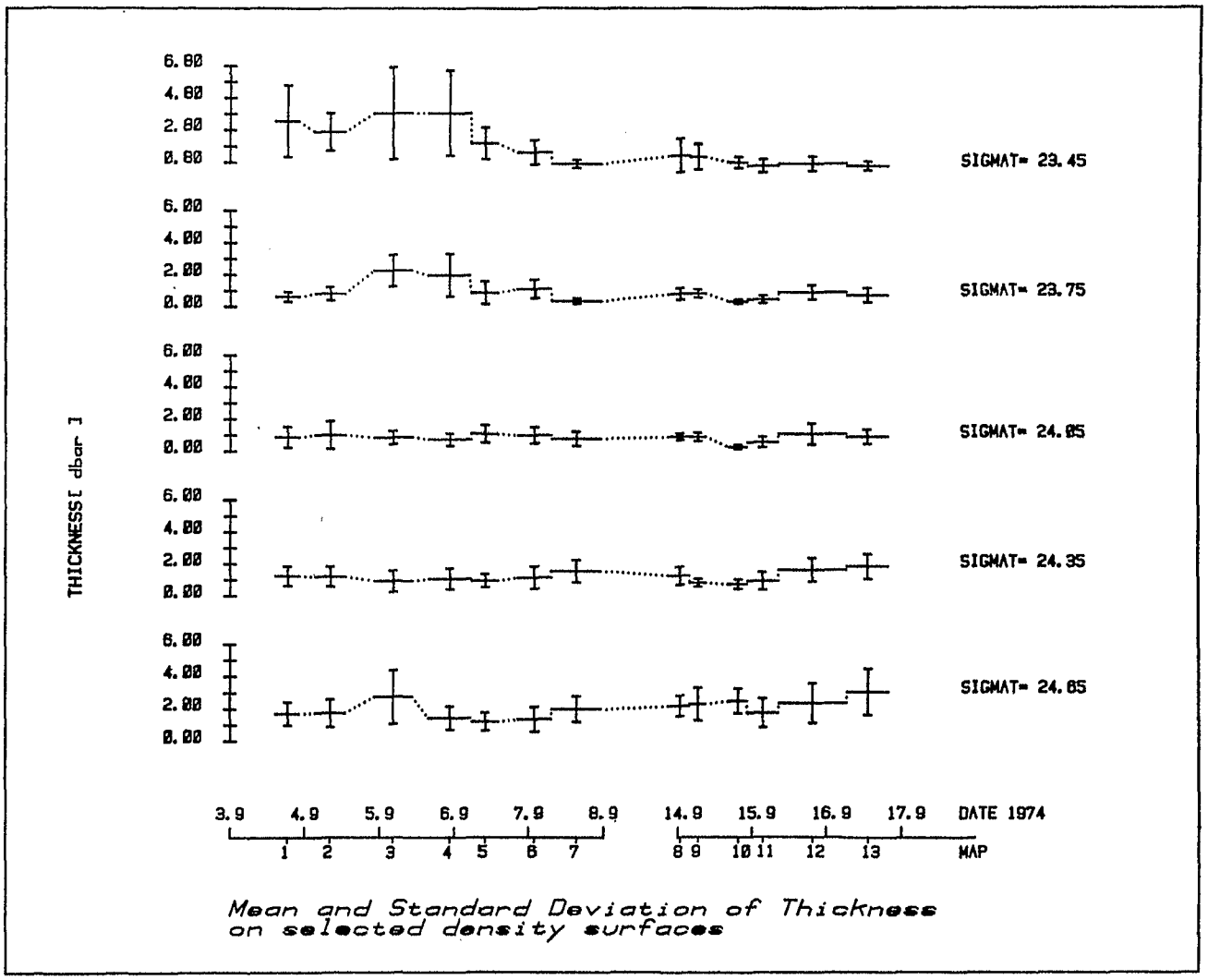

Figure 7.10 g): Mean and standard deviation of thickness on selected density surfaces for all thirteen Maps of the GATE Lagrangian Batfish Experiment.

MAP 1L1

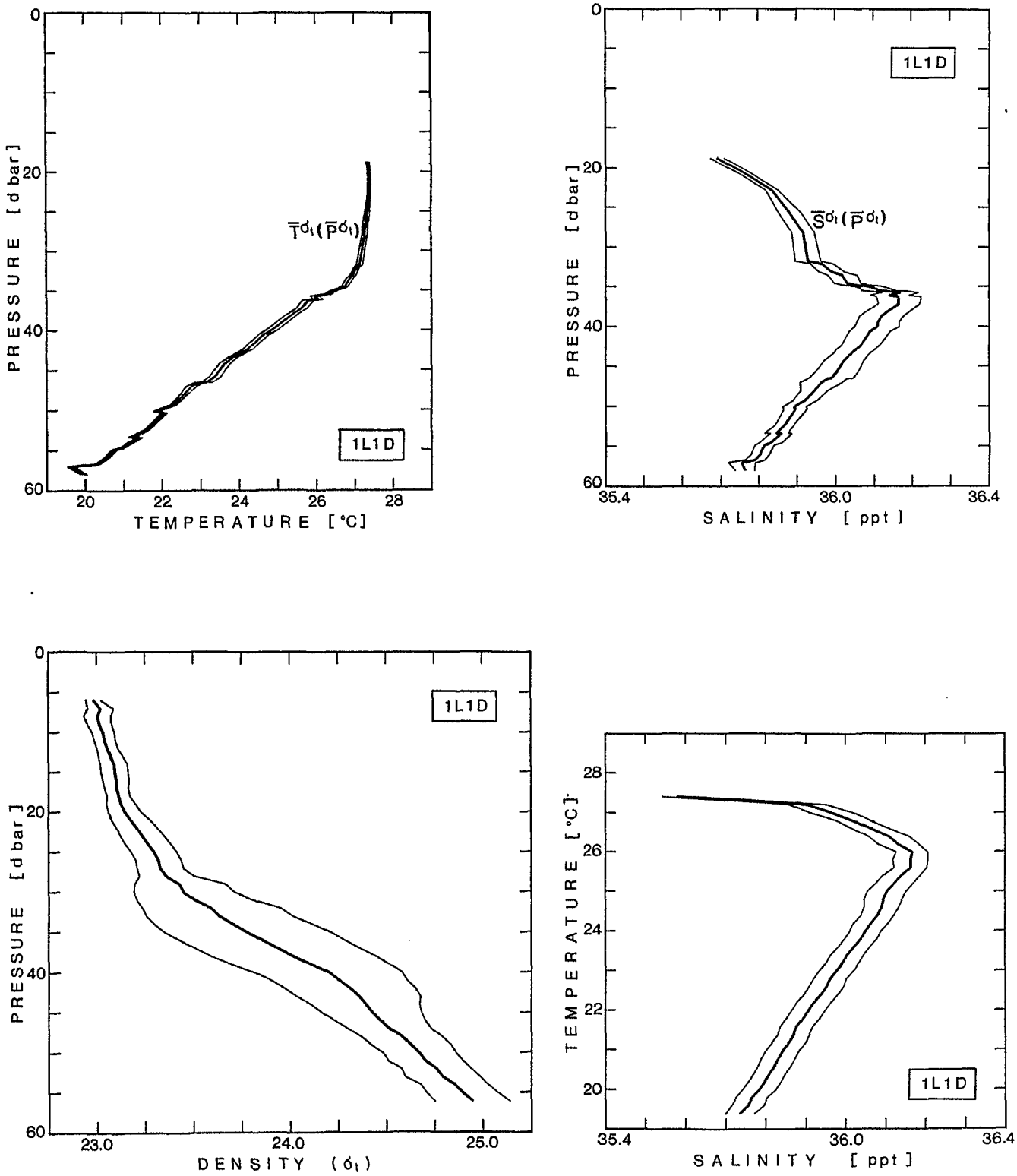

Fig. 7.11 a) : Profiles of the mean and standard deviation of potential temperature and salinity on surfaces of constant σ_T redrawn as functions of pressure using the mean relationship of σ_T to pressure (upper figures).

Profiles of the mean and standard deviation of density on surfaces of constant pressure and salinity on surfaces of constant potential temperature (lower figures).

MAP 1L2

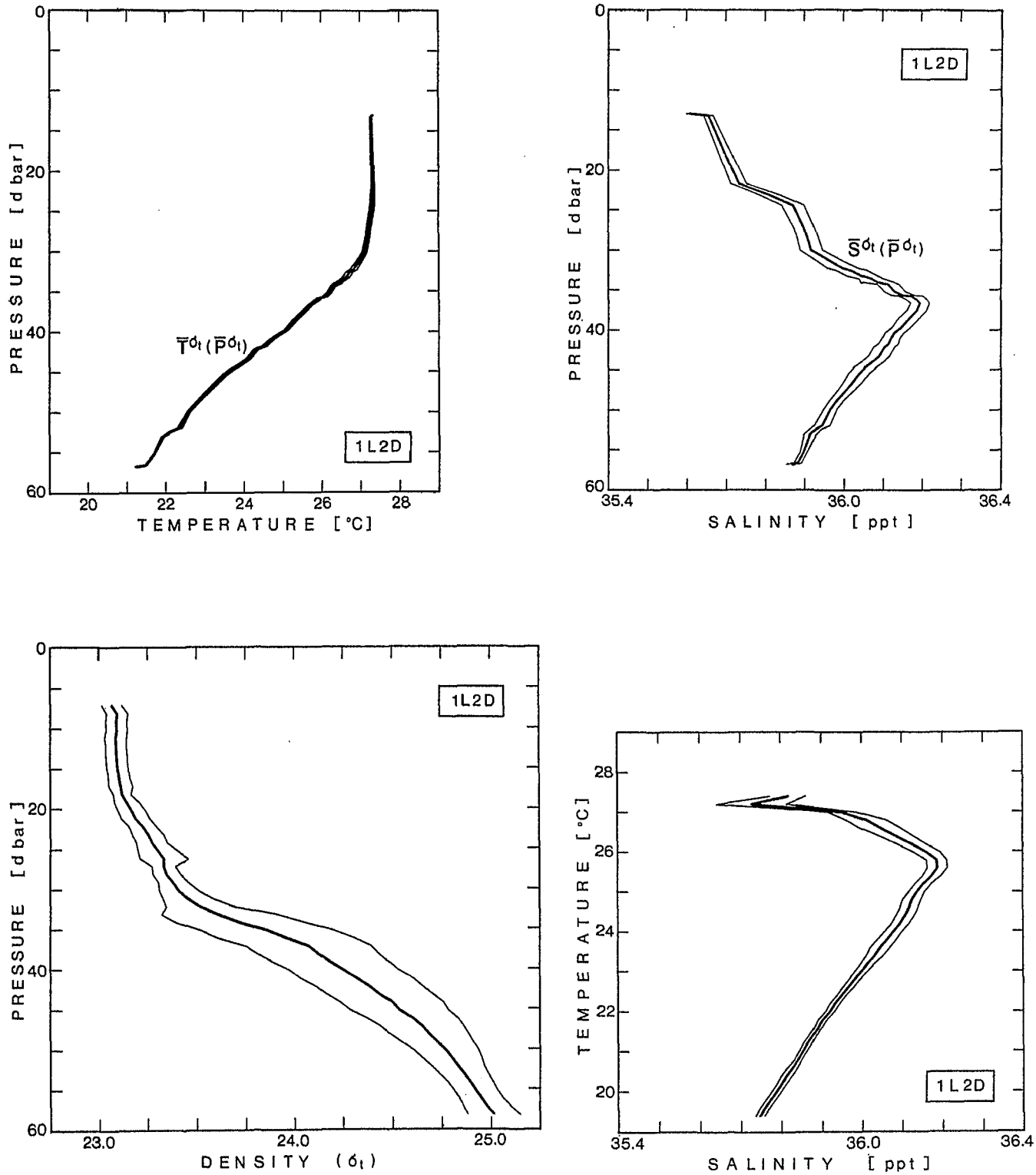

Fig. 7.11 b) : Profiles of the mean and standard deviation of potential temperature and salinity on surfaces of constant σ_T redrawn as functions of pressure using the mean relationship of σ_T to pressure (upper figures).

Profiles of the mean and standard deviation of density on surfaces of constant pressure and salinity on surfaces of constant potential temperature (lower figures).

MAP 1L3

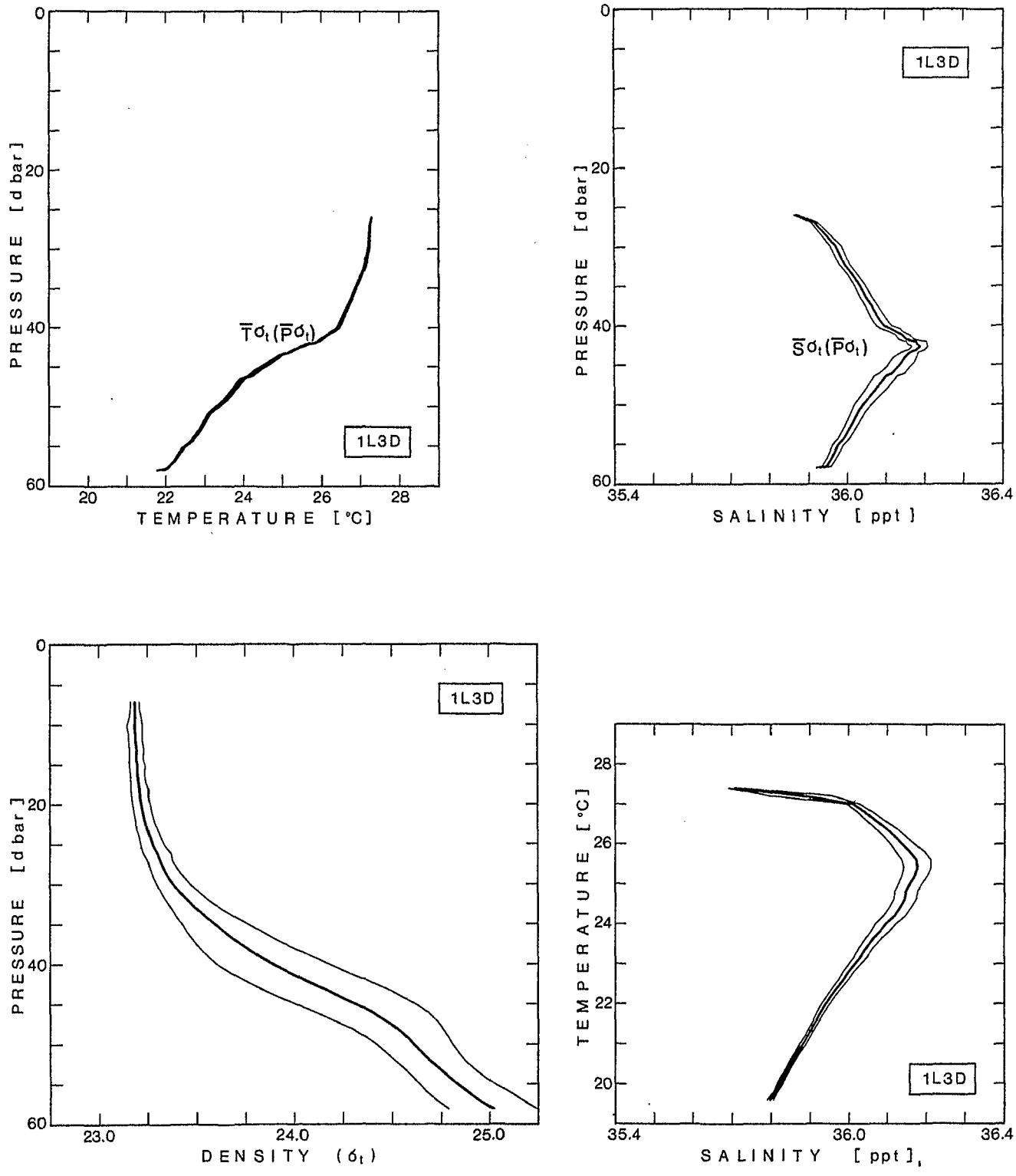

Fig. 7.11 c) : Profiles of the mean and standard deviation of potential temperature and salinity on surfaces of constant σ_T redrawn as functions of pressure using the mean relationship of σ_T to pressure (upper figures).

Profiles of the mean and standard deviation of density on surfaces of constant pressure and salinity on surfaces of constant potential temperature (lower figures).

MAP 1L4

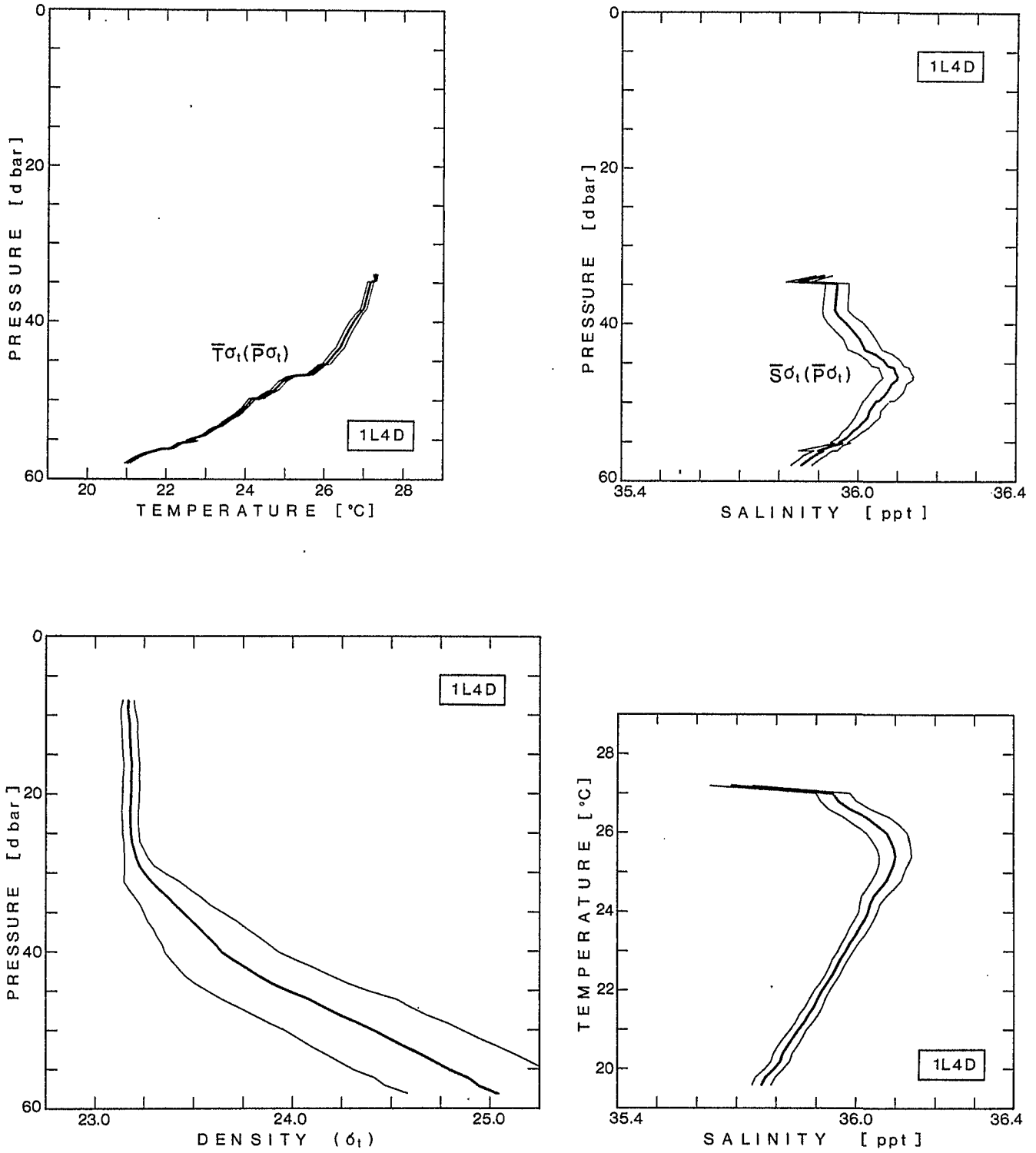

Fig. 7.11 d) : Profiles of the mean and standard deviation of potential temperature and salinity on surfaces of constant σ_T redrawn as functions of pressure using the mean relationship of σ_T to pressure (upper figures).

Profiles of the mean and standard deviation of density on surfaces of constant pressure and salinity on surfaces of constant potential temperature (lower figures).

MAP 1L5

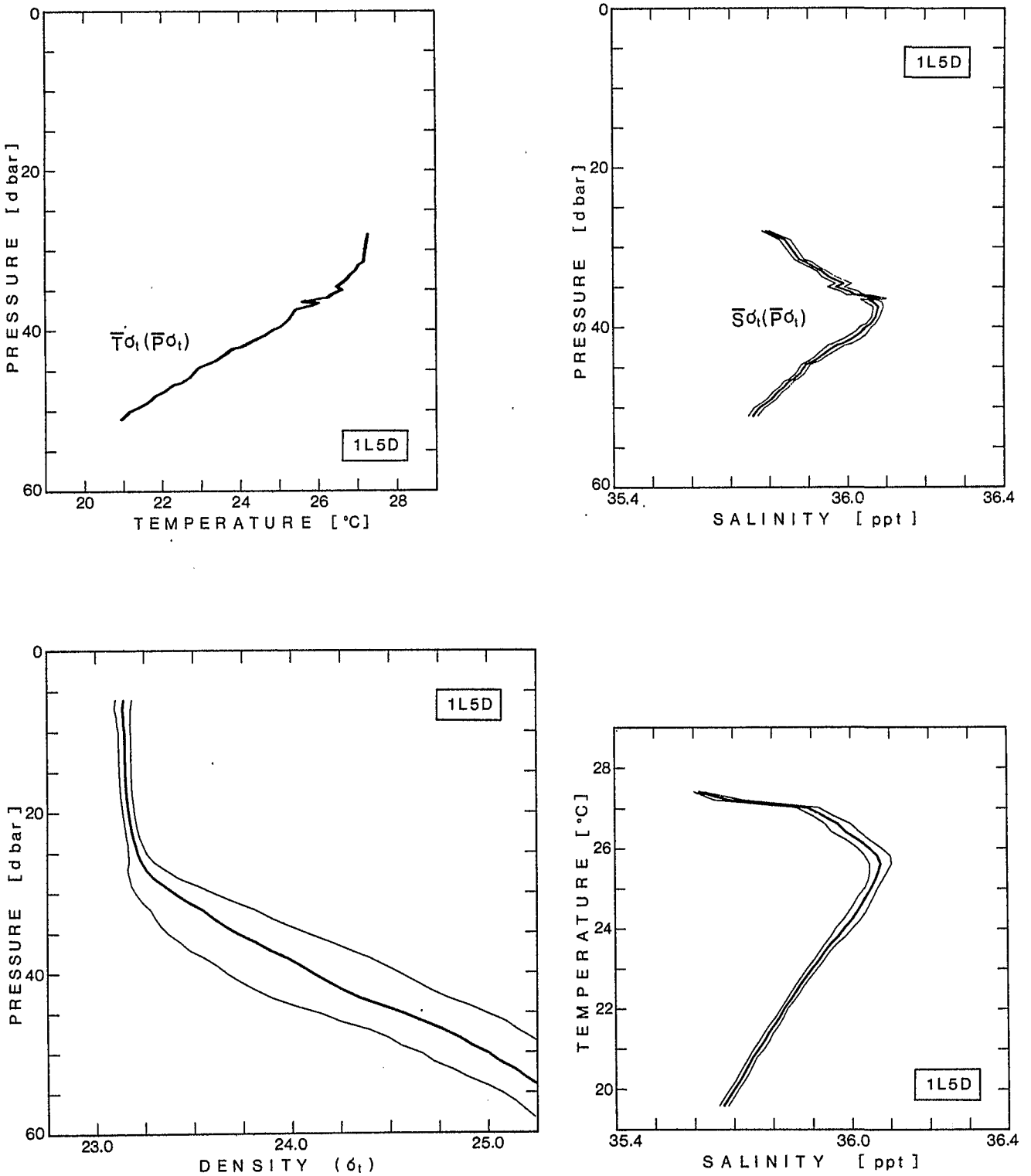

Fig. 7.11 e) : Profiles of the mean and standard deviation of potential temperature and salinity on surfaces of constant σ_T redrawn as functions of pressure using the mean relationship of σ_T to pressure (upper figures).

Profiles of the mean and standard deviation of density on surfaces of constant pressure and salinity on surfaces of constant potential temperature (lower figures).

MAP 1L6

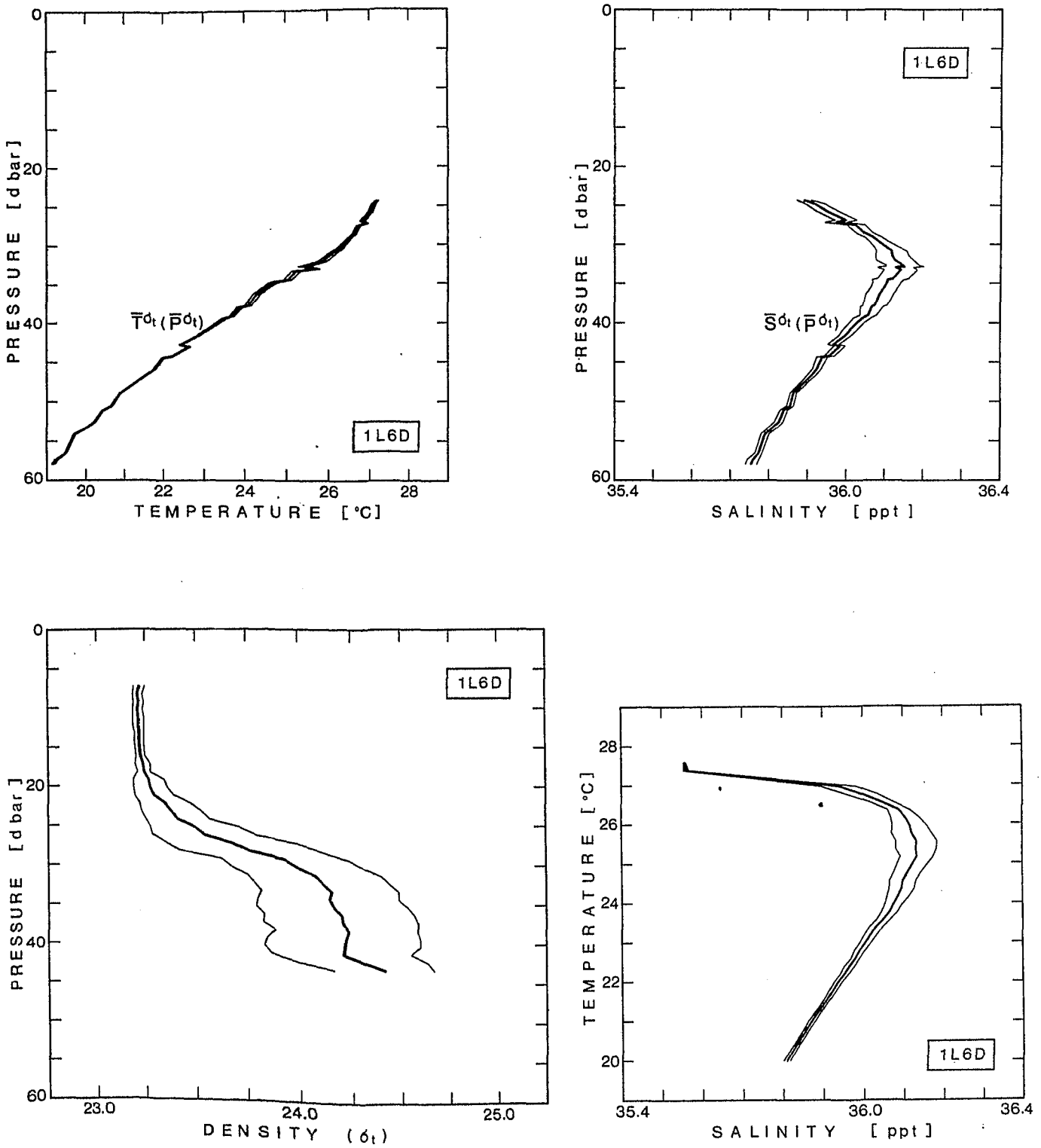

Fig. 7.11 f) : Profiles of the mean and standard deviation of potential temperature and salinity on surfaces of constant σ_T redrawn as functions of pressure using the mean relationship of σ_T to pressure (upper figures).

Profiles of the mean and standard deviation of density on surfaces of constant pressure and salinity on surfaces of constant potential temperature (lower figures).

MAP 1L7

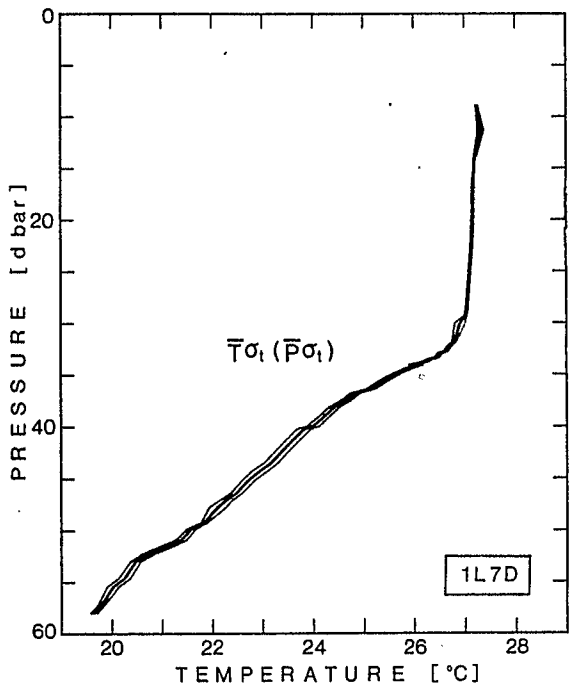

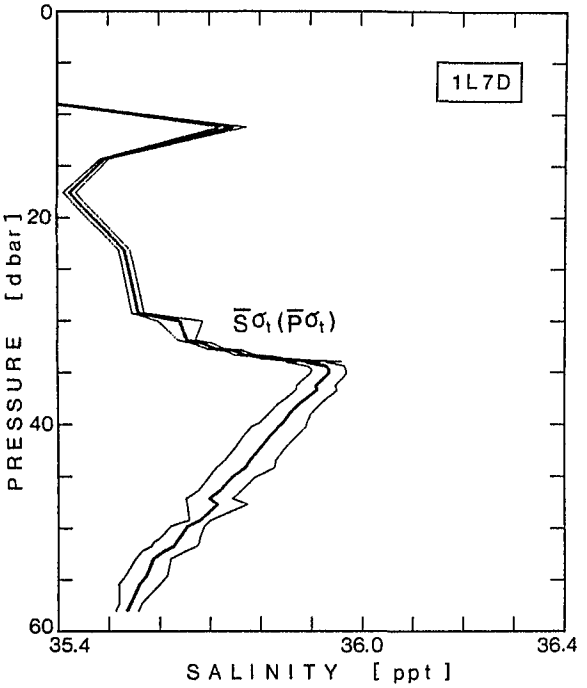

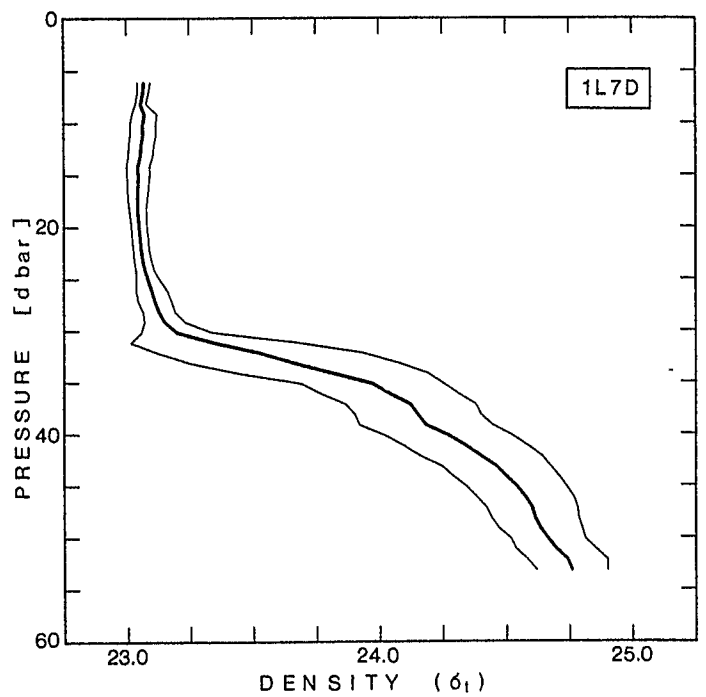

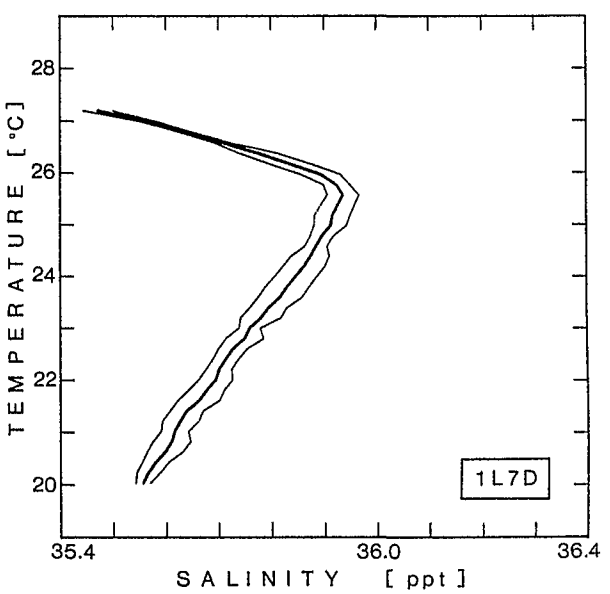

Fig. 7.11 g) : Profiles of the mean and standard deviation of potential temperature and salinity on surfaces of constant σ_T redrawn as functions of pressure using the mean relationship of σ_T to pressure (upper figures).

Profiles of the mean and standard deviation of density on surfaces of constant pressure and salinity on surfaces of constant potential temperature (lower figures).

MAP 2L1

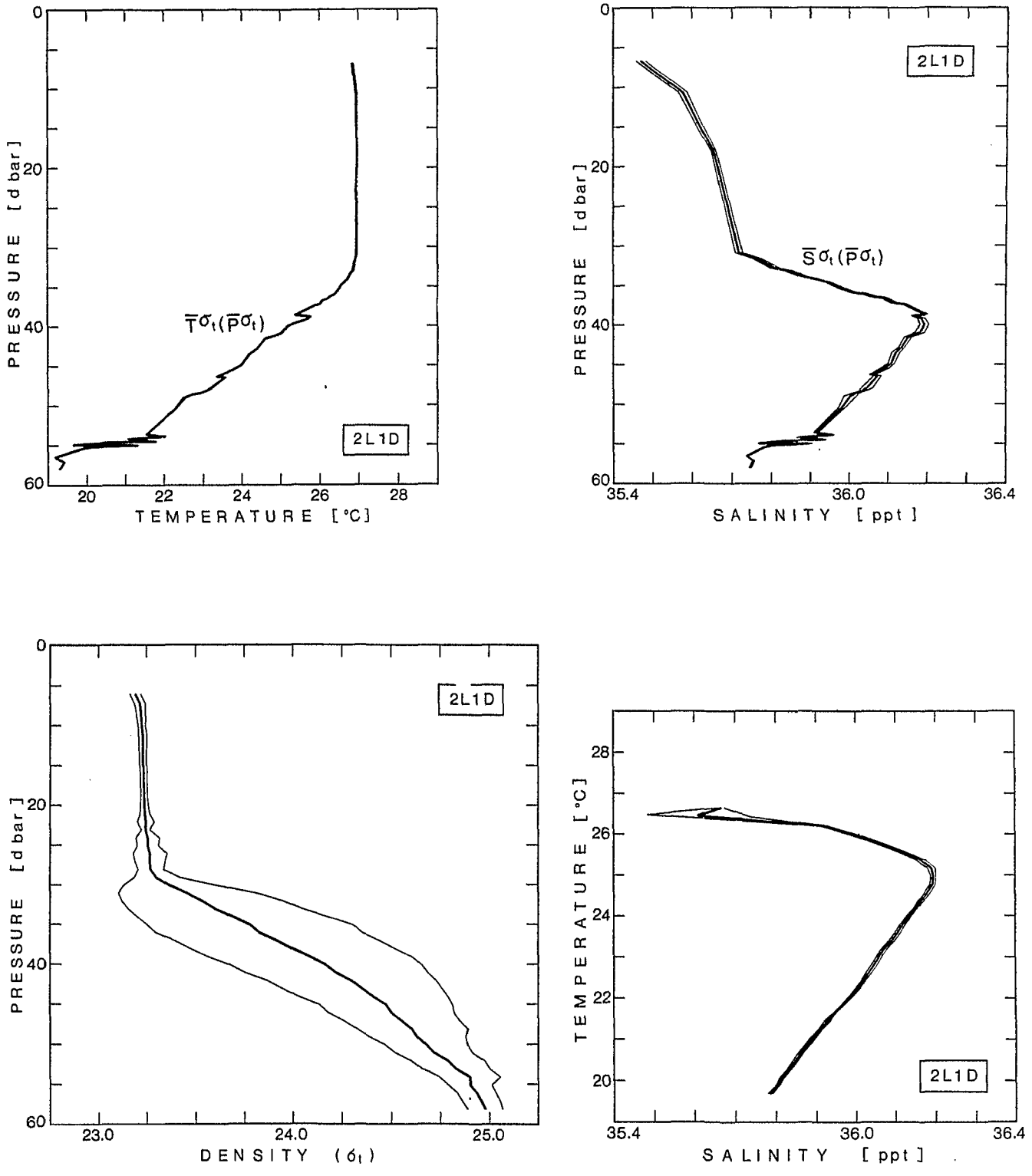

Fig. 7.11 h) : Profiles of the mean and standard deviation of potential temperature and salinity on surfaces of constant σ_T redrawn as functions of pressure using the mean relationship of σ_T to pressure (upper figures).

Profiles of the mean and standard deviation of density on surfaces of constant pressure and salinity on surfaces of constant potential temperature (lower figures).

MAP 2L2

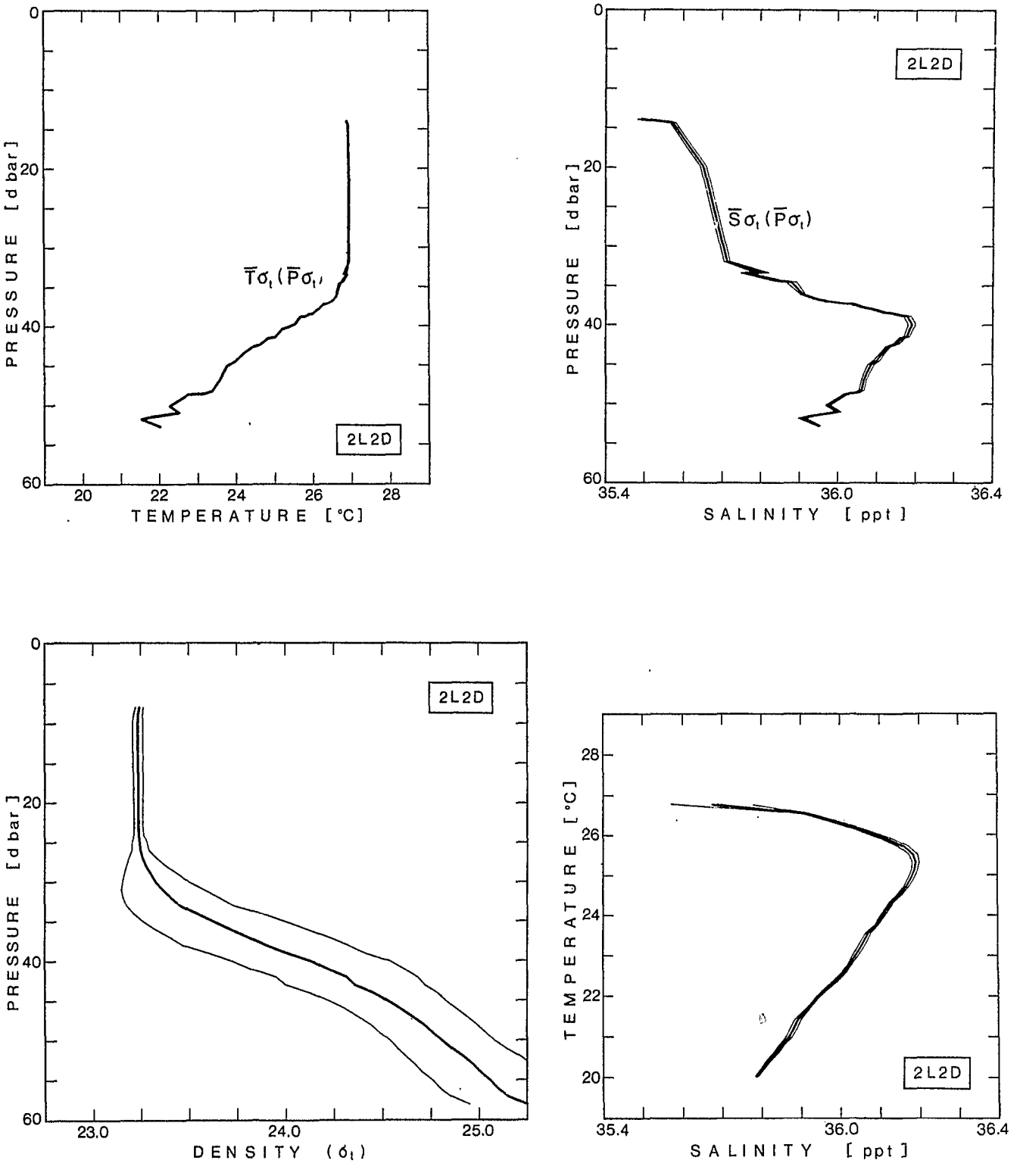

Fig. 7.11 i) : Profiles of the mean and standard deviation of potential temperature and salinity on surfaces of constant σ_T redrawn as functions of pressure using the mean relationship of σ_T to pressure (upper figures).

Profiles of the mean and standard deviation of density on surfaces of constant pressure and salinity on surfaces of constant potential temperature (lower figures).

MAP 3L1

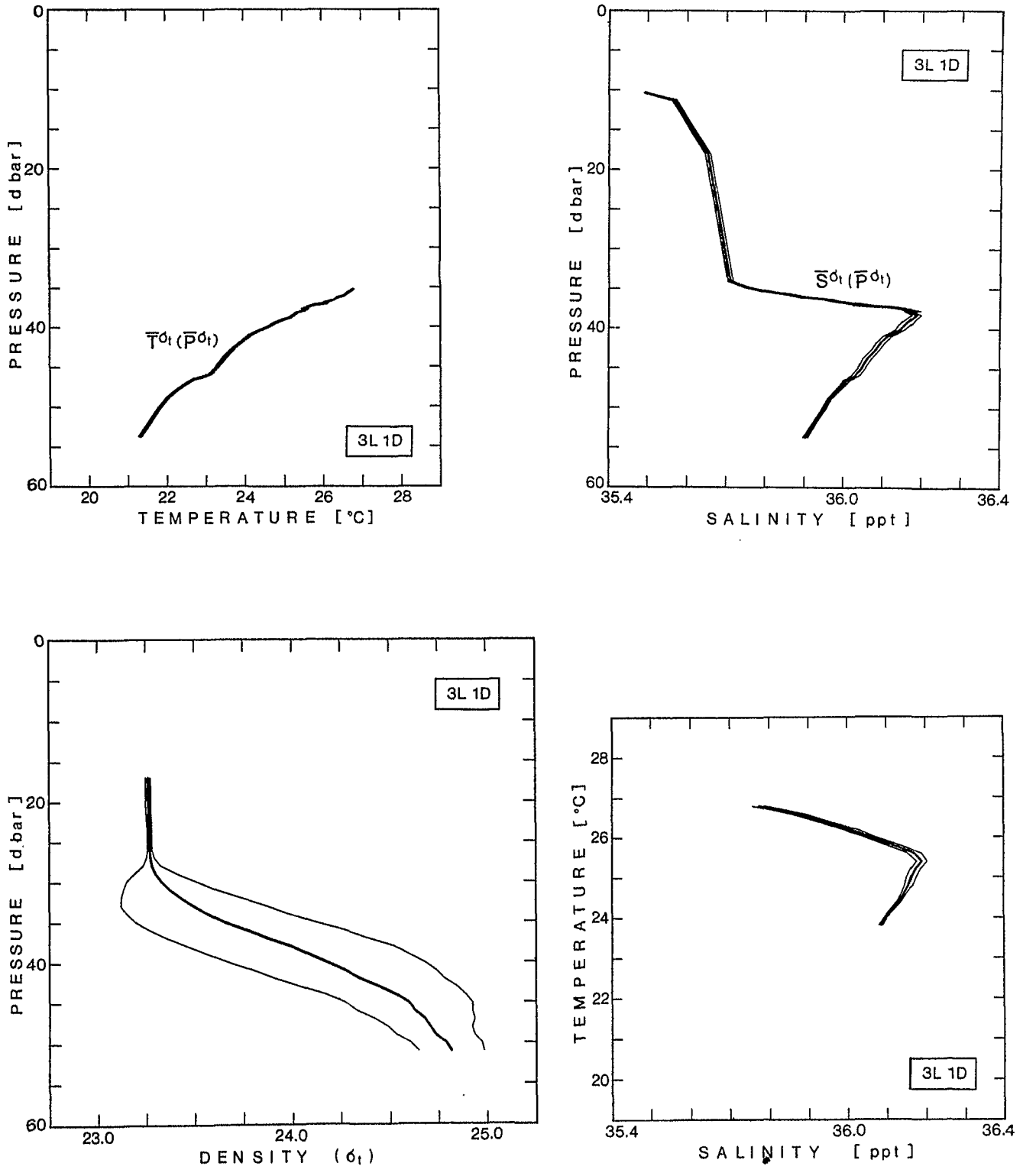

Fig. 7.11 j) : Profiles of the mean and standard deviation of potential temperature and salinity on surfaces of constant σ_T redrawn as functions of pressure using the mean relationship of σ_T to pressure (upper figures).

Profiles of the mean and standard deviation of density on surfaces of constant pressure and salinity on surfaces of constant potential temperature (lower figures).

MAP 3L2

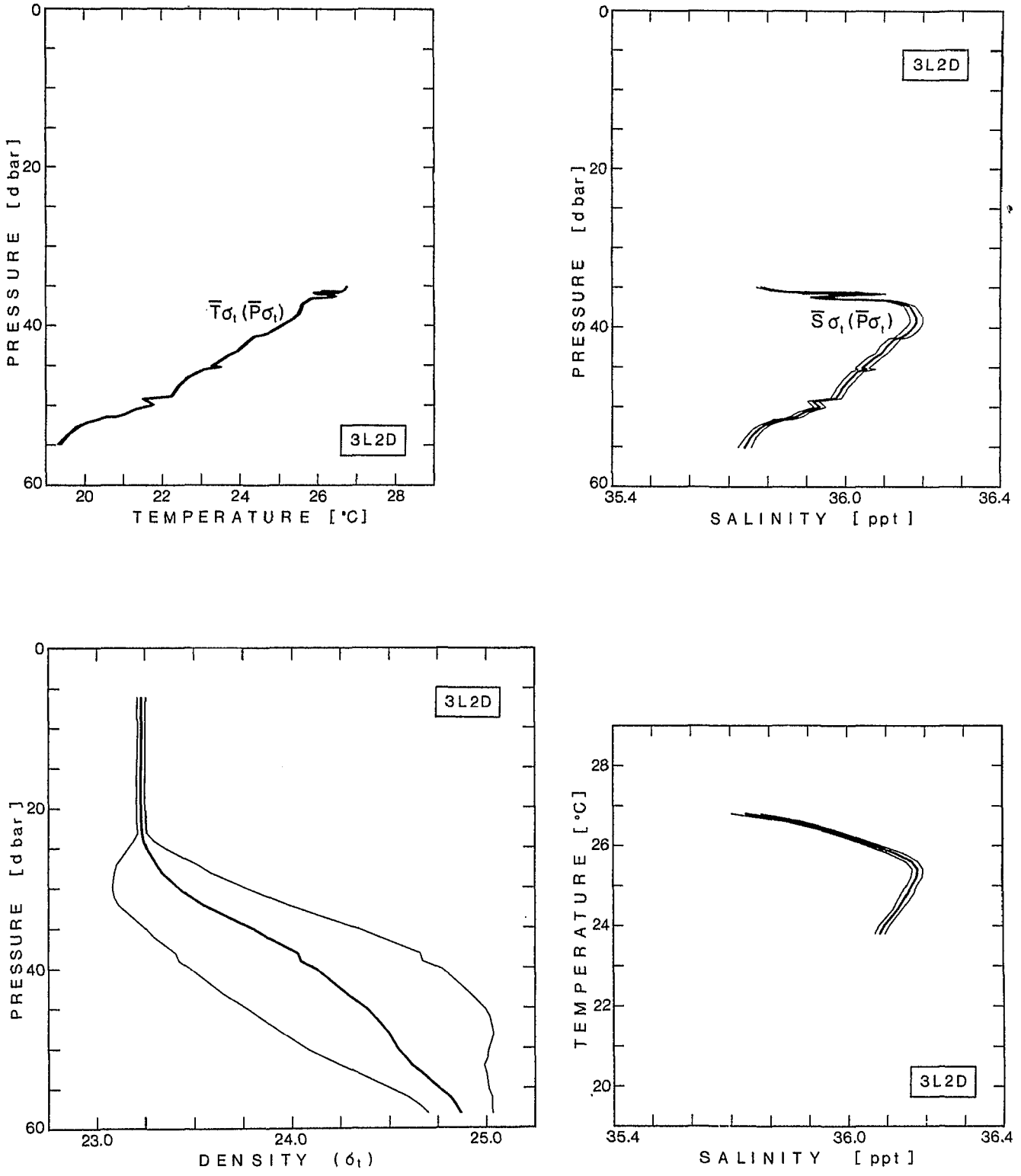

Fig. 7.11 k) : Profiles of the mean and standard deviation of potential temperature and salinity on surfaces of constant σ_T redrawn as functions of pressure using the mean relationship of σ_T to pressure (upper figures).

Profiles of the mean and standard deviation of density on surfaces of constant pressure and salinity on surfaces of constant potential temperature (lower figures).

MAP 3L3

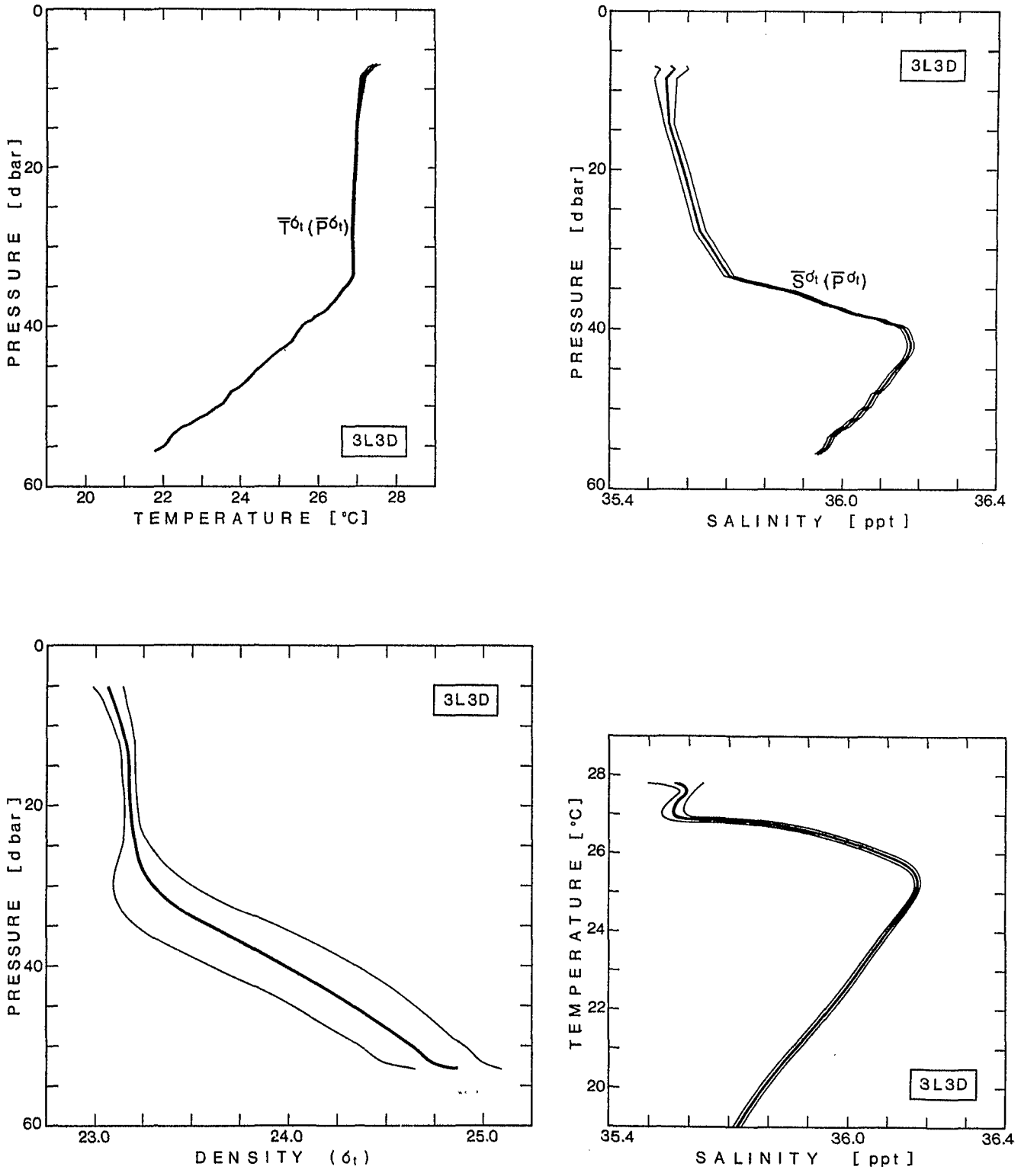

Fig. 7.11 1) : Profiles of the mean and standard deviation of potential temperature and salinity on surfaces of constant σ_T redrawn as functions of pressure using the mean relationship of σ_T to pressure (upper figures).

Profiles of the mean and standard deviation of density on surfaces of constant pressure and salinity on surfaces of constant potential temperature (lower figures).

MAP 3L4

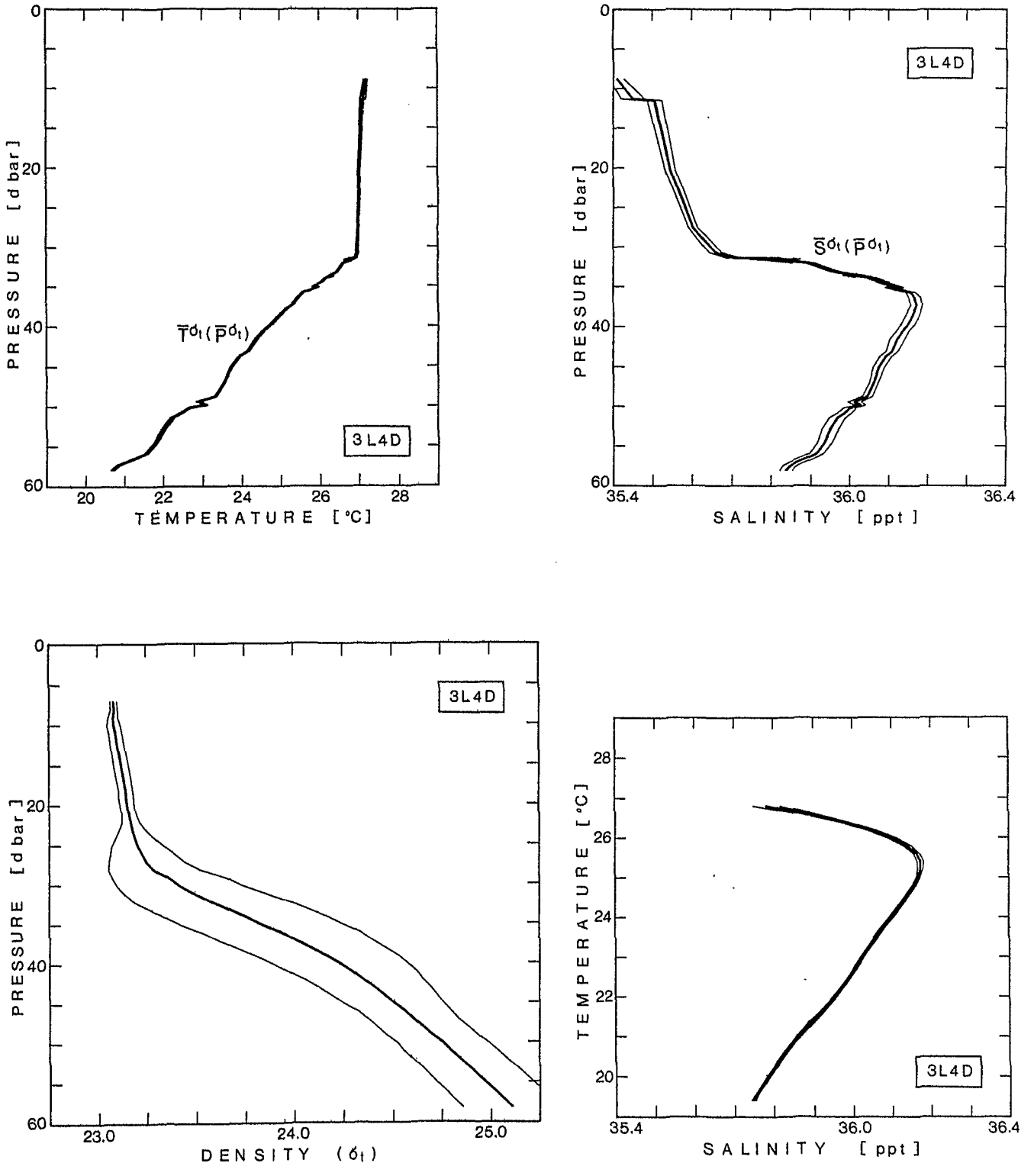

Fig. 7.11 m) : Profiles of the mean and standard deviation of potential temperature and salinity on surfaces of constant σ_T redrawn as functions of pressure using the mean relationship of σ_T to pressure (upper figures).

Profiles of the mean and standard deviation of density on surfaces of constant pressure and salinity on surfaces of constant potential temperature (lower figures).

POTENTIAL TEMPERATURE ON ISOPYCNIC SURFACES

MAP 1L1 Units: 10^{-2} K MAP 1L2

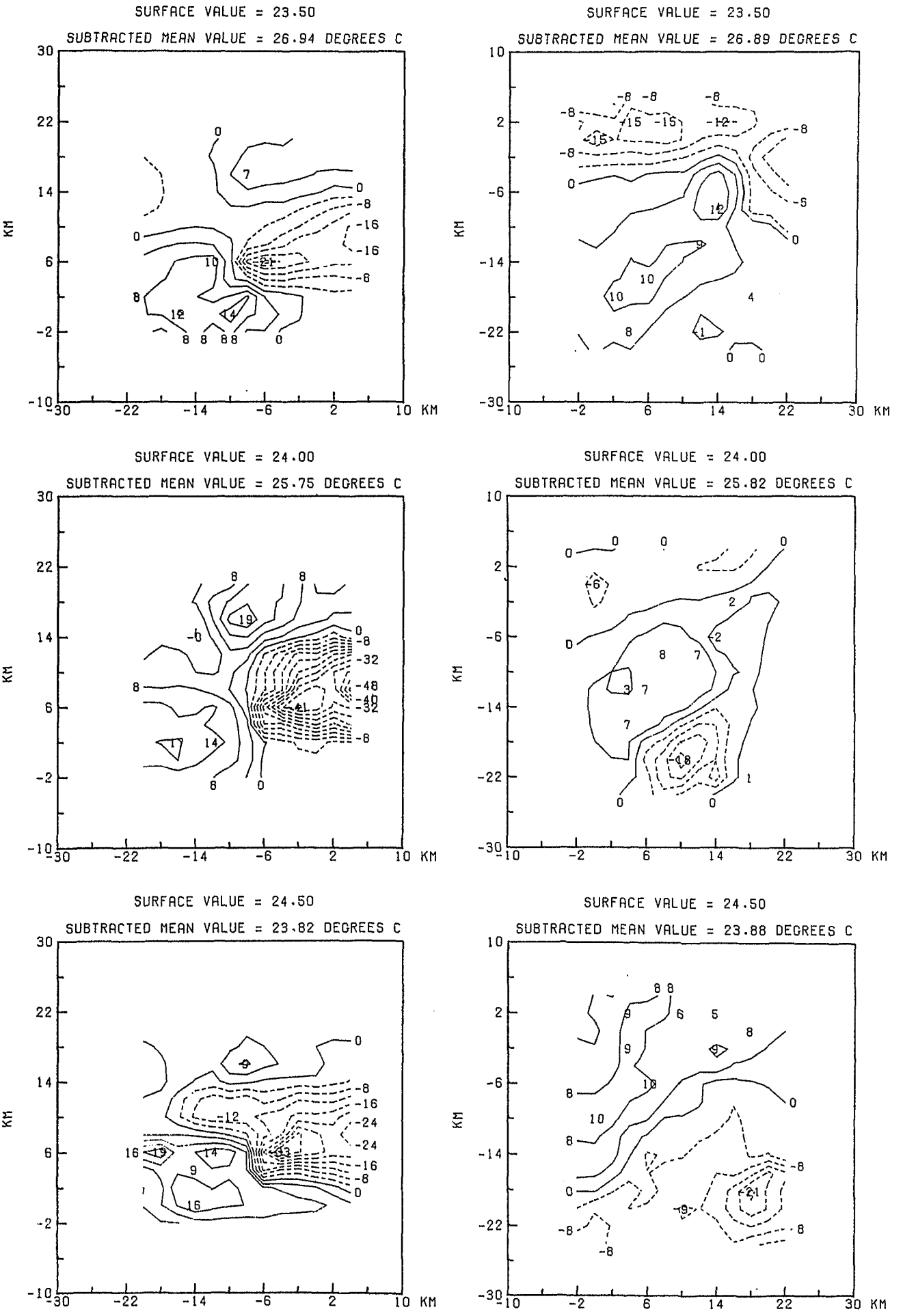

CONTOUR INTERVAL: 40 mK CONTOUR INTERVAL: 40 mK

Fig. 7.12 :

POTENTIAL TEMPERATURE ON ISOPYCNIC SURFACES

MAP 1L3 Units: 10^{-2} K MAP 1L4

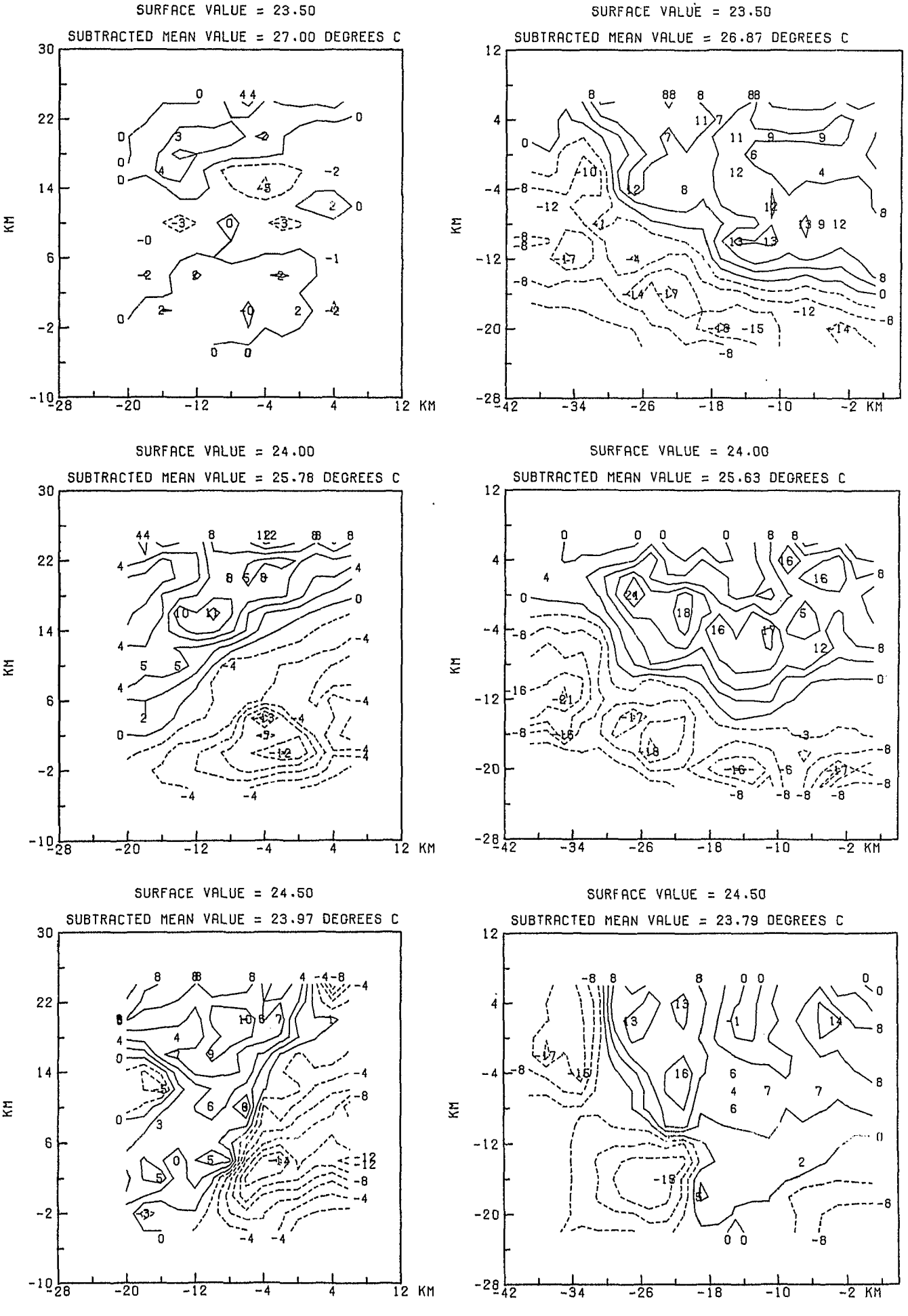

CONTOUR INTERVAL: 20 mK CONTOUR INTERVAL: 40 mK

Fig. 7.12 :

POTENTIAL TEMPERATURE ON ISOPYCNIC SURFACES

MAP 1L5 Units: 10^{-2} K

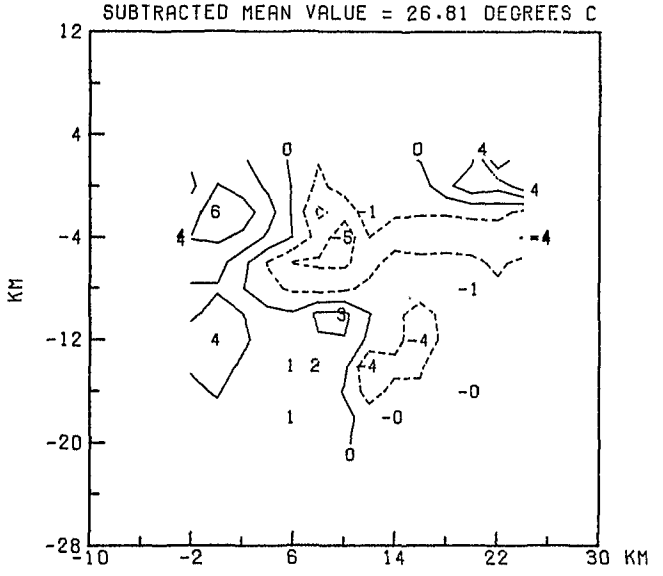

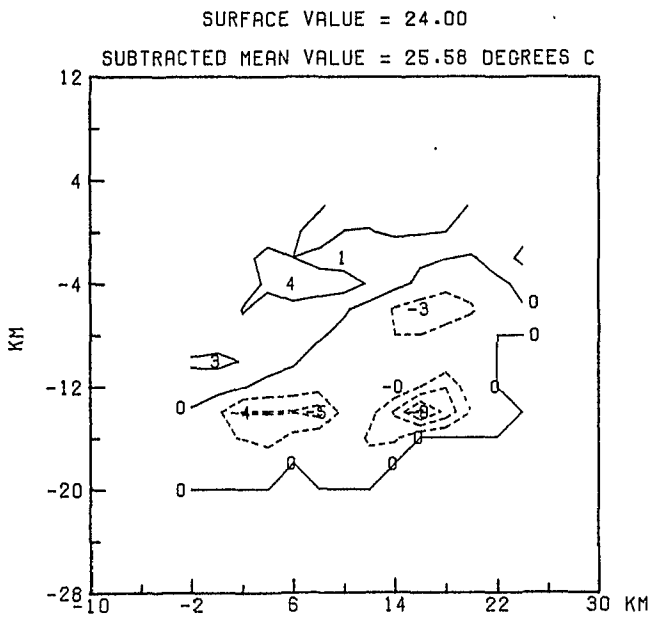

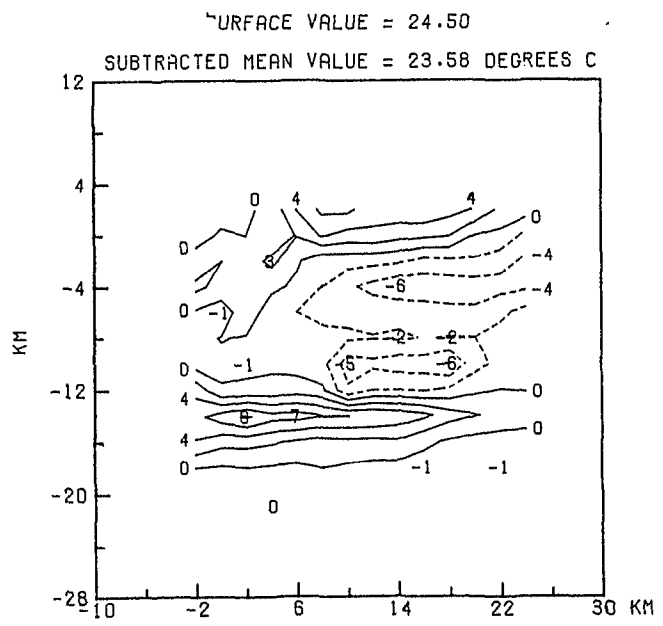

MAP 1L6

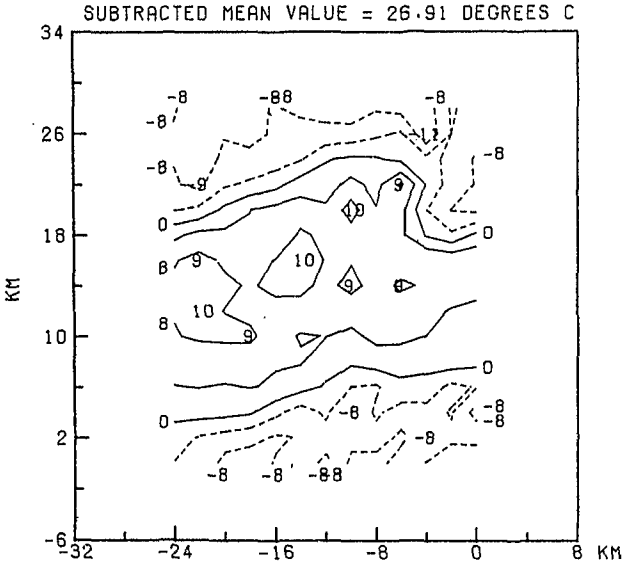

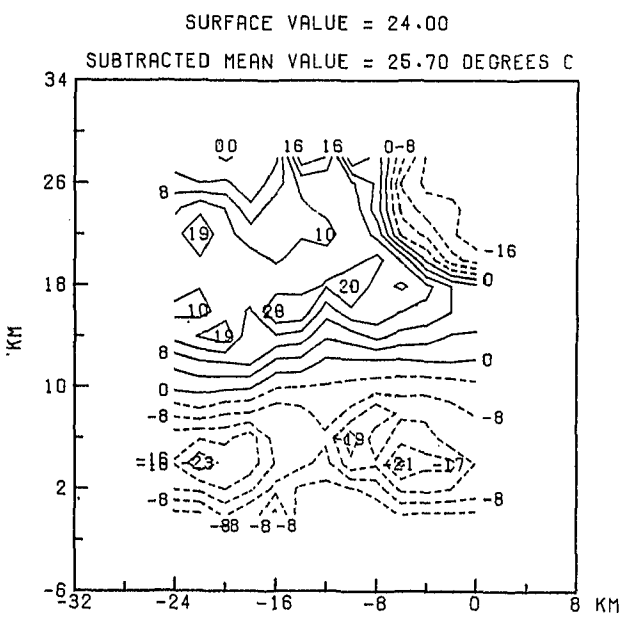

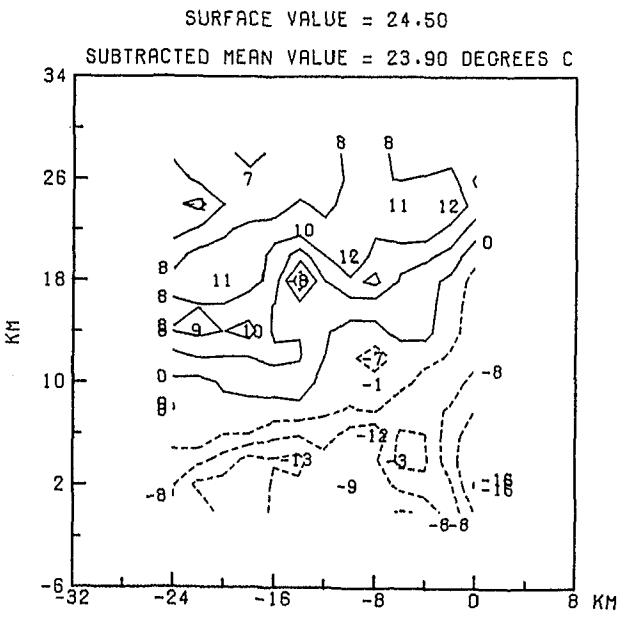

CONTOUR INTERVAL: 20 mK

CONTOUR INTERVAL: 40 mK

Fig. 7.12 :

POTENTIAL TEMPERATURE ON ISOPYCNIC SURFACES

Units: 10^{-2} K

MAP 1 L 7

SURFACE VALUE = 23.50

SUBTRACTED MEAN VALUE = 26.42 DEGREES C

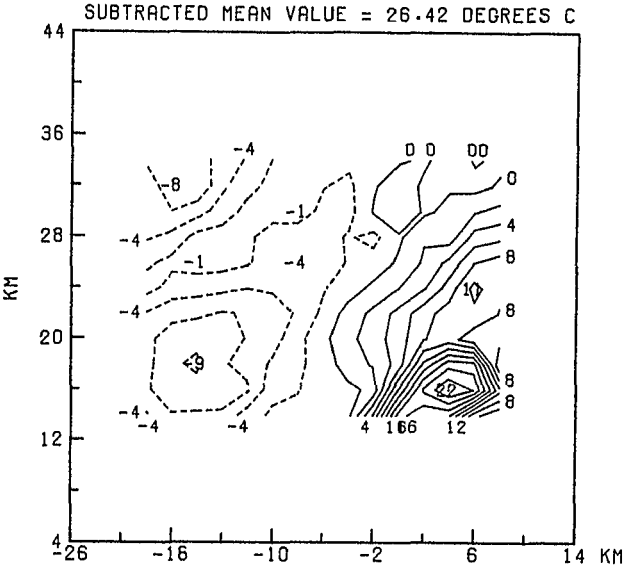

SURFACE VALUE = 24.00

SUBTRACTED MEAN VALUE = 25.15 DEGREES C

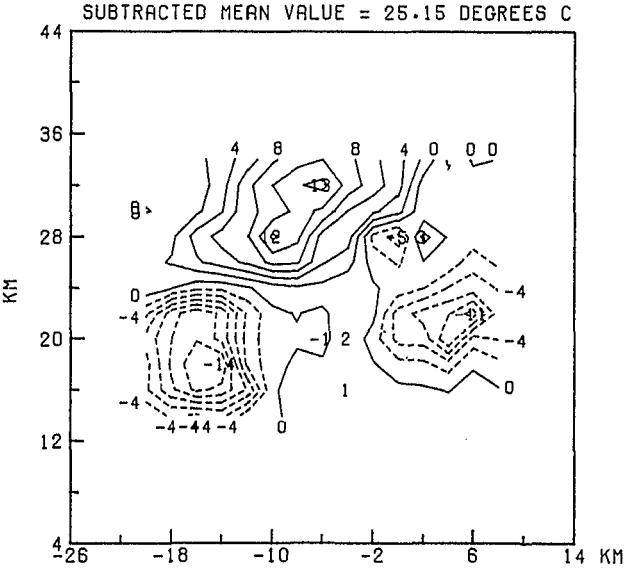

SURFACE VALUE = 24.50

SUBTRACTED MEAN VALUE = 23.13 DEGREES C

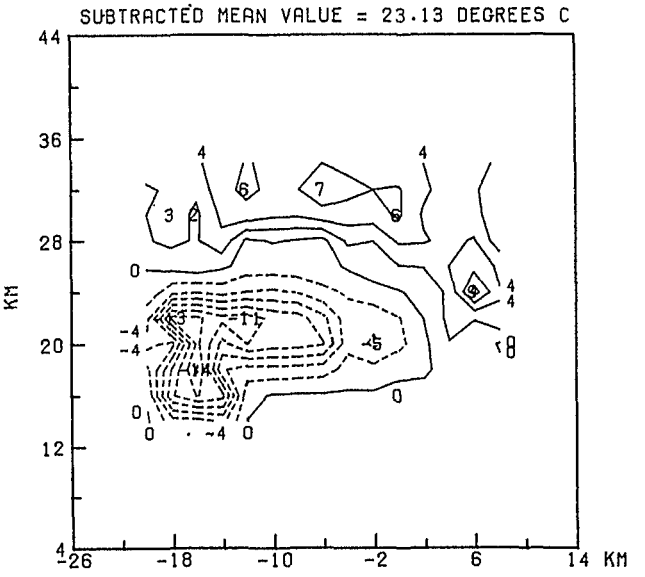

CONTOUR INTERVAL: 20 mK

Fig. 7.12 :

POTENTIAL TEMPERATURE ON ISOPYCNIC SURFACES

Units: 10^{-2} K

MAP 2L1

SURFACE VALUE = 23.50

SUBTRACTED MEAN VALUE = 26.69 DEG. C

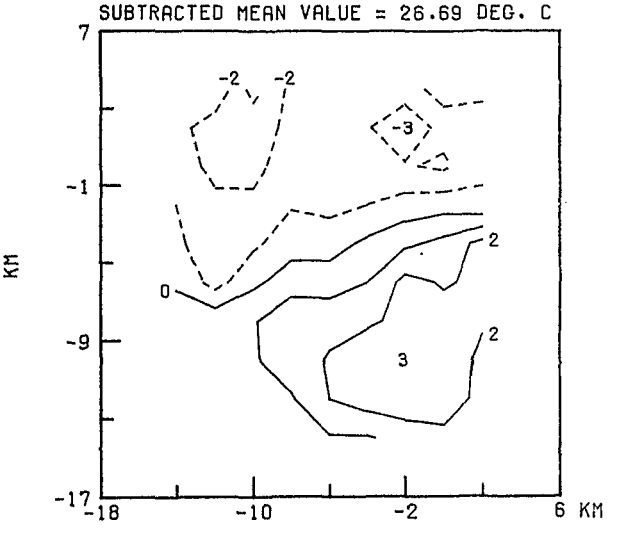

MAP 2L2

SURFACE VALUE = 23.50

SUBTRACTED MEAN VALUE = 26.68 DEG. C

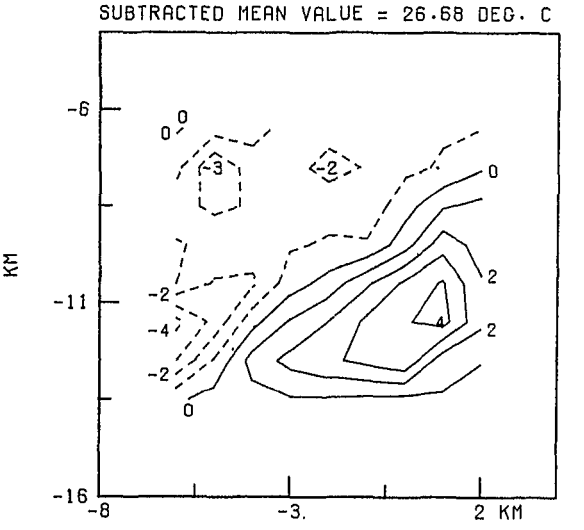

SURFACE VALUE = 24.00

SUBTRACTED MEAN VALUE = 25.78 DEG. C

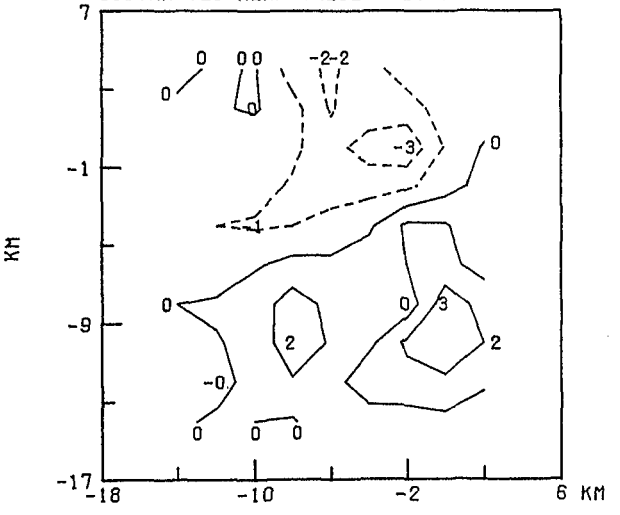

SURFACE VALUE = 24.00

SUBTRACTED MEAN VALUE = 25.77 DEG. C

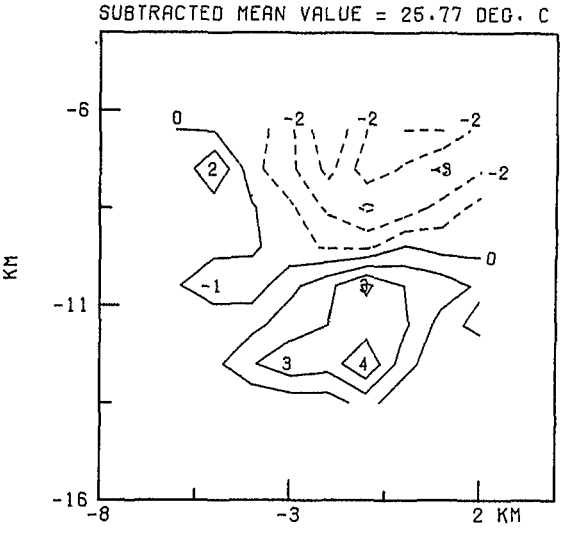

SURFACE VALUE = 24.50

SUBTRACTED MEAN VALUE = 23.98 DEG. C

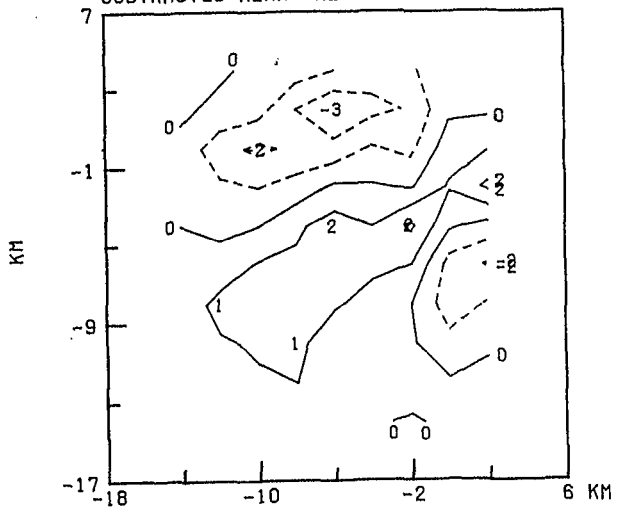

SURFACE VALUE = 24.50

SUBTRACTED MEAN VALUE = 23.97 DEG. C

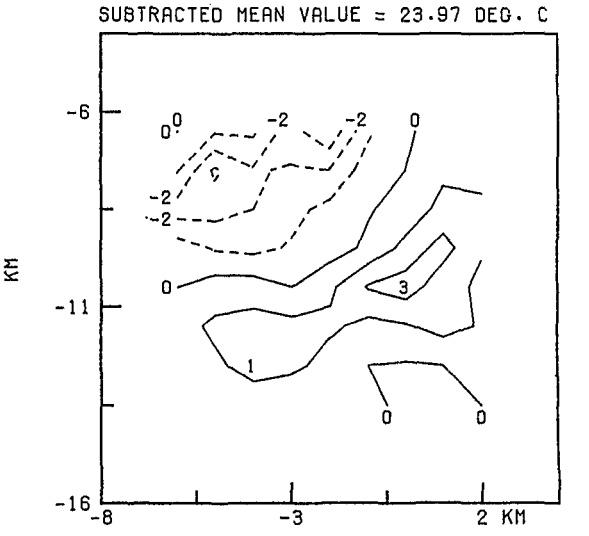

CONTOUR INTERVAL: 10 mK

CONTOUR INTERVAL: 10 mK

Fig. 7.12 :

POTENTIAL TEMPERATURE ON ISOPYCNIC SURFACES

Units: 10^{-2} K

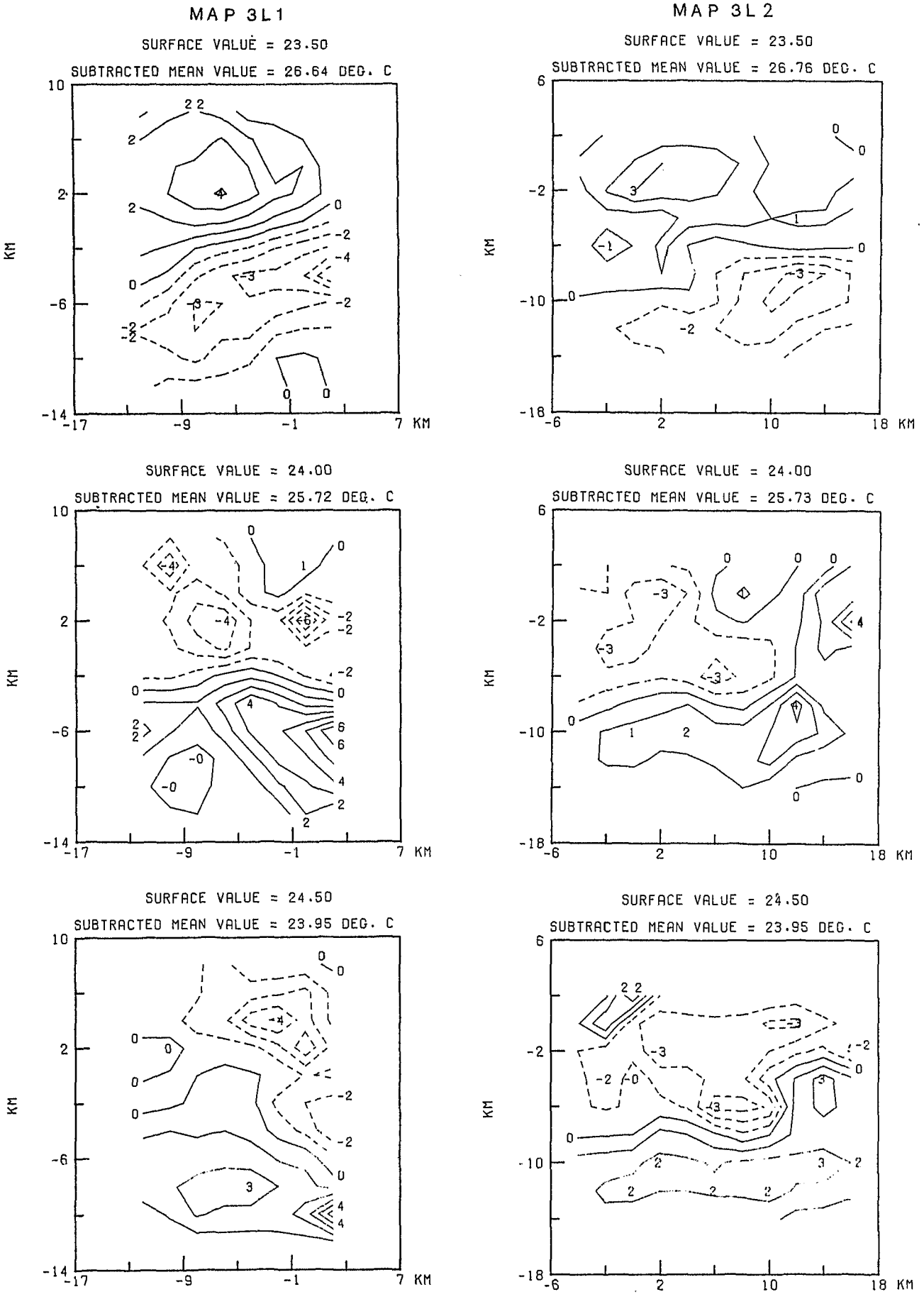

CONTOUR INTERVAL: 10 mK

CONTOUR INTERVAL: 10 mK

Fig. 7.12 :

POTENTIAL TEMPERATURE ON ISOPYCNIC SURFACES

Units: 10^{-2} K

MAP 3L3

SURFACE VALUE = 23.50

SUBTRACTED MEAN VALUE = 26.64 DEGREES C

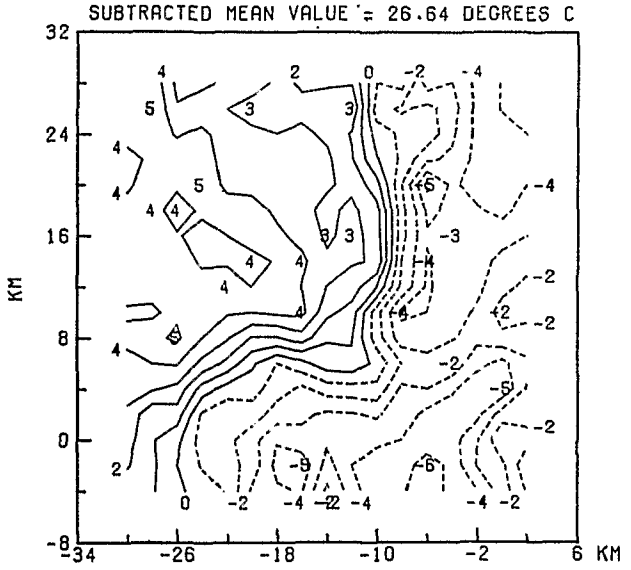

MAP 3L4

SURFACE VALUE = 23.50

SUBTRACTED MEAN VALUE = 26.64 DEG. C

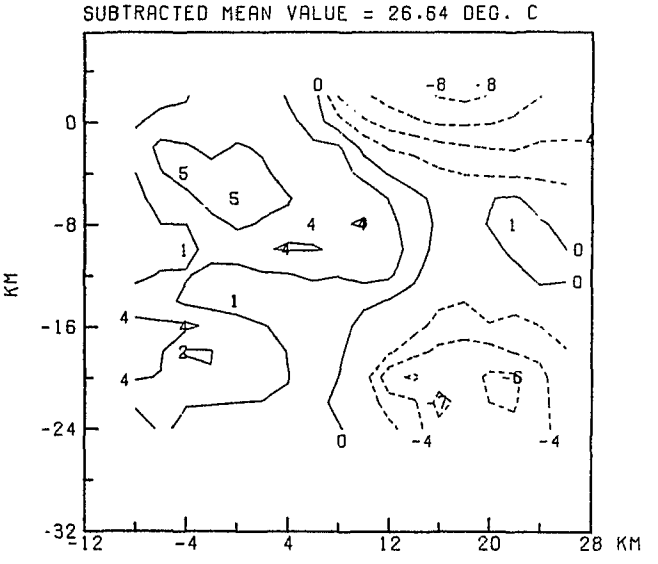

SURFACE VALUE = 24.00

SUBTRACTED MEAN VALUE = 25.73 DEGREES C

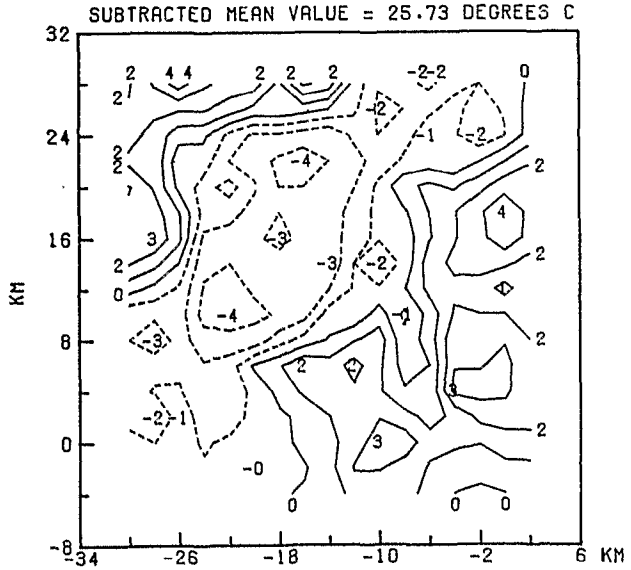

SURFACE VALUE = 24.00

SUBTRACTED MEAN VALUE = 25.73 DEG. C

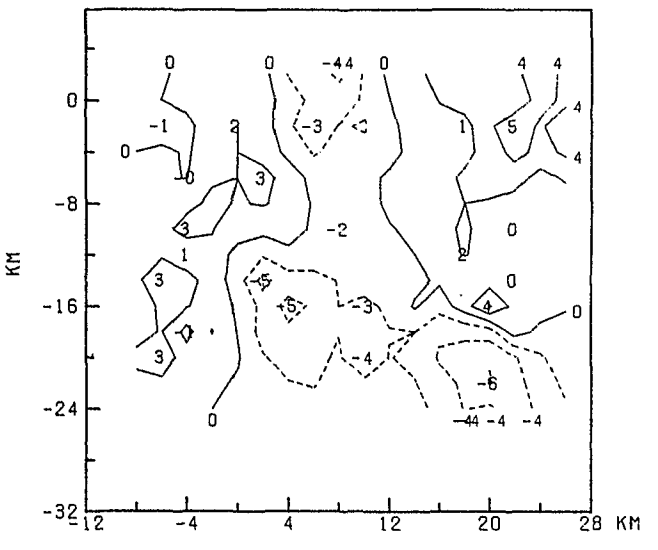

SURFACE VALUE = 24.50

SUBTRACTED MEAN VALUE = 23.96 DEGREES C

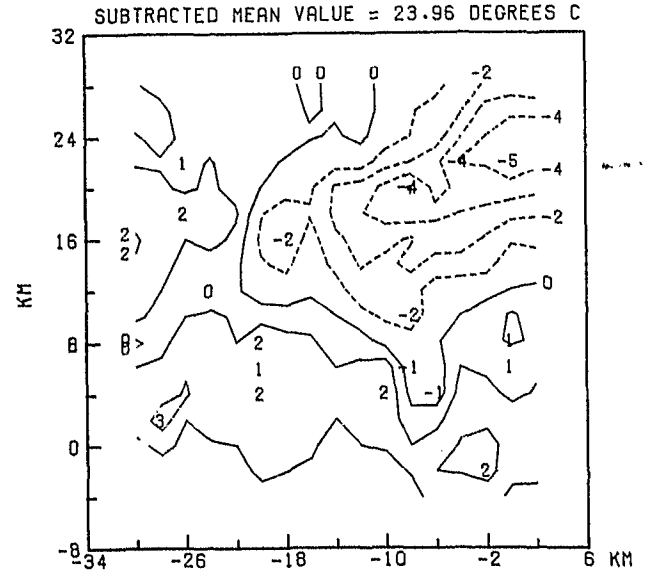

SURFACE VALUE = 24.50

SUBTRACTED MEAN VALUE = 23.94 DEG. C

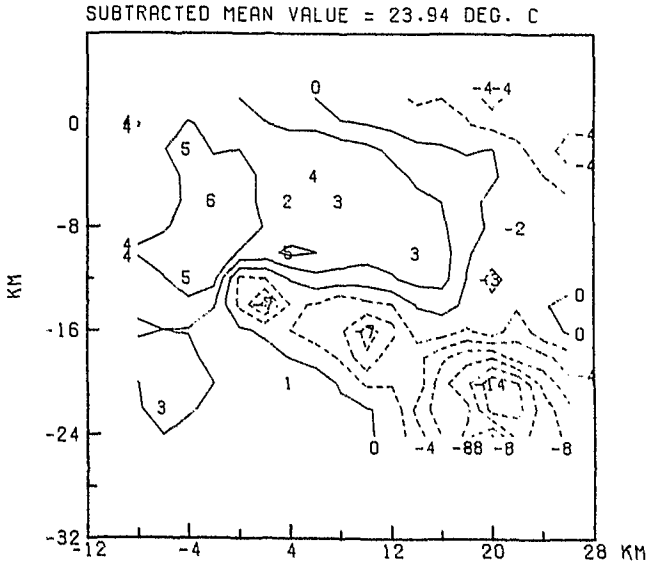

CONTOUR INTERVAL: 10 mK

CONTOUR INTERVAL: 20 mK

Fig. 7.12 :

THICKNESS BETWEEN ISOPYCNIC SURFACES

MAP 1L1 Units: dbar MAP 1L2

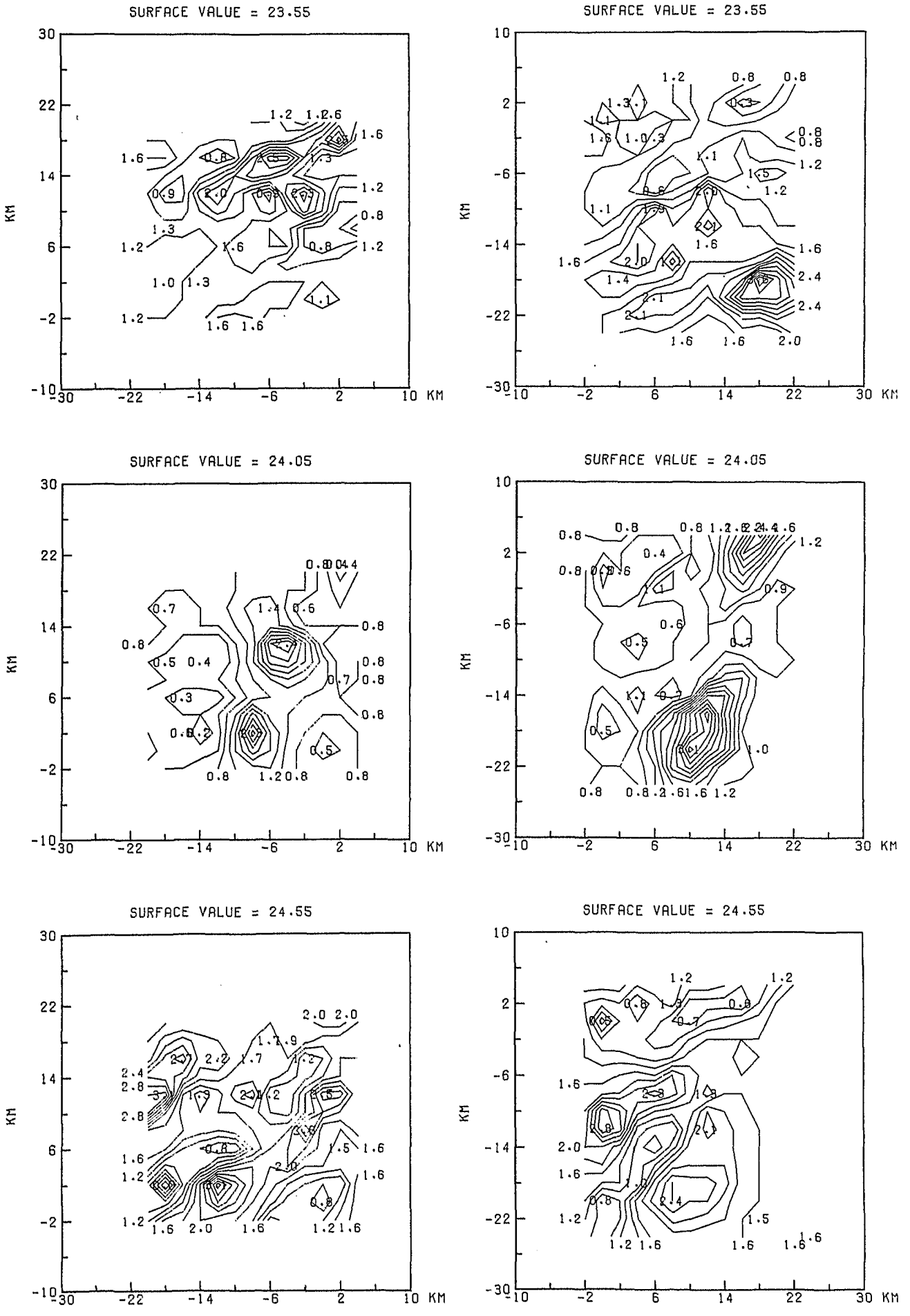

CONTOUR INTERVAL: 0.2 dbar Fig. 7.13 CONTOUR INTERVAL: 0.2 dbar

THICKNESS BETWEEN ISOPYCNIC SURFACES

MAP 1L3 Units: dbar MAP 1L4

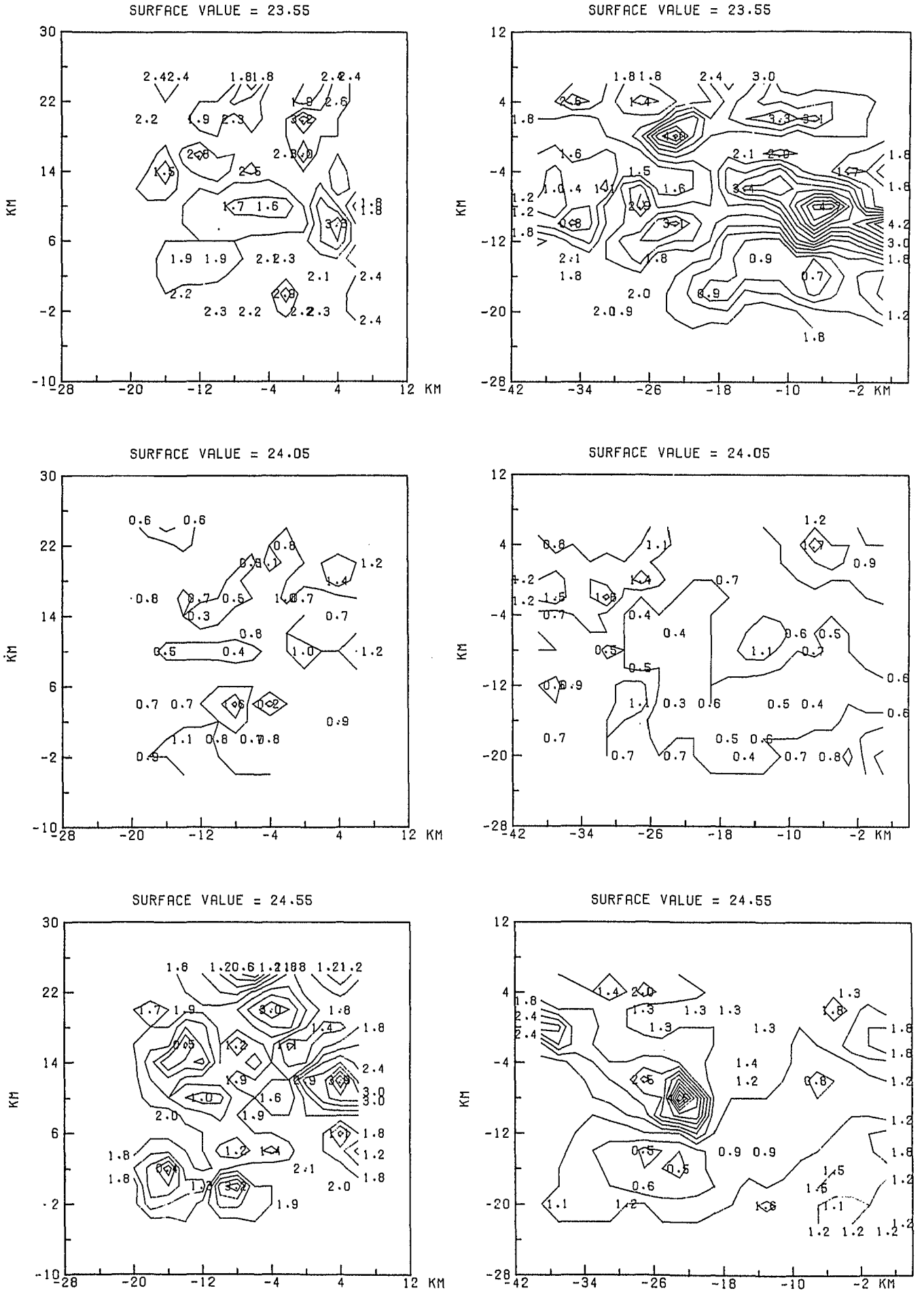

CONTOUR INTERVAL: 0.3 dbar Fig. 7.13 CONTOUR INTERVAL: 0.3 dbar

THICKNESS BETWEEN ISOPYCNIC SURFACES

MAP 1L5 Units: dbar MAP 1L6

SURFACE VALUE = 23.55

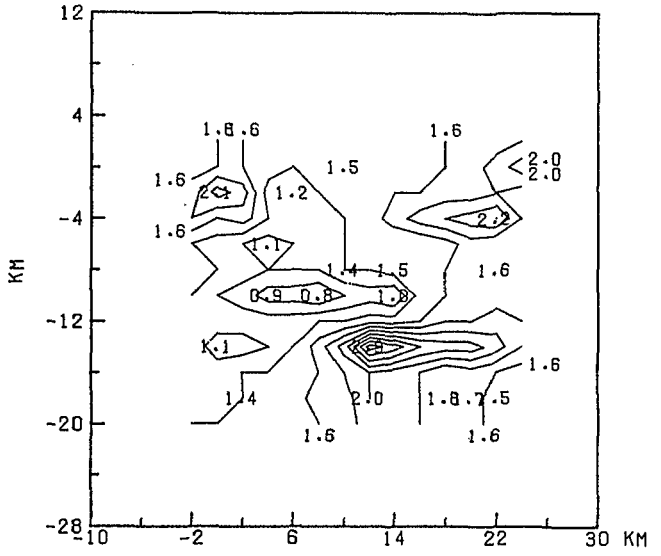

SURFACE VALUE = 23.55

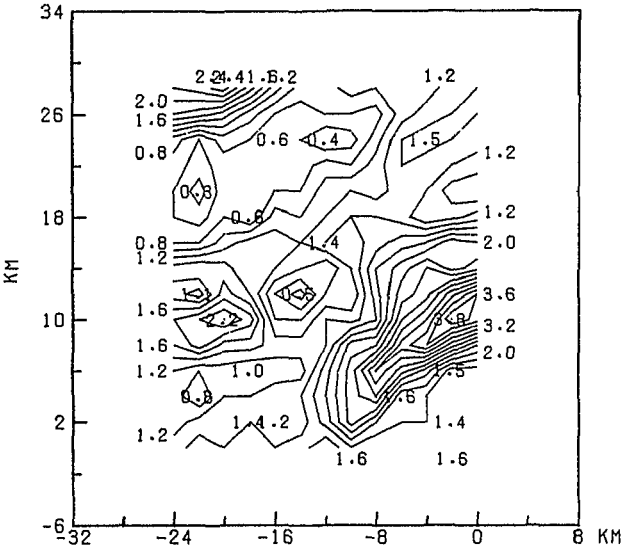

SURFACE VALUE = 24.05

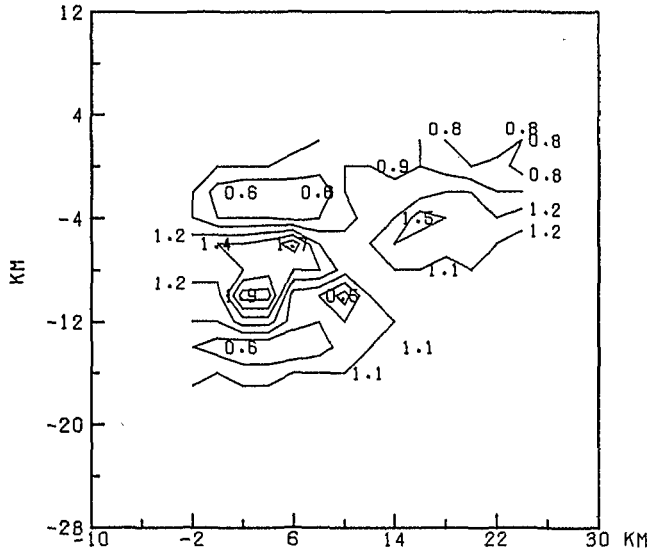

SURFACE VALUE = 24.05

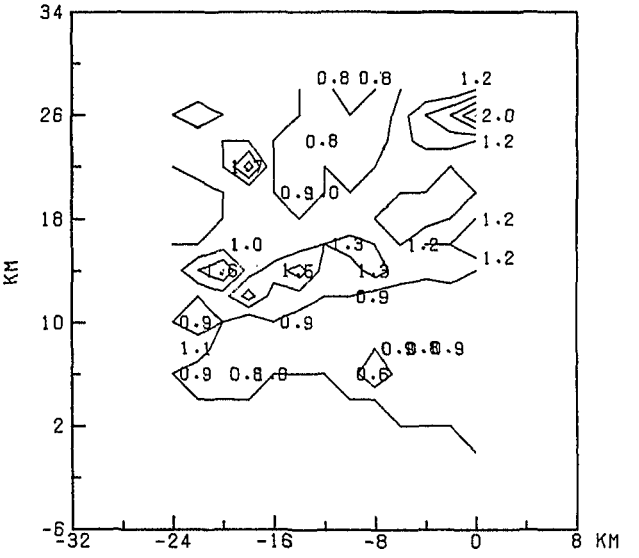

SURFACE VALUE = 24.55

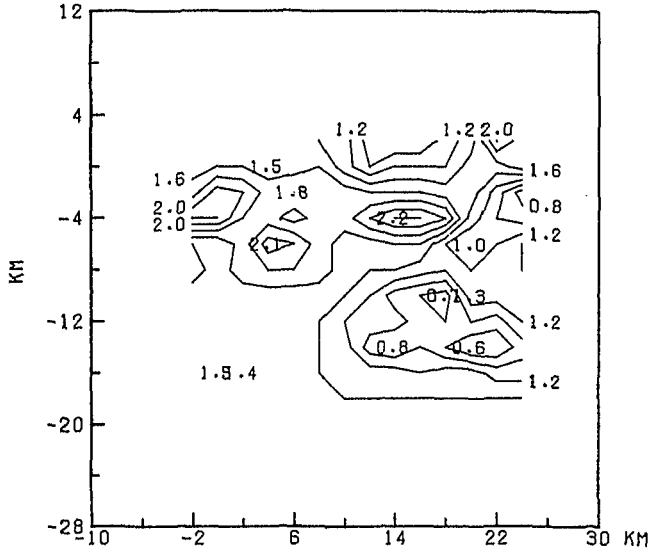

SURFACE VALUE = 24.55

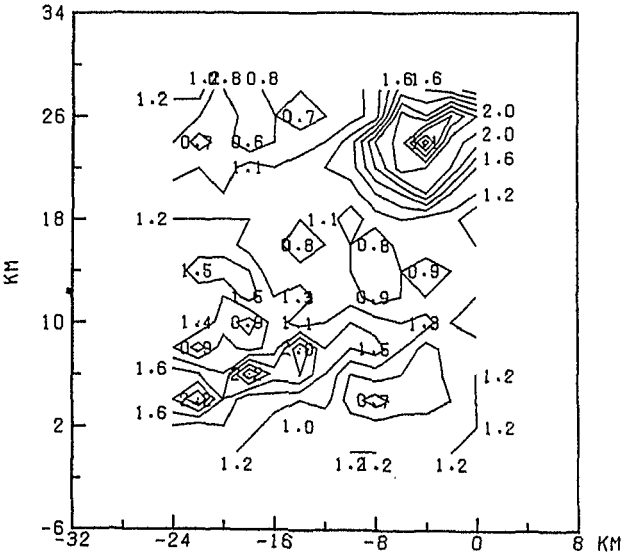

CONTOUR INTERVAL: 0.2 dbar

Fig. 7.13

CONTOUR INTERVAL: 0.2 dbar

THICKNESS BETWEEN ISOPYCNIC SURFACES

Units: dbar

MAP 1 L7

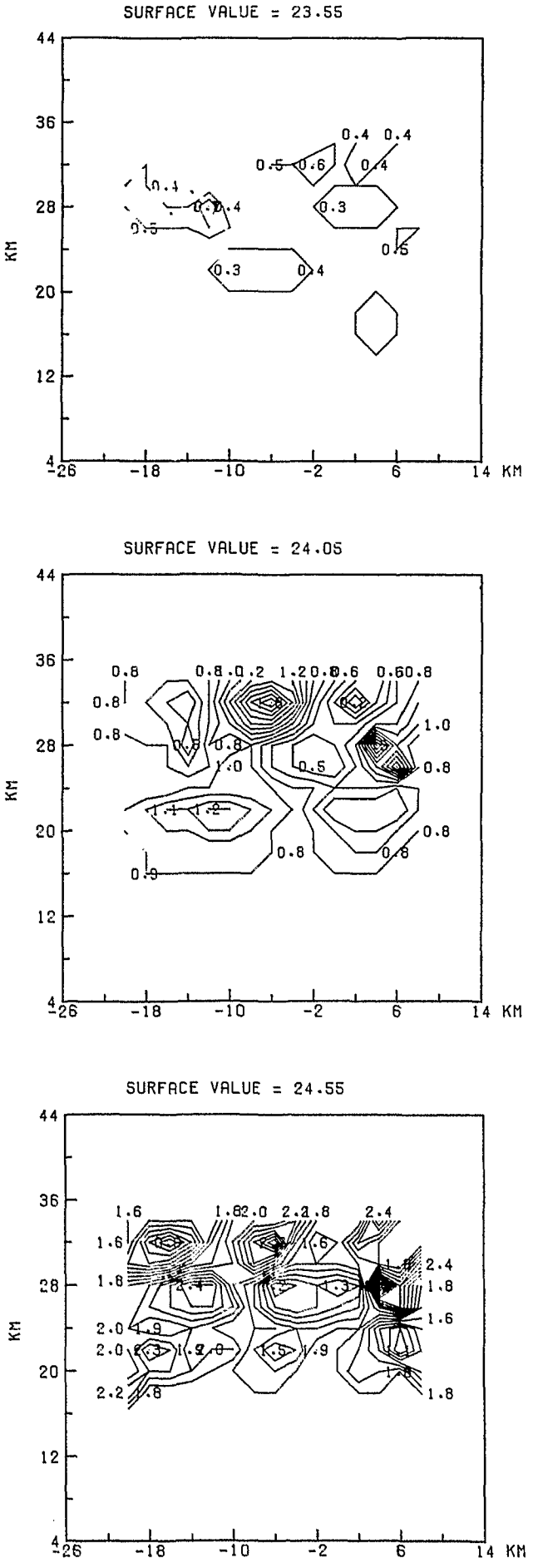

Fig. 7.13 CONTOUR INTERVAL: 0.1 dbar

THICKNESS BETWEEN ISOPYCNIC SURFACES

Units: dbar

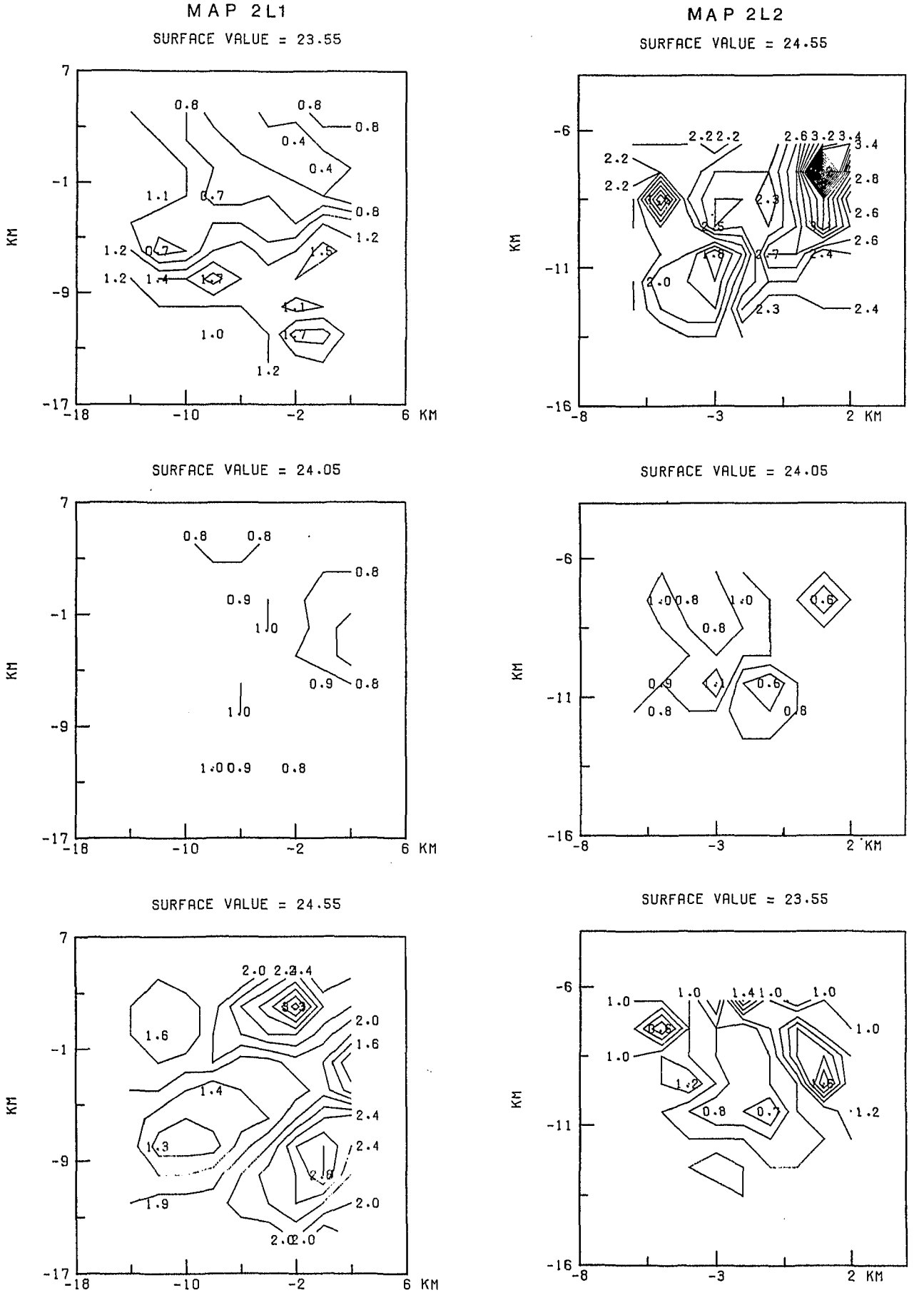

CONTOUR INTERVAL: 0.2 dbar Fig. 7.13 CONTOUR INTERVAL: 0.1 dbar

THICKNESS BETWEEN ISOPYCNIC SURFACES

Units: dbar

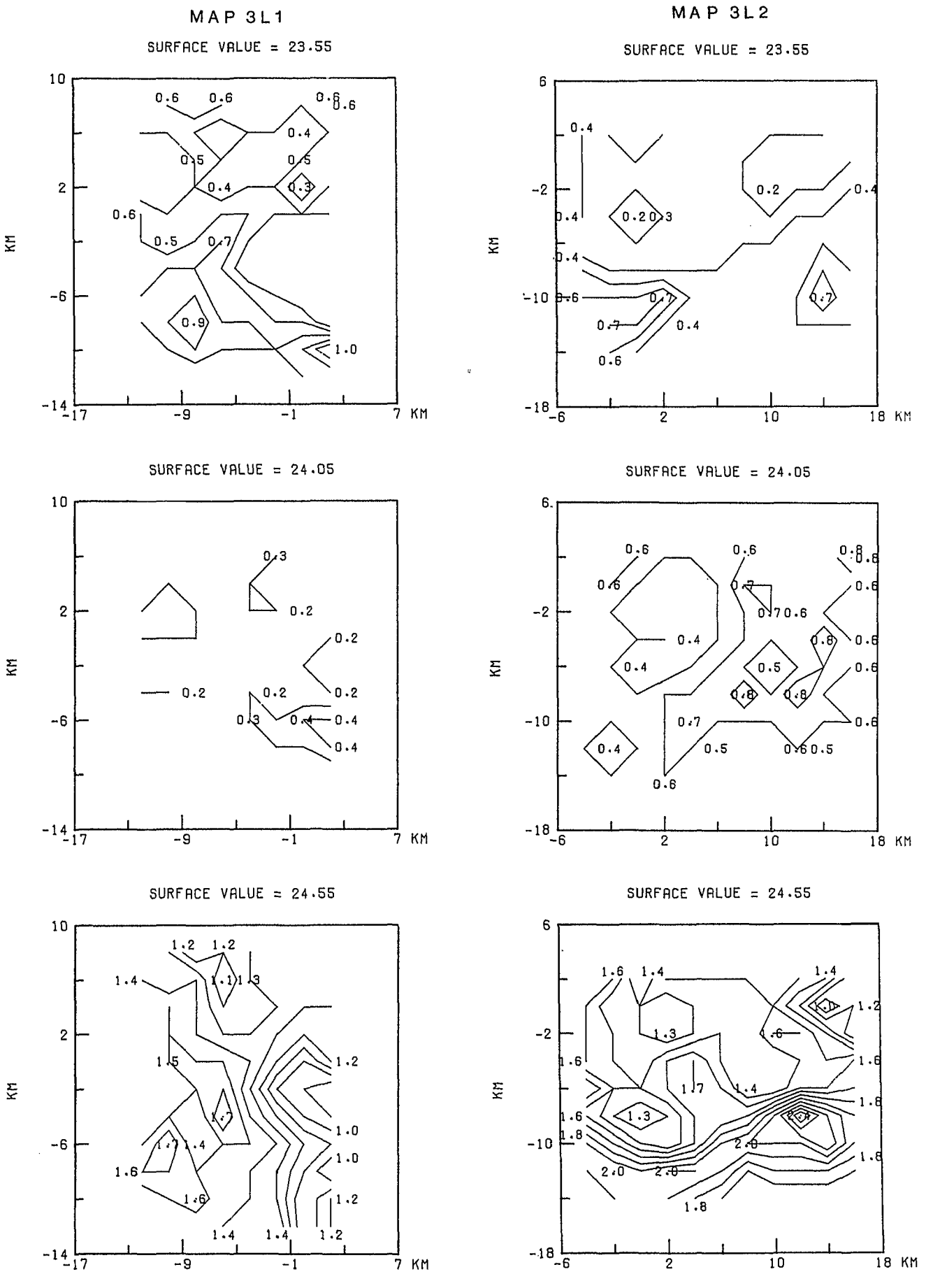

CONTOUR INTERVAL: 0.1 dbar Fig. 7.13 CONTOUR INTERVAL: 0.1 dbar

THICKNESS BETWEEN ISOPYCNIC SURFACES

Units: dbar

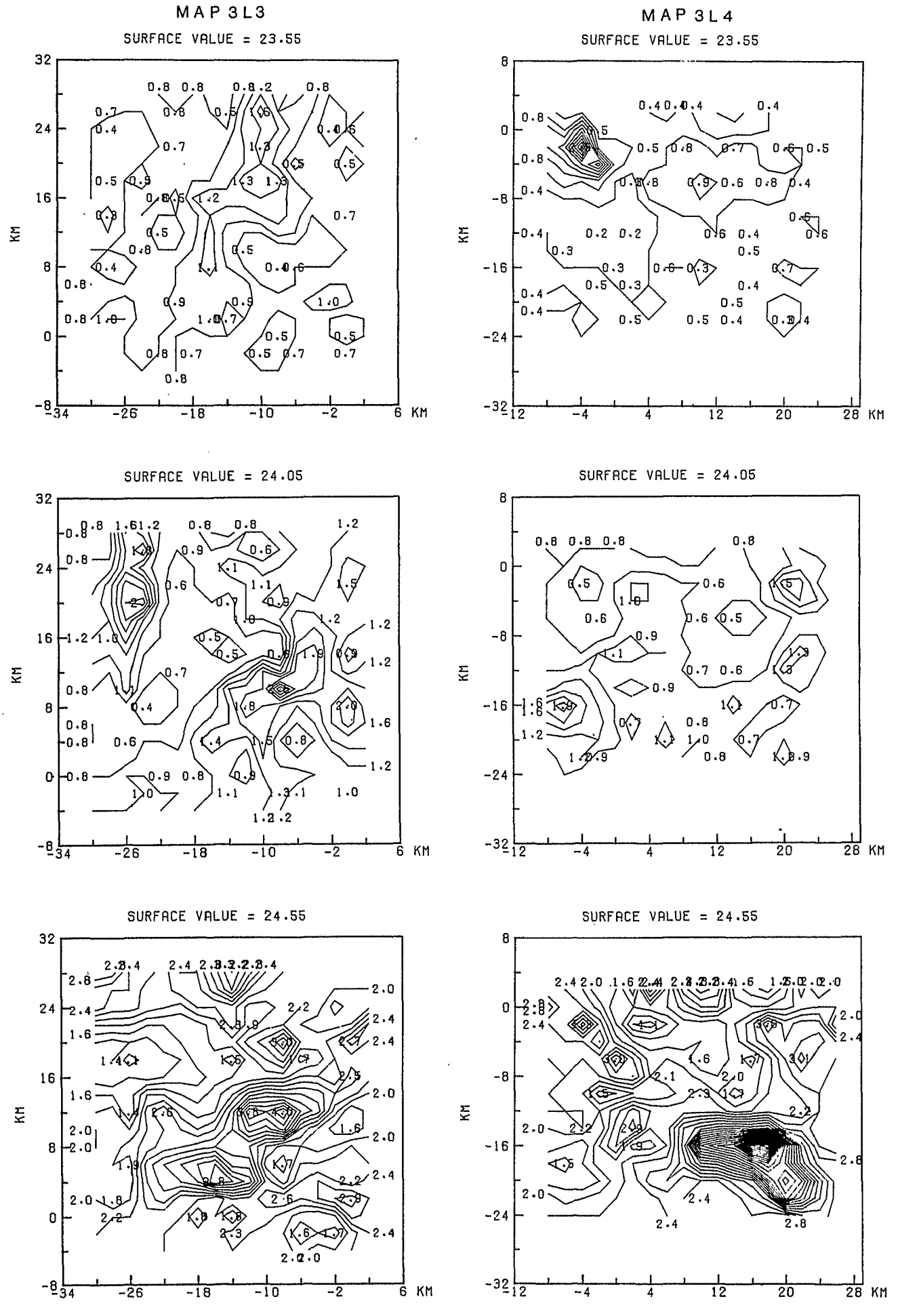

CONTOUR INTERVAL: 0.2 dbar

Fig. 7.13

CONTOUR INTERVAL: 0.2 dbar

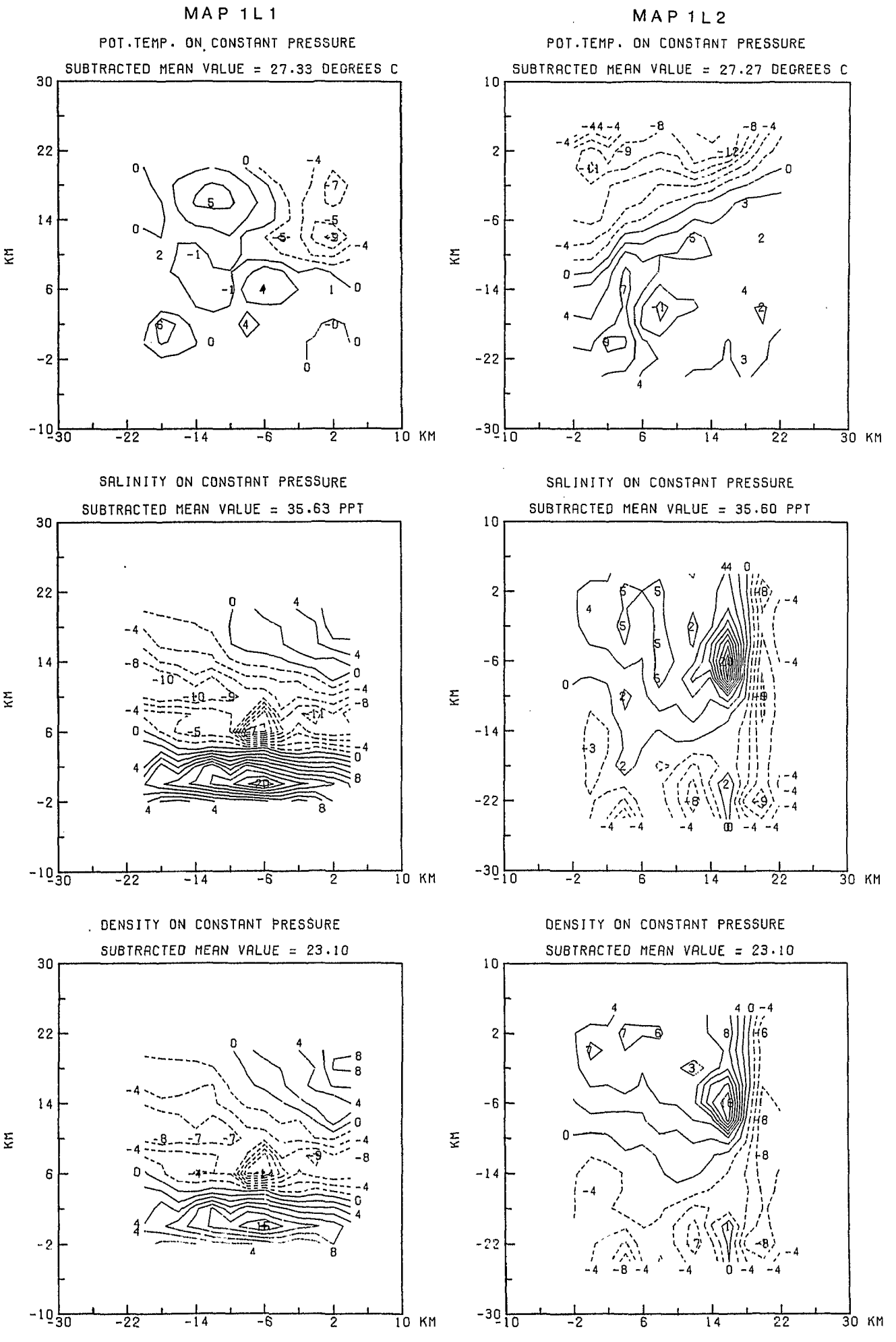

Figure 7.14 : UNITS: potential temperature: 10^{-2} K, salinity: 10^{-2} ppt, density: 10^{-2} kg m^{-3}, surface value: 16 dbar.

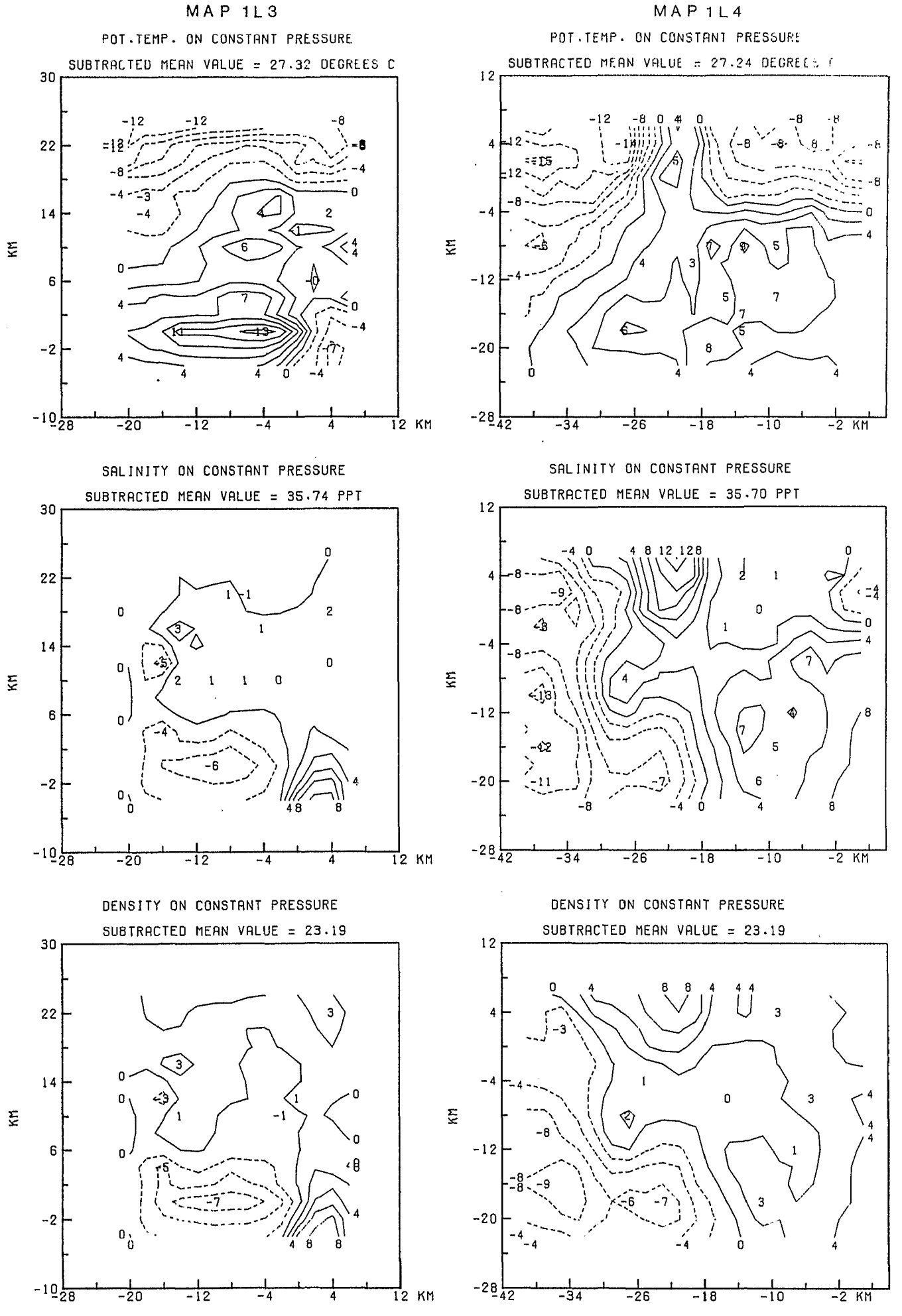

Figure 7.14 : UNITS: potential temperature: 10^{-2} K, salinity: 10^{-2} ppt, density: 10^{-2} kg m^{-3}, surface value: 16 dbar.

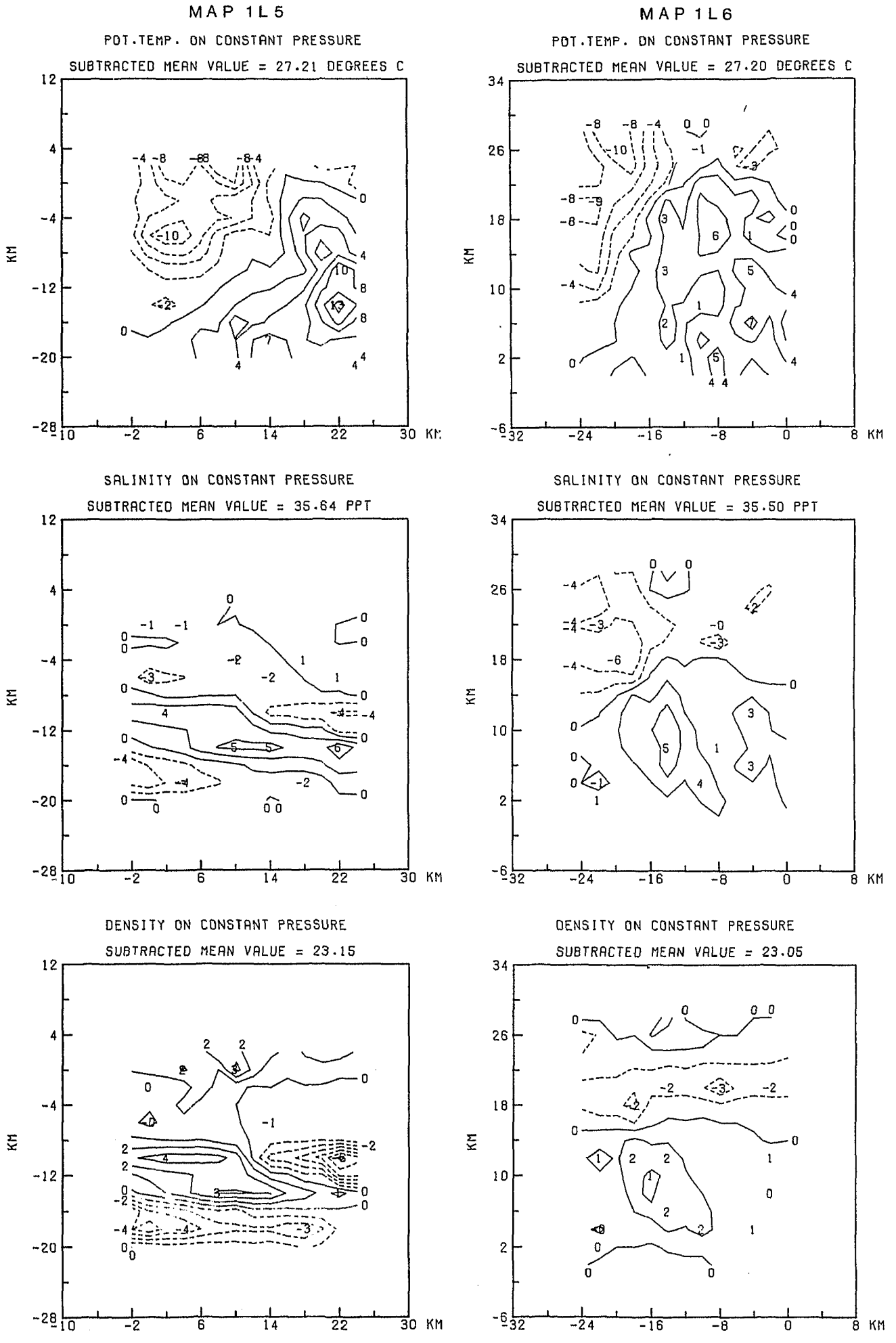

Figure 7.14 : UNITS: potential temperature: 10^{-2} K, salinity: 10^{-2} ppt, density: 10^{-2} kg m^{-3}, surface value: 16 dbar.

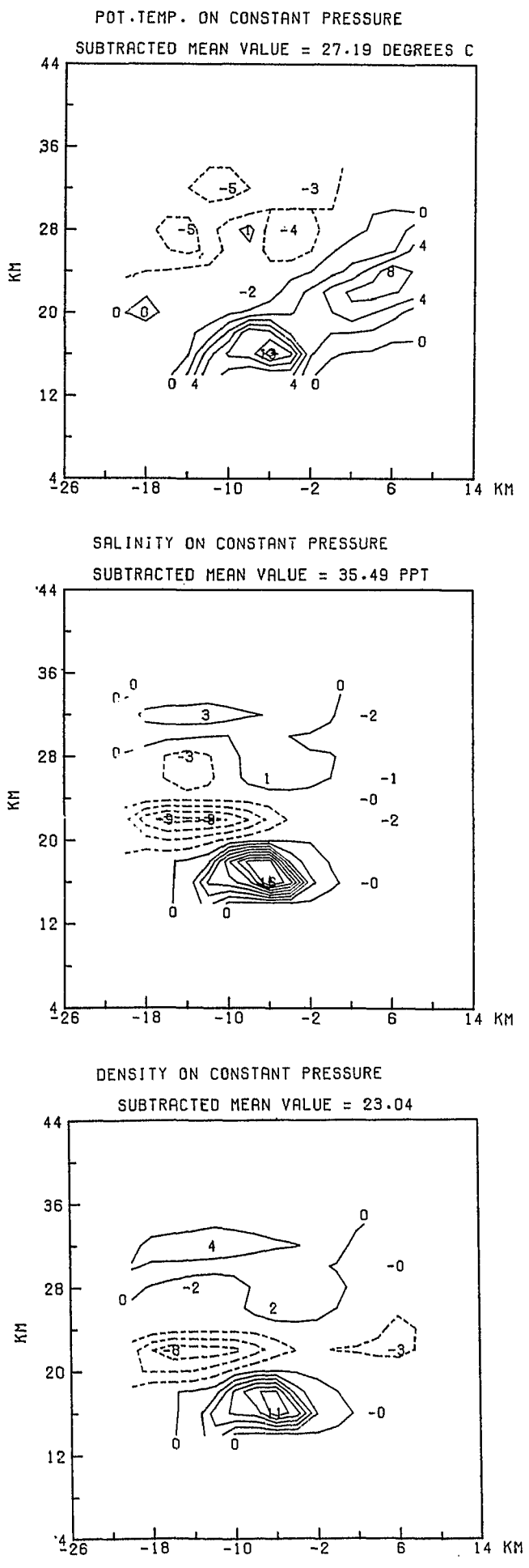

Figure 7.14 : UNITS: potential temperature: 10^{-2} K, salinity: 10^{-2} ppt, density: 10^{-2} kg m^{-3}, surface value: 16 dbar.

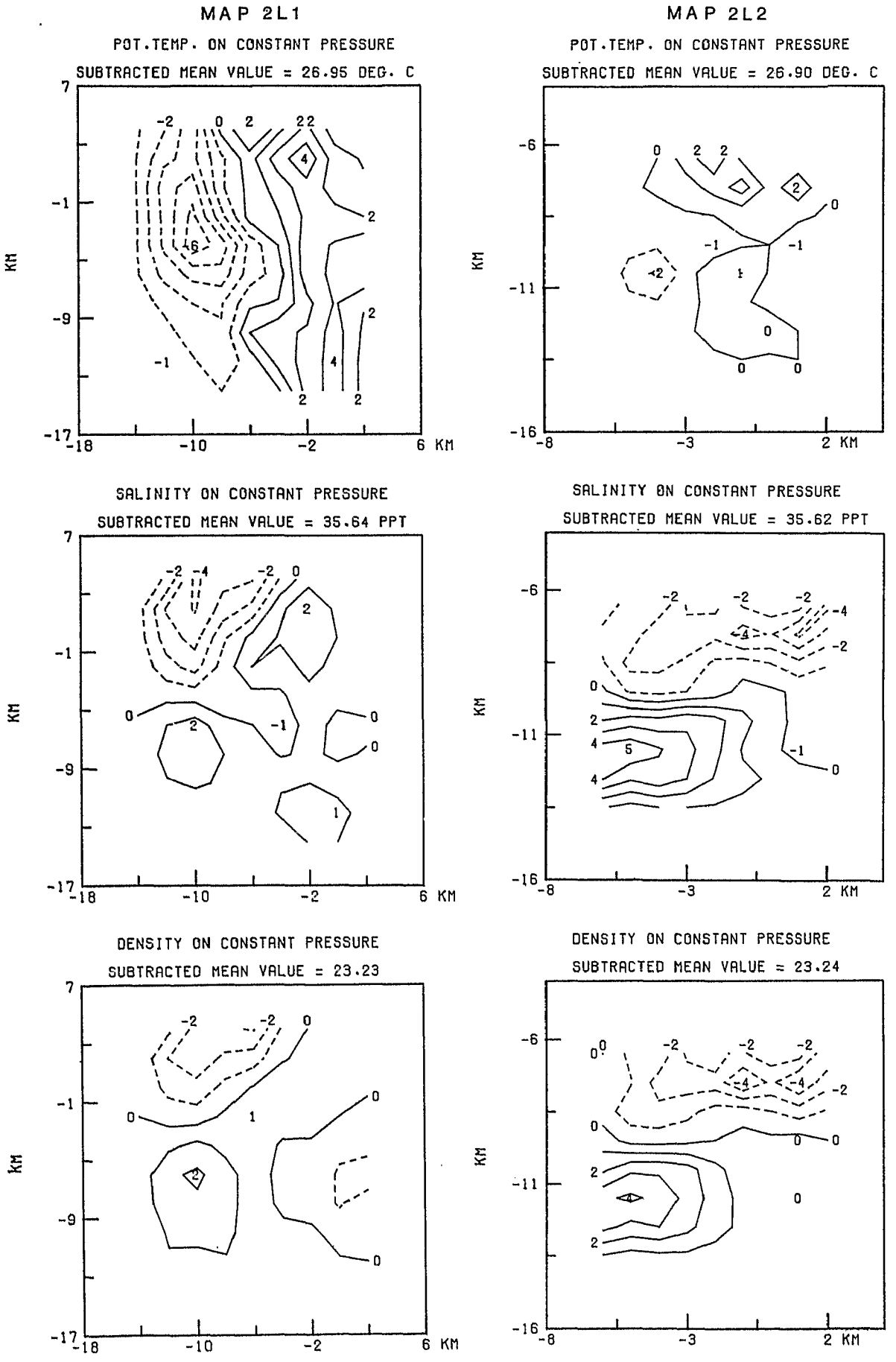

Figure 7.14 : UNITS: potential temperature: 10^{-2} K, salinity: 10^{-2} ppt, density: 10^{-2} kg m^{-3}, surface value: 16 dbar.

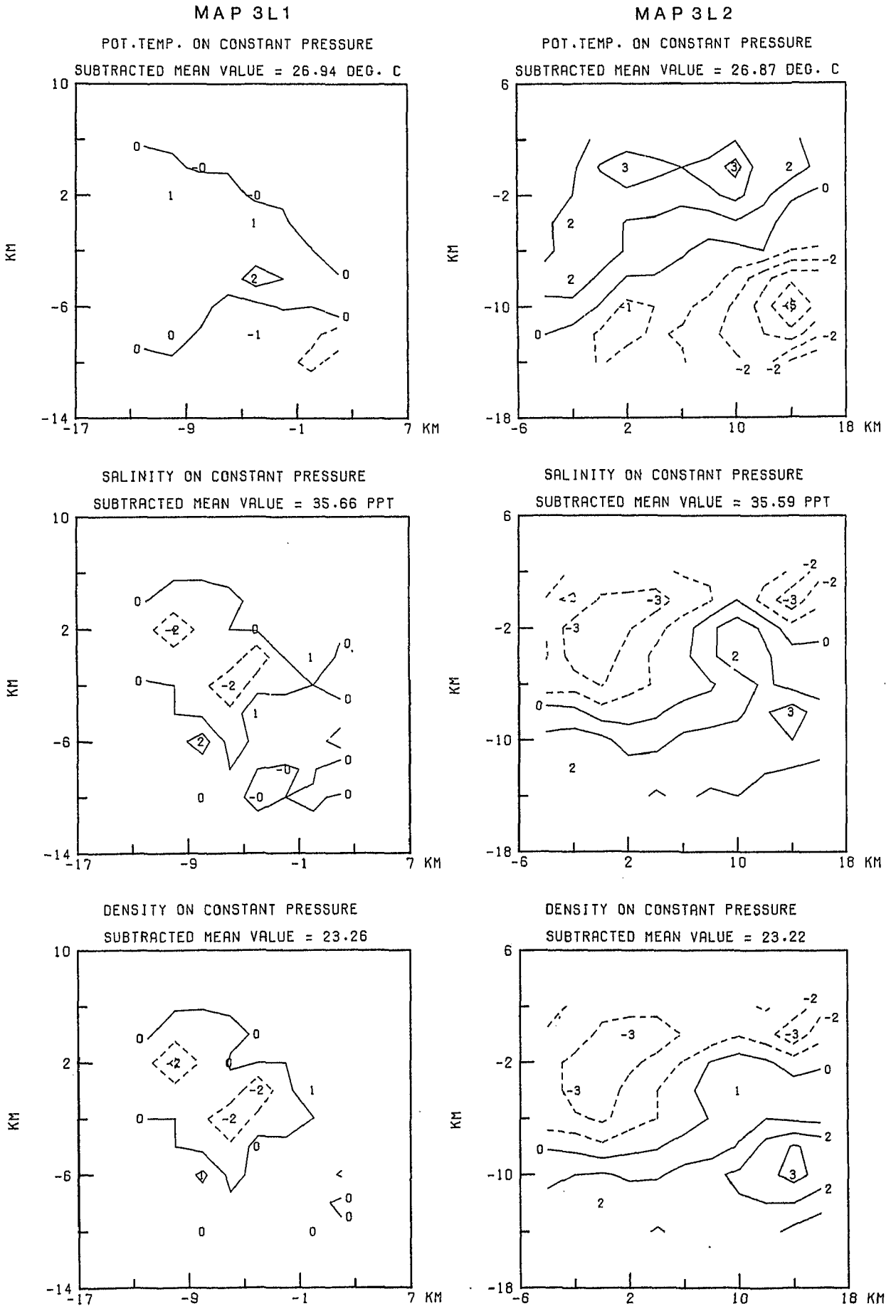

Figure 7.14 : UNITS: potential temperature: 10^{-2} K, salinity: 10^{-2} ppt, density: 10^{-2} kg m^{-3}, surface value: 16 dbar.

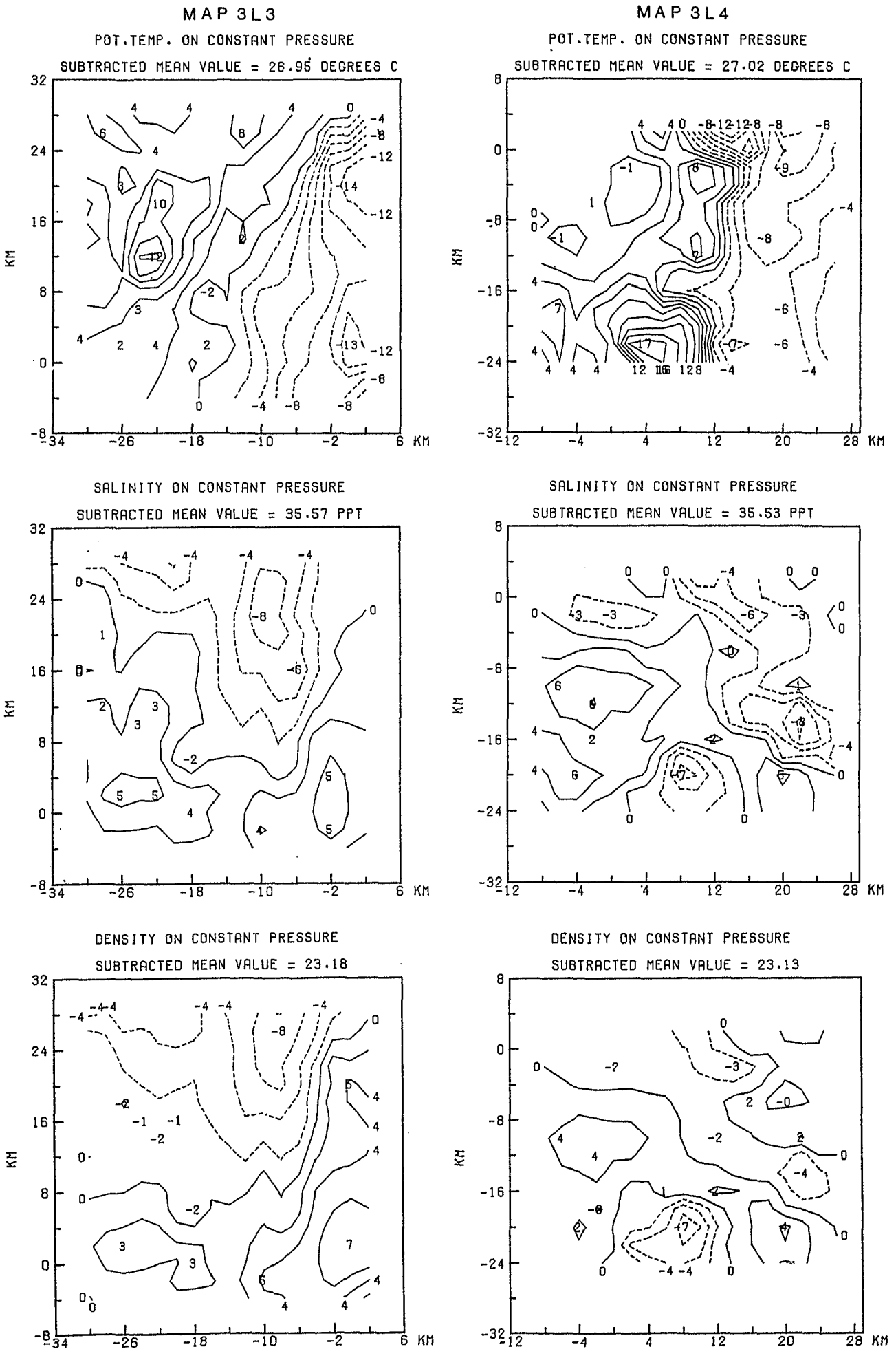

Figure 7.14 : UNITS: potential temperature: 10^{-2} K, salinity: 10^{-2} ppt, density: 10^{-2} kg m^{-3}, surface value: 16 dbar.

REFERENCES

Brown, N.L. (1974) A precision CTD microprofiler.
Proceedings of the IEEE International Conference on Engineering in the Ocean Environment, 42 pp.

Brown, N.L. and G. Morrison (1978) WHOI/Brown Conductivity, Temperature and Depth Microprofiler.
WHOI Technical Report 78-23. Unpublished manuscript.

Chee, L.S.H. (1977) An investigation of small scale fluctuations of sea surface temperature and salinity in the tropical convergence zone.
BSc Dissertation, University of Southampton.

Crease, J. and T. Sankey (1974) Algorithms for deriving oceanographic variables. Private communication.

Dessureault, J.G. (1976) "Batfish" - A depth controllable towed body for collecting oceanographic data.
Ocean Engineering 3, 99-111

Düing, W. (1980) GATE, Volume 2, Equatorial and A-Scale Oceanography.
Deep-Sea Res., Supplement II to Volume 26.

Düing, W., F. Ostapoff and J. Merle (1980) Physical Oceanography of the Tropical Atlantic during GATE.
Intergovernmental Oceanographic Commission and University of Miami, x + 117.

Eames, M.C. (1956) The configuration of a cable towing a heavy submerged body from a surface vessel.
Naval Research Establishment, Dartmouth, Nova Scotia. PHX-103. November 1956. Defence Research Board, Department of National Defence, Canada.

Elliott, J.A. and N.S. Oakey (1975) Horizontal coherence of temperature microstructure.
Journal of Physical Oceanography 5, 506-515.

Fofonoff, N.P., S.P. Hayes and R.C. Millard (1974) WHOI/Brown CTD Microprofiler: methods of calibration and data handling.
WHOI Technical Report 74-89.

GARP (1972) Experimental Design Proposal for the GARP Atlantic Tropical Experiment.
GATE Report No.1 (WMO/ICSU).

Halpern, D. (1975) Investigations of oceanic mesoscale structures near the ocean-atmosphere boundary.
Unpublished mansucript.

Hastenrath, S. and P.J. Lamb (1977) Climatic Atlas of the Tropical Atlantic and Eastern Pacific Oceans.
University of Wisconsin Press, Madison, 105 pp.

Hastenrath, S. and P.J. Lamb (1978) Heat Budget Atlas of the Tropical Atlantic and Eastern Pacific Oceans.
University of Wisconson Press, Madison, 104 pp.

ICSU/WMO (1975a) Preliminary Scientific Results of the GATE.
GATE Report 14.

ICSU/WMO (1975b) Report on the Field Phase of the GATE: Meteorological Atlas.
GATE Report 17.

Institute of Oceanographic Sciences (1975) GATE Phase III C-Scale Experiment. RRS "Discovery" Cruise 66, 31 August - 29 September 1974.
Cruise Report No. 20.

Käse, R.H. and R.A. Clarke (1978) High Frequency Internal Waves in the Upper Thermocline during GATE.
Deep-Sea Res. 25, 815-825.

Käse, R.H. and G. Siedler (1980) Internal Wave Kinematics in the Upper Tropical Atlantic.
Deep-Sea Res. Supplement I to Volume 26, 161-189.

Kassler, B. (1980) Die Verteilung von Dichteinversionen im GATE-Datensatz der RRS "Discovery".
Diplomarbeit, Universität Kiel.

Katz, E.J. (1969) Further Study of a Front in the Sargasso Sea.
Tellus 21, 259-269.

Katz, E.J. (1973) Profile of an isopycnic surface in the main thermocline of the Sargasso Sea.
J. Physical Oceanogr. 3, 448-457.

Kronfeld, U. (1982) Die Wärmebilanz der ozeanischen Deckschicht in einer mesoskaligen Front im GATE C-Gebiet.
Diplomarbeit, Universität Kiel.

Leach, H. (1984) Statistics of the three-dimensional isopycnal structure of thickness and temperature in the GATE "Discovery" Batfish Data.
In preparation.

Leach, H., P.J. Minnett and J.D. Woods (1984) The GATE Lagrangian Batfish Experiment.
Submitted to Deep-Sea Res.

Lewis, E.L. and R.G. Perkin (1978) Salinity: Its Definition and Calculation.
J. Geophys. Res. 83, 466-478.

MacVean, M.K. (1977) Models of Upper-Ocean Fronts.
Ph.D. Thesis, University of Southampton.

MacVean, M.K. (1980) Bericht an die DFG zum Projekt "Theoretische Untersuchung von ozeanischen Fronten".
Institut für Meereskunde, Kiel, unpublished.

MacVean, M.K. and J.D. Woods (1980) Redistribution of scalars during upper ocean frontogenesis - a numerical model.
Q. J. Roy. Met. Soc. 106, 293-311.

Merle, J. (1978) Atlas hydrologique saisonnier de l'Ocean Atlantique inter-tropical.
ORSTOM, Paris, 184 pp.

Minnett, P.J. (1978) Mesoscale Variability in the Tropical Thermocline during GATE.
Ph.D. Thesis, University of Southampton, vi + 265 pp.

Montgomery, R.B. (1938) Circulation in upper layers of southern North Atlantic deduced with use of isentropic analysis.
Papers in Physical Oceanography and Meteorology, 6(2), 55 pp.

Ostapoff, F., Y. Tarbeyer and S. Worthem (1973) Heat flux and precipitation estimates from oceanographic observations.
Science 180, 960-962

Parr, A.E. (1936) On the probable relationship between vertical stability and lateral mixing processes.
Journal du Conseil 11, 308-313.

Pegler, R.J. (1976) Sound speed variability on 1 to 20 km length scales in a tropical thermocline region.
MSc. Dissertation, University of Southampton.

Perkins, H.T. and J.C. Van Lear (1977) Simultaneous current-temperature profiles in the Equatorial Counter Current.
J. Phys. Oceanogr. 7, 264-271.

Philander, S.G.H. (1975) Field Phase report of the Oceanic Subprogramme. In: Report on the Field Phase of the GATE Scientific Programme.
GATE Report No. 16. ICSU/WMO, Geneva.

Rooth, C. (1973) Unpublished report on a cruise to the GATE-Area in 1973.

SCOR (1973) Proposal for a GATE Oceanographic Program.

Siedler, G. and J.D. Woods (1980) GATE, Volume 1, Oceanography and Surface Layer Meteorology in the B/C-Scale.
Deep-Sea Res., Supplement I to Volume 26

Siedler, G. and S.G.H. Philander (1982) Physics of the Upper Ocean.
Chapter 7 in The GARP Atlantic Tropical Experiment (GATE) Monograph.
GARP Publications Series No 25, WMO/ICSU, Geneva.

Tang, C. (1984) Statistics of static stability in the Batfish data from GATE.
In preparation.

Tucker, M.J. et al. (1970) Two component electromagnetic ship's log.
Journal of the Institute of Navigation, 23, 302-316

Van Leer, J.W. Düing, R. Erath, E. Kelly and A. Speidel (1974) The Cyclesonde: an unattended vertical profiler for scalar and vector quantities in the upper ocean.
Deep-Sea Res. 21, 385-450.

Voorhis, A.D. (1969) The horizontal extent and persistence of Thermal Fronts in the Sargasso Sea.
Deep-Sea Res. 16 (Supplement), 331-337.

Wilson, W.D. (1960) Equation for the Speed of Sound in Sea Water.
Journal of the Acoustic Society of America, 32, 1357.

Woods, J.D. (1968) Wave induced shear-instability in the summer thermocline.
Journal of Fluid Mechanics 32, 791-800.

Woods, J.D. (1974) Batfish Experiments on RRS "Discovery" during Phase III of GATE. Part 1: Measurements and analysis at sea.
Report, Department of Oceanography, University of Southampton.

Woods, J.D. (1980) The generation of thermohaline finestructure at fronts in the ocean.
Ocean Modelling 32, 1-4. Unpublished manuscript.

Woods, J.D. (1981) A Mesoscale Front in the North Atlantic Equatorial Counter Current.
Unpublished manuscript.

Woods, J.D. and R.L. Wiley (1972) Billow turbulence and ocean microstructure.
Deep-Sea Res. 19, 87-121.

Woods, J.D. and P.J. Minnett (1979) Analysis of mesoscale thermoclinicity with an example from the tropical thermocline during GATE.
Deep-Sea Res. 26, 85-96.

Woods, J.D., H. Leach and P.J. Minnett (1981) The GATE Lagrangian Batfish Experiment - Data Report.
Berichte aus dem Institut für Meereskunde Nr. 89